UNIVERSIDAD DE SANTIAGO DE COMPOSTELA
Facultad de Farmacia
Departamento de Farmacia y Tecnología Farmacéutica

Carburos de silicio biomórficos como cerámicas portadoras de fármacos para su aplicación en implantes óseos

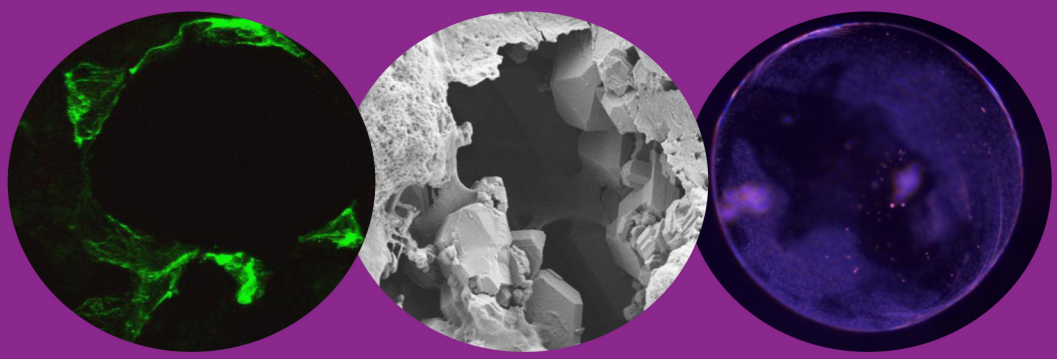

Patricia Díaz Rodríguez
Santiago de Compostela, 2014

Departamento de Farmacia y Tecnología Farmacéutica
Facultad de Farmacia
Campus Vida
15782 Santiago de Compostela

Carburos de silicio biomórficos como cerámicas portadoras de fármacos para su aplicación en implantes óseos

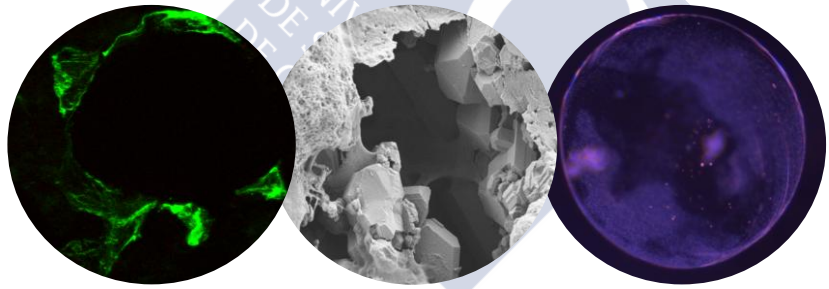

Patricia Díaz Rodríguez

Santiago de Compostela, 2014

USC
UNIVERSIDADE
DE SANTIAGO
DE COMPOSTELA

"Science is an imaginative adventure of the mind seeking truth in a world of mystery"

Sir Cyril Herman Hinshelwood

USC
UNIVERSIDADE
DE SANTIAGO
DE COMPOSTELA

Al comienzo de la tesis, éste parece el momento más deseado, escribir los agradecimientos, ya que es señal de que el trabajo ha llegado a buen término. Sin embargo, no resulta fácil resumir en un par de folios a todos aquellos que de una manera u otra han contribuido a la finalización de esta tesis. Espero no olvidarme de nadie y si lo hago, espero que me disculpéis.

En primer lugar, me gustaría expresar mi agradecimiento a mi directora de tesis *Mariana Landín Pérez* por su apoyo incondicional, sus consejos y su dirección desde el momento en el que me inicié en el mundo de la investigación.

Del mismo modo, quiero agradecer a todos los profesores del Departamento de Farmacia y Tecnología Farmacéutica, especialmente a *Ramón Martínez Pacheco, José Luis Gómez Amoza, Carmen Álvarez Lorenzo, Ángel Concheiro Nine* y *Francisco Otero Espinar* por su disponibilidad siempre que lo he necesitado.

Al Departamento de Física Aplicada de la Universidad de Vigo especialmente al profesor *Pío González*, la profesora *Julia Serra*, *Miriam* y *Cosme* por permitirme usar sus instalaciones y por su completa disponibilidad a lo largo de toda la tesis.

Al profesor *Henning Madry* y la profesora *Magali Cucchiarini* de la Universidad de Saarland por su amabilidad y por brindarme la oportunidad de realizar una estancia en su centro. También quiero agradecer a *Janina, Angelic, Amos, Jagi y Gertrud* por ser mi familia en Alemania y hacerme sentir como en casa desde el primer día.

A todos los miembros del Instituto de Ortopedia y Banco de Tejidos de la Universidad de Santiago de Compostela, *Maite, Silvia, Ana, Mari* y *Abel* por el buen trato y la ayuda recibida durante todos estos años.

A mis compañeros del Departamento de Farmacia y Tecnología Farmacéutica *Clara, Eva, Fani, Cibrán, Fran, Negin, Fernando Álvarez, Sandra, Rosalía, Julia, Patri, Bea, Elena*

Cutrín, Elena Raviña, Marga, Magdalena, Rocío, Andrea, Lorena y a aquellos que ya no están en el laboratorio pero que me han ayudado en todos estos años y que sin ninguna duda echo mucho de menos; *Ana Puga, Nano, Mariajo, Laura, Manolo, Luis, Álvaro, Abraham y Fernando.* Sin vosotros ésto no hubiera sido lo mismo.

A *Bárbara,* por compartir tantos buenos momentos juntas, tantas risas, por ser mi confidente y por iniciarme en el tute. A *Manuela,* por preocuparse siempre por todos y por tener una familia excepcional. A *Luis Díaz,* por ser capaz de generar un dialecto propio muy enriquecedor científicamente. A *Isa,* por conseguir sacarme una sonrisa sin importar si es lunes por la mañana o viernes por la noche. A *Alejandro,* por mantener la motivación de quien está empezando una tesis y contagiar ese sentimiento a quien le rodea. A *Sonia,* por regalarnos una sonrisa todos los días.

A *Catarina*, mi compañera de mesa, por darme siempre su opinión más sincera además de enseñarme los conceptos básicos de portugués. A *Susana Simoes,* por ser además de compañera de laboratorio, compañera de piso, gracias por estar siempre ahí. A *Ana Rey,* porque sin tí esta tesis no sería lo que es. Muchísimas gracias por compartir nuestra motivación, a veces excesiva, por la ciencia y ayudarme en todo lo que he necesitado. A *Lidia*, qué decir, simplemente gracias, gracias por aguantarme a tu lado tanto tiempo, gracias por escucharme y gracias por ayudarme siempre que lo he necesitado.

A mis amigos farmacéuticos *Sole, Luis, Silvia y Belén* que a pesar de llamarme friki, aguantan todas las charlas científicas que les doy y me animan en todo lo que me propongo. A *Josefa, Juan, Maruja, Moncho, Ana, David, Pablo, Luz, Ana Álvarez, Tamara y Manolo* por conseguir hacerme desconectar los fines de semana y por preocuparse siempre por mí.

A *Juan Carlos,* porque caiga lo que caiga siempre has estado a mi lado sin importar las consecuencias y por ser el copiloto ideal en este viaje.

A mi familia, especialmente a mis tíos *Suso, Teresa, Gloria, Manolo* y mis primos *Javi, Rubén y Yessica* porque de nada sirve llegar a la meta si te sientes solo. Gracias por hacerme sentir siempre arropada.

A mis abuelos *Irene, Dolores, Manuel* y *Ángel* aunque algunos ausentes, siempre presentes, por todos sus consejos y por haberme hecho la niña más feliz de este mundo.

A mi hermano *Efrén*, muchísimas gracias por apoyarme en todas mis decisiones y por valorarme tal y como soy.

A mis padres, *Aurea* y *Manuel* por enseñarme a ver las cosas siempre bajo el prisma de la positividad, a relativizar y a valorar las cosas realmente importantes en la vida. Este trabajo es vuestro también.

Finalmente, agradezco al Ministerio de Educación Cultura y Deporte por la beca FPU concedida que me ha permitido realizar esta tesis doctoral, a la Fundación Barrié de la Maza por permitirme hacer una estancia de investigación en la Universidad de Saarland y al proyecto POCTEP0330IBEROMARE1P por la financiación facilitada.

A TODOS, MUCHÍSIMAS GRACIAS

USC
UNIVERSIDADE
DE SANTIAGO
DE COMPOSTELA

Departamento de Farmacia y Tecnología Farmacéutica
Facultad de Farmacia
Campus Vida
15782 Santiago de Compostela

MARIANA LANDÍN PÉREZ, PROFESORA TITULAR DE FARMACIA Y TECNOLOGÍA FARMACÉUTICA, DE LA UNIVERSIDAD DE SANTIAGO DE COMPOSTELA,

CERTIFICA: Que la presente memoria titulada **"Carburos de silicio biomórficos como cerámicas portadoras de fármacos para su aplicación en implantes óseos"** elaborada por Dña. Patricia Díaz Rodríguez ha sido realizada bajo mi dirección en el Departamento de Farmacia y Tecnología Farmacéutica y, una vez concluida, autorizo su presentación a fin de que pueda ser juzgada por el tribunal correspondiente.

Y, para que conste, expido y firmo la presente certificación en Santiago de Compostela a 27 de Mayo de 2014

Mariana Landín Pérez

USC
UNIVERSIDADE
DE SANTIAGO
DE COMPOSTELA

ÍNDICE

Resumen

La incorporación de moléculas terapéuticas en las estructuras de los materiales implantables hace posible la liberación de fármacos *in situ* dando lugar a una nueva generación de sistemas biofuncionales. Este trabajo de investigación aborda la obtención de cerámicas a partir de precursores naturales mediante un proceso en dos etapas, lo que permite la síntesis de carburos de silicio biomórficos (bioSiCs).

Se estableció el potencial de los bioSiCs para la regeneración de tejido óseo, evaluando sus características morfológicas, las respuestas celulares que producen y su capacidad para cargar y liberar moléculas terapéuticas.

La síntesis de bioSiCs a partir de diferentes precursores naturales (pino, roble y sapelli) ha permitido obtener sistemas de propiedades morfológicas diversas. Su caracterización estructural y superficial ha permitido concluir que las cerámicas de mayor porosidad son las que resultan de la madera de pino; el mayor tamaño de poros se obtiene utilizando madera de roble como precursor y la madera de sapelli genera la cerámica más densa y rugosa, con la mayor interconectividad entre sus poros.

La evaluación de la biocompatibilidad de los tres sistemas cerámicos ha sido realizada mediante el cultivo con células madre mesenquimales mostrando excelentes resultados. Además, los sistemas que presentan mayor tamaño de poro inducen la

diferenciación celular, dando lugar a mayores concentraciones de indicadores de diferenciación osteoblástica.

El estudio de las interacciones de las cerámicas de carburo de silicio y sus precursores carbonáceos con los componentes tisulares y sanguíneos mostró los parámetros morfológicos y estructurales que las condicionan.

Los tres sistemas cerámicos fueron cargados con vancomicina mediante adsorción inespecífica generando perfiles de liberación dependientes de la estructura porosa. La actividad terapéutica ha sido evaluada mediante la capacidad para tratar un biofilm bacteriano y la capacidad de los sistemas de sapelli para inhibir su formación. Los sistemas de sapelli inhiben significativamente la formación del biofilm y todos los sistemas cargados disminuyen el número de unidades formadoras de colonia (CFUs) presentes.

El factor de crecimiento del endotelio vascular (VEGF) se incorporó en los bioSiCs mediante interacciones iónicas entre la proteína y los grupos funcionales de las superficies cerámicas. Los sistemas cargados mostraron un perfil de liberación sostenido y dependiente de la estructura porosa, capaz de mantener la bioactividad de la proteína tanto *in vitro* como *in vivo*. La adición de VEGF incorporado en la cerámica ha logrado obtener una diferenciación osteoblástica más rápida, lo que indica un efecto sinérgico entre el VEGF y la topografía de los bioSiCs.

Se han obtenido sistemas compuestos hidrogel-cerámica seleccionando como fase hidrogel una combinación de alginato y poloxamer. Los sistemas lograron perfiles de liberación de fármaco sostenidos, también condicionados por la morfología de los materiales. La evaluación *in vitro* de los sistemas cargados con indometacina mostró una adecuada capacidad antiinflamatoria para todos ellos, y además una disminución de la actividad catabólica de condrocitos osteoartríticos.

Los hidrogeles formados por alginato y poloxamer también fueron capaces de incluir vectores virales recombinantes adeno-asociados (rAAV) promoviendo su liberación sostenida y manteniendo su eficacia de transducción. El sistema polimérico con estructura más compacta ha obtenido un incremento de la expresión trangénica más prolongado. La incorporación de los hidrogeles cargados en los bioSiCs no ha sido capaz de obtener una adecuada eficacia de transducción siendo necesarios estudios adicionales.

En su conjunto, los resultados obtenidos confirman el elevado potencial de las cerámicas de carburo de silicio como sistemas biofuncionales con aplicación en implantes óseos. La posibilidad de emplear numerosos precursores naturales y varias técnicas de carga permitiría la selección del sistema más adecuado en función de la necesidad requerida.

USC
UNIVERSIDADE
DE SANTIAGO
DE COMPOSTELA

Summary

The incorporation of therapeutic molecules into implantable biomaterials for *in situ* drug release gives a novel generation of biofunctional materials. This research work is focused on the synthesis of ceramics derived from natural precursors by a two-step process, which allows biomorphic silicon carbides (bioSiCs) to be obtained.

bioSiCs potential to regenerate bone tissue was established by evaluating their morphological properties, their cellular responses produced and their ability to load and release therapeutic molecules.

The bioSiCs synthesis from different natural precursors (pine, oak and sapelli) has led to systems with various morphological properties. Their structural and surface characterization has led to the conclusion that higher porosity ceramics are those resulting from pine wood; the higher pore size is obtained using oak wood as precursor and sapelli wood generates the densest and the roughest ceramic, also with the highest pore interconnectivity.

The evaluation of the biocompatibility of the three ceramic structures has been performed by the cell culture with mesenchymal stem cells showing excellent results.

In addition, systems with larger pore size induced cell differentiation, leading to higher concentrations of osteoblastic differentiation markers.

The study of the interactions of silicon carbide ceramics and their carbonaceous precursors with tissue and blood components showed the morphological and structural parameters that modulate these interactions.

The three ceramic systems were loaded with vancomycin by unspecific adsorption showing porous structure dependent release profiles. The therapeutic activity of these systems was evaluated by the ability to treat a bacterial biofilm and the ability of sapelli systems to inhibit its formation. Sapelli systems significantly inhibit biofilm formation and all loaded systems were able to decrease the number of colony forming units (CFUs) present in the preformed biofilm.

The Vascular Endothelial Growth Factor (VEGF) was incorporated into the bioSiCs by ionic interactions between the protein and the functional groups of the ceramic surfaces. The loaded systems show a sustained release profile dependent on the porous structure which was able to maintain the bioactivity of the protein both *in vitro* and *in vivo*. The addition of VEGF into the ceramic has achieved a faster osteoblastic differentiation, indicating a synergistic effect between VEGF and bioSiCs topography.

Hydrogel-ceramic composite systems were obtained by mixing alginate and poloxamer. The systems achieved sustained release profiles of poorly soluble drugs, also modulated by the morphology of the materials. The *in vitro* evaluation of indomethacin loaded systems showed a satisfactory anti-inflammatory activity for all the samples and also a decrease of the catabolic activity of osteoarthritic chondrocytes.

The hydrogels formed by alginate and poloxamer were also capable of including recombinant adeno-associated viral vectors (rAAV) promoting their controlled release and maintaining their transduction efficiency. The polymeric system with the most

compact structure was able to obtain a longer increase in transgene expression. The incorporation of loaded hydrogels into bioSiCs has not been able to obtain adequate transduction efficiencies, additional studies being required.

Taken together, the results of this work confirm the high potential of silicon carbide ceramics as biofunctional systems with applications in bone implants. The large number of natural precursors and different loading techniques available, should allow the selection of the right fit in each case according to the required needs.

USC
UNIVERSIDADE
DE SANTIAGO
DE COMPOSTELA

Capítulo 1

Introducción general

USC
UNIVERSIDADE
DE SANTIAGO
DE COMPOSTELA

1.1

Implantable materials for local drug delivery in bone regeneration

USC
UNIVERSIDADE
DE SANTIAGO
DE COMPOSTELA

1.1.1 **Bone morphology**

Bone is one of the essential organs of the body playing key roles in shape and protection, muscle attachment, leverage for motion and haemopoiesis, being the highest mineral reservoir with 98% of the total body calcium (1, 2). The high tensile and loading strength of bone is the consequence of its composition (mainly hydroxyapatite (HAp) and collagen). Its distinctive structure with concentric layers of mineralized extracellular matrix around a central Haversian canal oriented in parallel to the longitudinal axis in compact bone, is the basis of its excellent biomechanical properties. There are two types of bone tissue, cancellous bone and compact bone each one playing different functions in the body (1, 2).

Cancellous bone, crucial in hematopoiesis, growth and calcium homeostasis, is under continuous remodeling. Compact bone is stronger and suffers less remodeling formed by this closely packed Harversian system (2, 3). This bone tissue is made up of four types of cells; osteoblasts, osteoclasts, osteocytes and mesenchymal progenitor cells.

Osteocytes act as mechanotraductors controlling the bone mineral homeostasis (2). Osteoblasts and osteoclasts make the continuous remodeling process of bone possible; the osteoblasts being responsible for the synthesis of the matrix and mineralization, while the osteoclasts releasing calcium and digesting the collagen matrix as a consequence of bone resorption (4, 5). The equilibrium between both is necessary for

adequate bone function, thus one of the parameters to be considered in the development of drug local release systems. Mesenchymal progenitor cells are the key in the bone healing process; because of being able to differentiate to either chondrocytes or osteoblasts (6).

1.1.2 **Bone fracture healing process**

In brief, bone regeneration could be divided into four steps (Figure 1.1.1). This process starts with the formation of a hematoma due to the disruption of the tissue integrity and disintegration of blood vessels. This provisional fibrin matrix is infiltrated by neutrophils, monocytes, lymphocytes, macrophages and activated platelets that secret cytokines and growth factors able to attract mesenchymal progenitor cells. These cells can be directly differentiated to osteoblasts in well apposed and stabilized fractures able to produce intramembranous bone formation or to chondrocytes in non-stabilized fractures or large defects causing endochondral bone formation. In this case, chondrocytes together with fibroblast produce a semi-rigid *soft callus* capable to provide mechanical support of the fracture. These cells proliferate and synthesize the cartilaginous matrix until all the fibrinous matrix is changed into cartilage. Then chondrocytes in the center of the matrix stop to proliferate and change their protein expression directing mineralization of the surrounding matrix and stimulating the adjacent pluripotent marrow cells differentiation to osteoblasts before their apoptosis. Osteoblasts invade the collagen matrix formed by chondrocytes forming a vascularized proteinaceus and mineralized bone matrix called *hard callus*. The final step is the bone remodeling process that converts the irregular woven bone into compact or cancellous bone (7-11).

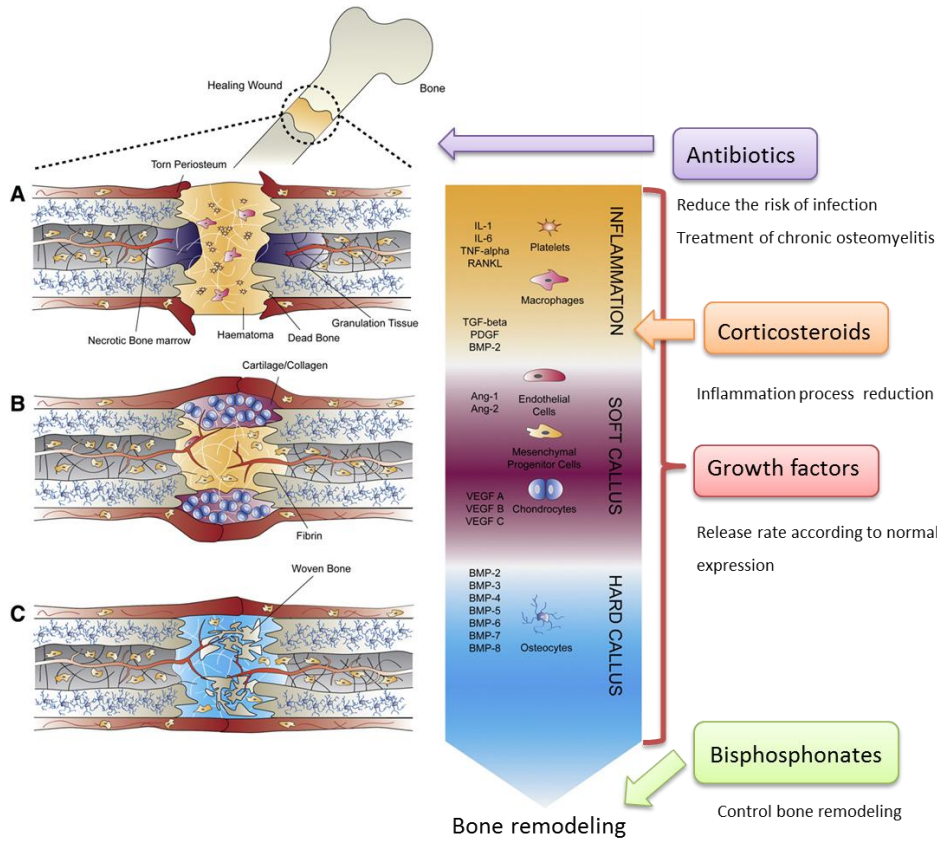

Figure 1.1.1 Bone healing steps and possible local drug release techniques from implant materials (adapted from (9) with permission of Elsevier). Bone morphogenetic protein (BMP), Interleukin (IL), Angiopoietin (Ang), Vascular endothelial growth factor (VEGF), platelet-derived growth factor (PDGF), transforming growth factor (TGF), tumor necrosis growth factor (TNF) and receptor activator of NF-κB (RANKL).

1.1.3 **Current materials for bone regeneration**

Some diseases such as fractures, tumors or infections give rise to damage bone of sufficient magnitude so that the natural mechanism of bone repair is not enough to recover its functionality. In such cases, the placement of bone grafts, preferably autologous bone is required. This option however, has several inconveniences, such as more prolonged surgery, limited availability of tissue, nerve damage, long lasting pain

and possible infection (3, 12-14). The use of alternative biomaterials that can be implanted enabling the recovery of bone functionality without the limitations of autologous grafts is an attractive approach for the treatment of several pathologies.

A biomaterial can be defined as a natural or synthetic product, able to perform an appropriate host response when implanted as a device to replace a functional part of the body. Biomaterials should be safe, economic and reliable (15). Moreover, they should have a structure that guarantees the adequate mechanical properties of the implant until the new bone tissue growth is enough to ensure its function (4). Ideally, biomaterials for bone replacement should also be biocompatible, osteoinductive, osteoconductive and, preferably, biodegradable.

The first biomaterial property to be analyzed is its biocompatibility. The biomaterial implantation should not cause adverse reactions such as inflammation that leads to cell death. They must allow the desired degree of incorporation into host tissues for an specific application to be obtained (5, 15, 16).

The osteoconductivity is defined as the ability to facilitate bone cell adhesion, proliferation and migration for biomaterial incorporation by the host tissues whereas osteoinduction is the direct material stimulation of bone formation. This term means that the biomaterial is able to stimulate the differentiation of mesenchymal progenitor cells to bone forming cell lineages helping with the *hard callus* formation. For this purpose biomaterials should have adequate macroporosity with high degree of interconnection. Those features enable cell migration, nutrient transport and tissue infiltration (17-19).

The degradation rate and its degradation products are also interesting characteristics to be considered. The biomaterial degradation rate should match the host tissue

growth without producing toxic products that may harm surrounded tissue (16, 20, 21).

Treatment by local drug release (growth factors, angiogenesis inductors, and guide cell proliferation, differentiation or migration factors) from implant biomaterials can provide an extra value to implantable systems. The use of loaded biomaterials for *in situ* drug release (Figure 1.1.1) can be an interesting strategy in treating bone pathologies or surgical complications and in facilitating bone regeneration, helping in patients' recovery (3, 14, 22).

The search for an ideal material able to simulate simultaneously both tissue morphology and functionality led to the development of a wide variety of new complex biomaterials. The need to ensure therapeutic success and facilitate patient recovery has made the combination of materials and therapeutic molecules a promising strategy in order to obtain "biofunctional systems" that meet the patient requirements with minimum systemic effects.

Biofunctional systems (biomaterial + drugs) must be easy to obtain and cost-effective, and simultaneously, they must be able to incorporate the appropriate amount of unaltered drug and/or growth factor (23, 24) and release it with suitable kinetics during a specific period of time in order to achieve adequate effectiveness and avoiding side effects. This is particularly important for some molecules like growth factors (25, 26) whose ineffective localization could cause ectopic bone formation (8).

The use of materials for medical purposes has a long tradition with their clinical orthopedic applications starting at the end of the 19th century (5). At present, the orthopedic biomaterials can be classified into four major groups; metals, ceramics, polymers and composites, which can be loaded with drugs using different mechanisms.

In the following paragraphs we will review the main types of biomaterials for implants, with particular reference to those that allow drug loading and release.

1.1.3.1 *Metals*

Historically, metals have been the most widely used materials in the recovery of bone function. They are clinically used for load bearing sites where they are the only materials that meet the mechanical requirements (5). There are three main groups of metals; cobalt-based alloys, stainless steels and titanium and Ti-based alloys. The use of titanium as surgical implants started at the late 30s and continues today (27). The natural and stable oxide layer formed on its surface leads to its excellent biocompatibility, allowing easy bone-implant integration (15, 28-30).

Metals have some advantages, such as high strength, ductility, hardness, formability and biocompatibility (27). However, their Young's modulus being higher than the bone one and their lack of osteoconduction and osteoinduction increase osteoclastogenesis and osteolysis, making their improvement necessary (31). Different modifications have been carried out in the last few decades for this purpose, such as surface modification of roughness and topography (16, 30), the coating with bioactive compositions (32), the obtaining of alloys with lower Young's modulus or the synthesis of trabecular metal with higher porosity that promote rapid tissue in-growth and strong implant fixation (16, 33-35).

Although metals are well tolerated in the body, to obtain a proper fixing of the implant and the prevention of infection and inflammation after surgery, continues to be a problem in the clinical practice (16, 36, 37). The loading of therapeutic molecules into metal based implants should help to avoid these side effects and, in some cases, provide osteoinduction. The conventional way for loading metal based implants is through the metal surface coating. Therapeutic molecules could be integrated into a polymeric

matrix (28, 34, 38-40) or a ceramic layer (35), adsorbed directly on to these implant coatings (36, 41-44), nonspecifically adsorbed on to the implant surface (45) or bound to the metal surface (30, 46, 47). Titanium is the most used metal for this purpose.

1.1.3.2 *Ceramics*

Ceramics are defined as inorganic non-metallic materials. It is a complex group including calcium phosphate based ceramics, silica based bioactive glasses and inert ceramics, such as zirconia and silicon carbides. Their use as biomedical materials dates back to late 1960s, when they were introduced to improve the applicability of the metals. Ceramics present, as main advantages, their lower wear rates at the articulating surface and the release of lower concentrations of inert wear particles (48, 49). They are hard refractory, polycrystalline compounds, difficult to shear plastically with high melting temperatures, low electric conductivity and corrosion resistance (15, 15, 48).

Ceramics could be classified into two major groups: biodegradable and non-absorbable ceramics.

1.1.3.2.1 Biodegradable ceramics

Their ability to interact with tissue environment facilitating their surface mineralization and therefore the bone growth makes them the most attractive group in tissue engineering. Biodegradable ceramics are reabsorbed after implantation by dissolution, thus being replaced by endogenous tissues. The degradation of the ceramic matrix leads to the formation of particles which are phagocyted by macrophages and giant cells whereas large material volumes are reabsorbed by osteoclast (33, 48, 50).

Calcium phosphate ceramics. As previously mentioned the main mineral component of bone is hydroxyapatite (HAp), a specific type of calcium phosphates. This fact justifies the interest in calcium phosphate ceramics when trying to simulate the natural bone

composition (41, 43). It has been shown that these ceramics are able to improve the bone bonding strength without inducing the formation of fibrous tissue showing excellent biocompatibility (49, 51). Despite the hydroxyapatite chemical composition being the closest to the mineral bone, its high stability makes the development of chemical modified derivatives with better aqueous solution properties to improve resorption rate *in vivo* necessary (50, 52-54).

Calcium phosphate ceramics degradation rate could be tailored by combining two or more calcium phosphates with different stability. Tricalcium phosphate (TCP) with Ca/P ratio of 1.5 and four polymorphs is widely used. The combination of β-TCP and hydroxyapatite named biphasic calcium phosphate is a material whose resorption rate can be modified according to the bone tissue regeneration and with higher osteoinduction over pure HAp, xenografts and in some cases autologous bone graft (48, 55, 56). It has been shown that these ceramics have been replaced *in vivo* by new and functional bone tissue which represents a significant advantage compared with other biomedical materials (56-58).

Calcium phosphate ceramics are commonly used for local drug delivery as porous scaffolds, coatings and self-hardening cements and in the latter years as nanoparticles (32).

As cements, one or more calcium phosphates can be mixed with an aqueous solution to give injectable pastes. After implantation and an *in situ* curing process, a final carbonate apatite product is formed which is characterized by an adequate mechanical strength that avoids the migration of the cement to undesirable sites (53, 59). Their ability to mold the defect site and their osteoconduction makes them attractive for orthopedic recovery, being approved by the Food and Drug Administration (FDA) in 1996 for the repairing of craniofacial defects in humans (60). Drugs could also be incorporated by mixing them into one or the two phases of their components (53).

Phosphate ceramic nanoparticles are high biocompatible and easy to handle. They are biodegradable giving no toxic degradation products. Nanoparticles can be used as drug delivery systems even for vectoring RNA and DNA. These nanoparticles could be obtained using various synthesis methods which lead to the efficient incorporation of antitumoral agents and proteins (32). These nanoparticles could also be coated by a drug-polymer solution forming nanocomposite systems which are able to release antibiotics and peptides (61-63).

A common combination is the use of ceramic coatings in metals which could be performed by different approaches; plasma spraying, sol-gel deposition, electrophoretic deposition, simultaneous vapor deposition, pulsed laser or electron beam deposition and biomimetic precipitation (32, 41). The final material is characterized by higher osteointegration than the substrate alone (42). However, most of these coating techniques use high processing temperatures making drug loading difficult (32). This makes biomimetic calcium phosphate-drug coprecipitation the most used technique in order to obtain drug loaded coating (64-66).

Calcium phosphate ceramic porous scaffolds could be loaded by specific and unspecific drug adsorption (67-69). However, the combination with polymers giving a final composite system is the most common technique (55, 70-72).

Bioactive glasses and glass-ceramics. Silica-based bioactive glasses are noncrystalline compounds made from fine ceramic crystallites in a glassy matrix, which present as the main advantages high surface reactivity, good degradation rate, osteoconduction and osteoinduction, creating an apatite layer precipitate in the presence of simulated body fluid (48, 49, 73-76). SiO_2 is the mayor constituent of the glass providing stability to the material by the formation of a covalently bonded network (73). The incorporation of new techniques in the obtaining process of bioactive glasses has lead to the production of mesoporous bioactive glasses which are characterized by well structured pore

channels with an average pore size of 5-20 nm and high surface area. Those properties make the loading of several therapeutic molecules or the surface modification to enhance drug affinity possible, and justify the high number of published studies on this subject (49, 73, 77-81).

1.1.3.2.2 Non absorbable ceramics

Non absorbable ceramics are materials that maintain their physical and mechanical properties once implanted into the patient. Alumina, zirconia and pyrolitic carbon are examples of this group. Their excellent biocompatibility, strength and toughness are their main advantages. However, they have a lack of long term stability and poor osteointegration properties (33, 48, 82). Non-oxide ceramics, such as silicon carbide or silicon nitride are considered more stable and not as sensitive to the characteristic slow crack growth of ceramics, which should lead to a better reliability. The obtaining of porous silicon carbide using the wood structure as template has lead to biomorphic silicon carbide ceramics (bioSiCs) characterized by consistent biomimetic microstructure, high degree of interconnectivity, high strength and thermal conductivity, good resistance to oxidation, biocompatibility and thermal conductivity whose final properties are controlled by the density and microstructure of the wood precursor (83-88).

1.1.3.3 *Polymers*

Polymers are the product of covalent bonding of small molecules called unimers forming long chain molecules widely used in biomedical devices (27). According to their origin they could be divided in two groups: natural and synthetic polymers.

1.1.3.3.1 Natural polymers

The most common natural polymers used in biomedical field are collagen, alginate, agarose, fibrin, chitosan and hyaluronic acid (5, 57). They are biodegradable, bioresorbable and versatile (24) and could be used as gels, porous scaffolds, films and nanofibers (24, 47).

Collagen is a structural protein of bones widely used in bone regeneration, the crosslinking with different agents to reduce its degradation rate is a commonly used technique to increase its stability (5, 17). A good alternative to collagen is the use of its denatured state, gelatin. The presence of sequences arginine-glycine aspartic acids in its structure improves osteointegration and stimulates the adhesion of osteoblasts (89).

Alginate is a polysaccharide present in brown algae, formed by D-mannuronic acid and L-glucuronic acid, this composition allows the binding of divalent cations (Ca^{2+}, Cd^{2+}, Cu^{2+}, Mn^{2+}) producing the gelation of the polymeric solution. Moreover, calcium is the most frequently used ion to promote gelation of alginate systems for biomedical applications due to its presence in the human body especially in bone tissue (89, 90). The use of this polymer has been successful in the controlled release of growth factors (24).

Chitosan is a hydrophilic polysaccharide with a similar structure to naturally formed glycosaminoglycans that could be degraded by human enzymes (3, 5). Its cationic nature facilitates the interaction with anionic glycosaminoglycans and proteoglycans which have great affinity to cytokines and growth factors. On the other hand due to its N-acetylglucosamine moiety, chitosan is able to interact directly with growth factors, receptors and adhesion proteins (91). This fact, together with its antibacterial activity and its appropriate physicochemical and biological properties, make it an excellent

material for the preparation of biomedical materials and drug delivery systems (34, 92, 93).

Agarose is used for many tissue engineering applications such as drug delivery or cell culture beads (57) whereas fibrin has been used as tissue sealant in surgery. For this application fibrin gels are prepared by the combination of fibrinogen and thrombin solutions containing calcium ions forming an adhesive glue adequate for the administration of endogenous plasma rich in growth factors (24, 90, 94).

Hyaluronic acid is a linear polysaccharide, essential component in extracellular matrix. It is characterized by high biocompatibility and may mediate in cellular signaling, wound repair and matrix organization. The use of this polymer in extracellular matrix biomimetic hydrogels has shown good results as growth factors delivery systems (95).

Other natural polymers have been useful as implantable bone drug delivery systems such as silk (96), chondroitin sulfate (25) and bacterial cellulose (97). Natural polymeric systems are able to load drugs into the polymeric matrix obtaining diffusion/erosion controlled drug release profiles (90, 98) that can be tailored modeling the drug load charge, the polymer weight and crosslinking variables (99).

1.1.3.3.2 Synthetic polymers

Although natural polymers present adequate biological properties their immunogenicity, the difficulty in processing and the potential risk of transmitting animal-originated pathogens make it necessary to obtain synthetic alternatives (47). Poly(α-esters) such as poly(caprolactone) (PCL), poly(propylene fumarate) (PPF), poly(lactic acid) (PLA), poly(glycolic acid) (PGA) and their copolymer poly(lactic-glycolic acid) (PLGA) and poly(ethylene glycol) (PEG) are broadly used in the medical field with minimal foreign body reaction (2, 3). These polymers have been approved by the FDA for their use in diverse clinical applications such as sutures, spinal fusion cages,

coronary stents, systemic drug delivery systems, nerve conduits and fixation screws (2, 43). PLGA is the most used as implantable bone material. Its degradation rate and mechanical properties could be tailored by selecting its molecular weight and copolymer ratio which makes this polymer attractive for controlled drug delivery systems applications (3, 24, 100, 101). Great efforts have been carried out in this field in order to obtain the perfect material with the adequate release profile; the use of PLGA microspheres alone or included into different matrices has been one of the most common technological approaches used to achieve the desirable bone local release. In this sense, good results have been obtained in the release of different therapeutic molecules as BMP-2 (102, 103), BMP-7, IGF (insulin-like growth factor), dexamethasone (104, 105), alendronate (106) or gentamicin (107). The main disadvantage of these molecules (PLA, PGA and PLGA) is their acidic degradation products as a consequence of their hydrolytic process that can cause the degradation of therapeutic molecules (91).

PCL is a biocompatible, biologically inert polymer whose mechanical properties and degradation rate could be also modified in order to obtain the desirable characteristics. It shows minimal toxicity and immune response (18, 25).

PPF is a linear polyester, highly biocompatible which has been shown to support and guide bone formation once crosslinked (108).

The ability of PEG to bind proteins or peptides giving stable nanosized complexes for their controlled release is used in the development of protein commercial drug delivery systems (57, 109). This polymer has also been useful for bone local delivery of BMPs (24).

The synthesis of new biodegradable polymers such as poly(lactic acid)-p-dioxane-poly(ethylene glycol) (PLA-DX-PEG) has been useful for the controlled release of BMP-

2. This polymer is able to undergo a sol-gel transition by the change of the temperature and its degradation rate could be tailored in order to achieve the desirable drug release profile (24, 110-113).

Although, the above mentioned polymers with elevate biocompatibility and biodegradability have high interest in the orthopedic field, the gold standard in polymers for orthopedic prostheses are poly(methyl methacrylate) (PMMA) cements and beads (114). They are characterized by their easy fabrication and excellent physical properties including tensile modulus, tensile strength, flexural rigidity and resistance to creep (15, 33). Today, the strategy approved for local antibiotic delivery in chronic osteomyelitis after surgical debridement of dead bone is the use of antibiotic loaded PMMA implants. However, the poor osteointegration and non-biodegradability of the polymer makes it necessary to perform additional surgery to remove the polymer device once the pathology is repaired (115, 116). Furthermore, the high drug doses loaded into the cements are not completely released due to the absence of degradation. For overcoming this limitation, different approaches have been made with better results as the incorporation of loaded PLGA microspheres into the cements (117) or the combination with other polymers (118).

1.1.3.4 *Composites*

As it can be deduced, each material has advantages and disadvantages. Not strange then that studies aimed at the collection and evaluation of composites are attracting increasingly attention. In the last few years new complex biomaterials have been developed in order to have the advantages of various materials simultaneously.

A composite could be defined as a continuous phase material, made from two or more ingredients with significantly different physical and/or chemical properties, whose characteristics are far from those of the raw materials (33). Several possible

combinations pointed out by Habraken and coworkers and Bose and coworkers (32, 119) can be used as implant material and also for local drug delivery. The most used combination is the inclusion of particles or fibers of calcium phosphate ceramics and bioactive glasses into biodegradable polymeric matrices (120). Composites of chitosan and PLA where PLA provides mechanical strength and stiffness whereas the cationic nature of chitosan minimizes the reduction of pH caused by the PLA degradation (91) are also employed or, with the same objective, mixtures of components able to release calcium and silicon ions, as bioactive glasses or phosphate ceramics with polymeric systems as PLGA (121) have been developed.

The combination of two types of ceramics in order to couple both mechanical properties and electrical conduction could be also used; an example is the case of carbon nanotubes and silica for obtaining a final material with good *in vitro* results stimulating cell proliferation of human osteoblasts after electrical stimuli (122).

More complex systems can also be synthesized including metals, ceramics and polymers. In many of them the stability of the polymeric component, mostly PLGA, is increased by the addition of the ceramic phase, calcium phosphates or bioactive glasses that neutralize the surrounding acid environment and reduce its autocatalytic effect (43). These ternary systems have been shown to be useful in controlled release of antibiotics (34).

1.1.4 **Therapeutic molecules with interest in bone regeneration**

Going back to Figure 1.1.1, it can be seen that the bone healing is an extremely complex process depending on different factors. Despite the great development of new materials in the few last years, the ideal implant material has not yet been developed. Some potential candidates, despite possessing appropriate porosity and mechanical properties, have a lack of osteoinduction. In this situation, their loading with bone

morphogenetic proteins and/or other growth factors should enhance their value by improving cellular attachment and bone formation (23, 123).

Although bone induction is important in the prosthesis osteointegration, implant fixation is also crucial in order to avoid its failure. It has been shown that the local administration of bisphosphonates, antiresorptive drugs, improve implant fixation *in vivo* (124). PMMA cements are characterized by low porosity and interconnectivity making the growth of bone cells into their inner structure difficult. This complication could be overcome by the addition of N-acetyl cysteine, a strong antioxidant that acts as a scavenging agent during the polymerization, increasing porosity and consequently osteoconductivity (125).

As can be seen the combination of biomaterials and drugs has lead to the enhancement of the material properties making the therapeutic success easier. Material-drug combinations are not only adequate for the improvement of implant materials but also allow local drug delivery. Local therapeutic treatments increase the time of permanence of the drug at the target site, maintain high local drug concentration and reduce the occurrence of side effects (23, 117).

In addition, the incorporation of labile therapeutic molecules as growth factors to biomaterial systems could enhance their stability protecting them from enzymatic or chemical degradation both in polymeric systems (126-128) and in ceramic matrices (13). The use of solid implant materials loaded with BMP-2 able to support enough space for cell growth has been found to be more adequate for bone regeneration than hydrogels. These systems have achieved higher levels of bone formation due to the stimulation of tisular compression, the key in bone induction (67, 129). Moreover, high implant volume of materials has produced a high bone formation (110). This could be explained by the influence of mechanical signals in the bone healing modulating

vascularization, inflammation, cell differentiation and migration enhancing the therapeutic activity of drug molecules (14).

Although a high number of molecules have been administered in bone therapy, antibiotics, growth factors and bisphosphonates are the groups more commonly used for local drug delivery from implant materials.

1.1.4.1 *Antibiotics*

Bone infections are caused by bacteria introduced through the blood stream (hematogenous) or from trauma, surgery or surrounded infected tissues (continuous focus). Several Gram-positive and Gram-negative organisms as *Staphylococcus epidermidis* or *Mycobacterium* sp can be involved in bone infections. However, *Staphylococcus aureus* and particularly, methicillin-resistant strain infections present the worst prognosis. In the clinical practice, the risk of bone infection is reduced by systemic antibiotic administration one or two hours before surgery (130). However, due to the low blood irrigation of bone, the systemic antibiotic administration would not be enough to assure a local concentration over the minimal inhibitory concentration (MIC) and to avoid bacteria growth (62, 131). The formation of bacterial biofilm, extremely resistant to both the immune system and antibiotics, is considered the primary cause of implant-associated infections. During the first hours after surgery, an implant is particularly susceptible to surface colonization and biofilm formation (132-135).

The use of implants loaded with antimicrobial agents, able to release the antibiotic at a concentration over the MIC for at least two days, is a promising approach in preventing post-operative infections (130). Despite of the efforts to avoid it, chronic osteomyelitis is still an important problem in orthopedic surgery. Its treatment makes a local release up to ten days of high drug concentration throughout the treatment

necessary. The ideal loaded device should promote a high dose during the first hours followed by a controlled release for up to one year (136). Currently, two methods are commonly used for the treatment of chronic osteomyelitis, intravenous injections or local implantation of calcium phosphate cements or PMMA beads loaded with antibiotics, normally gentamicin. PMMA beads are advantageous because of their high local concentrations of antibiotics for four weeks with minimal side effects and immunological reactions (136). However, PMMA systems present several inconveniences like the exothermic polymerization process for their development that causes temperature over 100 °C which is incompatible with some drugs loadings (137), their surface characteristics that make them adequate for bacterial biofilm growth (136) and their non-degradable character (49) which requires a second surgery for its extraction. All these limitations justify the efforts for developing improved antibiotic delivery systems useful in orthopedic surgery (136).

Aminoglycosides. This group includes the most studied antibiotics for bone regeneration, gentamicin, and also streptomicin, tobramicin, amikacin, sisomicin and netilmicin. They are active against Gram-positive and Gram-negative bacteria binding to the ribosome and inhibiting bacterial protein synthesis (59, 138). The most used is gentamicin included mainly into porous scaffolds (139-141) and bone cements (141, 142).

Glucopeptides. Vancomycin is a highly water soluble antibiotic, commonly used to treat methicillin-resistant *Staphylococcus aureus* osteomyelitis (143). Its main inconvenient is its high molecular weight that makes its loading into the materials difficult (144). It hampers the second stage of cell wall synthesis changing cellular membrane permeability and inhibiting RNA synthesis (145).

Fluoroquinolones. Enoxacin, ofloxacin, moxifloxacin, norfloxacin and ciprofloxacin have a broad antibacterial spectrum against Gram-positive, Gram-negative and mycobacteria. Among them, ciprofloxacin is the most widely used due to its low MIC for most

osteomyelitis pathogens (146, 147). Their mechanism of antibacterial action involves the cleavage of bacterial chromosomal DNA by the DNA gyrase (148).

β-lactam. This group includes penicillins (penicillin, amplicillin and amoxicillin) and cephalosporins (cephalotin, ceftriaxona, cefuroxime, cephazolin, ceftazidime, and cephalexin). Their common antibacterial mechanism involves the inhibition of membrane peptidoglycan synthesis. Cephalexin and cefuroxime have been shown to be useful in the treatment of bone infections (149, 150).

1.1.4.2 *Growth factors*

Growth factors are water-soluble bioactive proteins that influence bone regeneration promoting endogenous regeneration cascades, as shown in Figure 1.1.1. They are able to modulate the cell behavior by the union to membrane receptors that starts complex intracellular cascades which finally lead to the protein expression modification (3, 103). The high utility of bone morphogenetic proteins (BMP) in the stimulation of bone regeneration is well known. Currently, there are two BMPs (BMP-2 and BMP-7) approved by the FDA. BMP-2 has been shown to be the predominant cytokine during the bone remodeling process (151). A wettable and absorbable sponge or granules of collagen for the local administration of both BMPs are clinically used in anterior lumbar interbody fusion (152, 153).

The protein release profiles from the implant devices are essential for them to achieve an adequate therapeutic effect, this being properly bone repair when a controlled protein delivery is carried out (46, 103, 154-156). On the contrary, when protein release is fast, higher BMP concentrations are necessary (157, 158) and some side effects as osteolysis, ectopic bone formation or loss of motor or sensory function can be observed (159). The effective BMP dose depends on the application, the implant location and the animal species, making it difficult to extrapolate results from

experiments to clinical practice. The minimum dose required in primates and humans has been established in 1 mg/cm^3 of carrier material (160).

Different loading doses have been studied for improving bone regeneration results. Among them 10 mg/mm^3 (161) or 50 ng/mg polymer (113) have been pointed out as the best conditions. Moreover, a dose of 20 ng/mL per day gives a desirable regeneration effect while higher concentrations could cause osteoclastic bone resorption, heterotopic bone formation and the increased risk of cancer (55, 153, 162).

The ideal release profile for BMP-2 should have an initial burst followed by a continuous release for one or two weeks (163) at enough concentration to stimulate cells (50, 164). The desirable growth factor release profile should mimic the natural process of bone remodeling (8, 165) that includes several steps (Figure 1.1.1):

A) Inflammation (0-3 days); maximal levels of platelet derived growth factors (PDGF), IL-1, IL-6, TNF-α, TGF-β. PDGF stimulates cellular chemotaxis of macrophages, endothelial cells and mesenchymal stem cells associated with inflammatory responses, prophylaxis of infection and chemoattracts (71, 94, 164). TGF-β stimulates pluripotent marrow cells recruitment and differentiation to osteoblasts increasing bone formation (47, 166).

B) *Soft callus* formation (3-9 days); maximal levels of fibroblast growth factors (FGF). Local administration of bFGF has been shown to be useful in wound healing, angiogenesis, bone regeneration and organization (128, 167).

C) *Hard callus* formation (10-20 days); maximal levels of insuline growth factor (IGF) which influences proliferation and chemotaxis of osteoblasts and bone matrix formation (39). BMP-2 concentration increases at day 3 and returns at day 10 (168) while BMP-7 is expressed approximately after two weeks (169). The formation of new vessels is also important in this process and in intramembranous ossification

achieving high levels of vascular endothelial growth factor (VEGF) from day 5 to day 10 (25, 170).

One step forward is the combination of more than one growth factor trying to simulate the normal bone metabolism with an adequate mixture of cellular cytokines (151). A synergistic effect in the increasing of bone mineral density and in deep bone formation has been found when combining PDGF and VEGF (25), BMP-2 and VEGF (171, 172) or IGF-1 and BMP-2 (173).

Although there is a current available system for local release of growth factors (BMP-2 and 7) in a collagen matrix, it presents several immunological problems due to the xenogenic origin of collagen (24, 74). This fact together with the high doses included in these systems for adequate effects make the search for new synthetic materials to overcome these problems necessary (159, 174). Recently, growth factor local delivery systems have been reviewed by Mehta and coworkers 2012 and Lieneman 2012 (8, 9).

1.1.4.3 *Bisphosphonate*

Tumor induced hypercalcemia, Paget's disease, metastatic bone diseases and osteoporosis are treated with bisphosphonates as they promote the inhibition of osteoclasts which slow down the periprosthetic bone resorption and improve bone-implant contact and osteointegration (69, 175). Alendronate, the most representative bisphosphonate, is able to promote the activity and maturation of osteoblasts and the differentiation of mesenchymal stem cells to osteoblasts (176, 177). Risendronate and zolendronate have also been found to act as antitumoral drugs by the inhibition of cellular invasion (178).

1.1.4.4 *Corticosteroids*

Dexamethasone is a highly water soluble and costless corticosteroid, frequently used in bone regeneration experiments as the model drug. It has been found to induce osteoblastic differentiation *in vitro* and to increase alkaline phosphatase activity, the expression of osteocalcin and bone sialoproteins (43, 179).

1.1.4.5 *Hormones*

Calcium bone metabolism and therefore bone remodeling is regulated by a complex system of different hormonal signals (parathyroid hormone (PTH) and calcitonin) that change their expression levels as a function of the plasmatic calcium level. The local administration of these hormones included into biomaterial structures in order to stimulate bone formation has lead to controversial results. The intermittent treatment with PTH enhances bone formation while the sustained exposure causes bone resorption (180). However, the administration of calcitonin is able to restrain osteoclast and enhance the proliferation and differentiation of osteoblasts (181).

1.1.4.6 *Antitumoral drugs*

Usually bone cancer is the result of the spread of cancer from other organs. Its common treatment is the surgical removal of the cancerous tissue followed by the insertion of an orthopedic filling (182). Different antitumoral drugs have been used in the development of bone chemotherapy after tumor removal. One of the most used for the treatment of osteosarcoma is cisplatin with good therapeutic results (49, 183, 184).

The incorporation of iron ions into bioactive glasses has been also proposed as an adequate strategy for the treatment of bone tumors as the systems are able to

combine hyperthermia with local drug deliver capacity. The high temperature achieved after applying magnetic stimulation of the implant causes the tumor cells death (185).

1.1.4.7 *Others*

Simvastatin, a common hypolipidemic drug is also of interest because it has been reported to stimulate bone formation by inducing the expression of BMP-2 in different animal models, and therefore enhances osteogenesis and also induces osteoblastic differentiation of mesenchymal stem cells (186-189). Jeon and coworkers (190) found that its intermittent release from devices promotes osteoblastic stimulation while continuous stimulation reduces cell viability.

The proposal of the use of lactoferrin, a protein present in the granules of neutrophils and in breast milk with osteogenic purposes, is based on its ability to modify proliferation and differentiation of osteoblasts, increasing the calcification of extracellular matrix (191).

Lidocaine, is a local anesthetic that could be used for decreasing pain after the surgery. Its short half-life in blood serum (1.5-2 h) makes the design of controlled release systems necessary when using this drug (192).

Different therapeutic ions have also been studied as possible candidates for local controlled release from implants. Controlled release of silver ions (Ag) from tricalcium phosphate particles has shown an adequate protection against bacterial re-infection (193). Selenium (Se) released from coated titanium has anticancer activity *in vitro* against various cancer cell lines (182). Whereas strontium (Sr) promotes bone regeneration and inhibits bone resorption enhancing bone volume and microstructure (194, 195).

Some polymers also have therapeutic interest such as poloxamines. These triblock synthetic polymers formed by poly(ethylene oxide)-poly(propylene oxide) with an ethylenediamine core not only are adequate for drug solubilization but also (196) have the ability to promote osteoblastic differentiation of mesenchymal stem cells *in vitro* (197, 198). Other polymers are able to release proline when they are degraded, promoting an anti-inflammatory effect (199).

In the development of new complex systems it is also possible to combine two or more drugs from different groups. Combinations of antibiotics and growth factors have been found useful for the osteointegration process by both enhancing osteoblasts function and increasing antibacterial activity (29) while the combination of dexamethasone and alendronate has been shown to be useful for the enhancement of osteoblastic differentiation both *in vitro* and *in vivo* (176).

1.1.5 **Mechanism for loading drugs into implant materials and release kinetics**

Therapeutic molecules could be incorporated into the material matrix or adsorbed on the external biomaterial surface. Figure 1.1.2 shows the different mechanisms for loading implant materials with drugs. Drugs could be included during the material synthesis process (physical entrapment loading) or on the surface, after the final biomaterial is obtained. In the latter case, the drug can be nonspecifically adsorbed on the material surface, covalently linked to the surface or attached by physical interactions to the internal or external surface of the matrices or polymeric gel networks.

Metallic implants are usually drug loaded through the formation of a polymeric or ceramic coating therefore drug loading strategy depends mainly on the coating technique selected. However, some of titanium surface chemical modifications enhance

the presence of functional groups useful in the covalent bonding of BMP-2 showing a controlled release (30, 46).

Unspecific adsorption is normally used in ceramic systems when there is no affinity between the drug and the ceramic. Ceramic systems can also be loaded by directly mixing them with drug powders (32) or by co-precipitation (64, 65) (e.g. physical entrapment loading of the drug in calcium cements).

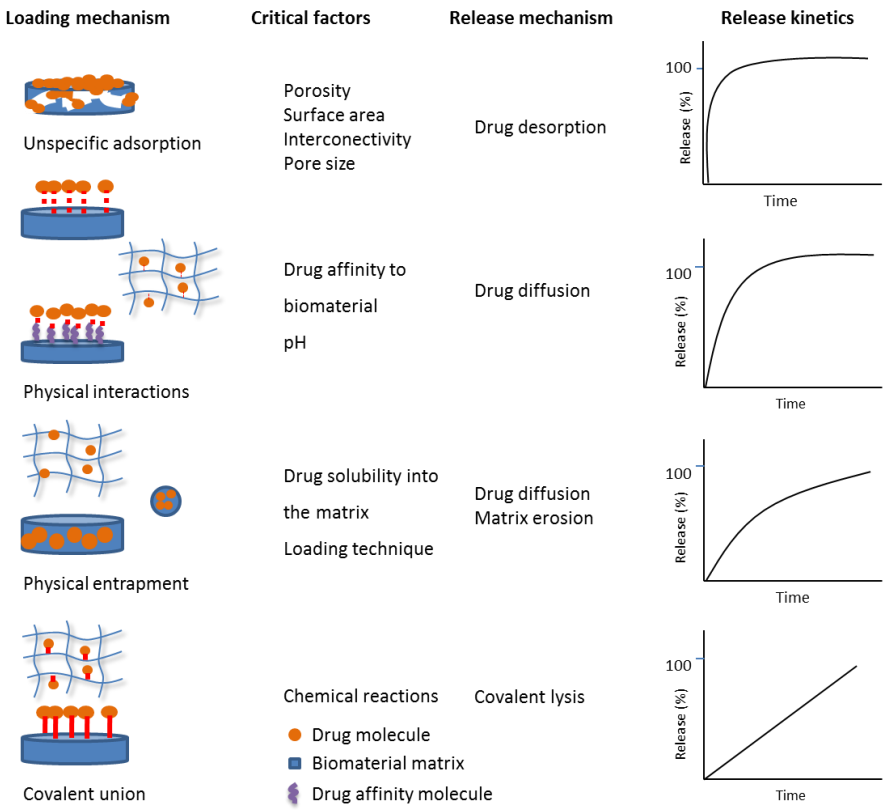

Figure 1.1.2 Drug loading techniques on biomaterials, critical factors and associated release mechanisms and profiles.

The functional groups of biodegradable ceramics confer great affinity for certain drugs such as bisphosphonates, obtaining the loading by physical interactions.

Polymeric implants are the most studied group. Those systems can be loaded with drugs using all techniques. Generally, those made with natural polymers make use of the physical interactions, while the synthetic polymers implants load drugs by physical entrapment (200).

1.1.5.1 *Unspecific adsorption*

The immersion of porous materials into high concentration drug solutions allows the drug loading by unspecific adsorption which are mainly dependent on structural parameters of the biomaterials like specific surface, total porosity and pore size distribution (201).

Once in contact with the dissolution medium, these loaded systems undergo the drug desorption. Release profiles are characterized by an initial burst effect caused by the fast dissolution of drug molecules adsorbed on the external structure followed by a release highly dependent on drug solubility and material pore structure (68, 139, 202). For similar total porosities, the presence of small size pores promotes drug sustained release due to the enhancement of the surface available for drug adsorption (77). On the contrary, big pores improve the water uptake and quick drug solubilization and release (203). The modulation of pore size distribution has been used as an approach to control and extend zolendronate drug release from mesoporous bioceramics (204). An alternative method could be applying vacuum during the loading process for obtaining slow drug release profiles. This procedure makes it possible for the loaded solution to reach the small size pores of the structure, hampering the wetting and the drug release (205). The incorporation of a polymeric coating as a complement of unspecific adsorption method has been used as a way to reduce the initial burst in antibiotic release profiles by creating a local drug diffusion barrier (206, 207).

When growth factors are loaded on polymeric electrospining fibers and scaffolds using unspecific adsorption methods fast and uncontrolled release profiles are achieved (99, 208). This makes the improvement of the loading techniques necessary in order to obtain a more controlled drug release.

1.1.5.2 *Physical interactions*

Physical interactions including hydrogen bonding, Van der Waals forces, electrostatic or hydrophobic interactions are widely used to load highly hydrophobic drugs in biomaterials and achieve desirable controlled release profiles (183, 209, 210).

With the exception of the hydrophobic interactions, all are highly dependent on pH conditioning for both drug loading and release processes. The modification of the pH medium is critical in protein loading and delivery and can be used as an approach to modulate protein release. At a pH lower than the protein isoelectric point, the molecule is positively charged whereas at pH higher than isoelectric point are negatively charged. This modification can increase or decrease the affinity of proteins for the biomaterial (211). If the proteins are loaded under hydrophobic conditions different pH values do not cause modification in protein release. The stabilization of the protein molecule under these conditions is unable to ionize at any pH (212).

The strong ionic interaction between bisphosphonates and divalent metal ions can be used as an approach for loading biomaterials. In the presence of those ions, bisphosphonates give a low soluble calcic salt precipitate that allows biomaterial surface loading by the formation of a drug coating and the consequent controlled release (42, 45). The electrostatic interactions between calcium phosphates and bisphosphonates are thought to be between two phosphate anions of calcium phosphate and two phosphonate groups of the bisphosphonate (183). These drugs have been shown to have high affinity to calcium phosphate and bioactive glasses obtaining good controlled

release systems (69, 176, 213, 214). The binding affinities of bisphosphonates for hydroxyapatite are different according to their molecular structure (from highest to lowest zolendronate > alendronate > ibandronate > risendronate > etidronate > clodronate) (215).

Also the ratio between calcium and phosphate, the surface charge of the ceramics and the surface hydrophobicity have an important influence on drug-ceramic affinity, being stronger for ceramics with the highest concentration of calcium (183, 215) and making the loading of hydrophobic carbon nanotubes by hydrophobic interactions possible (122).

It has been demonstrated that the therapeutic results of bisphosphonates are better when delivered locally, loaded on ceramic coatings, than after their systemic administration, finding an improved implant-bone contact (42, 216).

Acidic surfaces show greater capacity of bisphosphonate incorporation than the neutral surfaces, which allows the load with one higher dose of bisphosphonate in matrices that contain phosphorus due to interactions with the functional groups of the bisphosphonate (175).

The loading of growth factors as BMP-2 or VEGF in implants can also be performed through electrostatic interactions using heparin as mediator (217, 218). Heparin is a highly sulfated glycosaminoglycan able to bind many growth factors by electrostatic interactions between its negatively charged sulfate groups and the positively charged amino acid groups of proteins (219). The immobilization of the heparin molecule on biomaterial surface can be performed by different techniques like its binding to polymers by ionic interactions (219) or its chemical conjugation to polymeric systems (220) and demineralized bone matrices (221). The interaction of heparin with proteins not only enhances the drug content in the final material (17) with a controlled release

(217) but also stabilizes proteins, protecting them against proteolytic degradation and increasing their bioactivity (219).

Heparin can be also useful for loading other therapeutic molecules containing amine groups in their structure such as gentamicin. It has been shown that the combination of gentamicin and BMP-2 loaded using heparin immobilized on titanium surface, presents a suitable antibacterial activity and promotes pre-osteoblasts differentiation (29).

The mechanism for heparin immobilization has an important effect on drug release. When heparin is bound through ionic interactions, the biomaterial-heparin affinity plays a key role in the controlled release of the drug (219). On the contrary, when heparin is covalently linked to the biomaterial surface, it is the drug-heparin affinity, the drug diffusion and the system degradation which are the important variables in drug delivery (221). The drug concentration should not exceed the loading ability of the heparin, otherwise an inefficient loading of the implantable system is produced (37).

It is possible to synthesize therapeutic peptides including a mineral binding domain in their structure that allows their ionic interaction with calcium phosphates. Protein release from those loaded ceramics is highly influenced by the ceramic solubility that could be modified by changing the carbonate phase content (153). It has been shown that calcium phosphates have high affinity for some proteins (BMP-2, BSA) increasing the scaffold load capacity and being able to modulate their release (23, 55, 65). As an example, the high affinity of COO-, OH and NH_2 groups of BMP-2 and the negatively charged hydroxyapatite gives a strong interaction through water bridged hydrogen bonds that promotes the slow release of the protein (222, 223). Higher surface available for the interaction with proteins increases the loading ability (224). Those interactions could be also used for loading antibacterial peptides that simultaneously inhibit bacterial growth and enhance bone formation (225).

Additionally, bioactive glasses could interact with charged ampicillin (34), gentamicin (202) or vancomycin (226) obtaining systems with slow antibiotic release profiles. P-OH and Si-OH groups of bioactive glasses are able to generate hydrogen bonding with antibiotic hydroxil and amine groups. Those combinations would be sensitive to a pH that can be modulated to achieve the antibiotic controlled release (227, 228).

The increase of Si-OH groups of bioactive glasses raises the loading ability of proteins due to the presence of higher number of functional groups. This effect also depends on the molecular weight of the loaded protein. The higher molecular weight of protein, the lower its loading due to the need of larger available surface for the interaction with the scaffold (210). The inclusion of strontium into mesoporous bioactive glasses has been shown to be adequate in order to achieve a controlled release of dexamethasone (229).

Polymeric systems can also be loaded through physical interactions. Frequently, chemical modifications of natural polymers such as dextran have been carried out for increasing their affinity for BMP-2 (174). Another approach is to incorporate an additive to modulate the therapeutic molecule-polymer affinity. For example, the incorporation of keratose to collagen hydrogels increases growth factors affinity through ionic interactions giving final hydrogels with good controlled release properties during four weeks (230). On the contrary, the addition of chondroitin sulfate to collagen reduces its affinity for proteins by enhancing the polar groups of the hydrogels and the surface area, this modification allows a higher burst effect to be obtained that increases the osteoinductive activity *in vivo* possibly by the enhancement of chemotaxis (163).

The condroitin sulphate applied as a coating on PCL/β-TCP scaffolds has been also shown useful for promoting controlled release of BMP-2 for 15 days. Additionally, the amount of loaded protein can be controlled by the pH modification (161).

Chemical interactions also explain the different approaches of developing drug controlled release systems based on other polymers as gelatin or chitosan. Gentamicin interacts with gelatin through a Schiff reaction giving slow drug release profile particles. The drug loaded amount and the release mechanism (erosion, diffusion) can be determined by the selection of appropriated basic or acid gelatin (89, 191, 231).

The interactions between growth factors (TGF-β1) and chitosan allow the production of surface-loaded chitosan beads that release TGF-β1 at an adequate rate to promote osteoblastic differentiation (232).

Bone morphogenetic proteins could be incorporated into polyelectrolyte films by the pH modification (25, 161). In those systems drug release is determined by the charge, the temperature or the degradation of the polyelectrolyte multilayer (233).

1.1.5.3 *Physical entrapment*

Therapeutic molecules (antibiotics, growth factors and ions) can be physically entrapped into ceramics or polymeric systems during their synthesis or production process (234, 235). Homogeneous drug distribution is an important factor to be considered in the development of those systems in order to avoid an initial burst release. They generally achieve more prolonged release profiles than drug-adsorbed systems, the release controlled being mainly by diffusion and biomaterial erosion depending on the polymer degradation (2, 213).

For incorporating drugs into orthopedic cements, they can be physically mixed (181, 236) or dissolved (53) in one of the components of the cement system or in all of them. Both techniques have advantages and disadvantages. The addition of the drug in the solid phase allows more slow-release systems to be obtained, while incorporating the drug in the liquid phase gives rise to more homogeneous systems (170). The

incorporation of high amounts of drugs into these systems changes the properties of the final cement (237).

The extreme operation variables during cements production or their final characteristics (e.g. pH) can limit the utility of this loading procedure. As an example, the high temperature necessary for the polymerization process during PMMA cement production may accelerate thermo sensitive drug degradation (136). The pH of the cement is crucial to maintain the activity of therapeutic molecules degrading vancomycin at pH 9.5 (238). Finally, PMMA cements have a low porosity and an extremely slow degradation rate that limit the release of drugs physically entrapped into those materials (136).

In order to overcome these limitations, several polymers as carboximethycellulose (117) or ceramics as silica nanoparticles (142) can be mixed with PMMA cements. Those additives modify the porosity and/or the water uptake into the PMMA matrices enabling the dissolution and the release of the drug.

Drug release can be also improved by increasing the amount of drug into PMMA cements which promotes material fragility and its cracking (239) or through external stimuli like ultrasounds (240, 241).

An alternative to the PMMA is the use of calcium phosphate cements in which a hardening process takes place at room or body temperature. They have generally high intrinsic porosity that can even be improved by adding soluble organic additives (60, 242). It has been shown that calcium phosphate cements improve the therapeutic activity of certain proteins (53, 242) showing optimal release profiles for local release of antibiotics and anti-inflammatory drugs (243).

Techniques to incorporate therapeutic molecules into ceramics include its biomimetic coprecipitation forming a coating on metallic implants (35), the co-precipitation of

proteins and calcium phosphates (157, 162) and the physical mixture of drugs and ceramic powders (244). In order to modulate the drug release profile of the physical mixtures it is possible to add polymers or to compress them (146). All these techniques allow the production of biofunctional materials with better controlled drug release properties than the adsorption surface techniques.

The entrapment of drugs into polymeric network systems could be carried out using different technological approaches. The therapeutic molecule could be added to the water phase (171, 211, 245-249) of a polymer solution, mixed with the polymer powder (250, 251) or impregnated through supercritical fluids (93). The physical and rheological properties of the systems determine the drug release profile. The raw material composition (252), the molecular weight of polymers (129, 253, 254), the polymer concentration (60) and/or possible crosslinking conditions (255) are critical factors to be optimized for this type of implants.

In the last few decades, new pharmaceutical dosage forms as liposomes, microspheres and nanoparticles have extraordinarily developed, thus being possible to include them in the manufacture of bone implants to control drug release. They can be designed and optimized to obtain the desirable drug profile for each application (59, 100, 256-258).

PLGA microspheres and nanoparticles have been used for loading drugs in bone implants. The drug release from those particles is dependent on the PLGA hydrolysis and degradation (50, 102, 117, 223). The immobilization of microspheres or nanocapsules into calcium phosphates or PMMA cements, ceramics or polymeric systems cause a prolonged release of the loaded drugs (70, 117, 118, 169, 259-261). Moreover, the introduction of PLGA microspheres inside the cement minimized the burst release observed for PLGA microspheres alone and allows zero or first order drug release kinetics to be achieved (107, 117). Also, zero order kinetics can be

obtained by dexamethasone release including loaded PLGA nanoparticles on colloidal gels (262).

The combination of two types of nanocapsules of different properties has allowed to obtain BMP-2 and BMP-7 release system within a schedule program, achieving high degree of cell differentiation (169). More complex systems could be synthesize as the coating of microspheres with loaded nanospheres able to induce osteoblastic differentiation as well as the delivery of mesenchymal stem cells (104).

Microspheres can also be included in scaffolds by pressure sintering (263). It has been demonstrated that the formation of alternate layers with and without PTH microspheres lead to a system that promotes the pulse release of the hormone, controlled by erosion (180) and therefore improves osteoblasts activity.

Gelatin microspheres have also been used for local controlled release of gentamicin once included into calcium phosphate bone cements. The modification of the solubility of the cement by the addition of calcium sulphate has been shown to be useful in modulating release profiles (59).

The use of liposomes included into complex systems or attached to the external surface are adequate for the controlled release of vancomycin and dexamethasone (63, 259).

It is well known that nanoparticles can be internalized into the cellular cytoplasm adequate for intracellular dexamethasone and proteins delivery (32, 264).

1.1.5.4 *Chemical immobilization*

Chemical immobilization on bioactive glasses and hydrogels has been shown to be more adequate than physical interactions in order to avoid the burst release of BMP (9, 212).

The covalent union of peptides or proteins is also a common mechanism for loading drugs on polymeric materials. In these cases, the degradation of the covalent unions together with the diffusion through the polymeric system are the factors controlling drug release (9, 62, 265). Growth factors could be chemically modified or genetically engineered to contain functional groups such as thiols, acrylates or azides able to interact with different biomaterial surfaces (9).

This technique could also be used in order to achieve an adequate loading ability for allografts to simulate the osteoinduction of autologous bone by releasing osteoinductive peptides (266).

1.1.6. *In vitro* drug release studies

Drug solubility and therefore, *in vitro* drug dissolution results are influenced by an important number of factors as temperature, pH, medium polarity, dissolution interactions or medium ionic strength (150). An extensive review of the literature points out that there is a wide heterogeneity on the conditions of *in vitro* drug release studies from orthopedic implants.

Generally, media of pH 7.4 are used and trials are carried out at 37 °C to simulate physiological conditions. However, the other parameters of the process like the type of medium used, the volume of dissolution or stirring conditions are highly variable, making the interpretation of results and the comparison between different trials very difficult.

The most used dissolution medium is phosphate buffer saline (PBS) (25, 69, 164, 220). The medium selection significantly modifies the release kinetics obtained because it affects drug solubility. For example, the use of release medium with high salts concentration, could lead to the modification of drug release constant (267). The presence of ions in the solution changes the oriented structure of the water. The

interactions between ions and water cause ion-dipole electrostatic interactions and the formation of a hydration layer with different properties from free water. It has been shown that the use of cellular culture medium instead of phosphate buffer saline significantly reduces the drug release for BMP-2 due to its high ionic concentration and the presence of other molecules, such as glucose or amino acids (153).

Another dissolution medium, widely used, is the standard simulated body fluid (SBF). The ionic composition of the medium has been especially selected by Kokubo (22) as the most appropriate medium for evaluating the bioactivity of implant materials. It has been shown that the apatite layer induced when the material is immersed in physiological fluids hinders the diffusion of the drug, resulting in slowed released profiles (150). As it is presumed that this phenomenon takes place also *in vivo*, some authors (76, 268-270) have pointed out that release studies using SBF can be more appropriate to predict the actual behavior of loaded systems.

Temperature and pH are variables to be considered for testing release profiles from material implants, not only because of the possible effect on drug degradation, but also for their influence on the material properties especially when they are polymeric systems. Gelatin is sensitive to temperature, increasing drug release at high values (271). Different polymers could be ionized depending on the medium pH. Alginate, at pH higher than 5, has their mannuronic and glucuronic acid groups ionized, while carboxymethilcellulose needs a pH of 7.4 and chitosan a pH lower than 6. The ionization of polymers increases the matrix swelling, enhancing pore sizes and therefore drug release (89, 91, 250).

Loading drug amount can modify the release profile because of changes in drug gradient (72) and the possible changes in the biomaterial structure. When a large amount of drug is inside the pores, total porosity decreases, the access of medium is limited and therefore the release rate slows down (146). On the other hand, drug concentration

gradient is crucial in drug release process. This fact could be benefited by obtaining controlled release profiles. The use of fatty acid salts of gentamicin combined with gentamicin soluble salts are able to achieve an equilibrium between drug released and adsorbed on the ceramics surface, promoting a continuous release for up to 50 days (272). Assays should be carried out in sink conditions in order to avoid the back diffusion effect in drug elution (140). However, this condition accelerates drug release; it is expected *in vitro* that the drug clearance could be lower especially in poor irrigated tissues such as bone (258, 267). The amount of drug included into the biomaterial structure also modifies the biomaterial parameters. The use of dynamic release assays instead of static studies is an alternative to simulating the blood flow in bones. In those cases the concentration gradient acts as the driving force for drug release that seems to be faster compared to the results obtained in static condition tests (273).

Release profiles are extremely dependent on the method used to load the drug and the interactions established between the therapeutic molecule and the biomaterial (62). When the release from solid matrices is studied, especially implant materials loaded by an unspecific adsorption mechanism, a burst release effect is frequently observed (41). In those cases the porosity, pore size distribution, interconnectivity and tortuosity of the porous structure influence the drug release rate from the systems (73). High total porosity and pores larger than 100 μm have been described as critical factors for promoting osteoconduction in biomaterials (206). However, these characteristics favor the emergence of the undesirable burst effect. Modulation of porosity helps in the drug release control. The increase in mesoporosity enables a more prolonged drug release (2-50 nm) (49, 58) and pores smaller than 10 μm (micropores) allow the control of the release process (274). The effect of porosity can be modulated by the incorporation of highly water soluble ingredients to the matrices, for its immediate dissolution after contact with the dissolution medium and the formation of extra pores (275).

Internal and external surface area of the material also has an important effect on the drug release. The higher surface area values the stronger the contact with the dissolution medium, increasing drug release constant rate (240, 263) but also higher surface available to interact with drug molecules (163).

Drug included into polymeric systems are released following normally an initial burst (276) conditioned by hydration of the polymer, followed by a slow drug release by Fickian diffusion through the dissolution media or the hydrated gel and/or by the polymer erosion (18, 40, 277). The swelling degree and the degradation rate of the polymer are factors for controlling both loading and release of drugs and can be modulated by mixing polymers with different swelling degrees and degradation properties (40, 106). The combination of cellulosic polymers and ceramic systems has showed the usefulness of improving the controlled release of therapeutic molecules with different profiles depending on the loading strategy chosen. The homogeneous dispersion of drug, its concentration in the core of the device or forming a gradient allows the drug release during the whole process, during the initial stages or at the end of the polymer degradation (234).

The mechanism of diffusion from polymeric systems depends on the drug molecular size, drug solubility, hydrogel network structure and concentration gradient (34, 278). Generally, high molecular weight polymers slow down the release rate of therapeutic molecules while low molecular weight polymers cause higher burst effect (253, 254). Polymer concentration also determines the final network structure. High polymer concentrations hamper drug release by steric hindrance (60).

Polymer stability can be increased by controlling pH (101) or by chemical crosslinking (255) giving controlled release implant devices. As an example, functionalized dextrans have been used for the local delivery of BMP-2 with good *in vivo* results (279). It has

been described that some of these systems are able to release growth factors through cell-mediated polymer degradation mechanism (280).

Drug release profiles from polymeric or ceramic coatings (281) can be modulated by the thickness (282, 283) and the degradation properties of the coating (284, 285).

Natural filmogen polymers such as zein or chitosan are an attractive alternative to the controlled release of drugs from implants, being adequate for antitumorals, antibiotics and growth factors with kinetics dependent on drug solubility (40, 254, 286).

Additionally, some drug depending factors can be pointed out. The selection of high soluble (e.g. salts) or low soluble derivatives can be used as a technological approach to modulate the release profiles of some drugs, reducing the burst release or improving the dissolution process (192, 252, 287).

The inclusion of high concentrations of drugs could facilitate biomaterial degradation by system instability or due to the cellular chemotaxis affecting drug release profiles (111). When calcium phosphate cements are loaded, high amounts of drugs can modify their rheological properties and setting kinetics increasing the porosity of the final material and promoting fast release kinetics. The effect is strong for molecules that interact with calcium and phosphate ions (53, 243).

The inclusion of two proteins simultaneously into a hydrogel could affect the release of both proteins due to a competitive mechanism. As an example, the combination of SDF-1 (stromal cell-derived factor 1) and BMP-2 into a gelatin hydrogel increases the burst effect of SDF-1 (156).

1.1.6.1 *Drug release kinetic analysis*

Mathematical modeling of drug delivery and predictability of drug release from pharmaceutical formulations is a field of enormous importance that historically has attracted great attention (288).

Despite the conditions of the *in vitro* studies are really heterogeneous and not allowing easy comparisons between them, different authors have modeled the drug release behavior from implants, to make predictions about the therapeutic effect of the device (35), for comparing formulations (64) or for improving the understanding of the drug release mechanism (274).

The kinetics most commonly used to evaluate the release of drugs from implants are as follows (289, 290):

Zero order kinetics: $F = k_o t$, where F is the fraction of released drug at time t, and k_o is an apparent release rate. The release rate is independent on the drug concentration (64, 274). BMP-2 and insulin–like growth factor have been delivered at zero order kinetics or pseudo-zero order kinetics from crosslinked gelatin coating systems (168). Similarly, the release of ibuprofen from asymmetric coating titanium allows dependence on osmotic pressure (89). The release of other antibiotics and corticoids electrodeposited onto pure Ti dependent on-demand electrical stimulation can also follow zero order kinetic profiles (291).

First order kinetics: $\ln(1-F) = -k_1 t$, where F represents the fraction of drug released at time t, and k_1 is the first-order release rate constant. The release rate is dependent on drug concentration, drug solubility and diffusivity (35, 274).

Higuchi model: $F = k_H t^{1/2}$, where F represents the fraction of drug released at time t, and k_H is the Higuchi dissolution constant. This equation perfectly describes release

processes where drugs are dispersed in monolithic systems with no changes during the release process (constant porosity, no swelling…) and release is purely diffusion controlled with constant diffusion coefficients. This model has been shown to be adequate especially for the initial stages of drug delivery from calcium phosphate ceramics and calcium phosphate cements. After that, drug release is also modulated by matrix degradation (53, 64, 236, 243, 281).

Hixon-Crowell model: $Mo^{1/3} - Mt^{1/3} = k_s t$, where M_o is the initial amount of drug in the biomaterial, Mt is the remaining amount of the drug in the composite at time t, and k_S is the constant incorporating the surface volume relation. Dividing the above equation by $M_o^{1/3}$ and simplifying gives $(1-F)^{1/3} = 1 - k_E t$, $F = 1 - (M_t/M_o)$, where F represents the drug dissolved fraction at time t, and k_E is the release rate constant. This model describes systems where the drug release is dependent on the system erosion (64).

Korsmeyer-Peppas model: $F = k_P t^n$, where F represents the drug fraction released at time t, k_P is the release rate constant and n is the diffusional exponent which indicates the drug release mechanism n = 0.45 Fickian diffusion, 0.45 < n < 0.89 anomalous diffusion, n = 0.89 case II transport, n > 0.89 supercase II transport or typical zero-order release (57, 64). This model has been used to explain antibiotics release mechanisms from titanium coatings of calcium alginate and gelatin (51). The use of this model is also adequate for systems whose release profiles are controlled by various factors especially hydrophilic polymeric systems in where diffusion, dissolution and swelling are key parameters (57, 98, 250).

Weibull model: $F= M_o [1-e^{-(t-T)b/a}]$ where F represents the amount of drug dissolved as a function of time t. M_o is the total amount of drug being released, the release profiles are characterized by the relationship with the parameter shape that define the transport mechanism (61). This model, typically used for fractal system characterization, has been successfully applied for characterize drug dissolution from

mesoporous composite fibers (202). This model has also been found useful in the analysis of release kinetics from calcium phosphate bone cements with interaction between drug and cement component. In these cases different parameters modulate drug release as drug solubility, interaction between drug and cement composition and the precipitation of bone cement components (150).

The suitability of the therapeutic molecule release profile may extremely condition the therapeutic success of the implant. Different authors have analyzed these effects in order to obtain the adequate release profile for the success of growth factor treatments in stimulating an osteogenic response (168).

This field can be expected to become an integral part of implant devices development. The wide variety of materials available makes it unlikely that there will be one general theory applicable to any type of implant. It is much more likely that there will be a broad spectrum of diverse mathematical models, applicable to specific types of devices differing in composition, geometry and drug load. *In silico* prediction and optimization should help in accuracy and easiness of application of drug loaded bone implants.

1.1.7 **Translation to the human situation**

In vitro studies allow drug release profiles with good mathematical fitting to be obtained. However, results are particularly difficult to be extrapolated to the *in vivo* situation (286). If *in vitro-in vivo* correlations are always difficult for any administration route, these cases are even more problematic as the physiological environment is variable and dependent on multiple factors. Different authors have described high levels of antibiotic into the bone tissue after implantation of loaded materials despite the release kinetics *in vivo* were markedly slower than the one obtained *in vitro* during the release studies in PBS (149).

Several animal models (rats, mice, sheeps, rabbits, dogs, pigs…) have been used for the *in vivo* evaluation of drug loaded implanted materials (50, 70, 130, 149, 155, 279), showing that their therapeutic effect is highly dependent on the hematoma size, location and size of injury (292). All these parameters modify the physiological environment and therefore, the drug release (292).

A key factor in the elucidation of the *in vivo* results when studies are carried out using implants loaded with bone regeneration factors is to distinguish between the effect of the therapeutic molecule and the intrinsic bone regeneration characteristics of the animal. Adequate controls are needed. In some studies, not the BMP activity but the regeneration ability of the bone itself is responsible for the good therapeutic results (292).

1.1.8 **Future perspectives**

Successful bone regeneration requires the combination of many events, cells that undergo differentiation to form osteoblasts, biological factors that control growth and cell differentiation and cellular attachment, migration and proliferation (47). To help in this natural process and increasing therapeutic success, biomaterials play an important role. They must be properly tailored to obtain the correct properties and they can be loaded with growth factors to promote bone healing, antibiotics to reduce infections, analgesics and anti-inflammatories to reduce pain and recovery time or antitumoral drugs to avoid metastasis. They can also be used for gene-therapy purposes by incorporating DNA plasmids and small-interfering RNA. The sustained delivery of pDNA and siRNA from mesoporous silica nanoparticles (MSNPs) has been shown to increase the transfection levels of these molecules. All these applications need optimization and well organized strategies for the efficient delivery of drugs at target sites.

The delivery of cells with therapeutic activity is the next step in the development of biofunctional materials. It has been shown that the use of autologous bone marrow mononuclear cells and bone marrow mesenchymal stem cells increase angiogenesis and bone regeneration by the sustained release of bFGF (293, 294). Additionally, the combination of osteoblasts and BMP-2 has been found to stimulate alkaline phosphatase activity (295) and human bone marrow mesenchymal stem cells together with VEGF have been useful in the enhancement of the bone regenerative mechanism (296).

The bone drug delivery systems are considered combined (orthopedic materials + drug) systems by the FDA which requires a longer registration process than for traditional orthopedic implants hampering their clinical use (297).

The development of new local delivery systems for bone regeneration and/or the optimization of the already developed ones need expertise from both, biomaterial engineering and pharmaceutical technology fields which have been traditionally at a distance (41). Multidisciplinary works linking bone substitute production and the "know how" of pharmaceutical companies are crucial to facilitate the clinical use of these new materials.

1.1.9 **References**

1. Mezquita Pla C, Mezquita Pla J, Mezquita Mas B, Mezquita Mas P. Fisiología médica: del razonamiento fisiológico al razonamiento clínico. Mezquita Pla C, editor. Madrid: Panamericana; 2011.

2. Porter JR, Ruckh TT, Popat KC. Bone tissue engineering: A review in bone biomimetics and drug delivery strategies. Biotechnol Prog. 2009;25(6):1539-60.

3. Blitterswijk C, Thomsen P, Lindahl A, Hubbell JA, Williams D, Cancedda R, et al. Tissue engineering. 1st ed. Blitterswijk C, editor. London: Academic Press: Elsevier; 2008.

4. David IP. Orthopedic principles-A Resident´s guide. 1st ed. Heidelberg: Springer Berlin; 2005.

5. Barrere F, Mahmood TA, de Groot K, van Blitterswijk CA. Advanced biomaterials for skeletal tissue regeneration: Instructive and smart functions. Mater Sci Eng, R. 2008;R59(1-6):38-71.

6. Kugimiya F, Kawaguchi H, Kamekura S, Chikuda H, Ohba S, Yano F, et al. Involvement of endogenous bone morphogenetic protein (BMP) 2 and BMP6 in bone formation. J Biol Chem. 2005;280(42):35704-12.

7. Schindeler A, McDonald MM, Bokko P, Little DG. Bone remodeling during fracture repair: The cellular picture. Semin Cell Dev Biol. 2008;19(5):459-66.

8. Mehta M, Schmidt-Bleek K, Duda GN, Mooney DJ. Biomaterial delivery of morphogens to mimic the natural healing cascade in bone. Adv Drug Delivery Rev. 2012;64(12):1257-76.

9. Lienemann PS, Lutolf MP, Ehrbar M. Biomimetic hydrogels for controlled biomolecule delivery to augment bone regeneration. Adv Drug Delivery Rev. 2012;64(12):1078-89.

10. Kronenberg HM. Developmental regulation of the growth plate. Nature (London, UK). 2003;423(6937):332-6.

11. Cui FZ, Zhang Y, Wen HB, Zhu XD. Microstructural evolution in external callus of human long bone. Mater Sci Eng, C. 2000;C11(1):27-33.

12. Sopyan I, Mel M, Ramesh S, Khalid KA. Porous hydroxyapatite for artificial bone applications. Sci Technol Adv Mater. 2007;8(1-2):116-23.

13. Nie H, Soh BW, Fu Y, Wang C. Three-dimensional fibrous PLGA/HAp composite scaffold for BMP-2 delivery. Biotechnol Bioeng. 2007;99(1):223-34.

14. Willie BM, Petersen A, Schmidt-Bleek K, Cipitria A, Mehta M, Strube P, et al. Designing biomimetic scaffolds for bone regeneration: Why aim for a copy of mature tissue properties if nature uses a different approach? Soft Matter. 2010;6(20):4976-87.

15. Park J, Lakes RS. Biomaterials an introduction. 3er ed. Park J and Lakes RS, editors. New York: Springer; 2007.

16. Chandra P. Sharma. Biointegration of medical implant materials. 1st ed. Chandra P. Sharma, editor. Cambridge: Woodhead Publishing Limited; 2010.

17. Teixeira S, Yang L, Dijkstra PJ, Ferraz MP, Monteiro FJ. Heparinized hydroxyapatite/collagen three-dimensional scaffolds for tissue engineering. J Mater Sci: Mater Med. 2010;21(8):2385-92.

18. Yoon H, Kim G. A three-dimensional polycaprolactone scaffold combined with a drug delivery system consisting of electrospun nanofibers. J Pharm Sci. 2011;100(2):424-30.

19. Reves BT, Bumgardner JD, Cole JA, Yang Y, Haggard WO. Lyophilization to improve drug delivery for chitosan-calcium phosphate bone scaffold construct: A preliminary investigation. J Biomed Mater Res, Part B. 2009;90B(1):1-10.

20. Aoki K, Usui Y, Narita N, Ogiwara N, Iashigaki N, Nakamura K, et al. A thin carbon-fiber web as a scaffold for bone-tissue regeneration. Small. 2009;5(13):1540-6.

21. Khan W, Muthupandian S, Farah S, Kumar N, Domb AJ. Biodegradable polymers derived from amino acids. Macromol Biosci. 2011;11(12):1625-36.

22. Kokubo Tadashi. Bioceramics and their clinical applications. 1st ed. Kokubo Tadashi, editor. Cambridge: Woodhead Publiching Limited and CRC Press LLC; 2008.

23. Cushnie EK, Khan YM, Laurencin CT. Tissue-engineered matrices as functional delivery systems: Adsorption and release of bioactive proteins from degradable composite scaffolds. J Biomed Mater Res, Part A. 2010;94A(2):568-75.

24. Bessa PC, Casal M, Reis RL. Bone morphogenetic proteins in tissue engineering: The road from laboratory to clinic, part II (BMP delivery). J Tissue Eng Regener Med. 2008;2(2-3):81-96.

25. Shah NJ, MacDonald ML, Beben YM, Padera RF, Samuel RE, Hammond PT. Tunable dual growth factor delivery from polyelectrolyte multilayer films. Biomaterials. 2011;32(26):6183-93.

26. Ji W, Wang H, van den Beucken JJJP, Yang F, Walboomers XF, Leeuwenburgh S, et al. Local delivery of small and large biomolecules in craniomaxillofacial bone. Adv Drug Delivery Rev. 2012;64(12):1152-64.

27. Ratner B. Biomaterials science: an introduction to materials in medicine. 2nd ed. Ratner B, editor. Amsterdam: Elsevier Academic Press; 2004.

28. Swanson TE, Cheng X, Friedrich C. Development of chitosan-vancomycin antimicrobial coatings on titanium implants. J Biomed Mater Res, Part A. 2011;97A(2):167-76.

29. Lee D, Yun Y, Park K, Kim SE. Gentamicin and bone morphogenic protein-2 (BMP-2)-delivering heparinized-titanium implant with enhanced antibacterial activity and osteointegration. Bone. 2012;50(4):974-82.

30. Jonge LT, Leeuwenburgh SCG, Wolke JGC, Jansen JA. Organic-inorganic surface modifications for titanium implant surfaces. Pharm Res. 2008;25(10):2357-69.

31. Clark PA, Moioli EK, Sumner DR, Mao JJ. Porous implants as drug delivery vehicles to augment host tissue integration. Faseb J. 2008;22(6):1684,1693, 10.1096/fj.07-094789.

32. Bose S, Tarafder S. Calcium phosphate ceramic systems in growth factor and drug delivery for bone tissue engineering: A review. Acta Biomater. 2012;8(4):1401-21.

33. Guelcher SA, Hollinger JO. An introduction to biomaterials. Guelcher SA and Hollinger JO, editors. Florida: CRC-Taylor & Francis; 2006.

34. Patel KD, El-Fiqi A, Lee H, Singh RK, Kim D, Lee H, et al. Chitosan-nanobioactive glass electrophoretic coatings with bone regenerative and drug delivering potential. J Mater Chem. 2012;22(47):24945-56.

35. Yao C, Webster TJ. Prolonged antibiotic delivery from anodized nanotubular titanium using a co-precipitation drug loading method. J Biomed Mater Res, Part B. 2009;91B(2):587-95.

36. Xia W, Grandfield K, Hoess A, Ballo A, Cai Y, Engqvist H. Mesoporous titanium dioxide coating for metallic implants. J Biomed Mater Res, Part B. 2012;100B(1):82-93.

37. Wolf-Brandstetter C, Lode A, Hanke T, Scharnweber D, Worch H. Influence of modified extracellular matrices on Ti6AL4V implants on binding and release of VEGF. J Biomed Mater Res, Part A. 2006;79A(4):882-94.

38. Cheng S, Wei D, Zhou Y. Mechanical and corrosion resistance of hydrophilic sphene/titania composite coatings on titanium and deposition and release of cefazolin sodium/chitosan films. Appl Surf Sci. 2011;257(7):2657-64.

39. Strobel C, Bormann N, Kadow-Romacker A, Schmidmaier G, Wildemann B. Sequential release kinetics of two (gentamicin and BMP-2) or three (gentamicin, IGF-I and BMP-2) substances from a one-component polymeric coating on implants. J Controlled Release. 2011;156(1):37-45.

40. Abarrategi A, Civantos A, Ramos V, Sanz Casado JV, Lopez-Lacomba JL. Chitosan film as rhBMP2 carrier: Delivery properties for bone tissue application. Biomacromolecules. 2008;9(2):711-8.

41. Brohede U, Forsgren J, Roos S, Mihranyan A, Engqvist H, Stromme M. Multifunctional implant coatings providing possibilities for fast antibiotics loading with subsequent slow release. J Mater Sci: Mater Med. 2009;20(9):1859-67.

42. Peter B, Gauthier O, Laib S, Bujoli B, Guicheux J, Janvier P, et al. Local delivery of bisphosphonate from coated orthopedic implants increases implants mechanical stability in osteoporotic rats. J Biomed Mater Res, Part A. 2006;76A(1):133-43.

43. Son JS, Choi Y, Park E, Kwon T, Kim K, Lee K. Drug delivery from hydroxyapatite-coated titanium surfaces using biodegradable particle carriers. J Biomed Mater Res, Part B. 2013;101B(2):247-57.

44. Ren W, Zhang R, Hawkins M, Shi T, Markel DC. Efficacy of periprosthetic erythromycin delivery for wear debris-induced inflammation and osteolysis. Inflammation Res. 2010;59(12):1091-7.

45. Duan K, Fan Y, Wang R. Electrolytic deposition of calcium etidronate drug coating on titanium substrate. J Biomed Mater Res, Part B. 2005;72B(1):43-51.

46. Bae I, Yun K, Kim H, Jeong B, Lim H, Park S, et al. Anodic oxidized nanotubular titanium implants enhance bone morphogenetic protein-2 delivery. J Biomed Mater Res, Part B. 2010;93B(2):484-91.

47. Lee S, Shin H. Matrixes and scaffolds for delivery of bioactive molecules in bone and cartilage tissue engineering. Adv Drug Delivery Rev. 2007;59(4-5):339-59.

48. Boccaccini AR, Gough Julie E. Tissue engineering using ceramics and polymers. 1st ed. Boccaccini AR and Gough Julie E., editors. Cambridge: Woodhead Publishing Limited and CRC Press LLC; 2007.

49. Arcos D, Vallet-Regi M. Bioceramics for drug delivery. Acta Mater. 2013;61(3):890-911.

50. Hernandez A, Sanchez E, Soriano I, Reyes R, Delgado A, Evora C. Material-related effects of BMP-2 delivery systems on bone regeneration. Acta Biomater. 2012;8(2):781-91.

51. Xiao J, Zhu Y, Liu Y, Zeng Y, Xu F. An asymmetric coating composed of gelatin and hydroxyapatite for the delivery of water insoluble drug. J Mater Sci: Mater Med. 2009;20(4):889-96.

52. Dorozhkin SV. Bioceramics of calcium orthophosphates. Biomaterials. 2010;31(7):1465-85.

53. Ginebra M, Canal C, Espanol M, Pastorino D, Montufar EB. Calcium phosphate cements as drug delivery materials. Adv Drug Delivery Rev. 2012;64(12):1090-110.

54. Rojbani H, Nyan M, Ohya K, Kasugai S. Evaluation of the osteoconductivity of α-tricalcium phosphate, β-tricalcium phosphate, and hydroxyapatite combined with or without simvastatin in rat calvarial defect. J Biomed Mater Res, Part A. 2011;98A(4):488-98.

55. Kim J, Jeong I, Lee K, Jung U, Kim C, Choi S, et al. Volumetric bone regenerative efficacy of biphasic calcium phosphate-collagen composite block loaded with rhBMP-2 in vertical bone augmentation model of a rabbit calvarium. J Biomed Mater Res, Part A. 2012;100A(12):3304-13.

56. Dorozhkin SV. Biphasic, triphasic and multiphasic calcium orthophosphates. Acta Biomater. 2012;8(3):963-77.

57. Cabanas MV, Pena J, Roman J, Vallet-Regi M. Tailoring vancomycin release from β-TCP/agarose scaffolds. Eur J Pharm Sci. 2009;37(3-4):249-56.

58. Vallet-Regi M. Bone repair and regeneration: Possibilities. Materialwiss Werkstofftech. 2006;37(6):478-84.

59. Cai S, Zhai Y, Xu G, Lu S, Zhou W, Ye X. Preparation and properties of calcium phosphate cements incorporated gelatin microspheres and calcium sulfate dihydrate as controlled local drug delivery system. J Mater Sci: Mater Med. 2011;22(11):2487-96.

60. Weir MD, Xu HHK. High-strength, *in situ*-setting calcium phosphate composite with protein release. J Biomed Mater Res, Part A. 2008;85A(2):388-96.

61. Ignjatovic NL, Ninkov P, Sabetrasekh R, Uskokovic DP. A novel nano drug delivery system based on tigecycline-loaded calcium phosphate coated with poly-dl-lactide-co-glycolide. J Mater Sci: Mater Med. 2010;21(1):231-9.

62. Liu H, Webster TJ. Ceramic/polymer nanocomposites with tunable drug delivery capability at specific disease sites. J Biomed Mater Res, Part A. 2010;93A(3):1180-92.

63. Ma T, Shang B, Tang H, Zhou T, Xu G, Li H, et al. Nano-hydroxyapatite/chitosan/konjac glucomannan scaffolds loaded with cationic liposomal vancomycin: Preparation, *in vitro* release and activity against *staphylococcus aureus* biofilms. J Biomater Sci, Polym Ed. 2011;22(12):1669-81.

64. Nayak AK, Laha B, Sen KK. Development of hydroxyapatite-ciprofloxacin bone-implants using quality by design. Acta Pharm (Zagreb, Croatia). 2011;61(1):25-36.

65. Wu C, Zhang Y, Ke X, Xie Y, Zhu H, Crawford R, et al. Bioactive mesopore-glass microspheres with controllable protein-delivery properties by biomimetic surface modification. J Biomed Mater Res, Part A. 2010;95A(2):476-85.

66. Liu Y, Wu G, de Groot K. Biomimetic coatings for bone tissue engineering of critical-sized defects. J R Soc Interface. 2010;7(Suppl. 5):S631-47.

67. Kim C, Kim J, Kim J, Choi S, Chai J, Kim C, et al. Ectopic bone formation associated with recombinant human bone morphogenetic proteins-2 using absorbable collagen sponge and beta tricalcium phosphate as carriers. Biomaterials. 2005;26(15):2501-7.

68. Chai F, Hornez J-, Blanchemain N, Neut C, Descamps M, Hildebrand HF. Antibacterial activation of hydroxyapatite (HA) with controlled porosity by different antibiotics. Biomol Eng. 2007;24(5):510-4.

69. Capra P, Dorati R, Colonna C, Bruni G, Pavanetto F, Genta I, et al. A preliminary study on the morphological and release properties of hydroxyapatite-alendronate composite materials. J Microencapsulation. 2011;28(5):395-405.

70. Son JS, Appleford M, Ong JL, Wenke JC, Kim JM, Choi SH, et al. Porous hydroxyapatite scaffold with three-dimensional localized drug delivery system using biodegradable microspheres. J Controlled Release. 2011;153(2):133-40.

71. McCanless JD, Jennings LK, Cole JA, Bumgardner JD, Haggard WO. Induction of the early inflammatory-mediated cellular responses of fracture healing *in vitro* using platelet releasate-containing alginate/$CaPO_4$ biomaterials for early osteoarthritis prevention. J Biomed Mater Res, Part A. 2012;100A(5):1107-14.

72. Kim H, Knowles JC, Kim H. Development of hydroxyapatite bone scaffold for controlled drug release via poly(ε-caprolactone) and hydroxyapatite hybrid coatings. J Biomed Mater Res, Part B. 2004;70B(2):240-9.

73. Arcos D, Lopez-Noriega A, Ruiz-Hernandez E, Terasaki O, Vallet-Regi M. Ordered mesoporous microspheres for bone grafting and drug delivery. Chem Mater. 2009;21(6):1000-9.

74. Haidar ZS, Hamdy RC, Tabrizian M. Delivery of recombinant bone morphogenetic proteins for bone regeneration and repair. part B: Delivery systems for BMPs in orthopaedic and craniofacial tissue engineering. Biotechnol Lett. 2009;31(12):1825-35.

75. Vitale-Brovarone C, Baino F, Miola M, Mortera R, Onida B, Verne E. Glass-ceramic scaffolds containing silica mesophases for bone grafting and drug delivery. J Mater Sci: Mater Med. 2009;20(3):809-20.

76. Liu X, Xie Z, Zhang C, Pan H, Rahaman MN, Zhang X, et al. Bioactive borate glass scaffolds: *In vitro* and *in vivo* evaluation for use as a drug delivery system in the treatment of bone infection. J Mater Sci: Mater Med. 2010;21(2):575-82.

77. Wang H, Gao X, Wang Y, Tang J, Sun C, Deng X, et al. Bio-templated synthesis of mesoporous bioactive glass with a hierarchical pore structure. Mater Lett. 2012;76:237-9.

78. Colilla M, Manzano M, Vallet-Regi M. Recent advances in ceramic implants as drug delivery systems for biomedical applications. Int J Nanomed. 2008;3(4):403-14.

79. Wu C, Chang J, Xiao Y. Mesoporous bioactive glasses as drug delivery and bone tissue regeneration platforms. Ther Delivery. 2011;2(9):1189-98.

80. Vallet-Regi M, Balas F, Arcos D. Mesoporous materials for drug delivery. Angew Chem, Int Ed. 2007;46(40):7548-58.

81. Vallet-Regi M. Ordered mesoporous materials in the context of drug delivery systems and bone tissue engineering. Chem-Eur J. 2006;12(23):5934-43.

82. Chevalier J, Gremillard L. Ceramics for medical applications: A picture for the next 20 years. J Eur Ceram Soc. 2009;29(7):1245-55.

83. Singh M, Salem JA. Mechanical properties and microstructure of biomorphic silicon carbide ceramics fabricated from wood precursors. J Eur Ceram Soc. 2002;22(14-15):2709-17.

84. Lusquinos F, Pou J, Quintero F, Perez-Amor M. Laser cladding of SiC/Si composite coating on si-SiC ceramic substrates. Surf Coat Technol. 2008;202(9):1588-93.

85. Varela-Feria FM, Martinez-Fernandez J, de Arellano-Lopez AR, Singh M. Low density biomorphic silicon carbide: Microstructure and mechanical properties. J Eur Ceram Soc. 2002;22(14-15):2719-25.

86. Gonzalez P, Borrajo JP, Serra J, Chiussi S, Leon B, Martinez-Fernandez J, et al. A new generation of bio-derived ceramic materials for medical applications. J Biomed Mater Res, Part A. 2009;88A(3):807-13.

87. Lopez-Alvarez M, de Carlos A, Gonzalez P, Serra J, Leon B. Cytocompatibility of bio-inspired silicon carbide ceramics. J Biomed Mater Res, Part B. 2010;95B(1):177-83.

88. Will J, Hoppe A, Mueller FA, Raya CT, Fernandez JM, Greil P. Bioactivation of biomorphous silicon carbide bone implants. Acta Biomater. 2010;6(12):4488-94.

89. Xiao J, Zhu Y, Liu Y, Zeng Y, Xu F. A composite coating of calcium alginate and gelatin particles on Ti6Al4V implant for the delivery of water soluble drug. J Biomed Mater Res, Part B. 2009;89B(2):543-50.

90. Ma PX, Elisseeff J. Scaffolding in tissue engineering. 1st ed. Ma PX and Elisseeff J, editors. Florida: CRC Press; 2006.

91. Prabaharan M, Rodriguez-Perez MA, de Saja JA, Mano JF. Preparation and characterization of poly(L-lactic acid)-chitosan hybrid scaffolds with drug release capability. J Biomed Mater Res, Part B. 2007;81B(2):427-34.

92. Shi Z, Neoh KG, Kang ET, Wang W. Antibacterial and mechanical properties of bone cement impregnated with chitosan nanoparticles. Biomaterials. 2006;27(11):2440-9.

93. Duarte ARC, Mano JF, Reis RL. Preparation of chitosan scaffolds loaded with dexamethasone for tissue engineering applications using supercritical fluid technology. Eur Polym J. 2009;45(1):141-8.

94. Anitua E, Sanchez M, Orive G. Potential of endogenous regenerative technology for *in situ* regenerative medicine. Adv Drug Delivery Rev. 2010;62(7-8):741-52.

95. Prestwich GD. Hyaluronic acid-based clinical biomaterials derived for cell and molecule delivery in regenerative medicine. J Controlled Release. 2011;155(2):193-9.

96. Wu C, Zhang Y, Zhu Y, Friis T, Xiao Y. Structure-property relationships of silk-modified mesoporous bioglass scaffolds. Biomaterials. 2010;31(13):3429-38.

97. Shi Q, Li Y, Sun J, Zhang H, Chen L, Chen B, et al. The osteogenesis of bacterial cellulose scaffold loaded with bone morphogenetic protein-2. Biomaterials. 2012;33(28):6644-9.

98. Siepmann J, Peppas NA. Modeling of drug release from delivery systems based on hydroxypropyl methylcellulose (HPMC). Adv Drug Delivery Rev. 2001;48(2-3):139-57.

99. Niu X, Feng Q, Wang M, Guo X, Zheng Q. Porous nano-HA/collagen/PLLA scaffold containing chitosan microspheres for controlled delivery of synthetic peptide derived from BMP-2. J Controlled Release. 2009;134(2):111-7.

100. Fan D, De Rosa E, Murphy MB, Peng Y, Smid CA, Chiappini C, et al. Mesoporous silicon-PLGA composite microspheres for the double controlled release of biomolecules for orthopedic tissue engineering. Adv Funct Mater. 2012;22(2):282-93.

101. Liu G, Wu C, Fan W, Miao X, Sin D, Crawford R, et al. The effects of bioactive akermanite on physiochemical, drug-delivery, and biological properties of poly(lactide-co-glycolide) beads. J Biomed Mater Res, Part B. 2011;96B(2):360-8.

102. Habraken WJEM, Wolke JGC, Mikos AG, Jansen JA. PLGA microsphere/calcium phosphate cement composites for tissue engineering: *In vitro* release and degradation characteristics. J Biomater Sci, Polym Ed. 2008;19(9):1171-88.

103. Bodde EWH, Boerman OC, Russel FGM, Mikos AG, Spauwen PHM, Jansen JA. The kinetic and biological activity of different loaded rhBMP-2 calcium phosphate cement implants in rats. J Biomed Mater Res, Part A. 2008;87A(3):780-91.

104. Park JS, Yang HN, Woo DG, Jeon SY, Park K. The promotion of chondrogenesis, osteogenesis, and adipogenesis of human mesenchymal stem cells by multiple growth factors incorporated into nanosphere-coated microspheres. Biomaterials. 2010;32(1):28-38.

105. Luginbuehl V, Wenk E, Koch A, Gander B, Merkle HP, Meinel L. Insulin-like growth factor I-releasing alginate-tricalciumphosphate composites for bone regeneration. Pharm Res. 2005;22(6):940-50.

106. Samdancioglu S, Calis S, Sumnu M, Atilla Hincal A. Formulation and *in vitro* evaluation of bisphosphonate loaded microspheres for implantation in osteolysis. Drug Dev Ind Pharm. 2006;32(4):473-81.

107. Naraharisetti PK, Lee HCG, Fu Y, Lee D, Wang C. *In vitro* and *in vivo* release of gentamicin from biodegradable discs. J Biomed Mater Res, Part B. 2006;77B(2):329-37.

108. Hedberg EL, Kroese-Deutman HC, Shih CK, Crowther RS, Carney DH, Mikos AG, et al. *In vivo* degradation of porous poly(propylene fumarate)/poly(-lactic-co-glycolic acid) composite scaffolds. Biomaterials. 2005;26(22):4616-23.

109. Park JK, Shim J, Kang KS, Yeom J, Jung HS, Kim JY, et al. Solid free-form fabrication of tissue-engineering scaffolds with a poly(lactic-co-glycolic acid) grafted hyaluronic acid conjugate encapsulating an intact bone morphogenetic protein-2/Poly(ethylene glycol) complex. Adv Funct Mater. 2011;21(15):2906-12.

110. Kato M, Namikawa T, Terai H, Hoshino M, Miyamoto S, Takaoka K. Ectopic bone formation in mice associated with a lactic acid/dioxanone/ethylene glycol copolymer-tricalcium phosphate composite with added recombinant human bone morphogenetic protein-2. Biomaterials. 2006;27(21):3927-33.

111. Kato M, Toyoda H, Namikawa T, Hoshino M, Terai H, Miyamoto S, et al. Optimized use of a biodegradable polymer as a carrier material for the local delivery of recombinant human bone morphogenetic protein-2 (rhBMP-2). Biomaterials. 2006;27(9):2035-41.

112. Saito N, Murakami N, Takahashi J, Horiuchi H, Ota H, Kato H, et al. Synthetic biodegradable polymers as drug delivery systems for bone morphogenetic proteins. Adv Drug Delivery Rev. 2005;57(7):1037-48.

113. Murakami N, Saito N, Takahashi J, Ota H, Horiuchi H, Nawata M, et al. Repair of a proximal femoral bone defect in dogs using a porous surfaced prosthesis in combination with recombinant BMP-2 and a synthetic polymer carrier. Biomaterials. 2003;24(13):2153-9.

114. Geurts J, Chris Arts JJ, Walenkamp GHIM. Bone graft substitutes in active or suspected infection. contra-indicated or not? Injury. 2011;42 Suppl 2:S82-6.

115. Gonzalez Corchon MA, Salvado M, de la Torre BJ, Collia F, de Pedro JA, Vazquez B, et al. Injectable and self-curing composites of acrylic/bioactive glass and drug systems. A histomorphometric analysis of the behavior in rabbits. Biomaterials. 2006;27(9):1778-87.

116. Kanellakopoulou K, Tsaganos T, Athanassiou K, Koutoukas P, Raftogiannis M, Skiadas I, et al. Comparative elution of moxifloxacin from norian skeletal repair system and acrylic bone cement: An *in vitro* study. Int J Antimicrob Agents. 2006;28(3):217-20.

117. Shi M, Kretlow JD, Nguyen A, Young S, Scott BL, Wong ME, et al. Antibiotic-releasing porous polymethylmethacrylate constructs for osseous space maintenance and infection control. Biomaterials. 2010;31(14):4146-56.

118. Diniz Oliveira HF, Weiner AA, Majumder A, Shastri VP. Non-covalent surface engineering of an alloplastic polymeric bone graft material for controlled protein release. J Controlled Release. 2008;126(3):237-45.

119. Habraken WJEM, Wolke JGC, Jansen JA. Ceramic composites as matrices and scaffolds for drug delivery in tissue engineering. Adv Drug Delivery Rev. 2007;59(4-5):234-48.

120. Mourino V, Boccaccini AR. Bone tissue engineering therapeutics: Controlled drug delivery in three-dimensional scaffolds. J R Soc Interface. 2010;7(43):209-27.

121. Wu C, Ramaswamy Y, Zhu Y, Zheng R, Appleyard R, Howard A, et al. The effect of mesoporous bioactive glass on the physiochemical, biological and drug-release properties of poly(DL-lactide-co-glycolide) films. Biomaterials. 2009;30(12):2199-208.

122. Vila M, Cicuendez M, Sanchez-Marcos J, Fal-Miyar V, Manzano M, Prieto C, et al. Electrical stimuli to increase cell proliferation on carbon nanotubes/mesoporous silica composites for drug delivery. J Biomed Mater Res A. 2013;101(1):213-21.

123. Schnettler R, Pfefferle H, Kilian O, Heiss C, Kreuter J, Lommel D, et al. Glycerol-L-lactide coating polymer leads to delay in bone ingrowth in hydroxyapatite implants. J Controlled Release. 2005;106(1-2):154-61.

124. Wermelin K, Aspenberg P, Linderbaeck P, Tengvall P. Bisphosphonate coating on titanium screws increases mechanical fixation in rat tibia after two weeks. J Biomed Mater Res, Part A. 2008;86A(1):220-7.

125. Suzuki T, Kubo K, Hori N, Yamada M, Kojima N, Sugita Y, et al. Nonvolatile buffer coating of titanium to prevent its biological aging and for drug delivery. Biomaterials. 2010;31(18):4818-28.

126. Hu Y, Cai K, Luo Z, Jandt KD. Layer-by-layer assembly of β-estradiol loaded mesoporous silica nanoparticles on titanium substrates and its implication for bone homeostasis. Adv Mater (Weinheim, Ger). 2010;22(37):4146-50.

127. Kelpke SS, Zinn KR, Rue LW, Thompson JA. Site-specific delivery of acidic fibroblast growth factor stimulates angiogenic and osteogenic responses *in vivo*. J Biomed Mater Res, Part A. 2004;71A(2):316-25.

128. Gao Y, Zhu S, Luo E, Li J, Feng G, Hu J. Basic fibroblast growth factor suspended in matrigel improves titanium implant fixation in ovariectomized rats. J Controlled Release. 2009;139(1):15-21.

129. Kolambkar YM, Dupont KM, Boerckel JD, Huebsch N, Mooney DJ, Hutmacher DW, et al. An alginate-based hybrid system for growth factor delivery in the functional repair of large bone defects. Biomaterials. 2010;32(1):65-74.

130. Viguier E, Bignon A, Laurent F, Goehrig D, Boivin G, Chevalier J. A new concept of gentamicin loaded HAP/TCP bone substitute for prophylactic action: *In vivo* pharmacokinetic study. J Mater Sci: Mater Med. 2011;22(4):879-86.

131. Sendi P, Zimmerli W. Antimicrobial treatment concepts for orthopaedic device-related infection. Clin Microbiol Infect. 2012;18(12):1176-84.

132. Anagnostakos K, Schroeder K. Antibiotic-impregnated bone grafts in orthopaedic and trauma surgery: A systematic review of the literature. Int J Biomater. 2012:538061, 9.

133. Ehrlich GD, Stoodley P, Kathju S, Zhao Y, McLeod BR, Balaban N, et al. Engineering approaches for the detection and control of orthopaedic biofilm infections. Clin Orthop Relat Res. 2005(437):59-66.

134. Stoodley P, Sauer K, Davies DG, Costerton JW. Biofilms as complex differentiated communities. Annu Rev Microbiol. 2002;56:187-209.

135. Arciola CR, Campoccia D, Speziale P, Montanaro L, Costerton JW. Biofilm formation in *staphylococcus* implant infections. A review of molecular mechanisms and implications for biofilm-resistant materials. Biomaterials. 2012;33(26):5967-82.

136. Nandi SK, Mukherjee P, Roy S, Kundu B, De DK, Basu D. Local antibiotic delivery systems for the treatment of osteomyelitis-A review. Mater Sci Eng, C. 2009;29(8):2478-85.

137. Brin YS, Nyska A, Domb AJ, Golenser J, Mizrahi B, Nyska M. Biocompatibility of a polymeric implant for the treatment of osteomyelitis. J Biomater Sci, Polym Ed. 2009;20(7-8):1081-90.

138. Kittinger C, Marth E, Windhager R, Weinberg AM, Zarfel G, Baumert R, et al. Antimicrobial activity of gentamicin palmitate against high concentrations of *staphylococcus aureus*. J Mater Sci: Mater Med. 2011;22(6):1447-53.

139. Tadic D, Welzel T, Seidel P, Wuest E, Dingeldein E, Epple M. Controlled release of gentamicin from biomimetic calcium phosphate *in vitro*. comparison of four different incorporation methods. Materialwiss Werkstofftech. 2004;35(12):1001-5.

140. Silverman LD, Lukashova L, Herman OT, Lane JM, Boskey AL. Release of gentamicin from a tricalcium phosphate bone implant. J Orthop Res. 2007;25(1):23-9.

141. Ensing GT, Hendriks JGE, Jongsma JE, van Horn JR, van der Mei HC, Busscher HJ. The influence of ultrasound on the release of gentamicin from antibiotic-loaded acrylic beads and bone cements. J Biomed Mater Res, Part B. 2005;75B(1):1-5.

142. Shen S, Ng WK, Shi Z, Chia L, Neoh KG, Tan RBH. Mesoporous silica nanoparticle-functionalized poly(methyl methacrylate)-based bone cement for effective antibiotics delivery. J Mater Sci: Mater Med. 2011;22(10):2283-92.

143. Gentry LO. Management of osteomyelitis. Int J Antimicrob Agents. 1997;9(1):37-42.

144. Flórez J, Armijo JA, Mediavilla A. Farmacologia humana. 5th ed. Flórez J editor. Barcelona: Elsevier Masson; 2008.

145. Watanakunakorn C. Mode of action and *in-vitro* activity of vancomycin. J Antimicrob Chemother. 1984;14(Suppl. D):7-18.

146. Castro C, Sanchez E, Delgado A, Soriano I, Nunez P, Baro M, et al. Ciprofloxacin implants for bone infection. *in vitro-in vivo* characterization. J Controlled Release. 2003;93(3):341-54.

147. Koort JK, Maekinen TJ, Suokas E, Veiranto M, Jalava J, Knuuti J, et al. Efficacy of ciprofloxacin-releasing bioabsorbable osteoconductive bone defect filler for treatment

of experimental osteomyelitis due to *staphylococcus aureus*. Antimicrob Agents Chemother. 2005;49(4):1502-8.

148. Wolfson JS, Hooper DC. The fluoroquinolones: Structures, mechanisms of action and resistance, and spectra of activity *in vitro*. Antimicrob Agents Chemother. 1985;28(4):581-6.

149. Nandi SK, Kundu B, Mukherjee P, Mandal TK, Datta S, De DK, et al. *In vitro* and *in vivo* release of cefuroxime axetil from bioactive glass as an implantable delivery system in experimental osteomyelitis. Ceram Int. 2009;35(8):3207-16.

150. Hesaraki S, Nemati R. Cephalexin-loaded injectable macroporous calcium phosphate bone cement. J Biomed Mater Res, Part B. 2009;89B(2):342-52.

151. Sun X, Su J, Bao J, Peng T, Zhang L, Zhang Y, et al. Cytokine combination therapy prediction for bone remodeling in tissue engineering based on the intracellular signaling pathway. Biomaterials. 2012;33(33):8265-76.

152. Epstein NE. Commentary on research of bone morphogenetic protein discussed in review article: Genetic advances in the regeneration of the intervertebral disc. Surgical Neurology International. 2013;22(4 (suppl 2)):S 106-8.

153. Suarez-Gonzalez D, Barnhart K, Migneco F, Flanagan C, Hollister SJ, Murphy WL. Controllable mineral coatings on PCL scaffolds as carriers for growth factor release. Biomaterials. 2012;33(2):713-21.

154. Fu K, Xu Q, Czernuszka J, McKenna CE, Ebetino FH, Russell RGG, et al. Prolonged osteogenesis from human mesenchymal stem cells implanted in immunodeficient mice by using coralline hydroxyapatite incorporating rhBMP2 microspheres. J Biomed Mater Res, Part A. 2010;92A(4):1256-64.

155. Woodard JR, Hilldore AJ, Lan SK, Park CJ, Morgan AW, Eurell JAC, et al. The mechanical properties and osteoconductivity of hydroxyapatite bone scaffolds with multi-scale porosity. Biomaterials. 2006;28(1):45-54.

156. Ratanavaraporn J, Furuya H, Kohara H, Tabata Y. Synergistic effects of the dual release of stromal cell-derived factor-1 and bone morphogenetic protein-2 from hydrogels on bone regeneration. Biomaterials. 2011;32(11):2797-811.

157. Wu G, Liu Y, Iizuka T, Hunziker EB. The effect of a slow mode of BMP-2 delivery on the inflammatory response provoked by bone-defect-filling polymeric scaffolds. Biomaterials. 2010;31(29):7485-93.

158. Hoshino M, Egi T, Terai H, Namikawa T, Kato M, Hashimoto Y, et al. Repair of long intercalated rib defects in dogs using recombinant human bone morphogenetic protein-2 delivered by a synthetic polymer and beta-tricalcium phosphate. J Biomed Mater Res, Part A. 2009;90A(2):514-21.

159. Trajkovski B, Petersen A, Strube P, Mehta M, Duda GN. Intra-operatively customized implant coating strategies for local and controlled drug delivery to bone. Adv Drug Delivery Rev. 2012;64(12):1142-51.

160. Matsushita N, Terai H, Okada T, Nozaki K, Inoue H, Miyamoto S, et al. A new bone-inducing biodegradable porous β-tricalcium phosphate. J Biomed Mater Res, Part A. 2004;70A(3):450-8.

161. MacDonald ML, Samuel RE, Shah NJ, Padera RF, Beben YM, Hammond PT. Tissue integration of growth factor-eluting layer-by-layer polyelectrolyte multilayer coated implants. Biomaterials. 2011;32(5):1446-53.

162. Wernike E, Hofstetter W, Liu Y, Wu G, Sebald H, Wismeijer D, et al. Long-term cell-mediated protein release from calcium phosphate ceramics. J Biomed Mater Res, Part A. 2010;92A(2):463-74.

163. Wang Y, Zhang L, Hu M, Wen W, Xiao H, Niu Y. Effect of chondroitin sulfate modification on rhBMP-2 release kinetics from collagen delivery system. J Biomed Mater Res, Part A. 2010;92A(2):693-701.

164. Phipps MC, Xu Y, Bellis SL. Delivery of platelet-derived growth factor as a chemotactic factor for mesenchymal stem cells by bone-mimetic electrospun scaffolds. PLoS One. 2012;7(7):e40831.

165. Gerstenfeld LC, Cullinane DM, Barnes GL, Graves DT, Einhorn TA. Fracture healing as a post-natal developmental process: Molecular, spatial, and temporal aspects of its regulation. J Cell Biochem. 2003;88(5):873-84.

166. Lee J, Kim K, Shin S, Rhyu I, Lee Y, Park Y, et al. Enhanced bone formation by transforming growth factor-β1-releasing collagen/chitosan microgranules. J Biomed Mater Res, Part A. 2006;76A(3):530-9.

167. Cartmell S. Controlled release scaffolds for bone tissue engineering. J Pharm Sci. 2009;98(2):430-41.

168. Raiche AT, Puleo DA. Cell responses to BMP-2 and IGF-I released with different time-dependent profiles. J Biomed Mater Res, Part A. 2004;69A(2):342-50.

169. Yilgor P, Tuzlakoglu K, Reis RL, Hasirci N, Hasirci V. Incorporation of a sequential BMP-2/BMP-7 delivery system into chitosan-based scaffolds for bone tissue engineering. Biomaterials. 2009;30(21):3551-9.

170. De la Riva B, Sanchez E, Hernandez A, Reyes R, Tamimi F, Lopez-Cabarcos E, et al. Local controlled release of VEGF and PDGF from a combined brushite-chitosan system enhances bone regeneration. J Controlled Release. 2010;143(1):45-52.

171. Zhang W, Wang X, Wang S, Zhao J, Xu L, Zhu C, et al. The use of injectable sonication-induced silk hydrogel for VEGF165 and BMP-2 delivery for elevation of the maxillary sinus floor. Biomaterials. 2011;32(35):9415-24.

172. Kempen DHR, Lu L, Heijink A, Hefferan TE, Creemers LB, Maran A, et al. Effect of local sequential VEGF and BMP-2 delivery on ectopic and orthotopic bone regeneration. Biomaterials. 2009;30(14):2816-25.

173. Chen F, Chen R, Wang X, Sun H, Wu Z. *In vitro* cellular responses to scaffolds containing 2 microencapsulated growth factors. Biomaterials. 2009;30(28):5215-24.

174. Maire M, Chaubet F, Mary P, Blanchat C, Meunier A, Logeart-Avramoglou D. Bovine BMP osteoinductive potential enhanced by functionalized dextran-derived hydrogels. Biomaterials. 2005;26(24):5085-92.

175. Colilla M, Izquierdo-Barba I, Vallet-Regi M. Phosphorus-containing SBA-15 materials as bisphosphonate carriers for osteoporosis treatment. Microporous Mesoporous Mater. 2010;135(1-3):51-9.

176. Shi X, Ren L, Tian M, Yu J, Huang W, Du C, et al. *In vivo* and *in vitro* osteogenesis of stem cells induced by controlled release of drugs from microspherical scaffolds. J Mater Chem. 2010;20(41):9140-8.

177. Chen J, Luo Y, Hong L, Ling Y, Pang J, Fang Y, et al. Synthesis, characterization and osteoconductivity properties of bone fillers based on alendronate-loaded poly(ε-caprolactone)/hydroxyapatite microspheres. J Mater Sci: Mater Med. 2011;22(3):547-55.

178. Daubine F, Cortial D, Ladam G, Atmani H, Haikel Y, Voegel J, et al. Nanostructured polyelectrolyte multilayer drug delivery systems for bone metastasis prevention. Biomaterials. 2009;30(31):6367-73.

179. Martins A, Duarte ARC, Faria S, Marques AP, Reis RL, Neves NM. Osteogenic induction of hBMSCs by electrospun scaffolds with dexamethasone release functionality. Biomaterials. 2010;31(22):5875-85.

180. Jeon JH, Puleo DA. Formulations for intermittent release of parathyroid hormone (1-34) and local enhancement of osteoblast activities. Pharm Dev Technol. 2008;13(6):505-12.

181. Li DX, Fan HS, Zhu XD, Tan YF, Xiao WQ, Lu J, et al. Controllable release of salmon-calcitonin in injectable calcium phosphate cement modified by chitosan oligosaccharide and collagen polypeptide. J Mater Sci: Mater Med. 2007;18(11):2225-31.

182. Tran PA, Sarin L, Hurt RH, Webster TJ. Titanium surfaces with adherent selenium nanoclusters as a novel anticancer orthopedic material. J Biomed Mater Res, Part A. 2010;93A(4):1417-28.

183. Palazzo B, Iafisco M, Laforgia M, Margiotta N, Natile G, Bianchi CL, et al. Biomimetic hydroxyapatite-drug nanocrystals as potential bone substitutes with antitumor drug delivery properties. Adv Funct Mater. 2007;17(13):2180-8.

184. Maekinen TJ, Veiranto M, Lankinen P, Moritz N, Jalava J, Toermaelae P, et al. *In vitro* and *in vivo* release of ciprofloxacin from osteoconductive bone defect filler. J Antimicrob Chemother. 2005;56(6):1063-8.

185. Wu C, Fan W, Zhu Y, Gelinsky M, Chang J, Cuniberti G, et al. Multifunctional magnetic mesoporous bioactive glass scaffolds with a hierarchical pore structure. Acta Biomater. 2011;7(10):3563-72.

186. Simoes SMN, Veiga F, Torres-Labandeira JJ, Ribeiro ACF, Concheiro A, Alvarez-Lorenzo C. Poloxamine-cyclodextrin-simvastatin supramolecular systems promote osteoblast differentiation of mesenchymal stem cells. Macromol Biosci. 2013;13(6):723-34.

187. Nyan M, Sato D, Oda M, Machida T, Kobayashi H, Nakamura T, et al. Bone formation with the combination of simvastatin and calcium sulfate in critical-sized rat calvarial defect. J Pharmacol Sci (Tokyo, Jpn). 2007;104(4):384-6.

188. Park J. The use of simvastatin in bone regeneration. Med Oral Patol Oral Cir Bucal. 2009;14(9):e485-8.

189. Tanigo T, Takaoka R, Tabata Y. Sustained release of water-insoluble simvastatin from biodegradable hydrogel augments bone regeneration. J Controlled Release. 2010;143(2):201-6.

190. Jeon JH, Puleo DA. Alternating release of different bioactive molecules from a complexation polymer system. Biomaterials. 2008;29(26):3591-8.

191. Takaoka R, Hikasa Y, Hayashi K, Tabata Y. Bone regeneration by lactoferrin released from a gelatin hydrogel. J Biomater Sci, Polym Ed. 2011;22(12):1581-9.

192. Irbe Z, Loca D, Vempere D, Berzina-Cimdina L. Controlled release of local anesthetic from calcium phosphate bone cements. Mater Sci Eng, C. 2012;32(6):1690-4.

193. Schneider OD, Loher S, Brunner TJ, Schmidlin P, Stark WJ. Flexible, silver containing nanocomposites for the repair of bone defects: Antimicrobial effect against E. coli infection and comparison to tetracycline containing scaffolds. J Mater Chem. 2008;18(23):2679-84.

194. Xin Y, Jiang J, Huo K, Hu T, Chu PK. Bioactive $SrTiO_3$ nanotube arrays: Strontium delivery platform on ti-based osteoporotic bone implants. ACS Nano. 2009;3(10):3228-34.

195. Forsgren J, Engqvist H. A novel method for local administration of strontium from implant surfaces. J Mater Sci: Mater Med. 2010;21(5):1605-9.

196. Simoes SMN, Veiga F, Torres-Labandeira JJ, Ribeiro ACF, Sandez-Macho MI, Concheiro A, et al. Syringeable pluronic-α-cyclodextrin supramolecular gels for sustained delivery of vancomycin. Eur J Pharm Biopharm. 2012;80(1):103-12.

197. Puga AM, Rey-Rico A, Magarinos B, Alvarez-Lorenzo C, Concheiro A. Hot melt poly-ε-caprolactone/poloxamine implantable matrices for sustained delivery of ciprofloxacin. Acta Biomater. 2012;8(4):1507-18.

198. Rey-Rico A, Silva M, Couceiro J, Concheiro A, Alvarez-Lorenzo C. Osteogenic efficiency of *in situ* gelling poloxamine systems with and without bone morphogenetic protein-2. Eur Cells Mater. 2011;21:317-40.

199. Yu SS, Koblin RL, Zacherman AL, Perrien DS, Hofmeister LH, Giorgio TD, et al. Physiologically relevant oxidative degradation of oligo(proline) cross-linked polymeric scaffolds. Biomacromolecules. 2011;12(12):4357-66.

200. Ozkan S, Kalyon DM, Yu X, McKelvey CA, Lowinger M. Multifunctional protein-encapsulated polycaprolactone scaffolds: Fabrication and *in vitro* assessment for tissue engineering. Biomaterials. 2009;30(26):4336-47.

201. Fan J, Lei J, Yu C, Tu B, Zhao D. Hard-templating synthesis of a novel rod-like nanoporous calcium phosphate bioceramics and their capacity as antibiotic carriers. Mater Chem Phys. 2007;103(2-3):489-93.

202. Hong Y, Chen X, Jing X, Fan H, Gu Z, Zhang X. Fabrication and drug delivery of ultrathin mesoporous bioactive glass hollow fibers. Adv Funct Mater. 2010;20(9):1503-10.

203. Rauschmann MA, Wichelhaus TA, Stirnal V, Dingeldein E, Zichner L, Schnettler R, et al. Nanocrystalline hydroxyapatite and calcium sulphate as biodegradable composite carrier material for local delivery of antibiotics in bone infections. Biomaterials. 2005;26(15):2677-84.

204. Manzano M, Lamberti G, Galdi I, Vallet-Regi M. Anti-osteoporotic drug release from ordered mesoporous bioceramics: Experiments and modeling. AAPS PharmSciTech. 2011;12(4):1193-9.

205. Kundu B, Nandi SK, Dasgupta S, Datta S, Mukherjee P, Roy S, et al. Macro-to-micro porous special bioactive glass and ceftriaxone-sulbactam composite drug delivery system for treatment of chronic osteomyelitis: An investigation through *in vitro* and *in vivo* animal trial. J Mater Sci: Mater Med. 2011;22(3):705-20.

206. Kundu B, Lemos A, Soundrapandian C, Sen PS, Datta S, Ferreira JMF, et al. Development of porous HAp and β-TCP scaffolds by starch consolidation with foaming method and drug-chitosan bilayered scaffold based drug delivery system. J Mater Sci : Mater Med. 2010;21(11):2955-69.

207. Soundrapandian C, Basu D, Sa B, Datta S. Local drug delivery system for the treatment of osteomyelitis: *In vitro* evaluation. Drug Dev Ind Pharm. 2011;37(5):538-46.

208. Nguyen T, Lee B. *In vitro* and *in vivo* studies of rhBMP2-coated PS/PCL fibrous scaffolds for bone regeneration. J Biomed Mater Res, Part A. 2013;101A(3):797-808.

209. Dong X, Wang Q, Wu T, Pan H. Understanding adsorption-desorption dynamics of BMP-2 on hydroxyapatite (001) surface. Biophys J. 2007;93(3):750-9.

210. Xue W, Bandyopadhyay A, Bose S. Mesoporous calcium silicate for controlled release of bovine serum albumin protein. Acta Biomater. 2009;5(5):1686-96.

211. Martinez-Sanz E, Ossipov DA, Hilborn J, Larsson S, Jonsson KB, Varghese OP. Bone reservoir: Injectable hyaluronic acid hydrogel for minimal invasive bone augmentation. J Controlled Release. 2011;152(2):232-40.

212. Schickle K, Zurlinden K, Bergmann C, Lindner M, Kirsten A, Laub M, et al. Synthesis of novel tricalcium phosphate-bioactive glass composite and functionalization with rhBMP-2. J Mater Sci: Mater Med. 2011;22(4):763-71.

213. Czuryszkiewicz T, Areva S, Honkanen M, Linden M. Synthesis of sol-gel silica materials providing a slow release of biphosphonate. Colloids Surf, A. 2005;254(1-3):69-74.

214. Wang C, Chen S, Chen C, Wang C, Wang G, Chang J, et al. The effect of the local delivery of alendronate on human adipose-derived stem cell-based bone regeneration. Biomaterials. 2010;31(33):8674-83.

215. Roussiere H, Fayon F, Alonso B, Rouillon T, Schnitzler V, Verron E, et al. Reaction of zoledronate with β-tricalcium phosphate for the design of potential drug device combined systems. Chem Mater. 2008;20(1):182-91.

216. Linderbaeck P, Areva S, Aspenberg P, Tengvall P. Sol-gel derived titania coating with immobilized bisphosphonate enhances screw fixation in rat tibia. J Biomed Mater Res, Part A. 2010;94A(2):389-95.

217. Chen L, He Z, Chen B, Yang M, Zhao Y, Sun W, et al. Loading of VEGF to the heparin cross-linked demineralized bone matrix improves vascularization of the scaffold. J Mater Sci: Mater Med. 2010;21(1):309-17.

218. Chung Y, Ahn K, Jeon S, Lee S, Lee J, Tae G. Enhanced bone regeneration with BMP-2 loaded functional nanoparticle-hydrogel complex. J Controlled Release. 2007;121(1-2):91-9.

219. Abbah S, Liu J, Lam RWM, Goh JCH, Wong H. *In vivo* bioactivity of rhBMP-2 delivered with novel polyelectrolyte complexation shells assembled on an alginate microbead core template. J Controlled Release. 2012;162(2):364-72.

220. Jeon O, Powell C, Solorio LD, Krebs MD, Alsberg E. Affinity-based growth factor delivery using biodegradable, photocrosslinked heparin-alginate hydrogels. J Controlled Release. 2011;154(3):258-66.

221. Sun B, Chen B, Zhao Y, Sun W, Chen K, Zhang J, et al. Crosslinking heparin to collagen scaffolds for the delivery of human platelet-derived growth factor. J Biomed Mater Res, Part B. 2009;91B(1):366-72.

222. Kim S, Gwak S, Kim B. Orthotopic bone formation by implantation of apatite-coated poly(lactide-co-glycolide)/hydroxyapatite composite particulates and bone morphogenetic protein-2. J Biomed Mater Res, Part A. 2008;87A(1):245-53.

223. Ruhe PQ, Boerman OC, Russel FGM, Spauwen PHM, Mikos AG, Jansen JA. Controlled release of rhBMP-2 loaded poly(DL-lactic-co-glycolic acid)/calcium phosphate cement composites *in vivo*. J Controlled Release. 2005;106(1-2):162-71.

224. Sohier J, Daculsi G, Sourice S, de Groot K, Layrolle P. Porous beta tricalcium phosphate scaffolds used as BMP-2 delivery system for bone tissue engineering. J Biomed Mater Res, Part A. 2010;92A(3):1105-14.

225. Kazemzadeh-Narbat M, Noordin S, Masri BA, Garbuz DS, Duncan CP, Hancock REW, et al. Drug release and bone growth studies of antimicrobial peptide-loaded calcium phosphate coating on titanium. J Biomed Mater Res, Part B. 2012;100B(5):1344-52.

226. El-Ghannam A, Jahed K, Govindaswami M. Resorbable bioactive ceramic for treatment of bone infection. J Biomed Mater Res, Part A. 2010;94A(1):308-16.

227. Xia W, Chang J. Well-ordered mesoporous bioactive glasses (MBG): A promising bioactive drug delivery system. J Controlled Release. 2006;110(3):522-30.

228. Zhu Y, Kaskel S. Comparison of the *in vitro* bioactivity and drug release property of mesoporous bioactive glasses (MBGs) and bioactive glasses (BGs) scaffolds. Microporous Mesoporous Mater. 2009;118(1-3):176-82.

229. Wu C, Fan W, Gelinsky M, Xiao Y, Simon P, Schulze R, et al. Bioactive SrO-SiO_2 glass with well-ordered mesopores: Characterization, physiochemistry and biological properties. Acta Biomater. 2011;7(4):1797-806.

230. de Guzman RC, Saul JM, Ellenburg MD, Merrill MR, Coan HB, Smith TL, et al. Bone regeneration with BMP-2 delivered from keratose scaffolds. Biomaterials. 2013;34(6):1644-56.

231. Kohara H, Tabata Y. Enhancement of ectopic osteoid formation following the dual release of bone morphogenetic protein 2 and Wnt1 inducible signaling pathway protein 1 from gelatin sponges. Biomaterials. 2011;32(24):5726-32.

232. Lee J, Seol Y, Kim K, Lee Y, Park Y, Rhyu I, et al. Transforming growth factor (TGF)-β1 releasing tricalcium Phosphate/Chitosan microgranules as bone substitutes. Pharm Res. 2004;21(10):1790-6.

233. Guo X, Chen M, Feng W, Liang J, Zhao H, Tian L, et al. Electrostatic self-assembly of multilayer copolymeric membranes on the surface of porous tantalum implants for sustained release of doxorubicin. Int J Nanomed. 2011;6:3057-64.

234. Vorndran E, Klammert U, Ewald A, Barralet JE, Gbureck U. Simultaneous immobilization of bioactives during 3D powder printing of bioceramic drug-release matrices. Adv Funct Mater. 2010;20(10):1585-91.

235. Ewald A, Hoesel D, Patel S, Grover LM, Barralet JE, Gbureck U. Silver-doped calcium phosphate cements with antimicrobial activity. Acta Biomater. 2011;7(11):4064-70.

236. Otsuka M, Nakagawa H, Ito A, Higuchi WI. Effect of geometrical structure on drug release rate of a three-dimensionally perforated porous apatite/collagen composite cement. J Pharm Sci. 2009;99(1):286-92.

237. Schnitzler V, Fayon F, Despas C, Khairoun I, Mellier C, Rouillon T, et al. Investigation of alendronate-doped apatitic cements as a potential technology for the prevention of osteoporotic hip fractures: Critical influence of the drug introduction mode on the *in vitro* cement properties. Acta Biomater. 2011;7(2):759-70.

238. Jiang P, Patel S, Gbureck U, Caley R, Grover LM. Comparing the efficacy of three bioceramic matrices for the release of vancomycin hydrochloride. J Biomed Mater Res, Part B. 2010;93B(1):51-8.

239. Hall EW, Rouse MS, Jacofsky DJ, Osmon DR, Hanssen AD, Steckelberg JM, et al. Release of daptomycin from polymethylmethacrylate beads in a continuous flow chamber. Diagn Microbiol Infect Dis. 2004;50(4):261-5.

240. Cai X, Chen X, Yan S, Ruan Z, Yan R, Ji K, et al. Intermittent watt-level ultrasonication facilitates vancomycin release from therapeutic acrylic bone cement. J Biomed Mater Res, Part B. 2009;90B(1):11-7.

241. Yan S, Cai X, Yan W, Dai X, Wu H. Continuous wave ultrasound enhances vancomycin release and antimicrobial efficacy of antibiotic-loaded acrylic bone cement *in vitro* and *in vivo*. J Biomed Mater Res, Part B. 2007;82B(1):57-64.

242. Lode A, Wolf-Brandstetter C, Reinstorf A, Bernhardt A, Konig U, Pompe W, et al. Calcium phosphate bone cements, functionalized with VEGF: Release kinetics and biological activity. J Biomed Mater Res A. 2007;81(2):474-83.

243. Ginebra M, Traykova T, Planell JA. Calcium phosphate cements: Competitive drug carriers for the musculoskeletal system? Biomaterials. 2006;27(10):2171-7.

244. Lucas-Girot A, Verdier M, Tribut O, Sangleboeuf J, Allain H, Oudadesse H. Gentamicin-loaded calcium carbonate materials: Comparison of two drug-loading modes. J Biomed Mater Res, Part B. 2005;73B(1):164-70.

245. Alves A, Duarte ARC, Mano JF, Sousa RA, Reis RL. PDLLA enriched with ulvan particles as a novel 3D porous scaffold targeted for bone engineering. J Supercrit Fluids. 2012;65:32-8.

246. Mabilleau G, Aguado E, Stancu IC, Cincu C, Basle MF, Chappard D. Effects of FGF-2 release from a hydrogel polymer on bone mass and microarchitecture. Biomaterials. 2008;29(11):1593-600.

247. Kaito T, Myoui A, Takaoka K, Saito N, Nishikawa M, Tamai N, et al. Potentiation of the activity of bone morphogenetic protein-2 in bone regeneration by a PLA-PEG/hydroxyapatite composite. Biomaterials. 2004;26(1):73-9.

248. Delgado JJ, Evora C, Sanchez E, Baro M, Delgado A. Validation of a method for non-invasive *in vivo* measurement of growth factor release from a local delivery system in bone. J Controlled Release. 2006;114(2):223-9.

249. Catauro M, Raucci M, Ausanio G. Sol-gel processing of drug delivery zirconia/polycaprolactone hybrid materials. J Mater Sci: Mater Med. 2008;19(2):531-40.

250. Ismail FA. Design and *in vitro* evaluation of polymeric formulae of simvastatin for local bone induction. Drug Dev Ind Pharm. 2006;32(10):1199-206.

251. Wu C, Luo Y, Cuniberti G, Xiao Y, Gelinsky M. Three-dimensional printing of hierarchical and tough mesoporous bioactive glass scaffolds with a controllable pore architecture, excellent mechanical strength and mineralization ability. Acta Biomater. 2011;7(6):2644-50.

252. Lee H, Ahn S, Kim GH. Three-dimensional Collagen/Alginate hybrid scaffolds functionalized with a drug delivery system (DDS) for bone tissue regeneration. Chem Mater. 2012;24(5):881-91.

253. Krasko MY, Golenser J, Nyska A, Nyska M, Brin YS, Domb AJ. Gentamicin extended release from an injectable polymeric implant. J Controlled Release. 2007;117(1):90-6.

254. Aviv M, Berdicevsky I, Zilberman M. Gentamicin-loaded bioresorbable films for prevention of bacterial infections associated with orthopedic implants. J Biomed Mater Res, Part A. 2007;83A(1):10-9.

255. Kim H, Knowles JC, Kim H. Porous scaffolds of gelatin-hydroxyapatite nanocomposites obtained by biomimetic approach: Characterization and antibiotic drug release. J Biomed Mater Res, Part B. 2005;74B(2):686-98.

256. Luciani A, Guarino V, Ambrosio L, Netti PA. Solvent and melting induced microspheres sintering techniques: A comparative study of morphology and mechanical properties. J Mater Sci: Mater Med. 2011;22(9):2019-28.

257. Le Ray A, Chiffoleau S, Iooss P, Grimandi G, Gouyette A, Daculsi G, et al. Vancomycin encapsulation in biodegradable poly(ε-caprolactone) microparticles for

bone implantation. influence of the formulation process on size, drug loading, *in vitro* release and cytocompatibility. Biomaterials. 2002;24(3):443-9.

258. Mondal T, Sunny MC, Khastgir D, Varma HK, Ramesh P. Poly(L-lactide-co-ε-caprolactone) microspheres laden with bioactive glass-ceramic and alendronate sodium as bone regenerative scaffolds. Mater Sci Eng, C. 2012;32(4):697-706.

259. Wang G, Babadagli ME, Uludag H. Bisphosphonate-derivatized liposomes to control drug release from Collagen/Hydroxyapatite scaffolds. Mol Pharmaceutics. 2011;8(4):1025-34.

260. Liu H, Zhang L, Shi P, Zou Q, Zuo Y, Li Y. Hydroxyapatite/polyurethane scaffold incorporated with drug-loaded ethyl cellulose microspheres for bone regeneration. J Biomed Mater Res, Part B. 2010;95B(1):36-46.

261. Kempen DHR, Lu L, Hefferan TE, Creemers LB, Maran A, Classic KL, et al. Retention of *in vitro* and *in vivo* BMP-2 bioactivities in sustained delivery vehicles for bone tissue engineering. Biomaterials. 2008;29(22):3245-52.

262. Wang Q, Wang J, Lu Q, Detamore MS, Berkland C. Injectable PLGA based colloidal gels for zero-order dexamethasone release in cranial defects. Biomaterials. 2010;31(18):4980-6.

263. Suciati T, Howard D, Barry J, Everitt NM, Shakesheff KM, Rose FR. Zonal release of proteins within tissue engineering scaffolds. J Mater Sci: Mater Med. 2006;17(11):1049-56.

264. Oliveira JM, Sousa RA, Malafaya PB, Silva SS, Kotobuki N, Hirose M, et al. *In vivo* study of dendronlike nanoparticles for stem cells "tune-up": From nano to tissues. Nanomedicine (New York, NY, U S). 2011;7(6):914-24.

265. Zurlinden K, Laub M, Jennissen HP. Chemical functionalization of a hydroxyapatite based bone replacement material for the immobilization of proteins. Materialwiss Werkstofftech. 2005;36(12):820-7.

266. Culpepper BK, Bonvallet PP, Reddy MS, Ponnazhagan S, Bellis SL. Polyglutamate directed coupling of bioactive peptides for the delivery of osteoinductive signals on allograft bone. Biomaterials. 2013;34(5):1506-13.

267. Li X, Wang X, Zhang L, Chen H, Shi J. MBG/PLGA composite microspheres with prolonged drug release. J Biomed Mater Res, Part B. 2009;89B(1):148-54.

268. Zhang X, Jia WT, Gu YF, Xiao W, Liu X, Wang DP, et al. Teicoplanin-loaded borate bioactive glass implants for treating chronic bone infection in a rabbit tibia osteomyelitis model. Biomaterials. 2010;31(22):5865-74.

269. Zhu M, Zhang L, He Q, Zhao J, Guo L, Shi J. Mesoporous bioactive glass-coated poly(L-lactic acid) scaffolds: A sustained antibiotic drug release system for bone repairing. J Mater Chem. 2011;21(4):1064-72.

270. Ferraz MP, Mateus AY, Sousa JC, Monteiro FJ. Nanohydroxyapatite microspheres as delivery system for antibiotics: Release kinetics, antimicrobial activity, and interaction with osteoblasts. J Biomed Mater Res, Part A. 2007;81A(4):994-1004.

271. Chen F, Zhao Y, Sun H, Jin T, Wang Q, Zhou W, et al. Novel glycidyl methacrylated dextran (dex-GMA)/gelatin hydrogel scaffolds containing microspheres loaded with bone morphogenetic proteins: Formulation and characteristics. J Controlled Release. 2007;118(1):65-77.

272. Vogt S, Kuehn K-, Gopp U, Schnabelrauch M. Resorbable antibiotic coatings for bone substitutes and implantable devices. Materialwiss Werkstofftech. 2005;36(12):814-9.

273. Gbureck U, Vorndran E, Barralet JE. Modeling vancomycin release kinetics from microporous calcium phosphate ceramics comparing static and dynamic immersion conditions. Acta Biomater. 2008;4(5):1480-6.

274. Chevalier E, Viana M, Cazalbou S, Chulia D. Comparison of low-shear and high-shear granulation processes: Effect on implantable calcium phosphate granule properties. Drug Dev Ind Pharm. 2009;35(10):1255-63.

275. Delgado JJ, Sanchez E, Baro M, Reyes R, Evora C, Delgado A. A platelet derived growth factor delivery system for bone regeneration. J Mater Sci: Mater Med. 2012;23(8):1903-12.

276. Fuentes G, Lara A, Peon E, Torres M. Preliminary evaluation of TEDMA/HEMA + HAP composites as bone substitutes and drug controlled delivery matrixes. Lat Am Appl Res. 2005;35(1):9-14.

277. Rath SN, Pryymachuk G, Bleiziffer OA, Lam CXF, Arkudas A, Ho STB, et al. Hyaluronan-based heparin-incorporated hydrogels for generation of axially vascularized bioartificial bone tissues: *In vitro* and *in vivo* evaluation in a PLDLLA-TCP-PCL-composite system. J Mater Sci: Mater Med. 2011;22(5):1279-91.

278. Thanyaphoo S, Kaewsrichan J. Synthesis and evaluation of novel glass ceramics as drug delivery systems in osteomyelitis. J Pharm Sci. 2012;101(8):2870-82.

279. Peng G, Wang J, Yang F, Zhang S, Hou J, Xing W, et al. *In situ* formation of biodegradable dextran-based hydrogel via michael addition. J Appl Polym Sci. 2013;127(1):577-84.

280. Yang F, Wang J, Hou J, Guo H, Liu C. Bone regeneration using cell-mediated responsive degradable PEG-based scaffolds incorporating with rhBMP-2. Biomaterials. 2013;34(5):1514-28.

281. Zamoume O, Thibault S, Regnie G, Mecherri MO, Fiallo M, Sharrock P. Macroporous calcium phosphate ceramic implants for sustained drug delivery. Mater Sci Eng, C. 2011;31(7):1352-6.

282. Kim H, Knowles JC, Kim H. Hydroxyapatite/poly(ε-caprolactone) composite coatings on hydroxyapatite porous bone scaffold for drug delivery. Biomaterials. 2003;25(7-8):1279-87.

283. Huang D, Zuo Y, Zou Q, Zhang L, Li J, Cheng L, et al. Antibacterial chitosan coating on nano-hydroxyapatite/polyamide66 porous bone scaffold for drug delivery. J Biomater Sci, Polym Ed. 2011;22(7):931-44.

284. Zhang LF, Sun R, Xu L, Du J, Xiong ZC, Chen HC, et al. Hydrophilic poly (ethylene glycol) coating on PDLLA/BCP bone scaffold for drug delivery and cell culture. Mater Sci Eng, C. 2008;28(1):141-9.

285. Li Z, Kong W, Li X, Xu C, He Y, Gao J, et al. Antibiotic-containing biodegradable bead clusters with porous PLGA coating as controllable drug-releasing bone fillers. J Biomater Sci, Polym Ed. 2011;22(13):1713-31.

286. Lin T, Lu C, Zhu L, Lu T. The biodegradation of zein *in vitro* and *in vivo* and its application in implants. AAPS PharmSciTech. 2011;12(1):172-6.

287. Schnieders J, Gbureck U, Thull R, Kissel T. Controlled release of gentamicin from calcium phosphate-poly(lactic acid-co-glycolic acid) composite bone cement. Biomaterials. 2006;27(23):4239-49.

288. Siepmann J, Siepmann F. Mathematical modeling of drug delivery. Int J Pharm. 2008;364(2):328-43.

289. Dash S, Murthy PN, Nath L, Chowdhury P. Kinetic modeling on drug release from controlled drug delivery systems. Acta Pol Pharm. 2010;67(3):217-23.

290. Costa P, Sousa Lobo JM. Modeling and comparison of dissolution profiles. Eur J Pharm Sci. 2001;13(2):123-33.

291. Sirivisoot S, Pareta RA, Webster TJ. A conductive nanostructured polymer electrodeposited on titanium as a controllable, local drug delivery platform. J Biomed Mater Res A. 2011 Dec 15;99(4):586-97.

292. Kempen DHR, Yaszemski MJ, Heijink A, Hefferan TE, Creemers LB, Britson J, et al. Non-invasive monitoring of BMP-2 retention and bone formation in composites for bone tissue engineering using SPECT/CT and scintillation probes. J Controlled Release. 2009;134(3):169-76.

293. Qu D, Li J, Li Y, Gao Y, Zuo Y, Hsu Y, et al. Angiogenesis and osteogenesis enhanced by bFGF *ex vivo* gene therapy for bone tissue engineering in reconstruction of calvarial defects. J Biomed Mater Res, Part A. 2011;96A(3):543-51.

294. Hisatome T, Yasunaga Y, Yanada S, Tabata Y, Ikada Y, Ochi M. Neovascularization and bone regeneration by implantation of autologous bone marrow mononuclear cells. Biomaterials. 2005;26(22):4550-6.

295. Green DW, Leveque I, Walsh D, Howard D, Yang X, Partridge K, et al. Biomineralized polysaccharide capsules for encapsulation, organization, and delivery of human cell types and growth factors. Adv Funct Mater. 2005;15(6):917-23.

296. Kanczler JM, Ginty PJ, Barry JJA, Clarke NMP, Howdle SM, Shakesheff KM, et al. The effect of mesenchymal populations and vascular endothelial growth factor delivered from biodegradable polymer scaffolds on bone formation. Biomaterials. 2008;29(12):1892-900.

297. Verron E, Khairoun I, Guicheux J, Bouler J. Calcium phosphate biomaterials as bone drug delivery systems: A review. Drug Discovery Today. 2010;15(13/14):547-52.

1.2

Cerámicas biomórficas de carburo de silicio como nuevos materiales para regeneración ósea

USC
UNIVERSIDADE
DE SANTIAGO
DE COMPOSTELA

Las cerámicas son un grupo heterogéneo de compuestos inorgánicos, refractarios, policristalinos, generalmente sólidos, formados por combinaciones de enlaces iónicos y covalentes. Presentan como principales características; elevadas temperaturas de fusión, reducida conductividad eléctrica y gran resistencia a la corrosión y a la deformación. Estas propiedades las convierten en adecuadas candidatas para aplicaciones biomédicas, en particular, para la reparación y sustitución de tejidos esqueléticos conectivos duros, como implantes dentales, tendones y ligamentos artificiales, recubrimientos y dispositivos de fijación ortopédica, dental y maxilofacial (1). Desde un punto de vista biomédico las cerámicas pueden dividirse en dos grandes grupos: cerámicas biodegradables y no reabsorbibles. Desde un punto de vista químico pueden clasificarse en función de si incluyen o no átomos de oxígeno en su estructura, es decir, en cerámicas oxídicas y no oxídicas (2).

Las cerámicas biodegradables (cerámicas de fosfato cálcico, vidrios bioactivos y cerámicas de vidrio) son las más empleadas con fines médicos. Generalmente, éstas son capaces de inducir la formación de hueso *in vitro* (2). Los vidrios bioactivos y las cerámicas de vidrio incluyen, por lo general, cerámicas oxídicas como SiO_2, Na_2O, CaO y P_2O_5, mientras que las cerámicas de fosfato cálcico simulan el componente cristalino principal de la fase mineral del hueso y están formadas por iones calcio y fosfato (3). Las cerámicas de fosfato cálcico pueden cristalizar en forma de mono-, di-,

tri- o tetra- fosfato de calcio, hidroxiapatita y sales de β-whitlockita dependiendo de la relación Ca/P, la temperatura y la presencia de agua e impurezas. Entre ellas, la hidroxiapatita es la más empleada debido a su similitud con el componente mineral del hueso (4).

Las cerámicas no reabsorbibles incluyen óxidos de circonio, alúmina, carbón pirolítico y carburos y nitruros de silicio. Éstas se utilizan comúnmente en aplicaciones ortopédicas que requieren soporte de carga, debido a su mayor resistencia a la deformación y a la fractura (4). Dentro de este grupo, el óxido de alúmina es el más empleado por sus excelentes propiedades tribológicas (4-6).

La necesidad de que los materiales no reabsorbibles implantados sean capaces de vascularizarse e integrarse en el tejido óseo, asegurando su viabilidad a largo plazo, ha conducido a la búsqueda de estructuras cerámicas porosas tridimensionales que permitan el crecimiento tisular sirviendo de andamios o "scaffolds". Para ello, requieren tener apropiada porosidad y distribución de tamaño de poros, así como una elevada interconectividad. Además, deben proporcionar la suficiente resistencia mecánica para restaurar la funcionalidad del tejido dañado.

Con el fin de conseguir estructuras porosas adecuadas se han empleado numerosas técnicas como la adición de agentes porógenos en el proceso de elaboración de la cerámica, la preparación de andamios de varias fases o la formación de esponjas mediante el empleo de gas (7). El uso de materiales de origen natural como moldes en la producción de dichas cerámicas podría ser otra atractiva alternativa.

1.2.1 **Materiales de origen natural como precursores en la síntesis de cerámicas**

El empleo de fuentes naturales (madera, algas o procesados de madera) como molde para la obtención de materiales cerámicos tridimensionales permite aprovechar

estructuras que han sido perfeccionadas por la evolución genética a lo largo del tiempo. Los procedimientos empleados pretenden conservar la excelente relación entre propiedades mecánicas y bajo peso de la madera original, así como su alta rigidez, elasticidad y la tolerancia a daños a micro y macro escala (8-10).

Los materiales cerámicos así obtenidos son pseudomórficos, similares al material de partida en cuanto a su macro, meso y microestructura (11, 12). La arquitectura jerarquizada de la madera hace posible una elevada resistencia a la fractura y a la deformación junto con una adecuada rigidez y firmeza del material y una reducida densidad (0,05-1 g/cm^3) (13).

La madera es un material complejo formado por celulosa, hemicelulosas y lignina, cuyo contenido en átomos de carbono es de aproximadamente un 50% en peso. Las maderas son materiales anisótropos, es decir, su comportamiento elástico y su resistencia a la deformación son dependientes de la dirección de la carga, siendo mayor en dirección axial que en las direcciones radial y tangencial. Los valores de elasticidad, tenacidad y resistencia dependen de la organización de las unidades básicas de la madera, las células tubulares alargadas (células del esclerénquima) que crecen paralelas a la dirección en la que lo hace el árbol (10, 14, 15).

Las maderas pueden clasificarse en dos grandes grupos: maderas duras de árboles de hoja caduca (angiospermas o dicotiledóneas) y maderas blandas (coníferas o gimnospermas). La selección de la madera precursora determina las propiedades finales de la cerámica biomórfica.

Las maderas duras se caracterizan por poseer una estructura compleja con grandes células de vaso llamadas tráqueas de 0,1 mm de diámetro. Sin embargo, las maderas blandas poseen una microestructura menos complicada con traqueidas o fibras de entre 30 y 50 µm de diámetro, pero sin vasos. Las fibras proporcionan el sistema de

transporte de agua y constituyen más de 90% de su volumen para la mayoría de tipos de madera blanda. Los canales para la circulación de agua y nutrientes, de tamaño y distribución variable en función del precursor natural seleccionado (16), constituyen un excelente medio de transporte para los gases o líquidos empleados en el proceso de conversión de la madera en sistemas cerámicos (13).

Como material de fácil obtención y bajo precio, la madera es el precursor más empleado para la producción de cerámicas (17). Sin embargo, la gran variabilidad interlote de los productos naturales, ha promovido la búsqueda de precursores alternativos, más fácilmente estandarizables, cuyas propiedades puedan controlarse adecuadamente. Así, se han desarrollado cerámicas a partir de fibras de celulosa, tableros de fibra prensada, polvo de resina de madera o pulpa de bambú y estructuras de papel o cartón (8, 10, 13). En ocasiones incluso se han fabricado con productos de desecho, como fibras de coco (13, 18, 19). Cuando se procesan estos materiales, las propiedades mecánicas de las cerámicas se ven empeoradas por la heterogeneidad de las estructuras y la porosidad de la materia prima, cuando ésta es inferior al 40% (18, 20).

1.2.2 **Tipos de cerámicas biomórficas**

La producción de materiales cerámicos a partir de precursores celulósicos ha dado lugar a la obtención de cerámicas biomórficas, cerámicas de madera o cerámicas celulares, denominadas también ecocerámicas ya que su proceso de producción es respetuoso con el medio ambiente (21-23).

Su obtención puede llevarse a cabo mediante procesos de biomineralización por la precipitación de fases inorgánicas (carbonatos, sulfatos o fosfatos) a baja temperatura (< 100 °C), lo que requiere tiempos de síntesis elevados, o producirse a elevada

temperatura mediante la infiltración con líquidos o gases, como por ejemplo Si, SiO_2, y CH_3SiCl_3, que conduce a la obtención de cerámicas de carburo de silicio (14).

En general, el proceso de síntesis de las cerámicas biomórficas a elevada temperatura comienza con el pre-procesamiento (moldeado, secado y pirólisis en atmósfera inerte) del material precursor. El calentamiento de los precursores celulósicos por encima de 600 °C asegura la descomposición de los componentes poliaromáticos de las preformas en componentes volátiles (H_2O, CO_2, ácidos, grupos carbonilo y alcoholes) y la formación de un precursor tridimensional de carbón amorfo que presenta la estructura original de la madera (11, 24, 25).

El precursor puede entonces mineralizarse a través de la infiltración con metales fundidos no reactivos (Mg o Al), con polímeros de baja viscosidad (polietileno, poli cloruro de vinilo, poliamida) o con polímeros precerámicos (polisiloxanos, polisilanos o policarbosilanos). La infiltración con líquidos, silicio o titanio, conduce a la formación de materiales compuestos de carburo/metal en los que la porosidad depende del exceso de líquido retenido en los poros.

A través de la infiltración sol-gel se han obtenido diferentes cerámicas biomórficas oxídicas como TiO_2, ZrO_2 y Al_2O_3 y también no oxídicas como TiC, TiN/C, ZrC, Si-Mo-C (16, 26-28). Todas ellas se caracterizan por poseer una baja densidad, porosidad abierta y una microestructura jerarquizada similar a la del precursor fibroso (27), propiedades que les otorgan gran potencial para diferentes aplicaciones como soportes catalíticos, soportes de filtros o de inmovilización de células vivas, microreactores avanzados, estructuras de aislamiento de calor, humedad y acústica, sensores de temperatura, materiales para blindaje electromagnético y muchos otros procesos para los que se requiera estabilidad a elevada temperatura (12, 29, 30). Entre las posibles aplicaciones de las cerámicas biomórficas, las utilidades en biomedicina han atraído gran

atención en los últimos años, en particular, de aquellas que contienen titanio, de las hidroxiapatitas y de los carburos de silicio.

Las cerámicas biomórficas que contiene titanio se obtienen mediante el tratamiento de diferentes tipos de madera con tetraisopropóxido de titanio, lo que da origen a matrices de titanio con poros orientados en una sola dirección (31).

La hidroxiapatita, que puede ser sintetizada mediante diversos procedimientos a partir de precursores naturales, da lugar a estructuras porosas que presentan buenas perspectivas en el ámbito de la ingeniería tisular ósea, ya que han mostrado la capacidad de estimular la formación de hueso nuevo (32, 33).

A pesar de que el proceso de bioceramización de madera presenta gran versatilidad, una buena parte de la investigación en este área se ha centrado en la producción de cerámicas de carburo de silicio, debido a la sencillez de su proceso de síntesis (19). El desarrollo de métodos rentables para la producción de estas cerámicas no oxídicas, de excelentes propiedades mecánicas y elevada resistencia a la fractura, ofrece nuevas oportunidades para su uso clínico (34).

1.2.3 **Cerámicas biomórficas de carburo de silicio**

El carburo de silicio (SiC) es un material que se encuentra en la naturaleza como el mineral extremadamente raro, moissanita. El polvo de SiC, producido por primera vez en 1893, puede estar presente en dos polimorfos cristalinos; con estructuras cúbicas o hexagonales denominadas β-SiC y α-SiC respectivamente, ambos con diferentes e interesante propiedades ópticas, térmicas y eléctricas (35).

De manera convencional es posible obtener piezas de carburo de silicio con formas específicas mediante diversos procesos; la sinterización o el prensado en caliente, la reacción carbotérmica de SiO_2, el enlazado por reacción, la pirólisis de polímeros o

procesos de deposición química por vapor. Sin embargo, estas elaboraciones suelen requerir temperaturas superiores a 2000 °C y resultan caras, lo que resta utilidad a los materiales para una amplia gama de aplicaciones (36).

En los últimos años se ha abordado el desarrollo de nuevos métodos de producción para obtener cerámicas biomórficas de carburo de silicio con menor consumo energético y por lo tanto menor coste (25, 37). Su porosidad abierta, ligereza y excelentes propiedades mecánicas en flexión y compresión son algunas de las ventajas del carburo de silicio biomórfico (bioSiC) frente al carburo de silicio convencional (38-41).

La Figura 1.2.1 sintetiza las diferentes opciones disponibles para la obtención de cerámicas biomórficas de carburo de silicio; la infiltración con silicio en fase vapor, la reducción carbotérmica y la infiltración con silicio líquido (20). Estos métodos requieren el empleo de altas temperaturas para la conversión de la madera en cerámicas (9, 14) y en todos ellos, la porosidad e interconexión de los poros del precursor determinan el proceso de infiltración (11, 24).

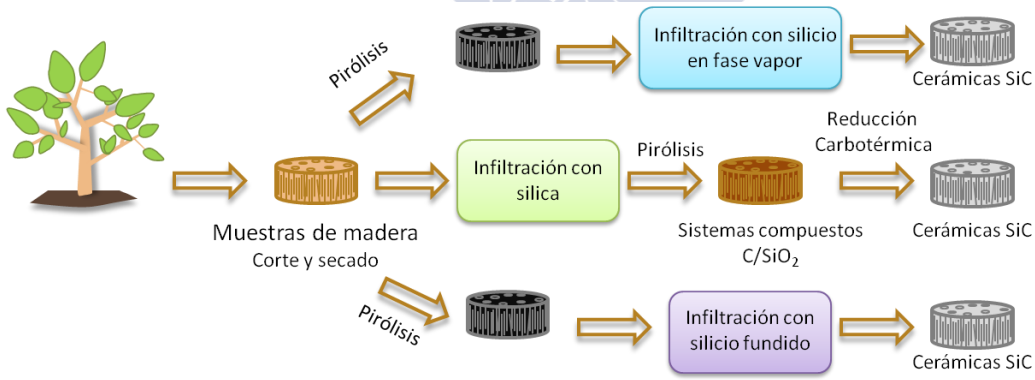

Figura 1.2.1 Métodos de síntesis del carburo de silicio biomórfico (bioSiC) a partir de madera y precursores procesados.

1.2.3.1 *Infiltración con silicio en fase vapor*

Este procedimiento de síntesis es versátil. Las piezas de madera desecadas y moldeadas de la forma apropiada se pirolizan e infiltran con vapor de silicio (Si_7, SiO_8 o CH_3SiCl_3) a elevada temperatura (27, 42). La elección del agente infiltrante permite la obtención de diferentes productos de silicio, como SiC-Si_3N_4, lo que permite además modular la resistencia a la oxidación del material (43, 44). Sin embargo, su principal inconveniente es la fuente de obtención del silicio, la descomposición de precursores metalorgánicos (45), lo que implica el empleo de altas temperaturas y largos procesos (26, 46).

1.2.3.2 *Reducción carbotérmica*

Cuando se emplea este procedimiento, las piezas de madera se infiltran con dióxido de silicio (SiO_2) y posteriormente se pirolizan. El SiO_2 puede ser obtenido directamente por una infiltración con silica gel o por el empleo de otros reactivos. Para la obtención del material deseado es necesario llevar a cabo varios ciclos de infiltración-pirólisis. El proceso se finaliza mediante una reducción carbotérmica a temperaturas superiores a 1000 °C de los precursores infiltrados y pirolizados. Este procedimiento da lugar a materiales principalmente formados por fase β-SiC (47) aunque la obtención de materiales puros SiC frecuentemente requiere tratamientos térmicos adicionales a temperaturas muy superiores debido a la formación de fases intermedias (48). La formación del carburo de silicio está determinada principalmente por las reacciones en fase de vapor, dando lugar a materiales de menor resistencia que los obtenidos por infiltración de silicio líquido (15).

Con el fin de mejorar los resultados de este procedimiento se han realizado diferentes estudios centrados en el control del vacío y/o de la presión durante la impregnación sol-gel con SiO_2 o en el uso de fluidos supercríticos (12, 45).

La infiltración sol-gel puede realizarse también utilizando otros reactivos, como tetraetilortosilicato (TEOS), poli(metilfenilvinilsilsesquioxano) (PMPVS), poli(metilhidrosiloxano) (PMHS) o poli(carbometilsilano) (PCMS) (27, 49, 50).

Este método es sencillo y de bajo coste, lo que constituye sus principales ventajas.

1.2.3.3 *Infiltración con silicio líquido (LSI)*

Según este procedimiento, las cerámicas biomórficas de carburo de silicio (bioSiCs) se fabrican mediante un proceso en dos etapas; una pirólisis controlada de la madera en atmósfera inerte, normalmente argón, seguida por una infiltración reactiva rápida y también controlada con silicio fundido a una temperatura superior al punto de fusión del silicio (1.410 °C) (36, 51-53).

$$C(s) + Si(l) \rightarrow \beta\text{-}SiC$$

Ecuación 1.2.1 Reacción química durante la síntesis de carburo de silicio mediante la infiltración con silicio líquido (14).

El material final está formado principalmente por β-SiC y silicio libre en la superficie de los poros, pero también puede contener algunos elementos traza como Al, S, B, Na (9, 14). El contenido medio de silicio se sitúa entre el 20 y el 30% (14).

La mayor parte de la pérdida de peso de la madera durante el proceso de pirólisis se lleva a cabo por encima de 500 °C. El uso de temperaturas superiores durante esta etapa promueve cambios estructurales, disminuyendo el tamaño de poro de la preforma de carbón y dificultando la posterior infiltración (54).

Las características de las maderas precursoras seleccionadas modulan la microestructura de la preforma de carbón y ésta a su vez condiciona el proceso de infiltración de silicio, ya que determina las fuerzas capilares y su cinética. Además, las

propiedades de la superficie del carbón influyen en el ángulo de contacto y la humectación con el silicio líquido. Por otra parte, la infiltración del carbón en la dirección axial favorece la conversión a carburo de silicio debido al transporte del fundido a través de los canales naturales del molde (20). Así, se obtiene una buena transmisibilidad de la microestructura entre la original de la madera, la del carbón vegetal y la de la cerámica de SiC final (55).

El silicio fundido interacciona con la preforma de carbón dando lugar a una reacción exotérmica espontánea que disuelve el carbón generando grupos Si-C que cristalizan. Si no hay suficiente silicio para disolver el carbón, la capa inicial de carburo de silicio formada inhibe las reacciones adicionales entre Si y C, y la formación de carburo de silicio posterior depende de un proceso de difusión, cuya importancia es alta a temperaturas superiores al punto de fusión del silicio. Este mecanismo explica las características microestructurales observadas en las muestras de carburo de silicio obtenidas (36, 56). Durante el proceso de infiltración, los poros de menor tamaño son eliminados debido a la expansión de volumen del 58% que se genera tras la cristalización del carburo de silicio (54).

Las condiciones en las que se produce el proceso de infiltración, además de la naturaleza del precursor, determinan la presencia de carbón residual que afectará negativamente a las propiedades de la cerámica (16, 52, 57). Por ello se han explorado diferentes opciones, como el uso de la radiación ultrasónica, con el fin de mejorar el proceso de infiltración y, por lo tanto, las propiedades finales de los materiales obtenidos (49).

La amplia variedad de maderas existente ofrece la posibilidad de producir cerámicas de carburo de silicio biomórfico con diferentes microestructuras tridimensional y propiedades a medida (densidad, porosidad abierta, interconectividad, resistencia a la fractura...) para la aplicación requerida (36, 37).

El método de infiltración con silicio líquido presenta diferentes ventajas para la producción de cerámicas biomórficas de carburo de silicio con respecto a los demás procedimientos (8, 52, 56-58):

- Resulta respetuoso con el medio ambiente ya que usa materiales renovables y el proceso es poco contaminante.
- Sus requerimientos energéticos y térmicos (reacción exotérmica) son reducidos.
- No precisa aditivos adicionales.
- El procedimiento es rápido y de bajo coste.

El carburo de silicio es químicamente inerte, no reabsorbible y extremadamente resistente a la corrosión y a la erosión. Los carburos de silicio son materiales semiconductores tanto térmica como eléctricamente (2.36 y 3.05 eV para β- y α-SiC, respectivamente). En general, las cerámicas de carburo de silicio son duras y resistentes, tanto a temperatura ambiente como a temperaturas superiores, y presentan buenas propiedades tribológicas (19, 59, 60). Su erosión se produce mediante la formación y propagación de grietas laterales y radiales.

La variabilidad observada en las propiedades de los carburos de silicio biomórficos se explica en función del material precursor y el proceso de fabricación empleado (temperatura de procesado, tiempo de reacción, relación C/Si empleada), ya que estos determinan su composición final, su microestructura (porosidad, morfología y distribución de tamaño de poro), su anisotropía y su densidad (8, 41).

Los efectos de cada variable implicada en su proceso de elaboración sobre sus propiedades se detallan a continuación:

1.2.3.3.1 Materia prima

La disposición de las células vegetales en la madera, conformando tráqueas o traqueidas, determina la microestructura del carburo de silicio biomórfico (17, 61). La densidad final de los bioSiCs que oscila entre 1,1 y 2,6 g/cm^3 (62) es también extremadamente dependiente de la madera precursora, habiéndose encontrado una relación lineal entre ambos parámetros (58):

$$\rho SiC=(2,39\mp0,01)\rho Wood \qquad R^2= 0,99$$

Ecuación 1.2.2 Relación entre la densidad de la madera precursora y la densidad de bioSiC.

El empleo de maderas y procesados de elevada densidad (madera de cedro prensada de alta densidad o tablones de alta densidad) conduce a muestras con una resistencia a la compresión dos veces superior a las obtenidas a partir de moldes de baja densidad (paulonia) (25).

El carburo de silicio biomórfico, presenta la anisotropía del material de partida, es decir, sus propiedades son también diferentes en dirección axial respecto a las direcciones radial o tangencial, aunque no de forma tan marcada como en la madera original. Estas diferencias son particularmente importantes en lo que se refiere a las características mecánicas y eléctricas (37, 63).

En las cerámicas biomórficas, a diferencia de sus maderas precursoras, la deformación en dirección axial no sólo depende de la compresión axial de las paredes celulares de la madera y en la compresión tangencial, la deformación no es sólo debida a la flexión plástica de las paredes celulares. Los sistemas cerámicos finales son complejos y su comportamiento no solamente está condicionado por las estructuras celulares implicadas (63).

La resistividad eléctrica del bioSiC aumenta con el contenido de silicio residual en dirección axial, mientras que en la dirección tangencial, este fenómeno no se observa (64).

El carácter anisotrópico mecánico de las muestras de carburo de silicio se puede modular mediante la infiltración con mezclas fundidas de Al_3-Si_9-Mg, obteniendo carburos de silicio compuestos, reforzados de aluminio, que presentan una mejor resistencia transversal a la compresión y una mayor rigidez (16).

1.2.3.3.2 Relación Si/C empleada

La relación inicial entre Si y C es un parámetro crítico durante el proceso de producción. Cuanto mayor es la cantidad de silicio respecto a la de carbón, más elevada es la proporción de SiC/C en el producto final, y por lo tanto, la densidad, la dureza y la resistencia mecánica del material obtenido (65).

Índices Si/C por debajo de 2,33 dan lugar a cerámicas con poros vacíos. La formación de cristales de carburo de silicio obturan los poros de la preforma de carbón y reducen la porosidad. Así, proporciones superiores a 2,33, dan lugar a materiales con poros parcial o completamente obturados con silicio residual (11, 66). Cuando la proporción de Si/C es mayor que tres, las cerámicas biomórficas obtenidas están formadas por SiC y Si residual y no presentan carbón sin reaccionar (26).

La cantidad de silicio residual condiciona, entre otras, las propiedades eléctricas del bioSiC, especialmente a temperaturas entre -268 y 228 °C. En este rango, el Si residual constituye una red interconectada, responsable de su comportamiento metálico. Este efecto no se observa a temperaturas superiores a 228 °C, en las que el bioSiC se convierte en un material semiconductor como consecuencia de la mayor contribución del carburo de silicio (37).

El exceso de silicio residual puede ser eliminado mediante su tratamiento con ácidos, usando una solución de ácido fluorhídrico (HF) y ácido nítrico (HNO_3) en una relación molar de 1,66 en agua. Controlada mediante un mecanismo de difusión, se lleva a cabo la reacción estequiométrica siguiente (67):

$$3Si + 12HF + 4HNO_3 \longrightarrow 3SiF_4 + 4NO + 8H_2O$$

Ecuación 1.2.3 Reacción estequiométrica de eliminación de silicio mediante tratamiento ácido.

El tiempo de tratamiento ácido determina el silicio residual y la aparición de poros que actúan como núcleos de formación de grietas. Tiempos de tratamiento extensos, mejoran la interconectividad de las muestras (68). Esta reacción también depende de la anisotropía y la porosidad de la muestra, siendo más rápida en la dirección axial y obteniéndose diferentes coeficientes de difusión eficaz en función de la porosidad.

1.2.3.3.3 Temperatura de procesado

La temperatura de procesado condiciona el proceso de infiltración de silicio y el tipo de producto final obtenido. A temperaturas alrededor de 1.550 °C se obtiene la forma β-SiC, mientras que entre 2.200 y 2.500 °C se producen los politipos hexagonales (α-SiC) (11, 66). Se ha demostrado que los bioSiCs producidos a altas temperaturas, son muy densos y tienen una elevada resistencia a la deformación (9).

1.2.3.3.4 Tiempo de reacción

El tiempo de reacción contribuye, al igual que la proporción Si/C utilizada, a la modulación de la relación entre el SiC y C en los materiales finales. A medida que el tiempo se incrementa, el porcentaje de carbón residual disminuye, y paralelamente, la porosidad del material y su resistencia a la fractura (26). El tiempo de reacción optimo

depende de la estructura porosa de la preforma de carbón, así como del tamaño del material infiltrado y de la temperatura empleada.

1.2.4 **Aplicaciones del carburo de silicio biomórfico**

Las cerámicas de carburo de silicio biomórfico poseen excelentes propiedades mecánicas y de resistencia a la oxidación, la corrosión, la temperatura y el desgaste que las hacen adecuadas para su empleo en aplicaciones de ingeniería avanzada, así como para el desarrollo de nuevos materiales con fines biomédicos (56).

1.2.4.1 *Soportes catalíticos*

Debido a su estructura porosa, los bioSiCs se han mostrado útiles como soportes catalíticos de níquel para la oxidación parcial de metano en la producción de gas de síntesis y también para la oxidación selectiva de H_2S, el tratamiento de gases de escape para motores de trabajo pesado y la deshidrogenación de n-butano. Además, su recubrimiento con zeolita permite incrementar la utilidad para esta aplicación, ya que ésta presenta una elevada superficie específica que contribuye positivamente a los procesos de adsorción, separación y catálisis (69).

1.2.4.2 *Refuerzo cerámico en hormigones*

El refuerzo de hormigones con partículas en forma de aguja de carburo de silicio es una forma efectiva para mejorar sus propiedades mecánicas mostrando, desde un punto de vista mecánico, resultados similares al refuerzo con filamentos metálicos pero con una mayor estabilidad química tras el proceso de curado (56, 70).

1.2.4.3 *Aplicaciones de alta temperatura*

Los bioSiCs se pueden emplear en el desarrollo de motores avanzados y como componentes estructurales de intercambiadores de calor (44, 49). Con el fin de

mejorar su conductividad térmica se puede obtener compuestos de cobre-carburo silicio, de forma que se combine, en un único material, la elevada conductividad térmica del cobre y el bajo coeficiente de expansión térmica del carburo de silicio, abriendo nuevas posibilidades para las aplicaciones de gestión térmica (54).

La capacidad de las cerámicas de silicio covalentes (SiC, Si_3N_4...) para formar una capa de óxido superficial (SiO_2) con una baja permeabilidad al oxígeno hace posible la obtención de materiales cuya resistencia a la oxidación es la más elevada de entre las cerámicas no oxídicas (41, 44, 49).

1.2.4.4 *Sistemas de filtración*

La microestructura de los carburos de silicio biomórfico los hace adecuados como materiales de filtración para la limpieza de gases en caliente en la industria de generación de energía eléctrica, donde se necesitan como principales características, una baja emisión y una elevada eficiencia. Para estas aplicaciones, se han propuesto como los más adecuados los obtenidos a partir de tablones de densidad media, con tiempos cortos de reacción (71).

1.2.4.5 *Aplicaciones biomédicas*

El carburo de silicio se ha propuesto como material de recubrimiento de dispositivos biomédicos (stents coronarios, válvulas) ya que es capaz de incrementar su hemocompatibilidad mediante la reducción de su trombogenicidad y de la respuesta inflamatoria (72-74). En los últimos años, el carburo de silicio se ha probado como material útil para el diseño y desarrollo de nuevos dispositivos biomédicos como membranas, agentes de diagnóstico por imagen y biosensores. Además, es particularmente interesante su potencial aplicación como biomaterial en implantes ortopédicos (59).

El hueso es un tejido complejo formado por una estructura jerárquica responsable de sus propiedades mecánicas. Se han producido numerosos desarrollos tecnológicos dirigidos a la producción de biomateriales artificiales, capaces de mimetizar la estructura ósea, que tras ser implantados, garanticen una adecuada osteoconducción y restauren la funcionalidad del tejido.

La búsqueda del perfecto andamio óseo se ha basado en un enfoque biomimético, la simulación de la composición química del hueso y/o su morfología para promover la estimulación de las células osteoblásticas. En este sentido, la macroporosidad y las propiedades de carga son cruciales. En general, los materiales organizados jerárquicamente, capaces de lograr una transmisión adecuada de las cargas mecánicas, presentan una buena osteoconductividad y promueven la osteointegración (75).

Las cerámicas biomórficas, cuya estructura mimetiza la de sus precursores naturales resultan materiales muy prometedores en el campo de la ingeniería de tejido óseo y medicina regenerativa (76). Como puede observarse en la Figura 1.2.2, existen importantes similitudes entre las estructuras óseas y las de los tejidos vegetales empleados en su producción.

En particular, el carburo de silicio biomórfico presenta indudables ventajas para este fin. Su porosidad interconectada, su fácil moldeado y su alta resistencia y tenacidad (8, 77) los convierten en candidatos potenciales para el desarrollo de prótesis que requieren el soporte de carga y simultáneamente, la difusión de nutrientes y productos de desecho (76). En estos casos, la porosidad de los materiales es un aspecto crucial. Los requisitos de porosidad total y/o tamaño de poro óptimos para una adecuada regeneración ósea, constituyen aspectos que no han sido completamente dilucidados (78, 79). Algunos autores han señalado que el tamaño de poro adecuado para facilitar la vascularización y el crecimiento óseo en su interior es de 100 μm, pero no se han establecido los requerimientos mínimos para asegurar la migración de los tipos de

células implicadas y la síntesis de matriz extracelular. La enorme variedad de recursos naturales disponibles como precursores debe permitir, sin duda, la selección de los más apropiados (80).

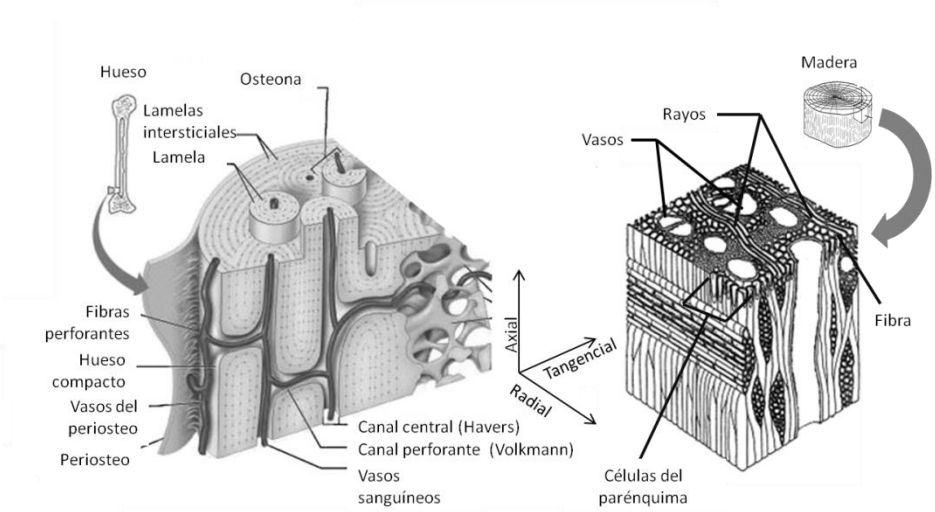

Figura 1.2.2 Comparación de la morfología ósea y la del tejido vegetal. Adaptado de (10, 75).

Con el fin de evitar la pérdida de masa ósea e incrementar la osteointegración es necesario también seleccionar cerámicas biomórficas de carburo de silicio con valores de rigidez a la compresión en el intervalo de 10 a 100 GPa, capaces de imitar las propiedades del hueso cortical humano (68).

Las excelentes propiedades tribológicas del carburo de silicio minimizan la probabilidad de generar productos de degradación del material, uno de los principales inconvenientes asociados a la utilización de materiales artificiales como sistemas implantables en el organismo. Su elevada resistencia a la corrosión en condiciones biológicas normales, reduce su velocidad de disolución a valores inferiores a 30 nm por año, lo que debe hacer posible el mantenimiento de sus propiedades mecánicas durante

largos períodos de tiempo tras su implantación asegurando la funcionalidad del tejido (59).

Los carburos de silicio biomórficos obtenidos a partir de diferentes orígenes han mostrado excelente biocompatibilidad (35, 80) sobre líneas celulares de osteoblastos (MG-63) y preosteoblastos (MC3T3-E1). Tras 24 horas de cultivo, las células osteoblásticas formaron una monocapa sobre la superficie de los biomateriales. Las células preosteoblásticas generaron, tras 28 días de ensayo, una matriz extracelular mineralizada (35). Por otra parte, la topografía superficial de algunos bioSiCs obtenidos a partir de precursores marinos (*Juncus maritimus*), condiciona físicamente el crecimiento de células preosteoblásticas de forma alineada sobre los canales nanométricos orientados de estas cerámicas (80).

La biocompatibilidad de estos materiales también ha sido evaluada *in vivo*. Los bioSiCs, implantados en el cóndilo del fémur de conejos, no promovieron reacciones adversas, ni el crecimiento de tejido fibroso, después de 12 semanas tras la cirugía (81, 82).

Las cerámicas de carburo de silicio no son bioactivas. Con el fin de dotar de esta propiedad a las potenciales prótesis, se han evaluado diferentes técnicas (deposición electroforética o con laser pulsado, tratamientos ácidos…) dirigidas a la modificación de sus características superficiales mediante recubrimientos con vidrios bioactivos o hidroxiapatita o la alteración de su composición superficial (83-87). El recubrimiento con vidrios bioactivos mejora la bioactividad promoviendo la formación de una capa de apatita tras 72 horas de inmersión en fluido corporal simulado (86, 87). Además, los sistemas recubiertos mantienen su biocompatibilidad, permitiendo el crecimiento celular adecuado y la adhesión de osteoblastos (MG-63) después de 24 horas de cultivo (83, 84, 88, 89).

Los tratamientos ácidos eliminan grupos Si de la superficie del material y promueven la producción de grupos $–COO^-$ capaces de reaccionar con calcio y generar una capa de hidroxiapatita cuando se sumergen en fluido corporal simulado. Este tipo de activación puede dar lugar a materiales adecuados para reemplazar hueso esponjoso (89).

La combinación de carburos de silicio biomórficos con otros materiales, permite el planteamiento de nuevas aplicaciones. En este sentido se han ensayado combinaciones de bioSiC y colágeno. Los sistemas elaborados son complejos, presentando una estructura central de fibras de colágeno electrodepositadas y mineralizadas, y una parte externa de carburo de silicio biomórfico obtenido de madera de sapelli. La implantación de andamios de carburo de silicio-colágeno ha permitido la reparación de defectos óseos *in vivo* en modelo animal de oveja, observándose una adecuada regeneración del tejido óseo y la formación de hueso nuevo con un área de contacto hueso-implante adecuada (90).

Los trabajos realizados hasta el momento con los carburos de silicio biomórfico, y en particular, los estudios *in vivo*, ponen de manifiesto el importante potencial de estas cerámicas como sustitutos óseos y dentales. Sin embargo, se desconocen algunos aspectos importantes como las posibilidades de modular su comportamiento mediante la selección de una microestructura concreta o la potencialidad de estos materiales para cargar y ceder moléculas terapéuticas, de conocido efecto sinérgico en la regeneración de tejido óseo (91).

La posibilidad de convertir los carburos de silicio biomórficos en materiales biofuncionales, con un elevado potencial en el tratamiento y la profilaxis de defectos óseos y/o patologías, requiere un conocimiento en profundidad de estos aspectos y justifican trabajos de investigación en este campo de conocimiento que tengan como objeto dichos materiales.

1.2.5 **Referencias**

1. Hench Larry L. An introduction to bioceramics. 2ª ed. Imperial College Press; 2013.

2. Guelcher SA, Hollinger JO. An introduction to biomaterials. Guelcher SA y Hollinger JO, editores. Florida: CRC-Taylor & Francis; 2006.

3. Kokubo Tadashi. Bioceramics and their clinical applications. 1ª ed. Kokubo Tadashi, editor. Cambridge: Woodhead Publiching Limited and CRC Press LLC; 2008.

4. Ratner B. Biomaterials science: an introduction to materials in medicine. 2ª ed. Ratner B, editor. Amsterdam: Elsevier Academic Press; 2004.

5. Park Joon B., Bronzino Joseph D. Biomaterials principles and applicactions. Park Joon B. and Bronzino Joseph D., editores. Florida: CRC Press LLC; 2003.

6. Park J, Lakes RS. Biomaterials an introduction. 3ª ed. Park J and Lakes RS, editores. New York: Springer; 2007.

7. Blitterswijk C, Thomsen P, Lindahl A, Hubbell JA, Williams D, Cancedda R, et al. Tissue engineering. 1st Ed ed. Blitterswijk C editor. London: Academic Press: Elsevier; 2008.

8. de Arellano-Lopez AR, Martinez-Fernandez J, Gonzalez P, Dominguez C, Fernandez-Quero V, Singh M. Biomorphic SiC: A new engineering ceramic material. Int J Appl Ceram Technol. 2004;1(1):56-67.

9. Cano Pavon JM, Vereda Alonso E, Siles Cordero MT, Garcia de Torres A, Lopez-Cepero JM. Use of spectroscopic techniques for the chemical analysis of biomorphic silicon carbide ceramics. Anal Chim Acta. 2005;528(1):129-34.

10. Greil P, Lifka T, Kaindl A. Biomorphic cellular silicon carbide ceramics from wood: II. mechanical properties. J Eur Ceram Soc. 1998;18(14):1975-83.

11. Yukhymchuk VO, Kiselev VS, Belyaev AE, Chursanova MV, Danailov M, Valakh MY. Synthesis, morphological and structural properties of bio-SiC ceramics. Funct Mater. 2010;17(4):520-7.

12. Li J, Ma H, Chi Z. Preparation of biomorphic SiC/C ceramics from pine wood via supercritical ethanol infiltration. Acta Geol Sin (Engl Ed). 2007;81(4):674-9.

13. Greil P, Vogli E, Fey T, Bezold A, Popovska N, Gerhard H, et al. Effect of microstructure on the fracture behavior of biomorphous silicon carbide ceramics. J Eur Ceram Soc. 2002;22(14-15):2697-707.

14. Greil P, Lifka T, Kaindl A. Biomorphic cellular silicon carbide ceramics from wood: I. processing and microstructure. J Eur Ceram Soc. 1998;18(14):1961-73.

15. Zhurinsh A, Locs J, Berzina-Cimdina L. Investigation of the feasibility of pyrolytic obtaining of porous biomorphic SiC ceramics. J Anal Appl Pyrolysis. 2009;85(1+2):544-8.

16. Wilkes TE, Young ML, Sepulveda RE, Dunand DC, Faber KT. Composites by aluminum infiltration of porous silicon carbide derived from wood precursors. Scr Mater. 2006;55(12):1083-6.

17. Gordic M, Bucevac D, Ruzic J, Gavrilovic S, Hercigonja R, Stankovic M, et al. Biomimetic synthesis and properties of cellular SiC. Ceram Int. 2014;40(2):3699-705.

18. Maity A, Kalita D, Kayal N, Ghosh J, Goswami T, Chakrabarti O, et al. Microstructural and mechanical characterisation of biomorphic SiC ceramics synthesised from coir fibreboard preform. Mater Sci Eng, A. 2013;565:72-9.

19. Maity A, Kalita D, Kayal N, Goswami T, Chakrabarti O, Gangadhar Rao P. Synthesis of biomorphic SiC ceramics from coir fibreboard preform. Ceram Int. 2012;38(8):6873-81.

20. Calderon NR, Martinez-Escandell M, Narciso J, Rodriguez-Reinoso F. Manufacture of biomorphic SiC components with homogeneous properties from sawdust by reactive infiltration with liquid silicon. J Am Ceram Soc. 2010;93(4):1003-9.

21. Kardashev BK, Smirnov BI, de Arellano-Lopez AR, Martinez-Fernandez J, Varela-Feria FM. Elastic and anelastic properties of SiC/Si ecoceramics. Mater Sci Eng, A. 2006;A442(1-2):444-8.

22. Munoz A, Martinez Fernandez J, Singh M. High temperature compressive mechanical behavior of joined biomorphic silicon carbide ceramics. J Eur Ceram Soc. 2002;22(14-15):2727-33.

23. Qian J, Jin Z. Preparation and characterization of porous, biomorphic SiC ceramic with hybrid pore structure. J Eur Ceram Soc. 2006;26(8):1311-6.

24. Wang Q, Jin G, Wang D, Guo X. Biomorphic porous silicon carbide prepared from carbonized millet. Mater Sci Eng, A. 2007;A459(1-2):1-6.

25. Lee DJ, Jang JJ, Park HS, Kim YC, Lim KH, Park SB, et al. Fabrication of biomorphic SiC composites using wood preforms with different structures. Ceram Int. 2012;38(4):3089-95.

26. Hou G, Jin Z, Qian J. Effect of holding time on the basic properties of biomorphic SiC ceramic derived from beech wood. Mater Sci Eng, A. 2007;A452-A453:278-83.

27. Vogli E, Sieber H, Greil P. Biomorphic SiC-ceramic prepared by si-vapor phase infiltration of wood. J Eur Ceram Soc. 2002;22(14-15):2663-8.

28. Hou G, Jin Z, Qian J. Effect of starting si contents on the properties and structure of biomorphic SiC ceramics. J Mater Process Technol. 2007;182(1-3):34-8.

29. Qian J, Wang J, Jin Z. Preparation of biomorphic SiC ceramic by carbothermal reduction of oak wood charcoal. Mater Sci Eng, A. 2004;A371(1-2):229-35.

30. Qian J, Wang J, Jin Z. Preparation and properties of porous microcellular SiC ceramics by reactive infiltration of si vapor into carbonized basswood. Mater Chem Phys. 2003;82(3):648-53.

31. Ota T, Imaeda M, Takase H, Kobayashi M, Kinoshita N, Hirashita T, et al. Porous titania ceramic prepared by mimicking silicified wood. J Am Ceram Soc. 2000;83(6):1521-3.

32. Qian J, Kang Y, Zhang W, Li Z. Fabrication, chemical composition change and phase evolution of biomorphic hydroxyapatite. J Mater Sci: Mater Med. 2008;19(11):3373-83.

33. Tampieri A, Sprio S, Ruffini A, Celotti G, Lesci IG, Roveri N. From wood to bone: Multi-step process to convert wood hierarchical structures into biomimetic hydroxyapatite scaffolds for bone tissue engineering. J Mater Chem. 2009;19(28):4973-80.

34. Chevalier J, Gremillard L. Ceramics for medical applications: A picture for the next 20 years. J Eur Ceram Soc. 2009;29(7):1245-55.

35. Lopez-Alvarez M, de Carlos A, Gonzalez P, Serra J, Leon B. Cytocompatibility of bio-inspired silicon carbide ceramics. J Biomed Mater Res, Part B. 2010;95B(1):177-83.

36. Varela-Feria FM, Ramirez-Rico J, Arellano-Lopez AR, Martinez-Fernandez J, Singh M. Reaction-formation mechanisms and microstructure evolution of biomorphic SiC. J Mater Sci. 2008;43(3):933-41.

37. Orlova TS, Popov VV, Quispe Cancapa J, Hernandez Maldonado D, Enrique Magarino E, Varela Feria FM, et al. Electrical properties of biomorphic SiC ceramics and SiC/Si composites fabricated from medium density fiberboard. J Eur Ceram Soc. 2011;31(7):1317-23.

38. Lusquinos F, Pou J, Quintero F, Perez-Amor M. Laser cladding of SiC/Si composite coating on Si-SiC ceramic substrates. Surf Coat Technol. 2008;202(9):1588-93.

39. Zawrah MF, El-Gazery M. Mechanical properties of SiC ceramics by ultrasonic nondestructive technique and its bioactivity. Mater Chem Phys. 2007;106(2-3):330-7.

40. Singh M, Salem JA. Mechanical properties and microstructure of biomorphic silicon carbide ceramics fabricated from wood precursors. J Eur Ceram Soc. 2002;22(14-15):2709-17.

41. Lee D, Kim YC, Adeel Umer M, Lim KH, Park SB, Hong SH. Oxidation behavior and ablation properties of MDF-based biomorphic SiC composites. Ceram Int. 2013;39(7):7475-81.

42. Egelja A, Gulicovski J, Devecerski A, Babic B, Miljkovic M, Boskovic S, et al. Synthesis of biomorphic SiC and SiO2 ceramics. J Serb Chem Soc. 2008;73(7):745-51.

43. Luo M, Hou G, Yang J, Fang J, Gao J, Zhao L, et al. Manufacture of fibrous α-Si_3N_4-reinforced biomorphic SiC matrix composites for bioceramic scaffold applications. Mater Sci Eng, C. 2009;29(4):1422-7.

44. Ghanem H, Alkhateeb E, Gerhard H, Popovska N. Oxidation behavior of silicon carbide based biomorphic ceramics prepared by chemical vapor infiltration and reaction technique. Ceram Int. 2009;35(7):2767-74.

45. Locs J, Berzina-Cimdina L, Zhurinsh A, Loca D. Optimized vacuum/pressure sol impregnation processing of wood for the synthesis of porous, biomorphic SiC ceramics. J Eur Ceram Soc. 2009;29(8):1513-9.

46. Vereda Alonso E, Garcia de Torres A, Siles Cordero MT, Cano Pavon JM. Quantitative determinations of SiC and SiO_2 in new ceramic materials by fourier transform infrared spectroscopy. Talanta. 2008;75(2):424-31.

47. Egelja A, Gulicovski J, Devecerski A, Ninic M, Radosavljevic-Mihajlovic A, Matovic B. Preparation of biomorphic SiC ceramics. Sci Sintering. 2008;40(2):141-5.

48. Rambo CR, Cao J, Rusina O, Sieber H. Manufacturing of biomorphic (si,ti,zr)-carbide ceramics by sol-gel processing. Carbon. 2005;43(6):1174-83.

49. Church TL, Fallani S, Liu J, Zhao M, Harris AT. Novel biomorphic Ni/SiC catalysts that enhance cellulose conversion to hydrogen. Catal Today. 2012;190(1):98-106.

50. Singh M, Salem JA. Mechanical properties and microstructure of biomorphic silicon carbide ceramics fabricated from wood precursors. J Eur Ceram Soc. 2002;22(14-15):2709-17.

51. Vereda Alonso E, Garcia de Torres A, Siles Cordero MT, Cano Pavon JM. Quantitative determinations of SiC and SiO_2 in new ceramic materials by fourier transform infrared spectroscopy. Talanta. 2008;75(2):424-31.

52. Presas M, Pastor JY, Llorca J, De Arellano-Lopez AR, Martinez-Fernandez J, Sepulveda R. Microstructure and mechanical properties of biomorphic SiC obtained from eucalyptus. Bol Soc Esp Ceram Vidrio. 2005;44(6):363-7.

53. Wang Y, Jin G, Guo X. Growth of ZSM-5 coating on biomorphic porous silicon carbide derived from durra. Microporous Mesoporous Mater. 2009;118(1-3):302-6.

54. Pappacena KE, Johnson MT, Xie S, Faber KT. Processing of wood-derived copper-silicon carbide composites via electrodeposition. Compos Sci Technol. 2010;70(3):485-91.

55. Qiao G, Ma R, Cai N, Zhang C, Jin Z. Mechanical properties and microstructure of Si/SiC materials derived from native wood. Mater Sci Eng, A. 2002;A323(1-2):301-5.

56. Zhu D, Gao M, Zhang S, Wu H, Pan Y, Liu Y, et al. A high-strength SiCw/SiC-Si composite derived from pyrolyzed rice husks by liquid silicon infiltration. J Mater Sci. 2012;47(12):4921-7.

57. Kaul VS, Faber KT, Sepulveda R, de Arellano Lopez AR, Martinez-Fernandez J. Precursor selection and its role in the mechanical properties of porous SiC derived from wood. Mater Sci Eng, A. 2006;A428(1-2):225-32.

58. Varela-Feria FM, Martinez-Fernandez J, de Arellano-Lopez AR, Singh M. Low density biomorphic silicon carbide: Microstructure and mechanical properties. J Eur Ceram Soc. 2002;22(14-15):2719-25.

59. Mahmoodi M, Ghazanfari L. Fundamentals of biomedical applications of biomorphic SiC. Prop Appl Silicon Carbide. 2011:297-343.

60. Leventis N, Sadekar A, Chandrasekaran N, Sotiriou-Leventis C. Click synthesis of monolithic silicon carbide aerogels from polyacrylonitrile-coated 3D silica networks. Chem Mater. 2010;22(9):2790-803.

61. Martinez Fernandez J, Munoz A, de Arellano Lopez AR, Valera Feria FM, Dominguez-Rodriguez A, Singh M. Microstructure-mechanical properties correlation in siliconized silicon carbide ceramics. Acta Mater. 2003;51(11):3259-75.

62. Gonzalez P, Borrajo JP, Serra J, Liste S, Chiussi S, Leon B, et al. Extensive studies on biomorphic SiC ceramics properties for medical applications. Key Eng Mater. 2004;254-256(Bioceramics):1029-32.

63. Martinez-Fernandez J, Valera-Feria FM, Singh M. High-temperature compressive mechanical behavior of biomorphic silicon carbide ceramics. Scr Mater. 2000;43(9):813-8.

64. Orlova TS, Smirnov BI, de Arellano-Lopez AR, Martinez Fernandez J, Sepulveda R. Anisotropy of electric resistivity of sapele-based biomorphic SiC/Si composites. Phys Solid State. 2005;47(2):229-32.

65. Gutierrez-Mora F, Goretta KC, Varela-Feria FM, Lopez ARA, Fernandez JM. Indentation hardness of biomorphic SiC. Int J Refract Met Hard Mater. 2005;23(4-6):369-74.

66. Yukhymchuk VO, Kiselov VS, Belyaev AE, Valakh MY, Chursanova MV, Danailov M, et al. Raman spectroscopy of bio-SiC ceramics. Phys Status Solidi A. 2011;208(4):808-13.

67. Robledo MJL, Ferrer RES, Leon AB, Fernandez JM, De Arellano Lopez AR. Mechanical properties of porous biomorphic SiC. Bol Soc Esp Ceram Vidrio. 2005;44(5):318-23.

68. Torres-Raya C, Hernandez-Maldonado D, Ramirez-Rico J, Garcia-Ganan C, de Arellano-Lopez AR, Martinez-Fernandez J. Fabrication, chemical etching, and compressive strength of porous biomimetic SiC for medical implants. J Mater Res. 2008;23(12):3247-54.

69. Wang Q, Sun W, Jin G, Wang Y, Guo X. Biomorphic SiC pellets as catalyst support for partial oxidation of methane to syngas. Appl Catal, B. 2008;79(4):307-12.

70. Sepulveda R, Robledo MJL, de Arellano Lopez AR, Fernandez JM, Dominguez C. Application of biomorphic SiC as a structural reinforcement in refractory concretes. Bol Soc Esp Ceram Vidrio. 2005;44(5):357-62.

71. Bautista MA, Cancapa JQ, Fernandez JM, Rodriguez MA, Singh M. Microstructural and mechanical evaluation of porous biomorphic silicon carbide for filtering applications in high temperature gasification processes. J Eur Ceram Soc. 2011;31(7):1325-32.

72. Okpalugo TIT, Ogwu AA, Maguire PD, McLaughlin JAD, Hirst DG. In-vitro blood compatibility of α-C:H:Si and α-C:H thin films. Diamond Relat Mater. 2004;13(4-8):1088-92.

73. Babapulle MN, Eisenberg MJ. Coated stents for the prevention of restenosis: Part I. Circulation. 2002;106(21):2734-40.

74. Li M, Cheng Y, Zheng YF, Zhang X, Xi TF, Wei SC. Surface characteristics and corrosion behaviour of WE43 magnesium alloy coated by SiC film. Appl Surf Sci. 2012;258(7):3074-81.

75. Sprio S, Ruffini A, Valentini F, D'Alessandro T, Sandri M, Panseri S, et al. Biomimesis and biomorphic transformations: New concepts applied to bone regeneration. J Biotechnol. 2011;156(4):347-55.

76. Lopez-Alvarez M, Gonzalez P, Serra J, de Carlos A, Chiussi S, Leon B. Innovative bioinspired SiC ceramics from vegetable resources. En: Khang G editor. Handbook of Intelligent Scaffold for Tissue Engineering and Regenerative Medicine. Singapore: Pan Stanford Publishing Pte. Ltd.;2012.

77. de Arellano-Lopez AR, Martinez-Fernandez J, Varela-Feria FM, Orlova TS, Goretta KC, Gutierrez-Mora F, et al. Erosion and strength degradation of biomorphic SiC. J Eur Ceram Soc. 2003;24(5):861-70.

78. Klenke FM, Liu Y, Yuan H, Hunziker EB, Siebenrock KA, Hofstetter W. Impact of pore size on the vascularization and osseointegration of ceramic bone substitutes in vivo. J Biomed Mater Res, Part A. 2008;85A(3):777-86.

79. Oh SH, Park IK, Kim JM, Lee JH. In vitro and in vivo characteristics of PCL scaffolds with pore size gradient fabricated by a centrifugation method. Biomaterials. 2007;28(9):1664-71.

80. Lopez-Alvarez M, Pereiro I, Serra J, Gonzalez P, de Carlos A. Porous silicon carbide scaffolds with patterned surfaces obtained from the sea rush *juncus maritimus* for tissue engineering applications. Int J Appl Ceram Technol. 2012;9(3):486-96.

81. de Carlos A, Borrajo JP, Serra J, Gonzalez P, Liste S, Leon B. In vitro cytotoxicity testing of wood-based biomorphic SiC ceramics. Key Eng Mater. 2005;284-286:581-4.

82. Gonzalez P, Borrajo JP, Serra J, Chiussi S, Leon B, Martinez-Fernandez J, et al. A new generation of bio-derived ceramic materials for medical applications. J Biomed Mater Res, Part A. 2009;88A(3):807-13.

83. Borrajo JP, Gonzalez P, Serra J, Liste S, Chiussi S, Leon B, et al. Cytotoxicity study of biomorphic SiC ceramics coated with bioactive glass. Bol Soc Esp Ceram Vidrio. 2006;45(2):109-14.

84. Borrajo JP, Gonzalez P, Serra J, Liste S, Chiussi S, Leon B, et al. Biomorphic silicon carbide ceramics coated with bioactive glass for medical applications. Mater Sci Forum. 2006;514-516(Pt. 2, Advanced Materials Forum III):970-4.

85. Borrajo JP, Serra J, Liste S, Gonzalez P, Chiussi S, Leon B, et al. Pulsed laser deposition of hydroxylapatite thin films on biomorphic silicon carbide ceramics. Appl Surf Sci. 2005;248(1-4):355-9.

86. Gonzalez P, Serra J, Liste S, Chiussi S, Leon B, Perez-Amor M, et al. New biomorphic SiC ceramics coated with bioactive glass for biomedical applications. Biomaterials. 2003;24(26):4827-32.

87. Rial L, Rodal P, Lopez-Alvarez M, Borrajo JP, Solla E, Serra J, et al. Bioceramic coatings on biomorphic SiC by electrophoretic deposition. Mater Sci Forum. 2008;587-588(Advanced Materials Forum IV):86-90.

88. de Carlos A, Borrajo JP, Serra J, Gonzalez P, Leon B. Behaviour of MG-63 osteoblast-like cells on wood-based biomorphic SiC ceramics coated with bioactive glass. J Mater Sci Mater Med. 2006;17(6):523-9.

89. Will J, Hoppe A, Mueller FA, Raya CT, Fernandez JM, Greil P. Bioactivation of biomorphous silicon carbide bone implants. Acta Biomater. 2010;6(12):4488-94.

90. Filardo G, Kon E, Tampieri A, Cabezas-Rodriguez R, Di Martino A, Fini M, et al. New bio-ceramization processes applied to vegetable hierarchical structures for bone regeneration: An experimental model in sheep. Tissue Eng, Part A. 2014;20(3-4):763-73.

91. Arcos D, Vallet-Regi M. Bioceramics for drug delivery. Acta Mater 2013;61(3):890-911.

Capítulo 2

Objetivos

USC
UNIVERSIDADE
DE SANTIAGO
DE COMPOSTELA

2. Objetivos

En los capítulos anteriores se ha puesto de manifiesto la necesidad de desarrollar sistemas avanzados para la profilaxis y el tratamiento de patologías del sistema musculoesquelético. La compleja estructura del tejido óseo, así como su función de sostén del organismo, condiciona extraordinariamente los requerimientos de los biomateriales empleados, que además de presentar una biocompatibilidad y estructura adecuadas, han de asegurar la recuperación de la funcionalidad del tejido. La incorporación de moléculas terapéuticas a los sistemas implantables puede permitir el tratamiento local de ciertas patologías y mejorar las respuestas celulares a los materiales, favoreciendo una mejor integración del implante e incluso modificando las propiedades del material, como se ha descrito en el Capítulo 1.1.

Las cerámicas biomórficas de carburo de silicio resultan materiales prometedores para la elaboración de implantes óseos no biodegradables, ya que poseen unas adecuadas propiedades mecánicas y estructurales y han mostrado unos excelentes resultados tras su implantación *in vivo,* como se ha indicado en el Capítulo 1.2. La disponibilidad de una amplia selección de precursores vegetales para su síntesis, permite la obtención de sistemas con microestructuras porosas muy diversas y por tanto, con potenciales diferencias en su comportamiento como biomateriales. Además, la incorporación de

moléculas terapéuticas en estos sistemas incrementa su versatilidad y su valor terapéutico.

El objetivo general de este trabajo es evaluar el potencial de tres cerámicas biomórficas de carburo de silicio de diferentes orígenes como materiales implantables, así como su capacidad para cargar y liberar moléculas terapéuticas con potencial efecto sobre ciertas patologías óseas o respuestas celulares. Ello debe permitir establecer criterios de utilidad para su empleo como materiales biofuncionales en regeneración ósea y/o el tratamiento de patologías asociadas.

El trabajo se presenta en los siguientes capítulos cuyos términos específicos se detallan a continuación:

1. Evaluación preliminar de la capacidad de carga de las cerámicas biomórficas mediante procesos de adsorción inespecífica de un antibiótico de amplio espectro, la vancomicina. Se seleccionó un sistema cerámico obtenido a partir de la madera de sapelli mediante un proceso de infiltración con silicio líquido. Se caracterizaron las propiedades morfológicas de los bioSiCs, se evaluó la biocompatibilidad de los sistemas y su capacidad para cargar y ceder el antibiótico en una cantidad suficiente para inhibir la formación del biofilm bacteriano.

2. Evaluación de las diferencias microestructurales de muestras de carburo de silicio biomórfico y su repercusión sobre la capacidad de carga de antibióticos (vancomicina) mediante procesos de adsorción inespecífica. Para la obtención de los bioSiC se emplearon tres precursores diferentes, madera de pino, roble y sapelli obtenidos también mediante un proceso de infiltración con silicio líquido. Se determinó la utilidad de los sistemas cargados para el tratamiento de biofilms bacterianos previamente formados.

3. Evaluación de las interacciones entre componentes celulares y sanguíneos con los tres sistemas cerámicos empleados (pino, roble y sapelli) y con sus respectivos precursores de carbón. Se establecieron los parámetros microestructurales y superficiales de los materiales que condicionan las respuestas celulares (hemólisis, coagulación sanguínea, trombogenicidad y respuesta inmunológica).

4. Desarrollo de cerámicas biomórficas cargadas con VEGF (factor de crecimiento del endotelio vascular) mediante interacciones físicas entre la proteína y los grupos funcionales de la superficie cerámica. Se evaluó el efecto de la variación en la microestructura sobre la cesión del VEGF y el consiguiente proceso de vascularización *in vitro*. Adicionalmente, se estableció el efecto que la topografía de las cerámicas y la cesión de VEGF presenta sobre la diferenciación de células madre mesenquimales obtenidas a partir de médula ósea humana.

5. Diseño y síntesis de sistemas combinados (carburo de silicio biomórfico/alginato/poloxamer) para la liberación controlada de fármacos cargados por inclusión en una matriz de hidrogel. Se emplearon las tres cerámicas de carburo de silicio señaladas anteriormente como componente cerámico, y un hidrogel compuesto por la combinación de un polímero natural y otro sintético. Se determinó la actividad terapéutica de los sistemas combinados cargados con un antiinflamatorio, la indometacina, sobre macrófagos estimulados con lipopolisacárido y condrocitos osteoartríticos. Se evaluó la inflamación producida por las partículas de bioSiC obtenidas por desgaste mecánico, directamente relacionadas con el rechazo a implantes óseos.

6. Desarrollo de sistemas combinados (carburo de silicio biomórfico/alginato/poloxamer) para la liberación controlada de vectores virales con aplicación en terapia génica. Se desarrollaron diferentes hidrogeles y se seleccionaron aquellos cuya estructura porosa resulta más adecuada para la carga y cesión de vectores virales capaces de producir una transducción apropiada con el fin de incorporarlos en los sistemas cerámicos. Evaluación de la capacidad de transducción de los sistemas combinados.

Capítulo 3

Bio-inspired porous SiC ceramics loaded with vancomycin for preventing MRSA infections

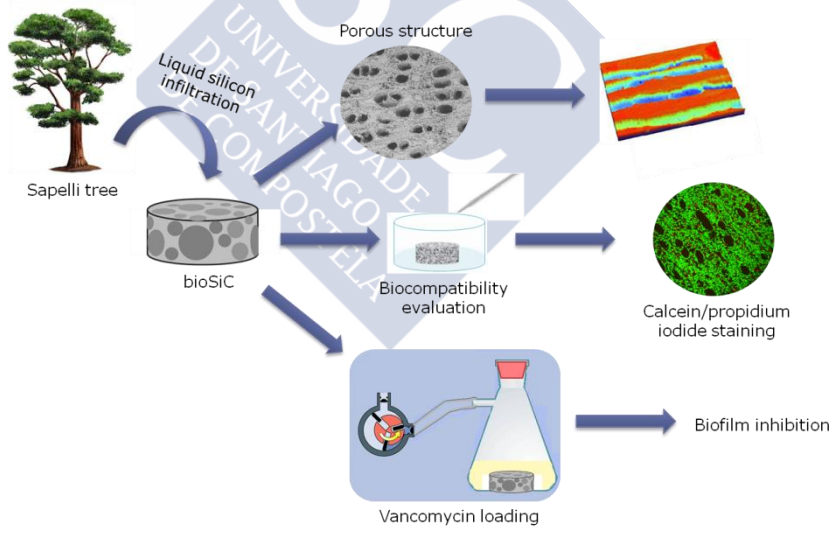

J Mater Sci Mater Med. 2011;22(2):339-347

USC
UNIVERSIDADE
DE SANTIAGO
DE COMPOSTELA

3.1 Abstract

Implant-related infections are a serious complication in orthopaedic and dental surgery resulting in prolonged hospitalization, high medical costs and patient mortality. The development of porous implants loaded with antibiotics may enable a local drug delivery for preventing surface colonization and biofilm formation. A new generation of bio-derived porous ceramic material that mimics hierarchical structures from nature was evaluated. Silicon carbide ceramics (bioSiCs) derived from sapelli wood were obtained by pyrolysis of *Entandrophragma cylindricum* wood followed by infiltration with molten silicon. This process renders disks that keep the bimodal pore size distribution (3 and 85 μm) of the original material and are highly cytocompatible (BALB/3T3 cell line). The ability of the bioceramic to load the antimicrobial agent vancomycin was evaluated by immersion of disks in drug solutions covering a wide range of concentrations. The disks released at pH 7.4 an important amount of drug during the first 2 h (up to 11 mg/g bioSiC) followed by a slower release, which is related to the presence of macro and mesopores. Finally, the antibiofilm effect against methicillin resistant *Staphylococcus aureus* was assessed and a considerable reduction (92%) of the bacterial film was observed. Results highlight the bioSiC potential as component of medicated medical devices.

3.2 Introduction

After roughly 100 years of clinical use of ceramics in dentistry and orthopaedics, there is still a need for novel biomaterials. Chevalier and Gremillard (1), in their recent and extensive review on ceramics for medical applications, stated the imperative need for obtaining novel, tough and stable materials (with special mention to non oxide ceramics as silicon carbide or silicon nitride) as orthopedic material candidates. Additionally, these authors pointed out the interest of developing those new materials through a biomimetic approach. Huebsch and Mooney (2) emphasize that there is a considerable body of research on the importance of physical variables, including topological and mechanical properties of biomaterials, in guiding a biological response. Some materials originated from living organisms, as bones, have outstanding properties due to their inorganic nature but also to their complex structural organization. To achieve a synthetic material that matches to bone, one has to take care of both these aspects. Bones are made up of a collection of materials built out of a common basic building block, the mineralized collagen fibril, that can be arranged in different patterns. All forms of bone possess mechanical strength and toughness out of reach from its constituent materials (3). Numerous attempts have been made to mimic the structure of bone (4–6). Highly porous calcium phosphate ceramic scaffolds or organic–inorganic composites are well known examples that have been used successfully (7), but none of them simultaneously combined the microscopic and macroscopic structure of the bone. Mimicking bone structure continues to be a challenging task.

Bio-derived silicon carbide based ceramics (bioSiC), obtained by Si-melt infiltration of carbonaceous scaffolds derived from wood templates have been proposed as new engineering ceramic materials with potential use in biomedical applications (8, 9). As a result of the evolution, wood combines a good balance between resistance/weight ratio and fluids circulation. BioSiC are non oxide ceramics that keep the complex natural

structural organization of wood, resembling to a certain extent that of bones. Biocompatible bioSiC can be produced with low cost, nearnet- shape and adequate mechanical properties (8–10). The possibility of varying the wood cellulosic preforms and/or the process variables makes the bioSiC approach extremely versatile and allows to tailor microstructures resulting in materials with different densities, morphologies, pore size distributions, levels of anisotropy, mechanical strength, etc. (8) and, thus, potentially useful as candidates for the development of orthopedic and dental implants.

Bone infections are typically caused by bacteria introduced from trauma, surgery, implant use, or by direct colonization from a proximal infection or via systemic circulation. Postoperative osteomyelitis is still an important problem in orthopedic and dental surgery (11). The bacterial biofilm, extremely resistant to both the immune system and antibiotics, is considered the primary cause of implant-associated infection. During the first 6 h after surgery, an implant is particularly susceptible to surface colonization and biofilm formation (11). Efficiency of the systemic treatment of osteomyelitis is limited by the difficult access of the antibiotic to the infection site (12, 13). The use of implants loaded with antimicrobial agents is a promising approach to prevent post-operative infections (14). The effectiveness of the antibiotic/device combinations is strongly dependent on the mechanism and the rate of drug release (15). Sub-inhibitory drug concentrations (i.e., those below the minimal inhibitory concentration) does not prevent the formation of a microbial biofilm and may even exacerbate complications or induce resistance in wound-site bacteria. An initial "burst" release from the device may sufficiently reduce the likelihood of the primary biofilm infection and, as a consequence, improve the prophylaxis against infection and speed-up the patients recovery. Recent studies have demonstrated that microporous materials may be particularly useful as drug-eluting implants. Porous hydroxyapatite enables more absorption and longer antibacterial activity (up to 2 days) *in vitro* than dense

hydroxyapatite (only 12 h) (16). On the other hand, mesoporous silica with a highly regular nano-porous structure and a vast surface area provided controlled release and an excellent protection for the loaded guest molecules (17).

The aim of the present work was to evaluate the potential of a bioSiC from sapelli wood for the loading and the release of vancomycin in order to prevent local bacterial infections, including biofilms formed by methicillin resistant *Staphylococcus aureus* (MRSA). To the best of our knowledge the suitability of bioSiC as drug delivery system has not been evaluated yet. Vancomycin is a highly soluble (>100 mg/mL) antimicrobial agent, which is usually administered systemically after bone surgery to prevent bacterial infection because of its broad spectrum and particular efficiency against staphylococci (18, 19). First, the porosity and topography of the bioSiC was characterized in detail in order to confirm the mimicking of the smart hierarchical structure of the tree template. Cytocompatibility and cell conductive properties were then tested. Finally, the ability of bioSiC to load vancomycin and to prevent the biofilm formation was evaluated and related to the particular hierarchical structure of the disks.

3.3 Materials and methods

3.3.1 **Bio-inspired silicon carbide**

Pieces of bioSiC were obtained from transversal cuts of sapelli wood (*Entandrophragma cylindricum*). The bioceramization process consisted of drying the wood at 60 °C for 24 h, after which pieces were subjected to a pyrolysis step up to 800 °C in an inert atmosphere with well controlled heating and cooling ramps. Finally, the carbon perform obtained was infiltrated with molten silicon at 1,550 °C in vacuum for 30 min (9). The final material was cut to obtain disks of Ø 6 mm x 2 mm.

3.3.2 **BioSiC characterization**

The microstructure and topography of bioSiC disks were evaluated by Scanning Electron Microscopy (SEM Philips XL 30), Interferometric Profilometry (WYKO NT-1100) and Confocal Laser Scanning Microscopy (CLSM Bio-Rad MRC 1024). The material density was determined, by triplicate, using a helium-air pycnometer (Quantacrome Mod. PY2, USA). The pore size distribution was evaluated by mercury intrusion porosimetry using a Micromeritics Autopore IV 9500 (Norcross, GA, USA) fitted with a 3 mL penetrometer for solids. The working pressures covered the range 0.6–2.5 x 10^4 psi. The specific surface area was evaluated by the Brunauer–Emmett–Teller (BET) method (20) which involved the determination of the amount of the adsorptive gas (N_2 in this case) required to cover the external and the accessible internal pore surface of the material with a complete monolayer. The disks were degassed by heating at 60 °C and 10^{-3} mmHg. Then, samples were exposed to N_2 gas at 77 K and 0.01–0.98 relative pressure on an automatic surface area analyzer (Micromeritics ASAP 2000, USA). The BET surface area (S_{BET}) was calculated from the isotherms according to the BET equation: S_{BET} (m^2/g) = 4.37 V_m (cm^3/g), where V_m is the volume of nitrogen necessary to form the monolayer.

3.3.3 **Cell viability test**

The *in vitro* cytocompatibility of bioSiC disks was tested, in triplicate, by using a BALB/3T3 cell line (CCL 163, ATCC, USA), according to the 10993-5 protocol of the International Standardization Organization (ISO). BioSiC disks were placed in 24-well plates. Then a cell suspension of 200,000 cells/well in 2 mL of DMEM (GIBCO®), supplemented with 10% fetal bovine serum (FBS) and 1% gentamicin, was added into the wells and the plate was incubated at 37 °C for 24 h in 5% of CO_2 and 90% of relative humidity environment. A control (cells without bioSiC disk) was treated in the same way. The bioSiC samples were collected and dyed in order to assess live/ dead

populations by means of a calcein/propidium iodide staining using confocal microscopy (Confocal Spectral Microscopy Leica TCS-SP2 LEICA, Wetzlar, Germany). To calculate their ratio (viability), live and dead populations were counted using a light microscope (Optiphot2, Nikon, Japan) with green and red filters and an Image Analysis software (Soft Imaging System GmbH, Version 3.2 Build 0.607). Cells remaining adhered to the tissue culture polystyrene (TCP) well were trypsinized and centrifuged. The pellet was resuspended with cell culture medium, cytospinned onto a glass slide, and dyed with calcein and propidium iodide.

3.3.4 **Vancomycin loading**

The high solubility in water of vancomycin enabled the loading of this antimicrobial agent into bioSiC disks by a simple immersion in 3 mL of drug aqueous solutions with concentrations ranging from 0.05 to 42.5 mg/mL. The disks were left in the drug solution for 24 h with mechanical shaking. Vacuum (75 mmHg) was applied for the first 2 h to eliminate the air from the pores of the pieces and to promote the flux of drug solution into the disks. The amount of vancomycin loaded in each disk was calculated as the difference between the initial and the final concentrations in the surrounding solution, determined by UV spectrophotometry at 280 nm (Agilent 8453, Böblingen, Germany). All the experiments were carried out in duplicate. Drug-loaded disks were desiccated at 40 °C until constant weight. BioSiC material loaded with vancomycin was evaluated as it was indicated above.

3.3.5 **Vancomycin release**

Dried drug-loaded disks were transferred to vials containing 3 mL of phosphate buffer (PBS) pH 7.4 at 37 °C and kept under mechanical shaking. Samples of the release medium were withdrawn at regular intervals and returned to the vial immediately after their drug concentration was measured spectrophotometrically at 280 nm. Water

uptake by the disks was monitored in parallel to the release tests by placing of dried disks in a Gay-Lussac pycnometer (Afora, Spain) and weighing the pycnometer at different times after filling with water.

3.3.6 **MRSA biofilm formation**

BioSiC material and vancomycin-loaded bioSiC disks, prepared by immersion in 42.5 mg/mL of drug solution during 24 h, were subjected to this microbiological study by using a clinical MRSA isolate. This bacterial isolate (recovered from a patient at the Ghent University Hospital, Ghent, Belgium) was grown on Tryptic Soy Agar (TSA) (Oxoid, Drongen, Belgium) at 37 °C. MRSA biofilms were formed in two different model systems. First, MRSA biofilms were formed in the Modified Robbins Devices (MRD), as described previously (21). In this system, growth medium is continuously replaced. Secondly, biofilms were formed on drug loaded-bioSiC disks using 24-well microtiter plates (MTP, Trasadingen, Switzerland). To this end, disks were placed in 1 mL MRSA suspensions with a density of appr. 10^6 CFU/mL (in 1:5 diluted Tryptic Soy Broth, TSB) for 1 h. Subsequently, disks were gently rinsed with 0.9% (w/v) NaCl to remove non-adherent cells and were placed in 1 mL diluted TSB for an additional 24 h at 37 °C. To quantify the biofilm formation in both methods the MRD and MTP, each disk was transferred to test tubes with 10 mL 0.9% (v/w) NaCl and the tubes were subjected three times to 30 s of sonication (Branson 3510, 42 kHz, 100 W, Branson Ultrasonics Corp., Danbury, USA) and 30 s of vortex mixing to detach the biofilm from the disks. Using this procedure all cells were removed from the disks and clumps of cells were broken apart. Sessile *S. aureus* cells were platted on TSA, and incubated at 37 °C for 48 h. Finally, the number of colony forming units (CFU) per disk was calculated by counting colonies on the plates. All experiments were carried out on at least 3 disks for each composition. The Student t test was used to evaluate the efficacy in reducing cell colonies and the differences between MRD and MTP methods.

3.4 Results

Processing variables during bioSiC production may affect the interconnected microstructure of the wood template. Morphological characterization of bioSiC was carried out by SEM micrographs (Figure 3.1) that evidenced the particular porous microstructure of the sapelli tree. Macropores (≈ 80 μm) in groups of two or three, characteristic of the sapelli tree (A), can be seen at the surface of the cross section of bioSiC. More in detail (B) a second population of mesopores (less than 10 μm) at the surface of the material can be noticed, with the silicon carbide crystals making the structure up (C). The walls of the vessels were maintained after infiltration giving a ceramic material with pores unidirectional connected, as it can be noted at the longitudinal section (Figure 3.2) characterized by interferometric profilometry (A) and confocal laser scanning microscopy (B).

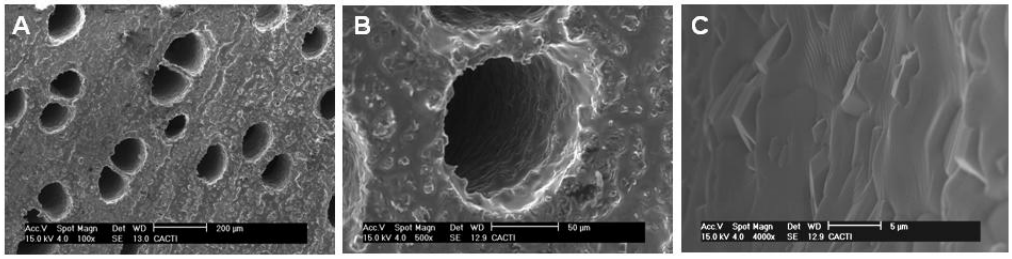

Figure 3.1 SEM micrographs (cross-section) of bioSiC ceramics produced from Sapelli wood. Three magnifications are shown: (A; X100), (B; X500) and (C; X4,000).

Microstructure was also confirmed from mercury intrusion porosimetry measurements (Figure 3.3). Results evidence a total intrusion volume of 0.243 ± 0.005 mL/g and a total porosity of 41.49 ± 0.05% with a bimodal pore size distribution (Figure 3.3) including macropores (mean diameter ≈ 85 μm) and mesopores (mean diameter ≈ 3 μm). Quantitative differences in the microstructural properties between vancomycin loaded

and unloaded bioSiC disks could not be established using mercury intrusion porosimetry.

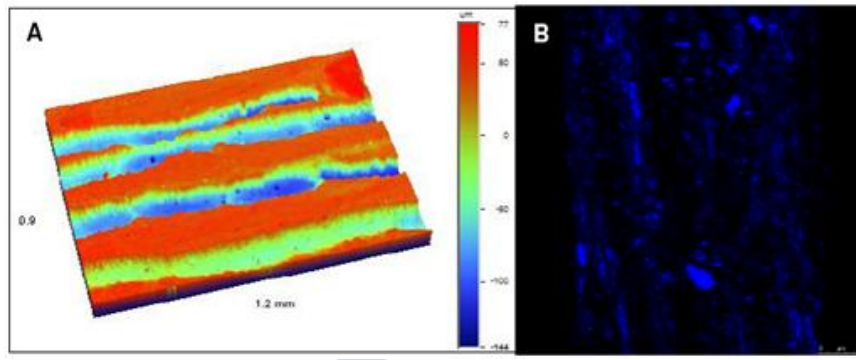

Figure 3.2 Topographic characteristics of a bioSiC ceramic (longitudinal section) by interferometric profilometry (A) and confocal laser scanning microscopy (B).

The nitrogen adsorption analysis confirmed the absence of microporosity and allowed the estimation of specific surface (1.198 ± 0.005 m^2/g).

The ability of bioSiC disks to sustain cell attachment and growth was assessed by an *in vitro* biocompatibility test following ISO 10993-5 procedure. The assays were conducted using Balb cell line. After 24 h in contact, a homogeneous well distributed layer of living cells and a significantly smaller amount of dead cells on the top of the bioSiC disks can be observed (Figure 3.4). The ratio between living and dead cells was used to calculate the viability of cells on the disk. The obtained values were 79.9% (sd 13.1) on bioSiC disks and 98.0% (sd 1.9) on the TCP from the wells. Vancomycin loaded bioSiC were also tested to assure *in vitro* biocompatibility achieving a percentage of cell viability of 95.8% (sd 6.0).

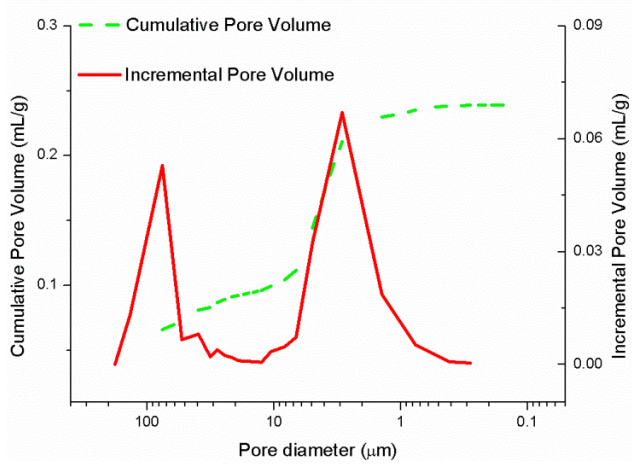

Figure 3.3 Pore size distribution and percentage of porosity of bioSiC derived from sapelli wood.

Figure 3.5 shows the adsorption curve of vancomycin on bioSiC material which relates the concentration of the solute on the adsorbent (mg vancomycin per gram of dried material) to the concentration of the solute in the surrounding solution at the equilibrium. The shape of the adsorption curve can be classified as Class S according to Giles and coworker classification (22). At the highest loading concentration studied (6 mg/mL) a significant amount of vancomycin (nearly 50 mg/g of bioSiC) was loaded.

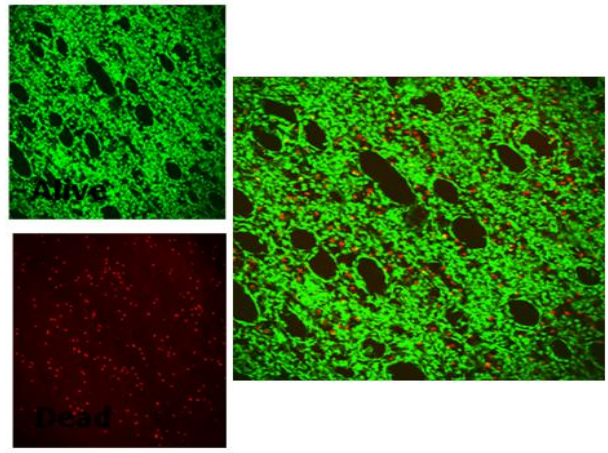

Figure 3.4 Calcein-propidium iodide staining observed by confocal microscopy 24 h after seeding on bioSiC samples. Living cells in green and dead cells in red.

When the loaded disks were immersed in 3 mL phosphate buffer pH 7.4 in order to simulate the release process under body conditions, a rapid release occurred during the first 2 h (Figure 3.6) followed by a slower rate. Figure 3.6 shows the profiles for the first hours (critical period after surgery) but the antibiotic release slowly continues for weeks. The total amounts released in the first 2 h are significantly lower but proportional to the amount of adsorbed vancomycin estimated from the adsorption experiments.

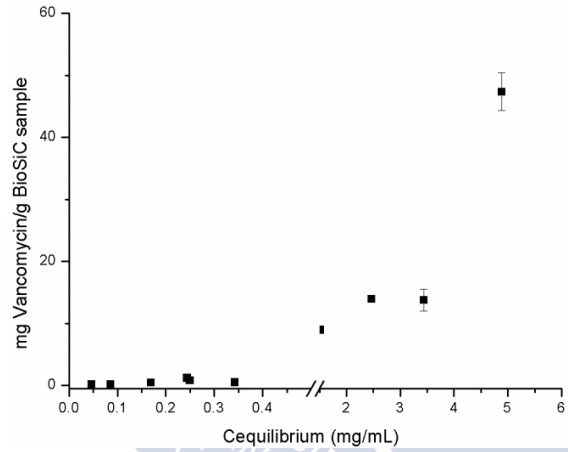

Figure 3.5 Vancomycin adsorbed on bioSiC samples (mg/g) versus vancomycin concentration at the equilibrium.

Finally, the effectiveness of bioSiC disks loaded by immersion in 42.5 mg/mL vancomycin solution to prevent MRSA biofilm formation was tested in two model systems, one (the MRD) in which the growth medium was continuously replaced and another one (the MTP) in which growth medium was not replaced. In the MRD, unloaded control disks contained on, average 6.76×10^4 CFU/disk while vancomycin-containing disks contained 4.57×10^4 CFU/disk (a reduction of 31.4%) (Figure 3.7) but the difference was not statistically significant. On the contrary, the antibiofilm effect in the MTP assay was much more pronounced and statistically significant ($t = 3.45$; 5 and 7 df $\alpha<0.05$), with control disks containing 1.10×10^4 CFU/disk and the vancomycin-

loaded disks presented only 5.50 x 10^2 CFU/disk (a reduction of 94.99%). Data indicate that vancomycin is being released in both model systems.

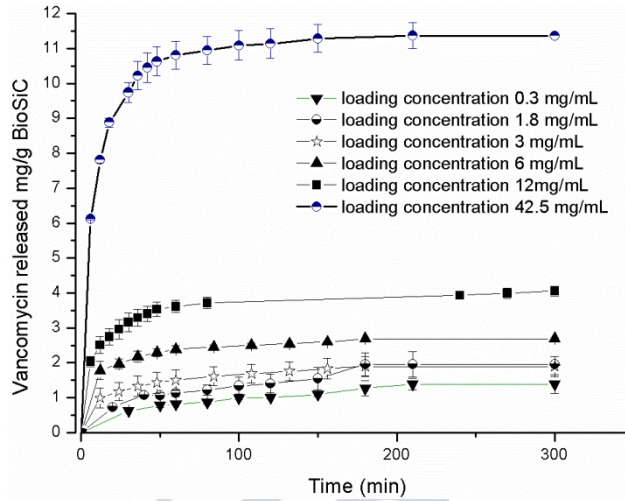

Figure 3.6 Vancomycin release from bioSiC samples at the different conditions studied.

3.5 Discussion

As a hardwood, sapelli wood microstructure includes three types of pores: vessels which are large cells to transport nutrients, and fibers and rays, which are smaller in diameter cells used for strength and storage (23). The vessels and fibers are elongated and run in the axial (longitudinal) direction of the tree. The rays are aligned perpendicularly to the vessels and fibers, in the transverse direction (24). The microstructure and the density of sapelli wood are particularly appealing for its use as scaffold molds, while the mechanical properties of the wood can be remarkably improved by a rapid and controlled mineralization. The preparation of biomorphic wood-based SiC consisted in the pyrolysis of the wood followed by gas phase infiltration with molten silicon (8). The resulting structure is expected to have a cellular structure of SiC with elongated silicon channels.

3.5.1 **BioSiC characterization**

3.5.1.1 *Morphological characterization*

SEM micrographs of bioSiC (Figure 3.1) evidenced the particular porous microstructure of the sapelli tree, with the characteristic groups of two and three macropores (≈ 80 µm), corresponding to vessels (A). The walls of the vessels resisted the reactive molten silicon infiltration resulting in a ceramic material with connected pores. At higher magnifications (B), a second population of mesopores (less than 10 µm) at the surface of the material can be noticed, with the silicon carbide crystals making up the structure both around the pores (B) and inside of them (C). Thus, the particular structure of wood is maintained in the bioSiC (8, 9), resulting in a complex organization with macro and microporosity, both key characteristics for the success of an implant material (1).

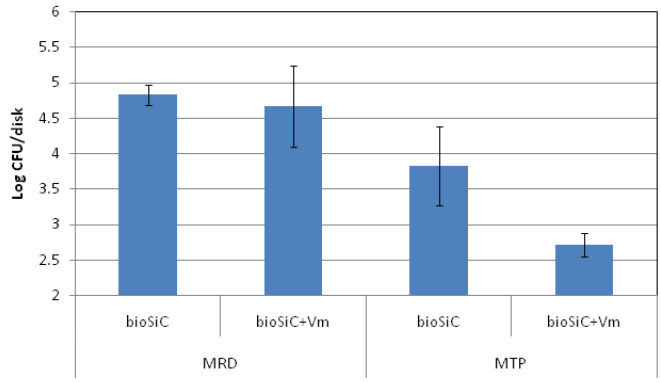

Figure 3.7 Log (number of CFU/disk) recovered in both biofilm model systems from bioSiC disks loaded or not with vancomycin. Error bars represent standard deviation.

Details of the topography and interconnected porosity were obtained by interferometric profilometry. The bioSiC longitudinal section image (Figure 3.2A) revealed the presence of long channels over 1 mm completely open and similar to the

original vascular system. Furthermore, additional information of the topography was obtained by CLSM. The autofluorescence image of bioSiC longitudinal section (Figure 3.2B) showed the porous character of the bio-ceramics and the interconnection grade. The fluorescence is emitted by the SiC crystals that constitute the material. Figures 3.1 and 3.2 illustrate that the hierarchically-structured vascular system of the vegetal precursor was replicated in the final bioinspired SiC ceramic.

3.5.1.2 *Pore size distribution*

To gain insight into the microporous structure, mercury intrusion porosimetry was carried out (Figure 3.3). The results indicated a bimodal pore size distribution with macropores (mean diameter 85 μm) and mesopores (mean diameter 3 μm). The total intrusion volume was 0.243 ± 0.005 mL/g with a total porosity of 41.49 ± 0.05%.

Material microstructure (volume and morphology of the macro and mesopores) has been pointed out as the key issue for the success of implantable materials in surgery (1) as the macroporosity controls the access of the tissues and biological fluids to the volume of the substitute and the microporosity deals with the adhesion of the cells. Moreover, according to current literature, vascularization only takes place when the implant material present pores greater than 5 μm and is maximal in pores of 60 μm (25). The unidirectional macropores (80 μm, Figure 3.1), the presence of a smaller size pore population and their high interconnectivity make the bioSiC from sapelli potentially able to be osteoconductive. Open-pore geometries with highly porous surface and microstructure enable the cell in-growth and reorganization and should provide the necessary space for angiogenesis.

It is important to notice that processing variables during bioSiC production may affect the interconnected microstructure of the wood template. Sapelli-based carbons exhibit bimodal distributions derived from its fiber and vessel pores in a range of 0.05–61 μm,

which can be partially modified through the infiltration process. In agreement with previous findings due to the volume expansion of ≈ 58% associated with the silicon carbide formation reaction, pores smaller than 1 μm are eliminated (9). Large pores, on average, also decrease in size due to carbide formation. However in some cases, the pore size distribution shifts towards larger sizes, which can be attributed to the breakage of struts during the expansion reaction, causing some pores to coalesce (9, 26). These unions could explain the macropores of 85 μm and mesopores of 3 μm found in the pore size distribution of bioSiC from sapelli

3.5.1.3 *Density and specific surface determination*

The density of the bioSiC disks from sapelli was 2.9 ± 0.2 g/cm^3, which is much higher than the value for pristine sapelli wood (0.64 g/cm^3). According to bibliographic data (13, 27), the density values obtained for bioSiC are closer to that of the cortical bone (1.7–2.0 g/cm^3) than other materials currently used in orthopaedics as the cobalt–chromium alloys (8.5 g/cm^3) or titanium alloys (3.4 g/cm^3). The sapelli-based bioSiC specific surface was estimated to be 1.198 ± 0.005 m^2/g, which is similar to that of commercial bone substitute materials, such as Interpore200® hydroxyapatite (2.64 m^2/g), Endobone® hydroxyapatite (0.7 m^2/g) or PerioGlass® (bioglass, 0.6 m^2/g) (28).

3.5.2 **Cell viability test**

The double staining showed that, after 24 h in contact, the cells adhere and grow on the bioSiC surface around the macropores (Figure 3.4). The increased fluorescence at the pores edges suggests that cells have colonized the inner surface of the pores. A homogeneously distributed layer of living cells (green) and a significantly smaller amount of dead cells (red) on the top of the bioSiC disks can be observed. The ratio between living and dead cells was used to calculate the viability of cells on the disk. The

obtained values were 79.9% (sd 13.1) on bioSiC disks, 98.0% (sd 1.9) and on the TCP from the wells. This indicates a good survival of cells on the bioSiC material (29, 30).

3.5.3 **Vancomycin loading**

Vacuum was applied to promote the penetration of the drug loading solution into the small pores of bioSiC. Vacuum should remove the air from smaller pores and force the entrance of water along the micropore channels. Adsorption isotherm of vancomycin on bioSiC material enabled to relate the concentration of the solute on the adsorbent (mg vancomycin per gram of dried material) to the concentration of the solute in the surrounding solution at the equilibrium (Figure 3.5). A Class S adsorption curve was obtained (22). This means that, as vancomycin at the outer solution increases, a monolayer of drug molecules is firstly adsorbed on the material and then successive layers of vancomycin can be piled up. This behavior is characteristic of the existence of unspecific interactions between solute molecules and the adsorbent interface. If the loading were only driven by the equilibration of the drug concentration between the outer solution and the inner aqueous phase of the disks, those disks immersed in 6 mg/mL drug solution could load up to 1.46 mg/g. However, the loading of those disks was nearly 50 mg/g, which confirms the relevance of the adsorption mechanism. The patterning of hydrophobic (e.g. carbon) and hydrophilic (e.g. silicon) regions in the surface of a material, as in the case of SiC, has been previously shown to be favorable for adsorption of DNA and proteins (31). This may be the case of vancomycin too.

One gram of drug-loaded (50 mg/g) bioSiC immersed in 1 L of medium may provide enough drug to exceed the minimum inhibitory concentration 90% (MIC90) of vancomycin against MRSA (0.25–2 μg/mL (32)).

3.5.4 **Vancomycin release**

Drug-loaded disks were immersed in 3 mL phosphate buffer pH 7.4 and no vacuum was applied in order to simulate the release process under physiological conditions. A rapid release occurred during the first 2 h, after which the release rate dramatically decreased. In Figure 3.6 the profiles for the first hours (critical period after surgery) are shown, but the slow antibiotic release continues for weeks. The total amounts released in the first 2 h are significantly lower but proportional to the adsorbed vancomycin. Since the experiments were carried out under sink conditions, this fact may be explained by the difficulty of the medium to access the smaller pores under atmospheric pressure. Thus, the delivery should start from greater pores, acting the small ones as reservoirs for the long term release. The amount of water that penetrates into the disks when no vacuum is applied was measured using a Gay-Lussac pycnometer. Five minutes after immersion 0.023 mL of water per gram penetrated into the disks. Two hours later the volume of water increased to 0.042 mL, which is less than a quarter of the volume obtained by mercury porosimetry. After 2 h, a progressive but minor increase in the water uptake occurred. The initially rapid entrance of water followed by a slower uptake explains the pattern of the vancomycin release profiles.

3.5.5 **Inhibition of MRSA biofilm formation**

The effectiveness of bioSiC disks loaded by immersion in 42.5 mg/mL vancomycin solution to prevent MRSA biofilm formation was tested in two model systems (Figure 3.7), one (the MRD) in which the growth medium was continuously replaced and another one (the MTP) in which growth medium was not replaced. In the MRD, unloaded control disks contained on average 6.72×10^4 CFU/disk while vancomycin-loaded disks contained 4.61×10^4 CFU/disk, which represents a reduction of 31.4% but not statistically significant. The anti-biofilm effect in the MTP was much more

pronounced and statistically significant, meaning a reduction of 92.2%. The more-pronounced anti-biofilm effect in the MTP can be explained by the gradual accumulation of vancomycin over time, while vancomycin is continuously washed away in the MRD model system.

3.6 Conclusions

BioSiC from sapelli has a bimodal pore size structure (3 and 85 μm modes) with a total porosity of 41.49% and a density similar to that of the bone. The specific surface area also resembles that of other commercial bone substitutes and enables high vancomycin loading. The combination of different pore sizes enables cell conductive properties and leads to a peculiar drug release pattern with an initially fast delivery (during the critical period for preventing surface colonization) followed by a slower release rate period. The effectiveness of vancomycin-loaded bioSiC against microbial infections was confirmed both under static and dynamic conditions, being able to reduce MRSA biofilm formation. These findings point out bioSiC as a promising biomimetic ceramic from arboreal origin for bone replacement.

3.7 References

1. Chevalier J, Gremillard L. Ceramics for medical applications: a picture for the next 20 years. J Eur Ceram Soc. 2009;29:1245–55.

2. Huebsch N, Mooney DJ. Inspiration and application in the evolution of biomaterials. Nature. 2009;462:426–32.

3. Weiner S, Wagner HD. The material bone: structure-mechanical function relations. Annu Rev Mater Sci. 1998;28:271–98.

4. Chen QZ, Boccaccini AR. Poly(D, L-lactic acid) coated 45S5 Bioglass-based scaffolds: processing and characterization. J Biomed Mater Res A. 2006;A-77:445–57.

5. Cui FC, Li Y, Ge J. Self-assembly of mineralized collagen composites. Mater Sci Eng R. 2007;R-57:1–27.

6. Peroglio M, Gremillard L, Chevalier J, Chazeau L, Gauthier C, Hamaide T. Toughening of bio-ceramics scaffolds by polymer coating. J Eur Ceram Soc. 2007;27:2679–85.

7. Vallet-Regi M, Balas F, Colilla M, Manzano M. Bone-regenerative bioceramic implants with drug and protein controlled delivery capability. Prog Solid State Chem. 2008;36:163–91.

8. de Arellano-López AR, Martínez-Fernández J, González P, Dominguez C, Fernández-Quero V, Singh M. Biomorphic SiC: a new engineering ceramic material. Int J Appl Ceram Technol. 2004;1:56–67.

9. González P, Borrajo JP, Serra J, Chiussi S, León B, Martínez- Fernández J, et al. A new generation of bioderived ceramic materials for medical applications. J Biomed Mater Res A. 2009;88:807–13.

10. Presas M, Pastor J, LLorca J, de Arellano-López A, Martínez- Fernández J, Sepúlveda R. Mechanical behavior of biomorphic Si/SiC porous composites. Scr Mater. 2005;53:1175–80.

11. Hetrick EM, Schoenfisch MH. Reducing implant related infections: active release strategies. Chem Soc Rev. 2006;35:780–9.

12. Wu P, Grainger W. Drug/device combinations for local drug therapies and infection prophylaxis. Biomaterials. 2006;27: 2450–67.

13. Rahaman MN, Yao A, Bal BS, Garino JP, Ries MD. Ceramics for prosthetic hip and knee joint replacement. J Am Ceram Soc. 2007;90:1965–88.

14. Zilberman M, Elsner JJ. Antibiotic-eluting medical devices for various applications. J Control Release. 2008;130:202–15.

15. Teller M, Gopp U, Neumann HG, Kühn KD. Release of gentamicin from bone regenerative materials: an *in vitro* study. J Biomed Mat Res B Appl Biomater. 2006;81B:23–9.

16. Lepretre S, Chai F, Hornez JC, Vermet G, Neut C, Descamps M, et al. Prolonged local antibiotics delivery from hydroxyapatite functionalized with cyclodextrin polymers. Biomaterials. 2009;30:6086–93.

17. Shi X, Wang Y, Varshney RR, Ren L, Zhang F, Wang DA. *In vitro* osteogenesis of synovium stem cells induced by controlled release of bisphosphate additives from microspherical mesoporous silica composite. Biomaterials. 2009;30:3996–4005.

18. Calhoun JH, Mader JT. Treatment of osteomyelitis with a biodegradable antibiotic implant. Clin Orthop Relat Res. 1997;341: 206–14.

19. Gitelis S, Brebach GT. The treatment of chronic osteomyelitis with a biodegradable antibiotic-impregnated implant. J Orthop Surg. 2002;10:53–60.

20. Stanley-Wood NG, Abdelkarim A, Johansson ME, Sadeghnejad G, Osborne N. The variation in, and correlation of, the energetic potential and surface areas powders with degree of uniaxial compaction stress. Powder Technol. 1990;69:16–26.

21. Coenye T, De Prijck K, De Wever B, Nelis HJ. Use of the Modified Robbins Device to study the in vitro biofilm removal efficacy of NitrAdine™, a novel disinfecting formula for the maintenance of oral medical devices. J Appl Microbiol. 2008;105:733–40.

22. Giles CH, MacEwan TH, Nakhwa SN, Smith D. Studies in adsorption. Part XI. A system of classification of solution adsorption isotherms, and its use in diagnosis of adsorption mechanisms and in measurement of specific surface areas of solids. J Chem Soc. 1960;111:3973–93.

23. Mizutani M, Takase H, Adachi N, Ota T, Daimon K, Hikichi Y. Porous ceramics prepared by mimicking silicified wood. Sci Technol Adv Mater. 2005;6:76–83.

24. Kleist G, Bauch J. Cellular UV microspectrophotometric investigation of sapelli heartwood (*Entandrophragma cylindricum*) from natural provenances in Africa. Holzforschung. 2001;55:117–22.

25. Dziubla TD, Lowman AM. Vascularization of PEG-grafted macroporous hydrogel sponges: a three-dimensional in vitro angiogenesis model using human microvascular endothelial cells. J Biomed Mater Res A. 2004;68A:603–14.

26. Pappacena KE, Gentry SP, Wilkes TE, Johnson MT, Xie S, Davis A, et al. Effect of pyrolyzation temperature on wood derived carbon and silicon carbide. J Eur Ceram Soc. 2009;29: 3069–77.

27. Hallab NJ, Jacobs JJ, Katz JL. Application of materials in medicine, biology, and artificial organs. In: Ratner BD, Hoffman AS, Schoen FJ, Lemons JE, editors. Biomaterials science: an introduction to materials in medicine. 2nd ed. London: Elsevier Academic Press; 2004. p. 532–9.

28. Weibrich G, Trettin R, Gnoth SH, Götz H, Duschner H, Wagner W. Determining the size of the specific surface of bone substitutes with gas adsorption. Mund Kiefer Gesichtschir. 2000;4: 148–52.

29. Neuss S, Apel C, Buttler P, Denecke B, Dhanasingh A, Ding X, et al. Assessment of stem cell/biomaterial combinations for stem cell-based tissue engineering. Biomaterials. 2008;29: 302–13.

30. Jagur-Grodzinski J. Polymers for tissue engineering, medical devices, and regenerative medicine. Concise general review of recent studies. Polym Adv Technol. 2006;17:395–418.

31. Cicero G, Galli G, Catellani A. Interaction of water molecules with SiC (001) surfaces. J Phys Chem B. 2004;108:16518–24.

32. Rouse MS, Steckelberg JM, Patel R. *In vitro* activity of ceftobiprole, daptomycin, linezolid and vancomycin against methicillin-resistant staphylococci associated with endocarditis and bone and joint infection. Diagn Microbiol Infect Dis. 2007;58: 363–5.

Capítulo 4

Suitability of biomorphic silicon carbide ceramics as drug delivery systems against bacterial biofilms

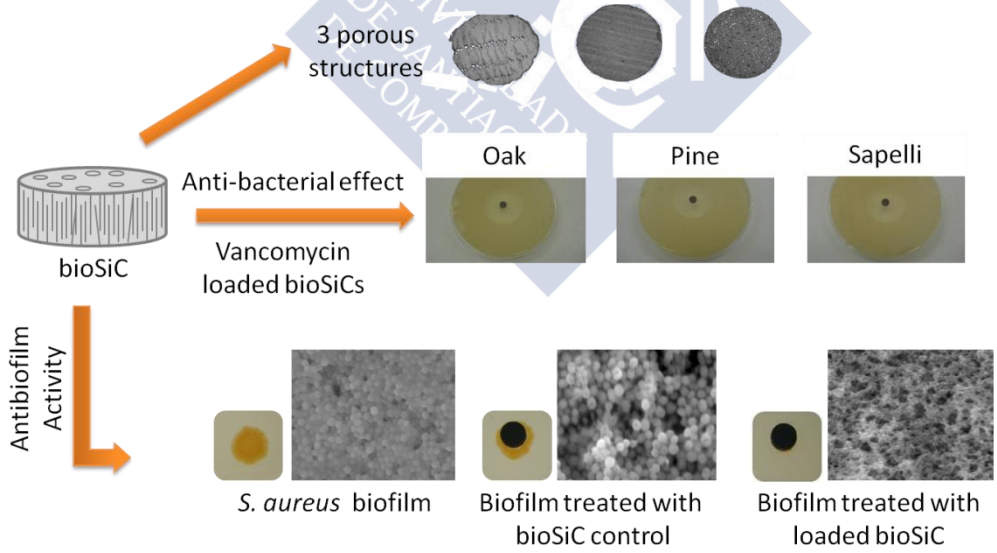

ISNR Pharmaceutics. 2013:104529, 9

USC
UNIVERSIDADE
DE SANTIAGO
DE COMPOSTELA

4.1 Abstract

The present work is aimed at getting a new insight into biomorphic silicon carbides (bioSiCs) as bone replacement materials. BioSiCs from a variety of precursors were produced, characterized, and loaded with a broad-spectrum antibiotic. The capacity of loaded bioSiCs for preventing and/or treating preformed *S. aureus* biofilms has been studied. The differences in precursor characteristics are maintained after the ceramic production process. All bioSiCs allow the loading process by capillarity, giving loaded materials with drug release profiles dependent on their microstructure. The amount of antibiotic released in liquid medium during the first six hours depends on bioSiC porosity, but it could exceed the minimum inhibitory concentration of *Staphylococcus aureus*, for all the materials studied, thus preventing the proliferation of bacteria. Differences in the external surface and the number and size of open external pores of bioSiCs contribute towards the variations in the effect against bacteria when experiments are carried out using solid media. The internal structure and surface properties of all the systems seem to facilitate the therapeutic activity of the antibiotic on the preformed biofilms, reducing the number of viable bacteria present in the biofilm compared to controls.

4.2 Introduction

The pathogenic events taking place on the surface of medical devices are primarily associated with the presence of microorganisms and their biofilms (1, 2). A biofilm is an intricate community of microorganisms embedded in a polysaccharide matrix, capable of attaching onto different kinds of surfaces developing a hard-to-eradicate infection (3). The adhesion of bacteria onto a surface (biological or artificial) depends on biophysical properties, such as wettability and/or electrostatic forces, and the production of specific factors such as polysaccharide intercellular adhesins that create links between the bacteria themselves and bacteria surface. Microorganisms reach the implanted medical devices during or immediately after orthopedic surgery, thus leading to further complications (4). Among postoperative problems, infections caused by *S. aureus* arise from the worst prognosis because of the ability of this microorganism to adhere to foreign bodies forming biofilms. The formation of biofilms is a key part in antibiotic resistance (5).

Different strategies have been developed to prevent biofilm formation after surgery by surface modification of biomaterials which in turn should modify the bacterial adherence (6) or the load and release of broad-spectrum antibiotics from the biomaterials, thus eliminating the incipient colonization (7, 8). When antibiotics are used, they can be embedded, absorbed into the material structure, or adsorbed on to the biomaterial surface (7, 8). The antibiotic release from the biomaterial must be sufficient to maintain the local concentration above the minimal inhibitory concentration (MIC) value during a sufficient period of time (9–12). Several studies aimed at the prevention of colonization and biofilm formation in implantable biomaterials have been reported (13). While postoperative osteomyelitis is still an important problem in orthopedic and dental clinical practice (14), studies on already formed biofilm treatments are much more limited.

Biomorphic silicon carbide (bioSiC) is a ceramic material obtained from natural resources with good mechanical properties, high biocompatibility, and osteoconductivity (15–17). BioSiCs have a smart hierarchical porous microstructure (pore size distribution, pore orientation, and total porosity) widely determined by the material used as wood cellulosic preform. In addition, the molten silicon infiltration, characteristic of its manufacturing process, produces a material with a close to the bone Young's modulus (18, 19). On this basis, bioSiC has been proposed as a candidate material for the production of bone substitutes able to prevent the loss of bone characteristic of other implants made with materials of greater strength (20) and a porous microstructure adequate to load and release antibiotics (16).

In a previous paper we have demonstrated the capacity of bioSiC from sapelli wood to load and release vancomycin, inhibiting bacterial adherence and preventing biofilm formation (16). The present work aims at extending this previous study to get an insight into new utilities of bioSiCs as bone replacement materials. To the best of our knowledge the suitability of biomorphic silicon carbides to treat already formed biofilms has not been verified yet. We have included bioSiCs from a variety of precursors and therefore different surface and microstructural characteristics, in order to establish any possible differences in its behavior, when the use of these antibiotic loaded bioSiCs for preventing or treating *S. aureus* biofilms is intended.

4.3 Materials and methods

4.3.1 **Bio-inspired silicon carbide**

Disks of bioSiC (Ø 6 mm x 2 mm) from wood precursors with different microstructures were obtained, pine (*Pinus pinaster*), oak (*Quercus robur*), and sapelli (*Entandrophragma cylindricum*), as previously reported by González and coworkers (15). The wood was dried at 60 °C during 24 hours, followed by pyrolysis at 1,000 °C in

argon atmosphere. The carbon preform obtained was then infiltrated with molten silicon in vacuum at 1,550 °C for 30 min.

4.3.2 **BioSiC characterization**

The material density was determined, in triplicate, using a helium-air pycnometer (Quantachrome Mod. PY2, USA).

The pore size distribution was evaluated by mercury intrusion porosimetry (Micromeritics AutoPore IV 9500, Norcross, GA, USA) using a 3 mL penetrometer for solids.

The specific surface area was evaluated by adsorption of nitrogen using the Brunauer-Emmett-Teller (BET) method. The disks were degassed by heating at 60 °C and 10^{-3} mmHg. Samples were exposed to N_2 gas at 77 K and 0.01–0.98 relative pressure using an automatic surface area analyzer (Micromeritics ASAP 2000, USA). BioSiC disks morphology was characterized by Scanning Electron Microscopy (SEM, Philips XL 30).

4.3.3 **Vancomycin loading**

Vancomycin solutions (42.5 and 85 mg/mL) were prepared by direct dissolution of vancomycin hydrochloride (Fagron Bach: 06L2101) in ultrapure water. Fixed volumes of each solution (30 µL) were added on to the disks. Drug-loaded disks were dried at 40 °C until a constant weight was reached.

4.3.4 **Vancomycin release in dissolution medium**

Dried drug loaded disks were transferred to vials containing 1 mL of phosphate buffer saline (PBS) pH 7.4 at 37 °C and maintained under mechanical shaking. Release medium samples were withdrawn at regular intervals. The vancomycin concentration was evaluated spectrophotometrically at 280 nm (Agilent 8453, Germany).

4.3.5. **Vancomycin elution on agar plates *in vitro***

Staphylococcus aureus ATCC 292135 was purchased from the Spanish Collection of Type Cultures (CECT), cultured in brain infusion broth (Liofilchem, Italy) overnight at 37 °C in atmospheric conditions, adjusted to 0.5 McFarland units, and used to inoculate Mueller-Hinton Agar (MHA) plates. Immediately, dried vancomycin loaded disks were centered on the inoculated MHA plates, incubated for 24 hours aerobically at 37 °C, and then the inhibition halos were measured. Once the halos were measured, the disks were transferred to freshly inoculated MHA plates, as reported before. This procedure was repeated every 24 h until absence of inhibition.

We have analyzed the release of vancomycin from the three types of samples in different media in order to compare the behavior of different bioSiCs in loading and releasing antibiotics and to confirm their utility in preventing *S. aureus* growth and also treating already formed *S. aureus* biofilm.

4.3.6 ***S. aureus* biofilm formation and antibiofilm activity of loaded bioSiCs**

Biofilms of *S. aureus* were induced on cellulose nitrate membrane filters according to that described by other authors with some protocol modifications (21, 22). Aliquots (15 µL) of an overnight culture of *S. aureus* grown in brain heart infusion broth (0.5 McFarland) were seeded on to cellulose nitrate membrane filters (13.0 mm diameter, 0.22 µm pore diameter; Millipore, USA) previously situated on MHA plates. Seeded membrane filters on MHA plates were incubated for 1 day at 37 °C in atmospheric conditions. Biofilms of *S. aureus* were induced.

Dried bioSiC-vancomycin disks (dose = 2.54 mg) were placed in the center of the membranes containing the biofilm and incubated at 37 °C. Unloaded bioSiC disks ($control_1$) and sterile paper disks impregnated with 20 µL of a standard vancomycin solution used in microbiological studies ($control_2$) (1.5 mg/mL) were used as controls.

After incubation for 24 or 48 hours, the dried bioSiC-vancomycin disks and controls were carefully removed, and the treated biofilms were then washed with 5 mL of phosphate buffer saline (PBS) (pH 7.4) to eliminate nonadherent cells, finally transferred to a vial containing 5 mL of PBS (pH 7.4), and vigorously vortexed for 1 min to suspend adhered cells. The cell suspensions obtained were 10-fold diluted in PBS. Aliquots (50 µL) of each dilution were seeded on to MHA plates and the colony forming units (CFUs) were counted after 48 hours of incubation at 37 °C in atmospheric conditions. This protocol minimized residual activity of the antibiotic. Alternatively, induced biofilms, treated with loaded bioSiCs, and controls were directly studied after gold coating using Scanning Electron Microscopy (SEM, Zeiss EVO LS 15, Germany).

4.3.7 **Statistical Analysis**

Results are expressed as means and standard deviations. Statistical significant differences between treatments were evaluated by analysis of variance (ANOVA) and Fisher's Least Significant Difference (LSD) using Statgraphics Centurion® X64 software.

4.4 Results

4.4.1 **BioSiC characterization**

Trees are classified into two main groups, softwoods and hardwoods. For the study we have included three wood materials, one softwood, pine, and two hardwoods, oak and sapelli.

Morphological characterization of bioSiC from those different precursors was carried out by SEM micrographs of the transverse surface of material pieces (Figure 4.1).The major difference between the anatomy of hardwoods and softwoods is the lack of vessels in softwood which are substituted in this type of wood by smaller tracheids (5–

50 µm) to conduct the fluid in the trunk. This anatomical peculiarity is the origin of the variations in mechanical properties between softwood and hardwood. As it can be seen, the variations in the internal structures and distribution of vessels, fibers, and rays of the precursors can be still detected after the infiltration of molten silicon. BioSiCs show structures extremely dependent of the source material. Pine bioSiC shows a roughness surface with small external pores while oak and sapelli bioSiCs present open external pores around 100 µm.

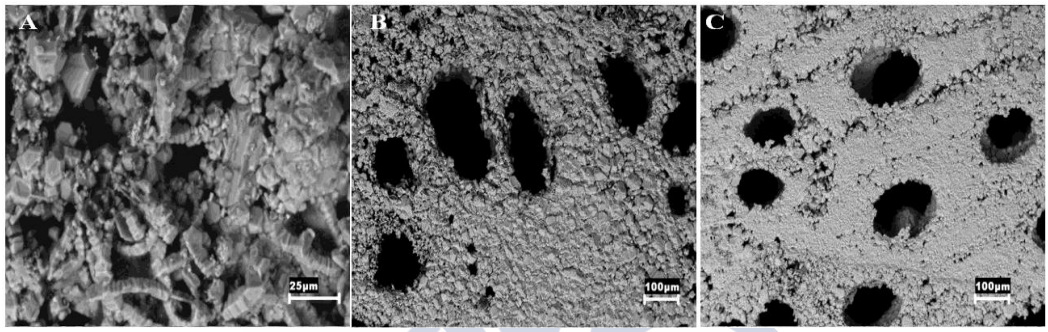

Figure 4.1 Transverse surface of different bioSiC pieces characterized by Scanning Electron Microscopy (SEM): (A) pine bioSiC, (B) oak bioSiC, and (C) sapelli bioSiC.

Mercury intrusion porosimetry results corroborate those observations (Figure 4.2 and Table 4.1) and also point out differences between the hardwoods selected. Pine wood gives the material with the highest porosity (46.97 ± 5.43%) characterized by numerous interconnected mesopores in the range of 1–10 µm (Figure 4.2A).

Oak wood results in the bioSiC of the lowest total porosity (27.85 ± 2.99%) and density and the highest specific surface characterized by the presence of an important number of macropores (Figure 4.2B) (mean diameter 141 ± 35 µm).

Sapelli bioSiC results (Figure 4.2C) are characteristic of a high porous material (40.72 ± 1.06%) with a bimodal pore size distribution with macropores (mean diameter 88 ± 31 µm) and mesopores (mean diameter 3.1 ± 1.6 µm). The agreement between the sapelli

bioSiC outcomes is consistent with our previous results in this material (16) pointing out the robustness in bioSiC production process.

The nitrogen adsorption analysis confirmed the absence of microporosity in the bioSiCs. Those variations in the bioSiC surfaces, microstructures and porosities should result in important variations in behavior with regard to their osteointegration and vascularization properties (23) and also in their capacity to load and release antibiotics.

Sample	P (g/cm^3)	HG	Specific surface (m^2/g)	HG	Porosity (%)	HG
Pine bioSiC	3.01 (0.01)	X	0.83 (0.05)	X	46.97 (5.43)	X
Oak bioSiC	2.90 (0.01)	X	1.10 (0.02)	X	27.85 (2.99)	X
Sapelli bioSiC	3.05 (0.01)	X	0.99 (0.05)	X	40.72 (1.06)	X

Table 4.1 BioSiC properties obtained by helium pycnometry, nitrogen adsorption and mercury intrusion porosimetry. Standard deviations are shown in parentheses. HG means homogeneous groups.

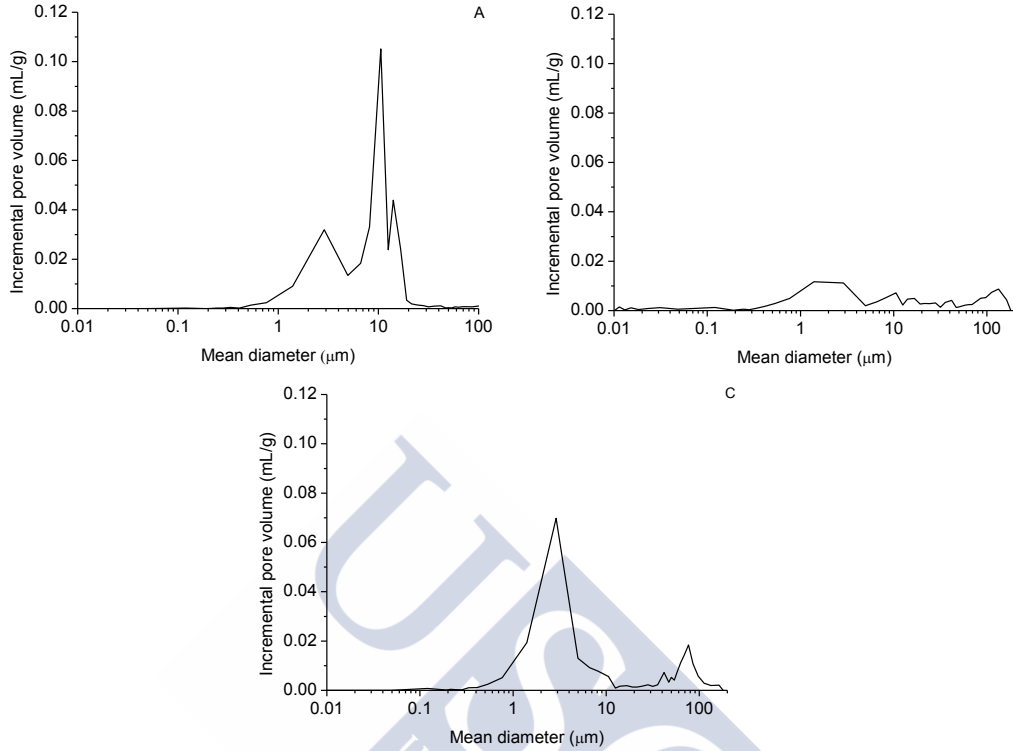

Figure 4.2 Pore size distribution obtained from mercury intrusion porosimetry of bioSiC of: (A) pine, (B) oak and (C) sapelli.

4.4.2 **Vancomycin release kinetics**

The microstructural characteristics and wettability properties of the bioSiCs allowed all of them to be loaded with a known amount of drug by simply adding the vancomycin solution on to the disks which completely penetrates and is maintained within the materials by capilarity.

When the loaded disks were immersed in 1 mL phosphate buffer pH 7.4 in order to simulate the release process a rapid delivery occurred during the first 90 minutes followed by a slower rate for all the samples. Figure 4.3 shows the profiles for the first hours (a critical period after surgery). The high hydrosolubility of vancomycin (>100

mg/mL) justifies the rapid initial delivery that should correspond to the adsorbed antibiotic on external surface and drug molecules with shorter diffusion pathway cause the prolongued controlled release of vancomycin for days.

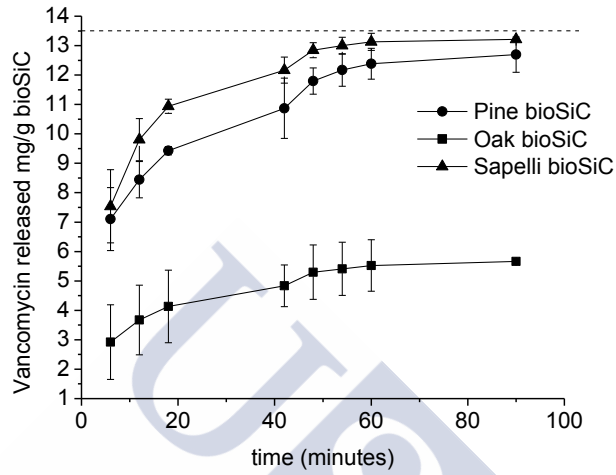

Figure 4.3 Release profiles of the low load concentration of vancomycin from three types of bioSiCs obtained from different precursors in PBS. The dashed lines (-) indicate the dose of vancomycin and correspond to 100% drug released.

Vancomycin release kinetics were analyzed using the Higuchi model (Table 4.2) that can accurately describe the release of water soluble drugs incorporated in porous solid matrices and allows materials to be compared (24). The good fit of release profiles to this model during the first stages indicates a characteristic diffusion mechanism of the drug through the bioSiC disks pores filled with medium. Differences in total porosity justify the slower release of vancomycin and lower values of K_H (Higuchi dissolution constant) observed for loaded oak disks.

Sample	K_H	R^2	F	freedom degress	α
Oak bioSiC	0.32 (0.07)	>0.90	>70	1 and 7	<0.01
Pine bioSiC	0.54 (0.15)	>0.94	>90	1 and 7	<0.01
Sapelli bioSiC	0.59 (0.06)	>0.86	>36	1 and 7	<0.01

Table 4.2. The release kinetics of vancomycin of loaded bioSiCs (Dose=1.27 mg/mL) by Higuchi model ($M= K_H *t^{0.5}$). Standard deviation in parentheses. K_H is the Higuchi release rate constant, R^2 is the square of the correlation coefficient, F is the F-ratio from the ANOVA of the regression and α is the probability of error.

For longer periods, the differences in the antibiotic release profiles in PBS medium from different materials can no longer be observed. Results do not show significant statistically differences between materials for the amount of drug released at 6 hours. In all the samples this amount of released vancomycin would exceed the minimum inhibitory concentration 90% of *Staphylococcus aureus* set to 1 μg/mL (22) even dipping disks in 1 liter of dissolution.

4.4.3 **Drug elution in agar plates *in vitro***

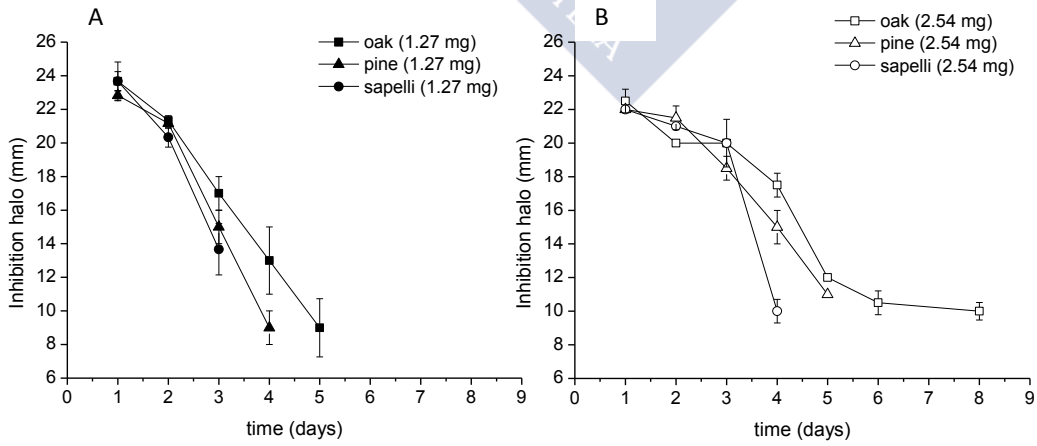

Figure 4.4 Inhibition halo profiles obtained from *Staphylococcus aureus* cultures treated with 1.27 mg and 2.54 mg vancomycin loaded bioSiCs.

The marked differences in vancomycin release profiles in liquid medium are reflected in the pattern of the inhibition halos of *S. aureus* generated by the treatment with loaded bioSiC disks (1.27 mg) in cultures on agar (Figure 4.4A). No significant statistical differences were found between the inhibition halos size of the three porous structures at the beginning of the experiment. The drug release rate is a critical factor that determines the time while the device system manages to overcome the minimum inhibitory concentration and therefore generate a measurable inhibition halo. Presumably, the amount of vancomycin transferred to the agar medium should depend also on the number of water molecules available to dissolve the drug and the external surface characteristics of the material. The lowest external surface of oak bioSiC and their big open pores in contact with the agar medium, contribute to explain the prolonged effect against bacteria found for this material.

Loaded sapelli, pine and oak bioSiC show no bacterial growth inhibitory effect after 3, 4 and 5 days of incubation respectively. It is possible to improve antibacterial activity against *S. aureus* by increasing the loaded vancomycin dose to 2.54 mg (figure 4.4B) achieving 4, 5 and 8 days for sapelli, pine and oak bioSiC respectively.

4.4.4 **Anti-biofilm activity**

Sample	$Control_1$	$Control_2$	Oak bioSiC	Pine bioSiC	Sapelli bioSiC
CFU (24 h) ± σ	98 ± 24	26 ± 3	11 ± 1	9 ± 2	7 ± 1
CFU (48 h) ± σ	86 ± 10	-	9 ± 2	3 ± 1	4 ± 0

Tabk 4.3. Number of CFUs of *S. aureus* on the biofilm at preset times (dilution 10^4)(Differences in colour show statistically significant differences).

Table 4.3 shows the number of CFUs counted after 24 and 48 hours of treatment of *S. aureus* biofilms previously formed with the different loaded bioSiC systems (dose = 2.54 mg) and controls. The gray scale illustrates the statistically significant differences

between groups. It is interesting to note that control$_2$ (standard solution of vancomycin), included as control at just 24 hours of treatment obtained a number of CFUs lower than those of control$_1$ (unloaded bioSiC) but significantly higher than CFUs after treatments with loaded bioSiCs. The sustained vancomycin release from all bioSiCs significantly reduces *S. aureus* biofilms indicating that the surface roughness and porous structure of the material could favor the penetration and the slow diffusion of drug through the glycocalyx matrix formed by bacterial population, improving biofilm treatments. The CFUs of *S. aureus* on oak bioSiC at 24 and 48 h were slightly higher than for pine and sapelli bioSiCs, However, results on agar (Figure 4.4B) showed a longer antibacterial effect on oak bioSiC (8 days for loaded oak bioSiC with 2.54 mg of vancomycin). This longer release should be enough to eradicate the infection and could explain the higher CFUs at 24 and 48 h.

As an example, SEM micrographs of the *S. aureus* induced biofilms together with the biofilms before and after 48h of treatment with the oak loaded and unloaded bioSiC are shown in Figure 4.5. As we can see the amount of bacteria after 48h in contact with the unloaded bioSiC (control$_1$) (Figure 4.5B) is similar to the non-treated biofilms (Figure 4.5A) and clearly higher than the biofilms treated with loaded BioSiC disks (Figure 4.5C) which surface appearance becomes clean as the original cellulose nitrate membrane.

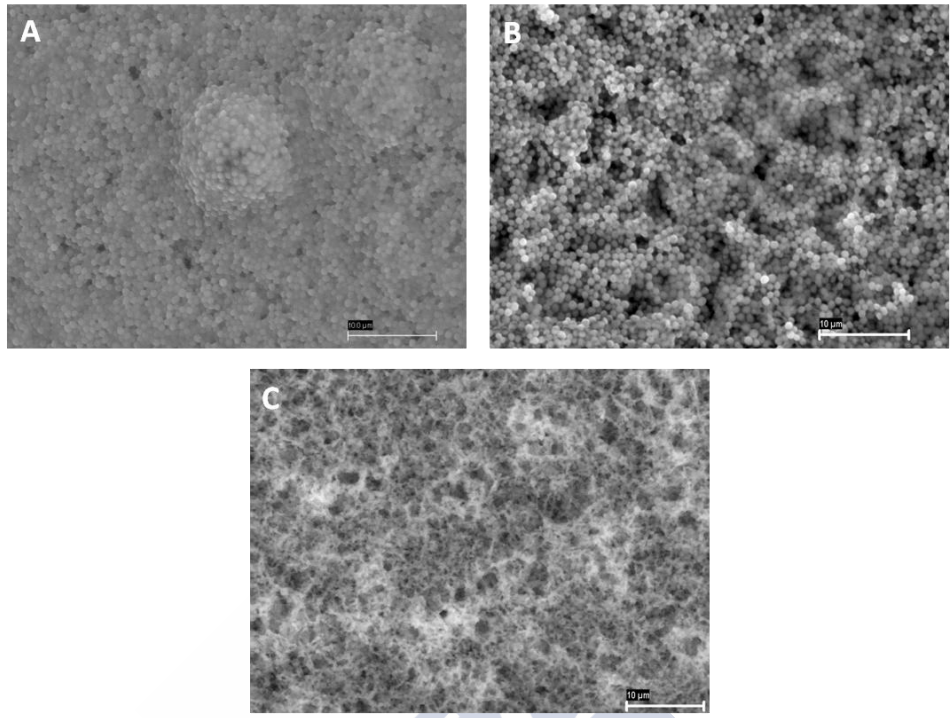

Figure 4.5 SEM micrographs of (A) induced biofilm on cellulose nitrate membrane, (B) induced biofilm treated with unloaded oak bioSiC (control$_1$) after 48 h incubation and (C) induced biofilm treated with vancomycin loaded (2.54 mg) oak bioSiC after 48h incubation.

4.5 Discussion

Wood is a natural material of complex hierarchical structure as a result of the orientation and alignment of cells that may serve as hierarchical template to generate novel biomorphic ceramics with meso and microstructures depending on the precursor selected. The morphology and arrangement of the different cells may vary widely between the different kind of woods, with large vessel cells dominating in hard wood and tracheids dominating in softwood. The diameter of the vessels and tracheids (named as pores) varies between 5 and 50 μm in softwood and between 1 and 300 μm in hardwood. While pine wood produces ceramics with a homogeneous porous

structure characterized by the presence of pores of small size, probably difficult to colonize by cells, sapelli and oak, produce ceramics with interesting porous structures which can be used as implants (25). The procedure selected in this work for the synthesis of bioSiCs from different natural resources allows systems with variable porosity, specific surface and density to be obtained. The characteristic cells of softwood and hardwood with a preferential orientation in the axial direction offer the possibility of transforming the bioorganic wood structure into an inorganic ceramic material with tailored physical and mechanical properties. Their surface characteristics and internal microstructure make them interesting candidates as potential delivery systems of therapeutic molecules (16).

The local administration of antibiotics through those porous systems would favor the therapeutic success, achieving a high dose of drug at the implant site and simultaneously reducing the adverse effects of systemic administration.

The vancomycin release study in PBS for all materials shows a quick antibiotic delivery during the first hours after implantation, characteristic of a high water soluble drug followed by a slow but prolonged release for days. The high initial drug release could act as an attack dose in response to the high risk of infection during the initial shock and the later controlled drug release keeps antibiotic concentration above the minimum inhibitory concentration (MIC), obtaining an extended antimicrobial therapeutic effect, preventing biofilm formation and inhibiting the occurrence of latent infections (26). Differences in drug release kinetics were found regarding the precursor materials; oak bioSiC having lowest porosity and the slowest antibiotic release rate. As a consequence, loaded oak bioSiC ceramics extend residual antimicrobial activity for longer than pine and sapelli when drug elution was tested on solid medium such as agar. An increase in the loaded dose, from 1.27 mg to 2.54 mg of vancomycin improves the effectiveness of the treatment, which in the case of the bioSiC from oak extend the

prevention of biofilm formation for a week in solid medium. The amount of water molecules and the drug concentration gradient at the prosthesis interface should also affect the antibacterial activity of loaded bioSiCs. Considering the physiological conditions in a bone-implant interface after surgery, where an inflammatory process is present and the inevitable antibiotic clearance due to blood and lymphatic stream takes place, we could expect a higher drug release *in vivo* than the one observed on agar. However, even with this slow drug release, obtained inhibition halos suggests the therapeutic potential of these systems.

After surgery a competition between cells and bacteria for the implant colonization is established (26). The release of vamcomycin locally from implants would favor osteoblast colonization while avoiding bacterial adhesion to the surface and therefore preventing the formation of biofilm. The formation of this organized structure confers resistance to antibiotics, hampers the therapeutic success of treatments and can lead to severe complications, such as destruction of local tissues, patient disability and morbidity and sometimes death (27). The biofilm hinders the penetration of drugs throughout (22, 28, 29). In this situation the antibiotic has poor activity against biofilm-embedded bacteria promoting resistances as a consequence of the continuing exposure to low drug concentrations (30).

The high molecular weight of vancomycin (31), the possible inhibition reactions with exopolysaccharides of the matrix and others factors could be responsible for the slow diffusion of this drug through biofilms. As result, the MIC90 of vancomycin is sharply increased in bacteria biofilms from 1 to 8 μg/mL (32). Our results indicate that vancomycin released from the bioSiCs was enough to treat *S. aureus* biofilms, progressively decreasing the number of viable bacterial cells embedded on the structured matrices. The rough structure of the scaffolds facilitates the antibiotic penetration through. On this basis, vancomycin loaded bioSiCs could be considered

potential candidates to produce implants for the substitution of infected prostheses in chronic infections reducing the risk of relapse.

4.6 Conclusions

There are statistically significant differences in surface characteristics, density and microstructure between bioSiCs from different origins. Despite their variations, all biomorphic silicon carbide ceramics were able to load and release vancomycin. Oak bioSiC with the highest specific surface, lowest total porosity and the biggest open pores shows a slow vancomycin release rate that promotes an antibacterial effect for more than a week for ceramics including 2.54 mg of drug. Differences between materials in preventing *S. aureus* biofilms, are not found for already formed *S. aureus* biofilm treatments.

The internal structure and surface properties of all the systems seem to facilitate the therapeutic activity of the antibiotic on the preformed biofilm, reducing the viable amount of bacterial colonies with time, by maintaining drug release over MIC for a long period of time. The use of bioSiC loaded systems is a promising strategy in order to prevent postsurgical periprosthetic infections but also to treat already present infections.

4.7 References

1. Davies DG, Parsek MR, Pearson JP, Iglewski BH, Costerton JW, Greenberg EP. The involvement of cell-to-cell signals in the development of a bacterial biofilm. Science. 1998;280:295–8.

2. Patel R. Biofilms and antimicrobial resistance. Clin Orthop Rel Res. 2005;437:41–7.

3. Costerton JW, Montanaro L, Arciola CR. Biofilm in implant infections: its production and regulation. Int J Artif Organs. 2005;28(11):1062-8.

4. Ehrlich GD, Stoodley P, Kathju S, Zhao Y, McLeod BR, Balaban N, et al. Engineering approaches for the detection and control of orthopedic biofilm infections. Clin Orthop Rel Res. 2005;437:59-66.

5. Stoodley P, Sauer K, Davies DG, Costerton JW. Biofilms as complex differentiated communities. Annu Rev Microbiol. 2002;56:187–209.

6. Forster H, Marotta JS, Heseltine K, Milner R, Jani S. Bactericidal activity of antimicrobial coated polyurethane sleeves for external fixation pins. J Orthop Res. 2004;22(3): 671–7.

7. Piozzi A, Francolini I, Occhiaperti L, Venditti M, Marconi W. Antimicrobial activity of polyurethanes coated with antibiotics: a new approach to the realization of medical devices exempt from microbial colonization. Int J Pharm. 2004;280(1-2):173-83.

8. Danese PN. Antibiofilm approaches: prevention of catheter colonization. Chem Biol. 2002;9:873–80.

9. Tambe SM, Sampath L, Modak SM. *In vitro* evaluation of the risk of developing bacterial resistance to antiseptics and antibiotics used in medical devices. J Antimicrob Chemother. 2001;47(5):589–98.

10. Anagnostakos K, Kelm J, Regitz T, Schmitt E, Jung W. *In vitro* evaluation of antibiotic release from and bacteria growth inhibition by antibiotic-loaded acrylic bone cement spacers. Biomed Mater Res B Appl Biomater. 2005;72(2):373-8.

11. Fujimura S, Sato T, Mikami T, Kikuchi T, Gomi K, Watanabe A. Combined efficacy of clarithromycin plus cefazolin or vancomycin against *Staphylococcus aureus* biofilms formed on titanium medical devices. Int J Antimicrob Agents. 2008;32(6):481-4.

12. McConeghy KW, LaPlante KL. *In vitro* activity of tigecycline in combination with gentamicin against biofilm-forming *Staphylococcus aureus*. Diagn Microbiol Infect Dis. 2010;68(1):1-6.

13. Arciola CR, Campoccia D, Speziale P, Montanaro L. Biofilm formation in *Staphylococcus* implant infections. A review of molecular mechanism and implications for biofilm-resistant materials. Biomaterials. 2012;33:5967-82.

14. Lange J, Troelsen A, Thomsen RW, Soballe K. Chronic infections in hip arthroplasties: comparing risk of reinfection following one-stage and two-stage revision: a systematic review and meta-analysis. Clin Epidemiol. 2012;4:57-73.

15. González P, Borrajo JP, Serra J, Chiussi S, León B, Martínez-Fernández J, et al. A new generation of bio-derived ceramic materials for medical applications. J Biomed Mater Res Part A. 2009;88(3):807-13.

16. Díaz-Rodríguez P, Landin M, Rey-Rico A, Couceiro J, Coenye T, González P. Bio-inspired porous SiC ceramics loaded with vancomycin for preventing MRSA infections. J Mater Sci-Mater Med. 2011;22(2):339-47.

17. López-Álvarez M, de Carlos A, González P, Serra J, León B. Cytocompatibility of bio-inspired silicon carbide ceramics. J Biomed Mater Res Part B. 2010;95(1):177-83.

18. Kaul VS, Faber KT, Sepúlveda R, de Arellano López AR, Martínez-Fernández J. Precursor selection and its role in the mechanical properties of porous SiC derived from wood. Mater Sc. Eng A, Struct Mater Prop Microstruct Process. 2006;428:225–32.

19. Greil P, Lifka T, Kaindl A. Biomorphic Cellular Silicon Carbide Ceramics from Wood: II. Mechanical Properties. J Eur Ceram Soc. 1998;18(14):1975-83.

20. Cabraja M, Oezdemir S, Koeppen D, Kroppenstedt S. Anterior cervical discectomy and fusion: Comparison of titanium and polyetheretherketone cages. BMC Musculoskelet Disord. 2012;13:172-181.

21. Lima KC, Fava LR, Siqueira JS. Susceptibilities of Enterococcus faecalis Biofilms to some antimicrobial medications. J Endod. 2001;27 (10):616-9.

22. Singh R, Ray P, Das A, Sharma M. Penetration of antibiotics through *Staphylococcus aureus* and *Staphylococcus epidermidis* biofilms. J Antimicrob Chemother. 2010;65:1955–8.

23. Klenke FM, Liu Y, Yuan H, Hunziker EB, Siebenrock KA, Hofstetter W. Impact of pore size on the vascularization and osteointegration of ceramic bone substitutes *in vivo*. J Biomed Mater Res Part A. 2008;85(3):777-86.

24. Jiang PJ, Patel S, Gbureck U, Caley R, Grover LM. Comparing the efficacy of three bioceramic matrices for the release of vancomycin hydrochloride. J Biomed Mater Res B Appl Biomater. 2010;93(1):51-8.

25. Roohani-Esfahani SI, Dunstan CR, Li JJ, Lu Z, Davies B, Pearce S, et al. Unique microstructural design of ceramic scaffolds for bone regeneration under load. Acta Biomater. 2013;9(6):7014-24.

26. Mouriño V, Boccaccini AR. Bone tissue engineering therapeutics: controlled drug delivery in three-dimensional scaffolds. J R Soc Interface. 2010;7(43):209-27.

27. Antoci VJ, Adams CS, Parvizi J, Davidson HM, Composto RJ, Freeman TA, et al. The inhibition of *Staphylococcus epidermidis* biofilm formation by vancomycin-modified titanium alloy and implications for the treatment of peroprosthetic infection. Biomaterials. 2008;29(35):4684-90.

28. Stewart PS, Costerton JW. Antibiotic resistance of bacteria in biofilms. Lancet. 2001;14:135-8.

29. Stewart PS. Theoretical aspects of antibiotic diffusion into microbial biofilms. Antimicrob Agents Chemother. 1996;40(11):2517-22.

30. Darouiche RO, Mansouri MD, Schneidkraut MJ. Comparative efficacies of telavancin and vancomycin in preventing device-associated colonization and infection by *Staphylococcus aureus* in rabbits. Antimicrob Agents Chemother. 2009;53(6):2626-8.

31. Salem AH, Elkhatib WF, Noreddin AM. Pharmacodynamic assessment of vancomycin-rifampicin combination against methicillin resistant *Staphylococcus aureus* biofilm: a parametric response surface analysis. J Pharm Pharmacol. 2011;63(1):73-9.

32. Rose WE, Poppens PT. Impact of biofilm on the *in vitro* activity of vancomycin alone and in combination with tigecycline and rifampicin against *Staphylococcus aureus*. J Antimicrob Chemother. 2009;63(3):485-8.

USC
UNIVERSIDADE
DE SANTIAGO
DE COMPOSTELA

Capítulo 5

Key parameters in blood-surface interactions of 3D bioinspired ceramic materials

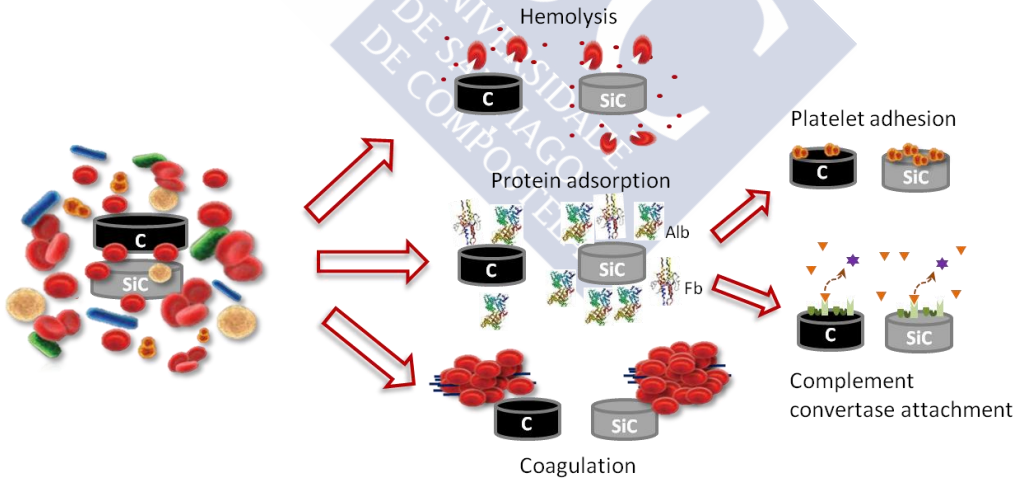

Materials Science and Engineering: C. 2014;41:232-239

USC
UNIVERSIDADE
DE SANTIAGO
DE COMPOSTELA

5.1 Abstract

Direct contact of materials with blood components may trigger numerous processes which ultimately lead to hemolysis, clot formation and recruitment of inflammatory cells. In this study, the blood-surface interactions for two inert bioinspired ceramic scaffolds obtained from natural resources; biomorphic carbon and silicon carbides (bioSiC) from different origins have been studied. The response of the blood in contact with carbon is well known. However, little has been identified on the influence of their 3D porous structure. Moreover, to our knowledge, there is no reference in the literature about the hemocompatibility of biomorphic silicon carbide as a porous scaffold. The experimental results showed the surface energy to be crucial to evaluate the hemocompatibility of a material however the surface topography and material porosity are also parameters to be considered. Surface roughness modifies clot formation whereas for protein adsorption total sample porosity seems to be the key parameter to be considered for hydrophilic materials (biomorphic silicon carbides), while the size of the pores determines the hemolytic response.

5.2 Introduction

Blood compatibility could be defined as the property of a device or a material which allows its function in contact with blood without causing adverse reactions (1). A hemocompatible blood contact material is a bio-inert product that has a non-inflammatory surface (2, 3) which stimulates neither the blood clotting nor the clot formation (4). Titanium, tantalum or stainless-steel, widely used for clinical devices, does not present good hemocompatibility. As reported by different authors (5, 6) this property must be improved by drug coating (e.g. heparin) for decreasing thrombosis risks. Inorganic coatings with carbon (7-9), gold (2), silicon carbide (10-12), titanium oxides and nitrides (13) or polysaccharide coatings (4, 14) are frequently used in order to increase the hemocompatibility of blood contacting medical implants. However, it is well known that clot formation, platelet activation and inflammation are also key processes in the normal tissue wound healing and modulate peri-implant bone healing and osteoconduction (15-19). Nevertheless high inflammatory reactions could promote chronic wound healing and fibrous tissue growth around the implant (20). Initial blood-material interactions play key roles in the integration of tissue engineering scaffolds, these being necessary to achieve a balance in the first steps of wound healing.

The material surface-water interaction, directly correlated with water contact angle (CA), is a crucial factor on the adhesion and activation of platelets. High contact angles minimize platelet adsorption, triggering blood coagulation and thrombosis (13). Surface roughness is an additional factor for blood compatibility because it increases the total surface exposed to blood. The greater the interaction, the higher the activation of the coagulation pathway will be (3, 16). Other material properties have also an effect on hemocompatibility like electrical resistivity (12) or ion releasing which could stimulate platelet activation, coagulation and thrombus formation (3). High efforts have been carried out in order to elucidate the interaction between material surface and blood

components but little is known about how the bulk properties of porous implant materials modulate these interactions.

Wood derived silicon carbide (bioSiC) is a ceramic material characterized by consistent microstructure, high strength and thermal conductivity, good resistance to oxidation and corrosion whose final properties are determined by the density and microstructure of the wood precursor (21-23). Their biomimetic structure, good biocompatibility and high interconnected porosity, make them useful for the manufacture of medical implants with adequate *in vivo* results (24-26).

During their manufacturing process, both the intermediate carbon biotemplates obtained after wood pyrolysis and the final product after silicon infiltration, maintain the original complex hierarchical microstructure of the wood (27) which makes them suitable for bone tissue engineering.

The microstructure of biomorphic silicon carbide can be selected using different wood precursors. It has been previously reported that the use of oak wood as precursor gives ceramics with low porosity (27.85%) while the use of pine or sapelli wood as templates gives materials with around 40% of porosity and lower specific surface (28).

The aim of this work is to evaluate the blood-surface interactions of bioinspired materials, bioSiCs and their intermediate carbon templates, obtained from different wood origins. The use of carbon (7-9) and SiC (2) as coating materials that reduce the thrombogenicity and inflammatory characteristics of biomaterials has been documented, but as far as we know, there is little information on the effect of their topography and microstructural 3D characteristics on their hemocompatibility properties and their interactions with whole untreated blood. We have evaluated the hemocompatibility of carbons and bioSiCs according to ISO 10993-4, testing the hemolysis, coagulation, thrombosis and immunology (complement activation)

parameters that should be evaluated for devices in contact directly or indirectly with blood.

5.3. Materials and methods

5.3.1 **BioSiC and carbon manufacture**

The selected wood precursors were pyrolyzed in an argon atmosphere at 1,000 °C according to the previously reported method (22) obtaining the desired carbon biotemplates (carbon disks Ø 6 mm x 2 mm).

The final bioSiCs were obtained by melt infiltration of the carbon precursors with silicon at 1,550 °C in vacuum conditions, triggering an exothermic reaction which ultimately results in the scaffolds. Woods of three different origins were used as raw materials: pine (*Pinus pinnaster*), oak (*Quercus robur*) and sapelli (*Entandrophragma cylindricum*).

5.3.2 **Surface characterization**

Surface topography was evaluated by interferometric profilometry (WYKO NT-1100, USA) obtaining the value of Rq (μm), average value of the square root of the deviation of the profile with respect to the median line, within the sample length.

The static contact angle was measured with distilled water using a Phoenix 300 goniometer (SEO, Korea) at room temperature.

In order to evaluate their microstructure, samples were analyzed by helium-air pycnometry (Quantacrome, PY2; USA), scanning electron microscopy (SEM Philips XL 30) and mercury intrusion porosimetry (Micromeritics Autopore IV 9500, Norcross, USA). Density (g/cm^3), total porosity (%) and pore size distribution were estimated.

The specific surface area (m^2/g) was obtained using the Brunauer-Emmett-Teller (BET) method which measures the amount of molecules of gas required to cover the external and internal accessible to nitrogen surface using an automatic surface area analyzer (Micromeritics ASAP 2000, USA).

5.3.3 **Blood-material interactions**

5.3.3.1 *Hemolysis test*

The evaluation of the percentage of hemolysis caused by carbon and bioSiC disks (6 mm Ø x 2 mm) was carried out according to the protocol explained elsewhere (29). Disks were hydrated with PBS (Phosphate buffer saline pH 7.4) for two hours. Then samples were placed into 10 mL plastic tubes containing 5 mL of human volunteers diluted blood (Centro de Transfusión de Galicia, Spain) (200 µL of blood in 5 mL of PBS) previously anticoagulated with EDTA (Ethylene Dinitrilo Tetraacetic Acid). After incubation for one hour at 37 °C, samples were centrifuged at 700 g for 10 min. The hemolytic activity was calculated as a function of the released hemoglobin which was measured by recording absorbance (Abs) of the supernatant using a UV-visible spectrophotometer (Agilent 8453, Germany) at 542 nm. Ultrapure water was used as the positive control (PC) (100% lysis) and empty plastic tubes as the negative control (NC). Results are expressed as hemolysis percentage that was obtained by the following equation:

$$\%\, Hemolysis\ = \frac{(Abs_{sample} - Abs_{NC})}{(Abs_{PC} - Abs_{NC})} \times 100$$

5.3.3.2 *Protein adsorption*

The adsorption of albumin (Alb) and fibrinogen (Fg) on to the materials as well as the ratio between them, are indicators of blood compatibility (7). Solutions of seroalbumin

bovine and human fibrinogen at physiological concentrations ([Alb]=30 mg/mL, Sigma Batch: 061M7010 and [Fb]=3 mg/mL, Acros Organics Batch: A0234700) in PBS (pH 7.4) were prepared. Additionally, different solutions were formulated; a staining solution with naphthol blue black (100 mg) (Sigma Batch: MKBC2601V), methanol (45 mL), glacial acetic acid (10 mL) and ultra-pure water (45 mL); a wash solution with 90% methanol, 8% ultra-pure water and 2% acetic acid, and an eluent solution with 50% ethanol, 50% NaOH (50 mM)/(0.1 mM) EDTA solution (5, 30). All reagents were of analytic grade.

Carbon and bioSiC samples were washed three times with ultra-pure water (MilliQ) and immediately placed in Eppendorf LoBind Microcentrifuge Tubes. Every protein solution (200 µL) was added to samples by triplicate. Samples were incubated at 37 °C for 60 min. The protein solutions were removed and samples were washed three times with ultra-pure water. 150 µL of the naphthol blue black staining solution were added to the samples and after 3 min, washed three times with the wash solution. The dye attached to the adsorbed proteins was removed using 150 µL of eluent solution and homogenizing on a plate shaker for 30 min at 300 rpm. After this time had passed, 100 µL of each sample solution was transferred to a 96-well plate. Dye amount was determined spectrophotometrically measuring the solution absorbance at 595 nm in a plate reader (FLUOstar OPTIMA, BMG Labtech). Nitrocellulose membranes were used to obtain the calibration curves of protein adsorbed (µg)/surface area (mm^2) between 19.09 µg/mm^2 and 1.59 µg/mm^2. The adsorption of albumin and/or fibrinogen values, was expressed as micrograms of protein by squared millimeters of the material surface (µg /mm^2). The Alb/Fib ratio was obtained by dividing the amount of albumin between the amount of fibrinogen. This ratio gives information on the cell behavior in the surface material.

5.3.3.3 *Coagulation evaluation*

Samples, previously hydrated for two hours with PBS, were transferred to test tubes. Immediately, 0.1 mL of untreated human volunteer blood was added to the samples. After 30 min of incubation (37 °C), 5 mL of distilled water was added. The clot formation was evaluated as a function of the final hemoglobin released after incubation. Red blood cells not embedded in thrombus were hemolyzed by adding distilled water. The hemoglobin content released was assessed colorimetrically using a UV-visible spectrophotometer (Agilent 8453, Germany) at 542 nm. The released hemoglobin is inversely proportional to the thrombus formed. Empty test tube was used as blank whereas distilled water. Triplicate samples were used in order to obtain the amount of the thrombus formed.

5.3.3.4 *Platelet adhesion test*

Anticoagulated healthy volunteers' blood was centrifuged (Avanti 30, Beckman, USA) at 220 g for 15 min to obtain platelet-rich plasma (PRP) (31).

Carbon and bioSiC disks, previously hydrated for 30 min with PBS, were placed in 24-well plates. 0.8 mL of PRP were added to each well and incubated at 37 °C. After 30 min the PRP was removed and the samples were fixed and dehydrated for Scanning Electron Microscopy evaluation (SEM, Philips XL 30, USA). Medical steel was used as reference material.

5.3.3.5 *Complement convertase attachment*

Complement convertase assay was purchased from HaemoProbebv (Groningen, The Netherlands) as a ready-to-use test kit. Disks were incubated with plasma provided by the kit for 15 min at room temperature in order to promote the formation of the complement convertase complex due to the interaction between the material surface

and the complement factor proteins. Unbound complement proteins were eliminated by washing the samples. Washed disks were incubated at room temperature for 24 hours in a medium with a specific chromogenic substrate with a sequence similar to C5 cleavage site. The union between the formed complement convertase complex and the chromogenic substrate was measured by recording the absorbance at 405 nm. The results were expressed as milligrams of complement convertase complex formed by sample volume (cm^3). Medical steel (MS), polymethylsiloxane (PDMS) and low-density polyethylene (LDPE) plates provided by HaemoProbebv were used as reference materials.

5.3.4 **Statistical analysis**

Results were expressed as means and standard deviations. The statistical significant differences between materials were established by the analysis of variance (ANOVA). When the F-ratio suggests that the difference between the population means was significant, the least significant difference (LSD) test was used to compare populations taken in pairs. ANOVA and LSD were performed by Statgraphics Centurion®X64 software.

5.4. Results and discussion

5.4.1 **Surface characterization**

Material surface properties are crucial in terms of their interaction with tissue components (1, 32). Both the carbons resulting from the process of wood pyrolysis and the bioSiCs resulting from the carbon infiltration with silicon have varying properties depending on the source material (27, 28, 33).

Figure 5.1 points out the significant differences between the materials selected for the experiments regarding their density, porosity and surface area. The pyrolyzation of

wood gives a low density material with high porosity and surface area. However, the subsequent infiltration which involved the spontaneous formation of silicon carbide crystals, gives materials with higher density and lower porosity and surface area. Depending on the wood origin, both carbons and silicon carbides have a variety of properties, materials from pine being the ones with the highest porosity while the oak source materials have the lowest one (28). Moreover, the carbon and SiC from sapelli are characterized by intermediate porosities and specific surfaces.

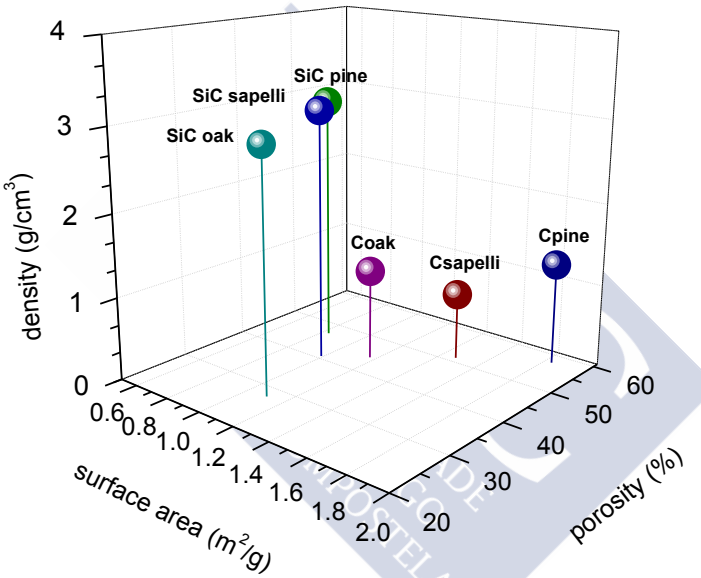

Figure 5.1 Relationship between the percentage of porosity, the surface area obtained by nitrogen adsorption and the helium picnometry density of the different carbon and bioSiC samples. BioSiC sample properties were extracted from the previous work (28).

Surface roughness determines the external area exposed to the blood, which is a crucial aspect in blood compatibility evaluation. Rough surfaces may cause stronger and faster blood coagulation (15, 30). In fact, the production of biomaterials of rough surfaces has been proposed as promoting clot formation in order to prevent blood leaking and allowing the tissue ingrowth inside the pores (16). Interferometric

profilometry photographs (Figure 5.2) graphically show large differences in pore structure and surface, both between the silicon carbides and their respective precursors, and between carbons and silicon carbides from different origins.

Red represents bumps on the material surface, while blue means depressions on the surface. Surface roughness is characterized by the root mean square average (Rq (μm)) at 5X magnification. According to the results, in general, data carbon samples have higher values of roughness than bioSiCs. Among the different vegetal precursors, sapelli origin gives the carbon and the bioSiC of the highest roughness compared to others. The carbon infiltration with silicon at high temperature leads to the reduction of the surface roughness as the silicon carbide crystals cover the surface irregularities present in the precursors.

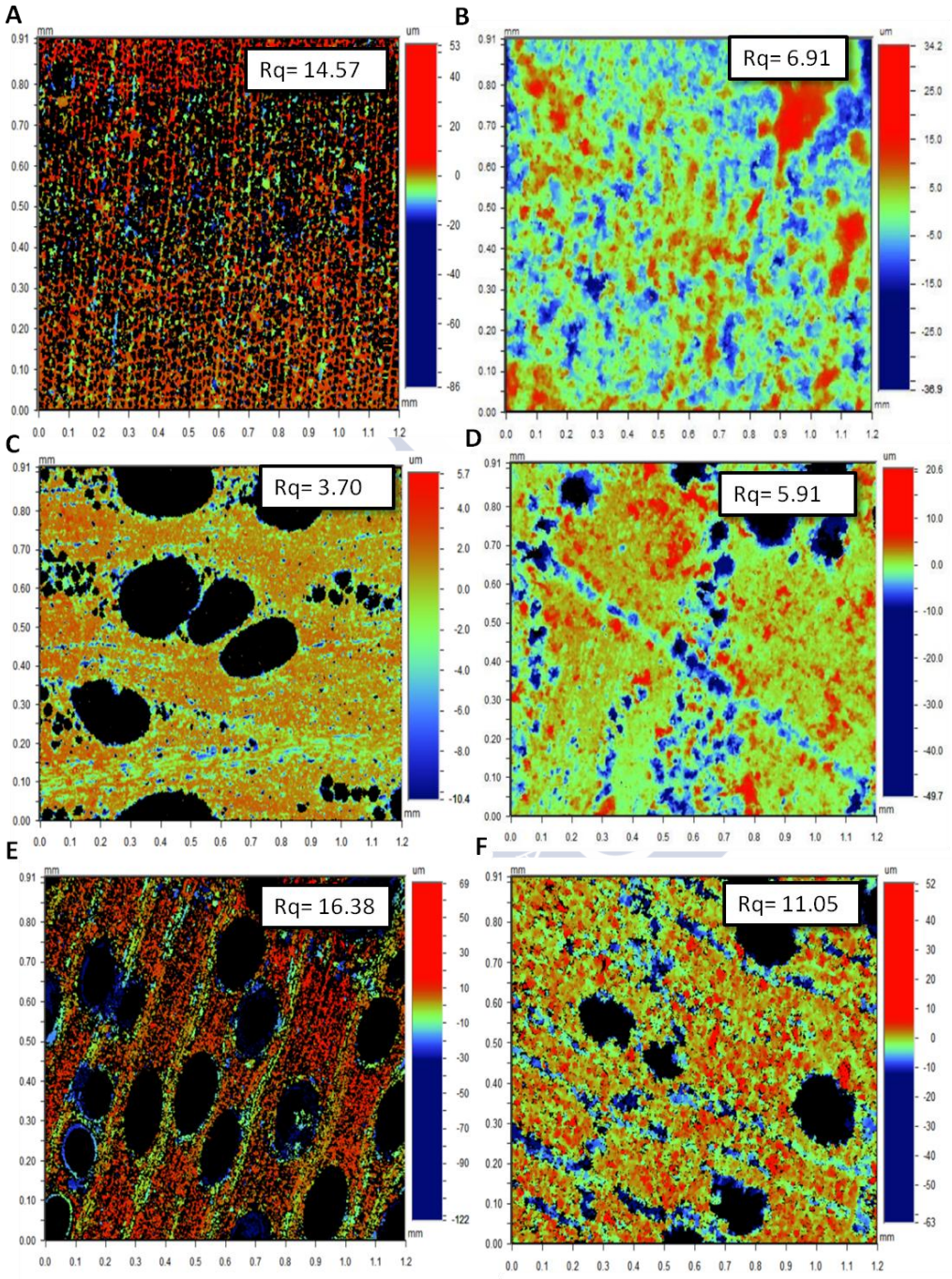

Figure 5.2 Interferometric profilometry images and surface roughness values obtained from them for: (A) pine carbon, (B) pine bioSiC, (C) oak carbon, (D) oak bioSiC, (E) sapelli carbon and (F) sapelli bioSiC.

Surface wettability obtained by contact angle measurement is directly related to the surface energy and can be correlated with biological interactions. The contact angle reflects the balance between the liquid-liquid molecules interactions and the biomaterial surface-liquid molecule attraction forces (1). Materials with an aqueous contact angle lower than 65° are considered hydrophilic surfaces. Higher aqueous contact angles are characteristic of hydrophobic surfaces. As the contact angle decreases the surface energy increases. It is accepted that contact angles lower than 45° correspond to high energy surfaces and contact angles higher than 75° with low energy surfaces (34). Surface hydrophility and energy have been used to predict the adhesion of cells to surfaces (35-37). There are no statistical significant differences between different wood precursors, neither in carbon nor in silicon carbide samples, regarding contact angle values. The results are expressed as mean and standard deviation. According to our results (Figure 5.3) all carbon samples have a high contact angle (mean 86 ± 2°), being classified as hydrophobic surfaces of low surface energy. On the contrary, all the bioSiC samples are characterized by a low contact angle (mean 38 ± 7°) and high wettability. Silicon infiltration leads to the formation of biomaterials of high hydrophilicity and surface energy.

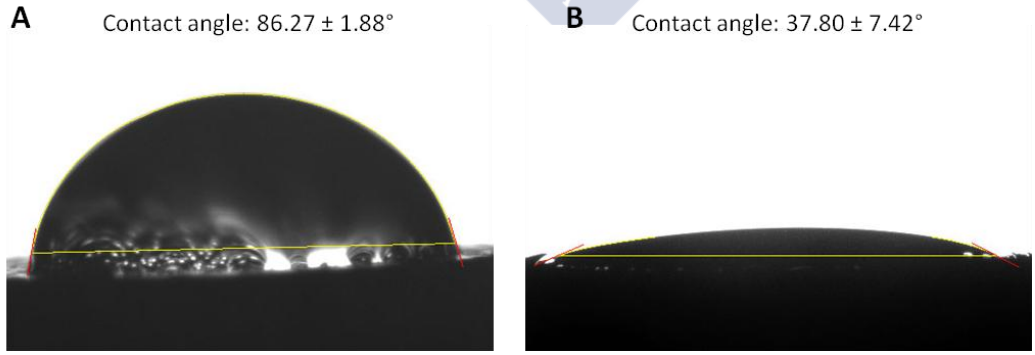

Figure 5.3 Contact angle obtained with distilled water of: (A) pine carbon, (B) pine bioSiC.

5.4.2 **Blood-material interactions**

5.4.2.1 *Hemolysis test*

The interaction of biomaterials with red blood cells is one of the most common methods of evaluating the hemocompatibility of materials. This interaction could lead to the damage of their cellular membrane or the erythrocytes lysis and, as a consequence, the release of their intracellular hemoglobin (38). The amount of released hemoglobin should be small to ensure the absence of toxicity of the implanted material. Figure 5.4 shows the percentage of hemolysis obtained after the direct contact between blood and both carbons and silicon carbide samples. Despite the carbons having higher surface roughness and external surface than silicon carbide samples, their direct interaction with diluted blood caused lower hemolysis percentages than with the bioSiC samples, probably due to differences in their hydrophilicity. The hydrophobicity of carbons could prevent their interaction with red blood cells. There are no differences in the hemocompatibility between carbon samples. Their mean hemolysis values below 5% allow them to be classified as non-hemolytic surface materials (38).

On the other hand, there are statistical significant differences between hemolysis values for hydrophilic bioSiC materials where microstructural properties seem to have a role. In a previous paper, statistical significant differences between the microstructural parameters of bioSiCs from sapelli, oak and pine were pointed out. Significant differences in specific surface, porosity and pore size distribution between oak bioSiC and the other two materials were assessed (28). Oak bioSiC has the highest surface area together with an important number of macropores (mean diameter 141 μm) where erythrocytes can penetrate easily (erythrocytes mean diameter 7.5 μm). On the contrary, mesopores in the range 1–10 μm present in the pine bioSiC and the high proportion of mesopores (mean diameter 3 μm) characteristic of sapelli bioSiC do not

facilitate the interaction of erythrocytes with the whole surface of those materials. As it can be seen, hemolysis is not correlated with the external surface exposed to the blood obtained by interferometric profilometry, but it seems that for hydrophilic surfaces the pore size is crucial for the hemolysis evaluation, maybe because there is a critical pore size above which the erythrocytes (mean size 7.5 μm) are able to penetrate into the materials.

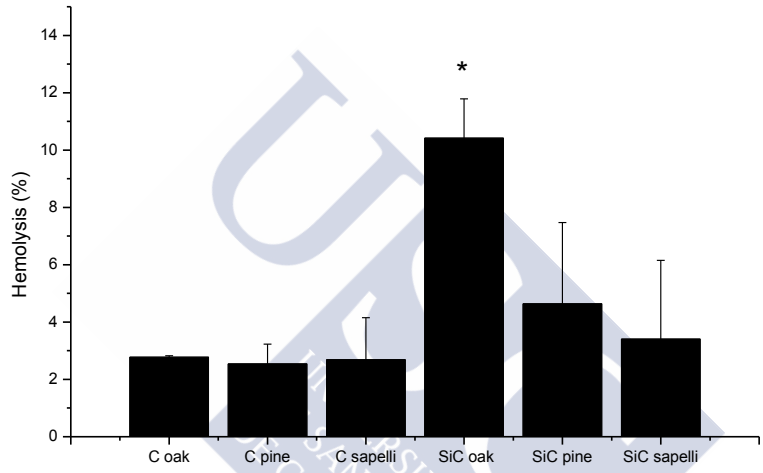

Figure 5.4 Hemolysis of red blood cells after the incubation of carbon (C) and bioSiC (SiC) samples with whole blood. The homogeneous groups are indicated by an equal number of asterisks (*) above the columns.

5.4.2.2 *Protein adsorption*

The study of biomaterial surface protein adsorption is critical for the *in vitro* evaluation of a new biomaterial (35). The body reacts and recognizes external materials by foreign body reactions and blood clotting. The coagulation process starts with the adsorption of plasma proteins, which ultimately leads to the formation of blood clotting. Albumin, fibrinogen and IgG are the proteins with the highest concentration in plasma, the

composition of the protein layer formed on biomaterial-blood interface depends on the properties of the materials and is correlated with the biological response (39). A material presenting an adsorption to albumin greater than the adsorption to fibrinogen, should promote a desirable cellular response. It is known that the adsorption of albumin, which is a hydrophilic protein, is correlated with the reduction of platelet adhesion and thromboresistance. On the contrary, the preferential adsorption of fibrinogen, which is a hydrophobic protein, is associated with a high platelet adhesion and activation (7, 40, 41). Figure 5.5 shows the results of protein adsorption for the biomaterials studied, the reference material and the positive control. For all samples, except for the positive control, the amount of the adsorbed albumin was higher than the amount of fibrinogen, characteristic of materials which causes low platelet adhesion and activation. All the biological reactions are based on the surface adsorption of proteins, in an initial step albumin is adhered to the surface generating a protein layer that will be replaced by adhesion proteins that are recognized by integrin receptors and transforms the biomaterial into a biologically recognizable material suitable for cell adhesion and the consequent tissue integration (35). The high albumin adhesion to the biomaterials surface could also indicate an adequate initial step for latest cellular recognition and tissue ingrowth. We also found lower fibrinogen/albumin ratios on carbon samples. According to other authors an increase on hydrophobicity enhances the adsorption of albumin and decreases the one of fibrinogen. However, proteins adsorbed on this type of biomaterials have a higher resistance to being displaced by other plasma proteins making the next steps of cell attachment and tissue integration difficult (41, 42).

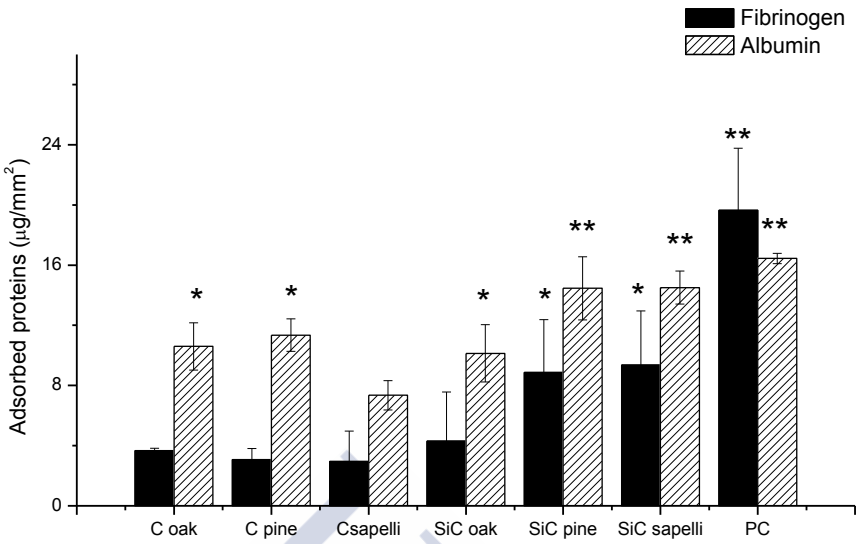

Figure 5.5 Adsorbed fibrinogen (black bars) and bovine serum albumin (striped bars) on to the different carbons and bioSiC materials studied and the positive control (nitrocellulose membranes). The homogeneous groups are indicated by an equal number of asterisks (*) above the columns.

5.4.2.3 *Coagulation evaluation*

The clot formation could be started by surface-mediated reactions or through factors derived from tissues. Both pathways lead to the formation of thrombin. The factors involved in the first surface-mediated reactions pathway are XII, XI, prekallikrein and high-molecular-weight kininogen (43). On the other hand, the extrinsic pathway is initiated by the activation of factor VII. The final formation of the thrombin gel leads to the entrapment of red blood cells into its structure causing the reduction of the number of free blood cells available for their lysis after the addition of water and the consequent decrease of released hemoglobin (15, 44).

Figure 5.6 shows the final amount of hemoglobin released after the incubation of untreated whole blood with the different biomaterials (carbons, bioSiCs, and the NC). The negative control gives the values of released hemoglobin when no clot is formed. The clotting formation is higher in those systems with low contact angle which also have higher protein adsorption. Hydrophilic surfaces are able to interact highly with biological components according to previously reported results (42).

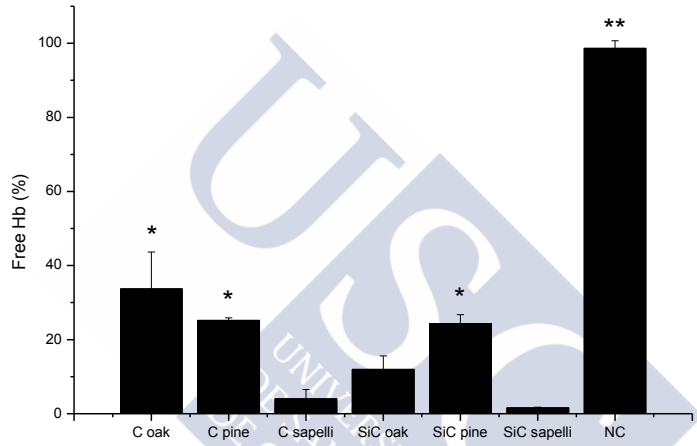

Figure 5.6 Final amount of hemoglobin released after the incubation of untreated whole blood with the different biomaterials and negative control. The homogeneous groups are indicated by an equal number of asterisks (*) above the columns.

Systems obtained from sapelli wood, are characterized by the highest values of surface roughness which cause the lowest free blood cells as a consequence of the higher clot formation. This could be explained by their higher surface area being in direct contact with the blood components. These inert materials show an excellent blood biocompatibility. In the case of hydrophilic and hydrophobic porous structures their ability to stimulate medium initial blood clot seems to be dependent on the surface roughness. In these cases the formation of the clot, initial step in wound healing and correlated with protein adhesion, could lead to the formation of new functional tissue

through the material pores. Although higher surface roughness means higher external surface exposed to the blood no effects of this parameter could be observed in the protein adsorption, showed before, wherein total porosity seems to be the key parameter to be analyzed. This fact could be explained because clot formation is a superficial event while protein adhesion could take place in all the porous structure of the material.

5.4.2.4 *Platelet adhesion*

Platelets are non-nucleated cells extremely sensitive to vascular damage which occupy approximately 0.33% of the total blood volume. Their discoid shape at normal state changes into irregular spheres with pseudopods when they are activated. The platelet activation after their adhesion to artificial surfaces or injured blood vessels causes the extracellular release of their granule contents stimulating other platelets and leading to their aggregation (45). Figure 5.7 shows SEM photographs of platelets on the biomaterials (carbons, bioSiCs and medical steel). The activation and aggregation of platelets are characterized by well-defined morphological changes which can be classified in five phases (45). According to this classification, all the samples are characterized by the presence of platelets with rounded morphology (phase 1) suggesting that platelets are not activated neither in medical steel (Figure 5.7G) nor in silicon carbide (Figure 5.7D-F). An important number of platelets are attached on medical steel surface showing a regular shape.

Platelet adhesion seems to be higher for bioSiC samples than for carbons which correspond to materials with high surface energy. It has been described that materials with high surface energy enhance cell attachment as a consequence of their ability to promote protein adsorption (34). This could be explained by the high hydrophilicity that causes high protein adsorption and the adhesion of platelets to artificial surfaces mediated by platelet glycoproteins. These proteins act as a receptor for adhesive

plasma proteins that facilitate cell attachment such as vitronectin, fibronectin and fibrinogen. Although carbon samples shown also good protein adhesion, the high affinity of these surface samples for the proteins makes the displacement of the initial protein layer by adhesive proteins difficult which ultimately leads to a reduction in cell attachment as was mentioned above (41).

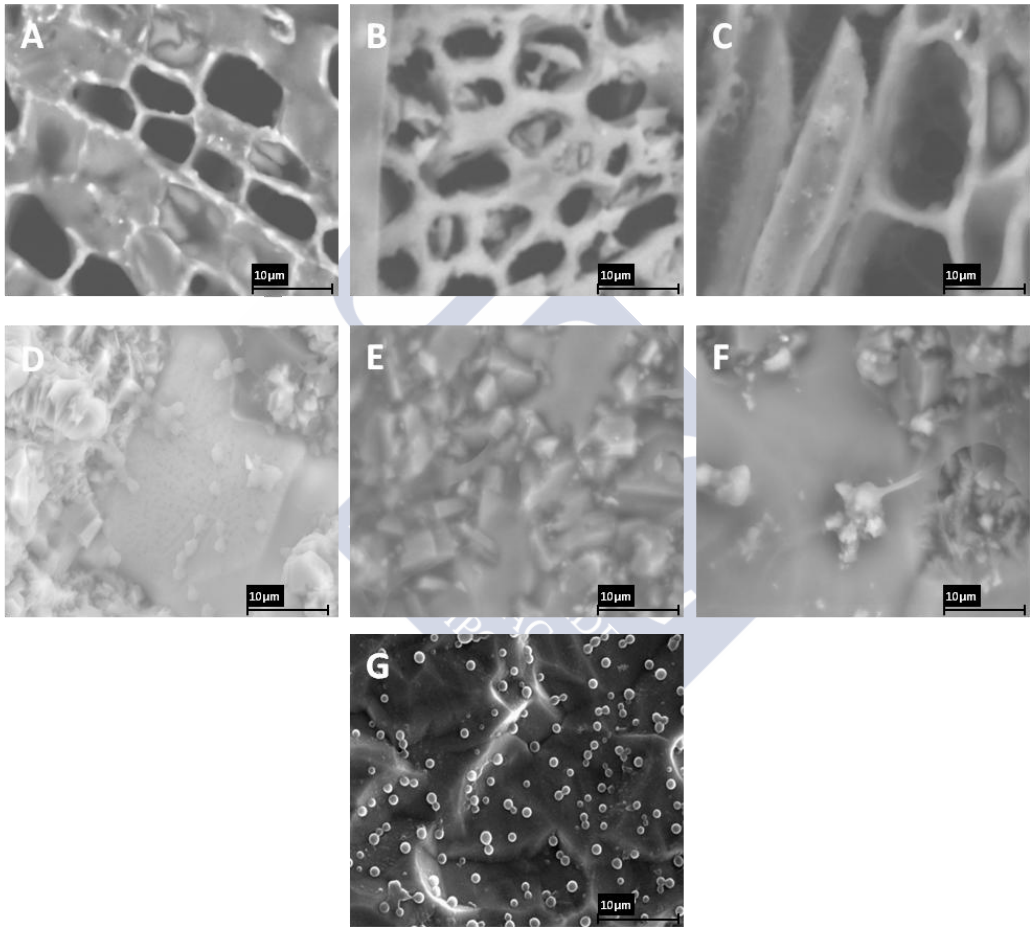

Figure 5.7 SEM micrographs of adherent platelets on different samples: (A) pine carbon, (B) oak carbon, (C) sapelli carbon, (D) pine bioSiC, (E) oak bioSiC, (F) sapelli bioSiC and (G) medical steel.

5.4.2.5 *Complement convertase attachment*

The complement system is composed of more than 30 different plasma proteins and membrane bound proteins involving three separate pathways: classical, alternative and lectin. This complex system contributes to switching on the innate inflammatory reactions and to cellular immune responses. The complement activation starts with the deposition of plasma proteins to the foreign surface, in normal physiological conditions most of the initial activated proteins is inactivated. When these proteins are recognized by others factors the amplification phase of the complement activation starts leading toward the formation of an enzyme named C5 convertase that converts C5 plasma protein to C5a and C5b (20). These two complement proteins cause the recruitment and activation of inflammatory cells, the lysis of pathogens and the increase of cellular immune response generating an inflammatory response (46). In order to quantify the amount of C5 convertase formed after the incubation of human plasma with the samples we added a substrate of this enzyme that is converted into a chromogenic substrate in the presence of this enzyme. According to the experimental data obtained (Figure 5.8), hydrophilic surfaces (bioSiC) facilitate complement activation obtaining in all the samples medium activation activity. The lower complement activation of the reference materials can be explained due to their smooth surface showing less surface area in contact with the plasma. According to what was previously reported, medium complement activation is needed for the normal wound healing process and plays key roles in inflammation, tissue regeneration and clearance of apoptotic and necrotic cells. The topical application of C5 has been found to be adequate in accelerate wound healing by increasing cell recruitment and that required for liver repair in an animal model. On the other hand, high activation of this system is found in chronic wound healing due to uncontrolled complement activation (18, 20). Furthermore in our

systems we found that complement activation is correlated with protein adsorption and in the same way with total material porosity.

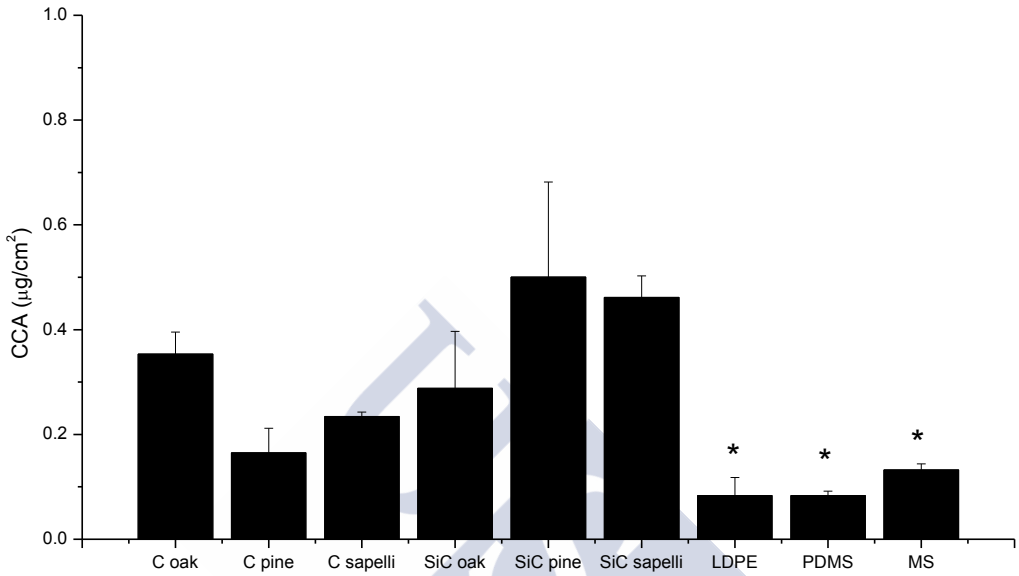

Figure 5.8 Activation of the complement convertase system after the incubation of the different samples and references with human serum. The homogeneous groups are indicated by an equal number of asterisks (*) above the columns.

5.5 Conclusions

Numerous studies have focused on the evaluation of external surface interactions with blood components but little is known about the effect of the internal structure in these interactions. We have analyzed the interactions with blood of two kinds of rough materials obtained from different natural resources, both having strong differences in surface wettability and roughness.

Every evaluated parameter was determined by a different crucial factor that modulates the biomaterial response. In hemolysis the key factors are pore size and wettability, for

protein adsorption and complement activation total surface area is the most important parameter, for platelet adhesion the contact angle is crucial whereas for clot formation roughness is the key factor.

The surface energy of carbon surfaces makes them promote low hemolysis and platelet activation. On the other hand, silicon carbide samples are characterized by a higher interaction with blood components due to its hydrophilicity.

These ceramic materials (bioSiC) have shown good hemocompatiblity, causing no platelet activation, medium complement activation and higher albumin adsorption than that of fibrinogen. These results suggest that these materials are good candidates for the clinical use as implants.

Results suggest that the evaluation of the interaction between blood and three-dimensional implant materials should include the testing of surface properties together with inner porous structure in order to consider the effects on the complete process.

5.6 References

1. Ratner B. Biomaterials science: an introduction to materials in medicine. 2nd ed. Ratner B, editor. Amsterdam: Elsevier Academic Press; 2004.

2. Babapulle MN, Eisenberg MJ. Coated stents for the prevention of restenosis: Part I. Circulation. 2002;106(21):2734-40.

3. Zheng CL, Cui FZ, Meng B, Ge J, Liu DP, Lee I-. Hemocompatibility of C-N films fabricated by ion beam assisted deposition. Surf Coat Technol. 2005;193(1-3):361-5.

4. Yoshioka T, Tsuru K, Hayakawa S, Osaka A. Preparation of alginic acid layers on stainless-steel substrates for biomedical applications. Biomaterials. 2003;24(17):2889-94.

5. Zha Z, Ma Y, Yue X, Liu M, Dai Z. Self-assembled hemocompatible coating on poly (vinyl chloride) surface. Appl Surf Sci. 2009;256(3):805-14.

6. Huang L, Yang M. Surface immobilization of chondroitin 6-sulfate/heparin multilayer on stainless steel for developing drug-eluting coronary stents. Colloids Surf, B. 2008;61(1):43-52.

7. Jones MI, McColl IR, Grant DM, Parker KG, Parker TL. Protein adsorption and platelet attachment and activation, on TiN, TiC, and DLC coatings on titanium for cardiovascular applications. J Biomed Mater Res. 2000;52(2):413-21.

8. Kim H, Moon M, Lee K, Seok H, Han S, Ryu J, et al. Mechanical stability of the diamond-like carbon film on nitinol vascular stents under cyclic loading. Thin Solid Films. 2008;517(3):1146-50.

9. McLaughlin JA, Maguire PD. Advances on the use of carbon based materials at the biological and surface interface for applications in medical implants. Diamond Relat Mater. 2008;17(4-5):873-7.

10. Li M, Cheng Y, Zheng YF, Zhang X, Xi TF, Wei SC. Surface characteristics and corrosion behaviour of WE43 magnesium alloy coated by SiC film. Appl Surf Sci. 2012;258(7):3074-81.

11. Okpalugo TIT, Ogwu AA, Maguire PD, McLaughlin JAD. Platelet adhesion on silicon modified hydrogenated amorphous carbon films. Biomaterials. 2003;25(2):239-45.

12. Okpalugo TIT, Ogwu AA, Maguire PD, McLaughlin JAD, Hirst DG. In-vitro blood compatibility of a-C:H:Si and a-C:H thin films. Diamond Relat Mater. 2004;13(4-8):1088-92.

13. Yang Y, Lai Y, Zhang Q, Wu K, Zhang L, Lin C, et al. A novel electrochemical strategy for improving blood compatibility of titanium-based biomaterials. Colloids Surf, B. 2010;79(1):309-13.

14. Chen M, Liang H, Chiu Y, Chang Y, Wei H, Sung H. A novel drug-eluting stent spray-coated with multi-layers of collagen and sirolimus. J Controlled Release. 2005;108(1):178-89.

15. Davies JE. Understanding peri-implant endosseous healing. J Dent Educ. 2003;67(8):932-49.

16. Park J, Lakes RS. Biomaterials an introduction. 3er ed. Park J and Lakes RS, editors. New York: Springer; 2007.

17. Lienemann PS, Lutolf MP, Ehrbar M. Biomimetic hydrogels for controlled biomolecule delivery to augment bone regeneration. Adv Drug Delivery Rev. 2012;64(12):1078-89.

18. Sinno H, Prakash S. Complements and the wound healing cascade: An updated review. Plast Surg Int. 2013;2013:146764.

19. Park JY, Davies JE. Red blood cell and platelet interactions with titanium implant surfaces. Clin Oral Implants Res. 2000;11(6):530-9.

20. Cazander G, Jukema GN, Nibbering PH. Complement activation and inhibition in wound healing. Clin Dev Immunol. 2012:534291, 14.

21. Singh M, Salem JA. Mechanical properties and microstructure of biomorphic silicon carbide ceramics fabricated from wood precursors. J Eur Ceram Soc. 2002;22(14-15):2709-17.

22. Varela-Feria FM, Martinez-Fernandez J, de Arellano-Lopez AR, Singh M. Low density biomorphic silicon carbide: Microstructure and mechanical properties. J Eur Ceram Soc. 2002;22(14-15):2719-25.

23. Lusquinos F, Pou J, Quintero F, Perez-Amor M. Laser cladding of SiC/Si composite coating on si-SiC ceramic substrates. Surf Coat Technol. 2008;202(9):1588-93.

24. Gonzalez P, Borrajo JP, Serra J, Chiussi S, Leon B, Martinez-Fernandez J, et al. A new generation of bio-derived ceramic materials for medical applications. J Biomed Mater Res , Part A. 2009;88A(3):807-13.

25. Lopez-Alvarez M, de Carlos A, Gonzalez P, Serra J, Leon B. Cytocompatibility of bio-inspired silicon carbide ceramics. J Biomed Mater Res , Part B. 2010;95B(1):177-83.

26. Filardo G, Kon E, Tampieri A, Cabezas-Rodriguez R, Di MA, Fini M, et al. New bio-ceramization process applied to vegetable hierarchical structures for bone regeneration: An experimental model in sheep. Tissue Eng, Part A. 2014;20(3-4):763-73.

27. Brandt B, Zollfrank C, Franke O, Fromm J, Goken M, Durst K. Micromechanics and ultrastructure of pyrolysed softwood cell walls. Acta Biomater. 2010;6(11):4345-51.

28. Diaz-Rodriguez P, Perez-Estevez A, Seoane R, Gonzalez P, Serra J, Landin M. Suitability of biomorphic silicon carbide ceramics as drug delivery systems against bacterial biofilms. ISRN Pharm. 2013:104529, 9.

29. Contreras-Garcia A, Bucio E, Concheiro A, Alvarez-Lorenzo C. Polypropylene grafted with NIPAAm and APMA for creating hemocompatible surfaces that load/elute nalidixic acid. React Funct Polym. 2010;70(10):836-42.

30. Ma WJ, Ruys AJ, Mason RS, Martin PJ, Bendavid A, Liu Z, et al. DLC coatings: Effects of physical and chemical properties on biological response. Biomaterials. 2007;28(9):1620-8.

31. Remuzzi G, Marchesi D, Mecca G, de Gaetano G, Silver M. Platelet hypersensitivity in the nephrotic syndrome. Proc Eur Dial Transplant Assoc. 1979;16:487-94.

32. Amor N, Geris L, Vander Sloten J, Van Oosterwyck H. Computational modelling of biomaterial surface interactions with blood platelets and osteoblastic cells for the prediction of contact osteogenesis. Acta Biomater. 2011;7(2):779-90.

33. Calderon NR, Martinez-Escandell M, Narciso J, Rodriguez-Reinoso F. The role of carbon biotemplate density in mechanical properties of biomorphic SiC. J Eur Ceram Soc. 2009;29(3):465-72.

34. Guelcher SA, Hollinger JO. An introduction to biomaterials. Guelcher SA and Hollinger JO, editors. Florida: CRC-Taylor & Francis; 2006.

35. Arima Y, Iwata H. Effect of wettability and surface functional groups on protein adsorption and cell adhesion using well-defined mixed self-assembled monolayers. Biomaterials. 2007;28(20):3074-82.

36. Ishizaki T, Saito N, Takai O. Correlation of cell adhesive behaviors on superhydrophobic, superhydrophilic, and micropatterned Superhydrophobic/Superhydrophilic surfaces to their surface chemistry. Langmuir. 2010;26(11):8147-54.

37. Lourenco BN, Marchioli G, Song W, Reis RL, van Blitterswijk CA, Karperien M, et al. Wettability influences cell behavior on superhydrophobic surfaces with different topographies. Biointerphases. 2012;7(1-4):46.

38. Henkelman S, Rakhorst G, Blanton J, van Oeveren W. Standardization of incubation conditions for hemolysis testing of biomaterials. Mater Sci Eng, C. 2009;29(5):1650-4.

39. Thakurta SG, Miller R, Subramanian A. Adherence of platelets to in situ albumin-binding surfaces under flow conditions: Role of surface-adsorbed albumin. Biomed Mater (Bristol, U K). 2012;7(4):045007/1,045007/10.

40. Li Y, Neoh KG, Kang E. Plasma protein adsorption and thrombus formation on surface functionalized polypyrrole with and without electrical stimulation. J Colloid Interface Sci. 2004;275(2):488-95.

41. Nonckreman CJ, Fleith S, Rouxhet PG, Dupont-Gillain CC. Competitive adsorption of fibrinogen and albumin and blood platelet adhesion on surfaces modified with nanoparticles and/or PEO. Colloids Surf, B. 2010;77(2):139-49.

42. Huang Z, Chen M, Pan S, Chen D. Effect of surface microstructure and wettability on plasma protein adsorption to ZnO thin films prepared at different RF powers. Biomed Mater (Bristol, U K). 2010;5(5):054116/1,054116/6.

43. Saito H. Purification of high molecular weight kininogen and the role of this agent in blood coagulation. J Clin Invest. 1977;60(3):584-94.

44. Takemoto S, Kusudo Y, Tsuru K, Hayakawa S, Osaka A, Takashima S. Selective protein adsorption and blood compatibility of hydroxy-carbonate apatites. J Biomed Mater Res, Part A. 2004;69A(3):544-51.

45. Nurdin N, Francois P, Mugnier Y, Krumeich J, Moret M, Aronsson B, et al. Hemocompatibility evaluation of DLC- and SiC-coated surfaces. Eur Cell Mater. 2003;5:17,26; discussion 26-8.

46. Wahl SM, Arend WP, Ross R. Effect of complement depletion on wound healing. Amer J Pathol. 1974;75(1):73-90.

USC
UNIVERSIDADE
DE SANTIAGO
DE COMPOSTELA

Capítulo 6

Synergistic effect of VEGF and biomorphic silicon carbides topography on human bone marrow derived mesenchymal stem cells differentiation to osteoblasts

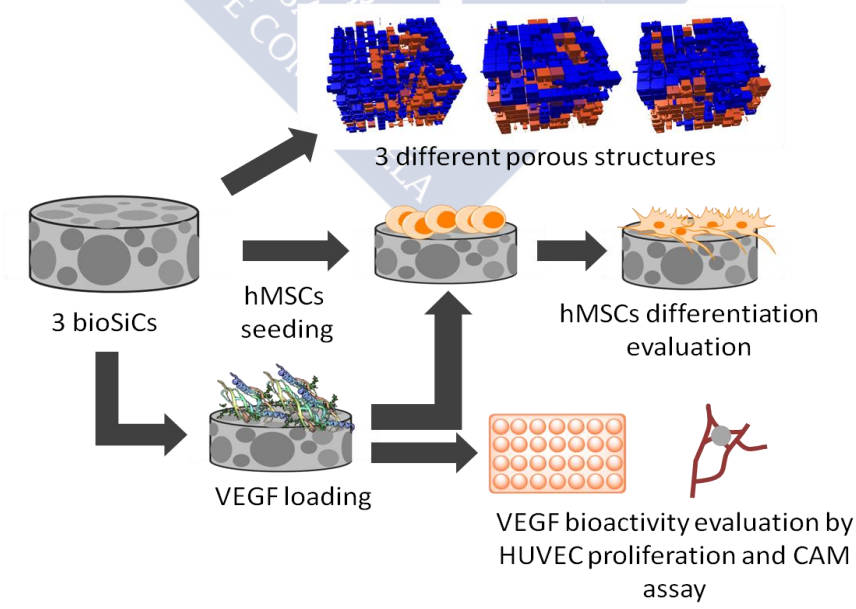

USC
UNIVERSIDADE
DE SANTIAGO
DE COMPOSTELA

6.1 Abstract

Topography features of biomaterials are able to modulate cell attachment, spreading and differentiation. The addition of growth factors to implantable biomaterials can modify these cellular responses, enhancing the therapeutic potential of the systems. The excellent biocompatibility of some biomorphic silicon carbide ceramics (bioSiCs) has been previously reported. However, the effect of their topography and surface properties on the behavior of cells has not yet been elucidated. The aim of this research is to establish the influence of bioSiCs surface topography on the differentiation of mesenchymal stem cells and the potential synergistic effect of the combination of ceramics and vascular endothelial growth factor (VEGF) on the osteoblastic differentiation. On this purpose, three porous bioSiCs from different natural precursors, with important differences in their microstructure were obtained. All bioSiCs show excellent biocompatibility results, being the largest pore size which promotes greater concentration of osteoblastic differentiation markers. Ceramics were loaded with VEGF through an ionic interaction mechanism, being the loaded systems able to achieve a controlled release of VEGF for up to five days which is capable of stimulating the proliferation of human umbilical vein endothelial cells (HUVEC) and the *in vivo* angiogenesis in the chorioallantoic membrane. The combination of VEGF and bioSiCs allows to obtain a synergistic effect on osteoblastic differentiation.

6.2 Introduction

It is well known that the chemical composition of biomaterials as well as their wettability, crystallinity, surface topography and porous structure are able to regulate attachment, spreading, migration, morphology and function of cells, thus conditioning implant fixation and integration (1-11). Huge efforts have been carried out in order to produce the ideal biomaterial whose structure and composition are able to simulate both tissue morphology (organized hierarchical structures) and functionality. For this purpose, biomimetic and bioinspired strategies are commonly used. Their focus is to use or to mimic the natural extracellular matrix topography, composition or signals to stimulate cells by the natural way of integrin mediated activation and regulation of transduction signals (1). Good examples of bioinspiration and biomimetic strategies are the synthesis of gold films with nanotopography (10), the development of metal implants with micro/nano-topography (12, 13), the use of biomimetic hydrogels (10, 14) or the production of biomorphic ceramics (15).

Biomorphic silicon carbide ceramics (bioSiCs) have been proposed as good candidates for clinical use as implants. They are able to load and controlled release antibiotics with suitable release profile to treat or prevent implant related infections. Moreover, their morphology has been found to modulate tissue interactions (16).

It has been demonstrated that metals and ceramics with similar porous structure of bone tissue show better results than non-porous materials (12). Pore size, porosity and interconnectivity are crucial for the formation of new capillary blood vessels (angiogenesis) and bone ingrowth (2, 17-19).

Nutrient and oxygen support by blood stream is essential in the tissue integration of designed scaffolds making cell survival, prompt removal of metabolic products, delivery of growth factors and recruitment of mesenchymal progenitor cells possible (2, 17, 20).

Therefore, the angiogenesis stimulation to ensure functional vascularization into the pore network of biomaterials is an interesting approach in promoting osteointegration. Moreover, angiogenesis is also implicated in the bone healing process in both endochondral and intramembranous ossification and in the differentiation of human osteoblasts (20).

The addition of proangiogenic factors such as VEGF (Vascular Endothelial Growth Factor) or FGF-2 (Fibroblast Growth Factor 2) (21, 22) to both polymeric and ceramic biomaterials has been shown to increase new vessel formation (23). Moreover, the combination of both angiogenic and osteogenic growth factors has shown a synergistic effect, enhancing bone regeneration, mineral density and deep bone formation *in vivo* due to their interactive roles in bone development (24-27).

In general the use of VEGF produces good experimental results. However, there is a risk of the occurrence of side effects if its release rate is not suitable. Local and controlled growth factor release profiles should be achieved in order to prevent systemic side effects such as uncontrolled vascularization, tumour growth and retinopathies (20). Furthermore, due to the short half-life of this protein (90 min), a suitable carrier should be developed in order to maintain its effect on osteoblast differentiation and migration (28).

The aim of this work is to develop biofunctional silicon carbide systems loaded with VEGF able to stimulate the initial angiogenesis process and promote the differentiation of migrated mesenchymal stem cells to osteoblasts.

For this purpose, we have compared three biomorphic silicon carbides, with important differences in their microstructure, in order to obtain an insight into the effect of their topography and porous structure on both, protein controlled release and human bone marrow derived mesenchymal stem cells (hMSCs) differentiation.

6.3 Materials and methods

Biomorphic silicon carbide samples were obtained as previously reported by González and coworkers (29). Three types of wood were selected as precursors according to their differences in porous structure (16); oak (*Quercus robur*), pine (*Pinus pinnaster*) and sapelli (*Enthandrophragma cylindricum*) obtaining bioSiC disks (Ø 6mm × 2 mm). Before *in vitro* experiments bioSiC samples were sterilized by autoclaving at 2 atm and 121 °C for 20 min (Raypa AES-12, Spain).

The vascular endothelial growth factor (rVEGF165) was supplied by Prepotech (USA).

6.3.1 **Biomorphic silicon carbide physical characterization**

In a previous paper, bioSiC materials were characterized by mercury porosimetry (16). The mercury intrusion curves were used to create a 3D network model of the void space and the structural elements. Pore-structure investigation was carried out by PoreXpert® 1.3.511 software (PoreXpert Ltd, UK) in order to get a better understanding of how fluids could behave in bioSiC pores when they go into a biological medium. The connectivity (mean number of throats per pore), the pore skew and the throat skew and the correlation level (between 0, random structure, and 1, organization in the unit cell) were estimated and simultaneously optimized from the mercury intrusion porosimetry cumulative curves using the Boltzmann-annealed simplex algorithm (30). The four parameters should enable the generation of unit cells with percolation properties close to the real ones. The water penetration rate in the simulated structures was modelled using PorExpert® and the waterfront position was calculated using the Bosanquet equation (31). Modelling parameters are described elsewhere (32).

The macropore diameters were studied through an image analysis program analySIS® using Scanning Electron Microscopy (SEM) images.

The composition of silicon carbide samples was obtained by Fourier transform infrared spectroscopy (FT-IR) using the KBr technique (Bruker, IFS-66v, Germany) by the pulverization of the samples.

The surface energy of bioSiC samples was evaluated using a Phoenix 300 goniometer (SEO, Korea) at room temperature using solvents with different acid/base ratio (distilled water, diiode methane and glycerol) as controls. Surface energy was obtained by the Lewis acid/base with the geometric combining rule software.

6.3.2 **Evaluation of silicon carbide biocompatibility with hMSCs**

BioSiC samples were cultured with human bone marrow derived mesenchymal stem cells (hMSCs) isolated from human bone marrow tissue aspirates provided by the Instituto de Ortopedia y Banco de Tejidos Musculoesqueléticos of the University of Santiago de Compostela (Spain) and cultured on Dulbecco's Modified Eagle's Medium (DMEM) (Sigma-Aldrich, USA) supplemented with 1% penicillin/streptomycin (Sigma-Aldrich, USA) and 20% Fetal Bovine Serum (FBS) (Biochrom, Germany). Cells were seeded on the surface of biomorphic silicon carbide samples in 96-well plates with a density of 30,000 cells per well. Cell viability values were obtained after 5, 10 and 15 days of cell culture quantifying cell proliferation by the MTT commercial assay (Roche, Switzerland) and using cell seeded plates without bioSiC as 100% of cell viability.

Cells were seeded in 24-well plates with a density of 80,000 cells per well for up to 7 days. At 1, 2 and 7 days, cell culture medium was removed and cells were washed with Phosphate Buffered Saline (PBS). After the addition of 500 µL of the lysis solution to

the cells and to obtain the corresponding cell extracts, the levels of caspase-3 were quantified by an ELISA kit (Human Caspase-3 Instant ELISA, eBioscience, USA).

In the same way, bioSiC samples were cultured with hMSCs for 1, 2 and 5 days and the concentration of secreted interleukin-1β (IL-1β) was analyzed using an ELISA assay (BenderMedSystem, USA).

The hMSCs viability on the surface of material samples was also evaluated after 5, and 15 days of cell culture by confocal microscopy (LEICA TCS-SP2, Germany) using the cell live/dead staining calcein/propidium iodide technique (33).

6.3.3 **Evaluation of hMSCs differentiation on bioSiC samples**

Biomorphic silicon carbide samples were placed in 96-well plates and cultured for up to 15 days with hMSCs at a density of 30,000 cells per well. At 5, 10 and 15 days, 200 µL of cell culture supernatant were extracted and frozen at -20 °C for quantification of cytokines and the volume was replaced with fresh supplemented DMEM medium. Differentiation medium containing dexamethasone, ascorbic acid and β-glycerophosphate (34) was used as the positive control. Cells cultured without samples or additives were used as the negative control. At the preset times, the concentration of osteocalcin (Invitrogen ELISA kit, USA), osteopontin (IBL Human osteopontin assay kit, Germany) and ALP (alkaline phosphatase) enzyme (Takara bionic, Japan) were analyzed.

6.3.4 **Silicon carbide VEGF loading and *in vitro* release**

Porous samples of biomorphic silicon carbide ceramics were loaded with rVEGF165 through a volumetric addition (30 µL) of the protein solution in PBS + 0.1% of Bovine Serum Albumin (BSA) with a concentration of 0.013 µg/µL giving a final amount of protein of 380 ng in each disk. The amount of protein not adsorbed into the silicon

carbide samples during the loading procedure and remaining in the loading wells were quantified through an ELISA (RayBiotech, USA) assay.

The protein release profiles from the bioSiC material were obtained by immersing the loaded disks into plastic tubes with 5 mL of PBS supplemented with 0.1% of BSA in order to avoid the denaturalization of the VEGF. Aliquots (200 µL) of the release medium were withdraw at preset times (10, 25, 60, 120, 180 min and 1, 2, 5, 10 and 15 days) and frozen into low bind tubes for the quantification of the protein by the ELISA assay mentioned above. The volume was replaced with fresh medium. The concentration of released VEGF during the cell culture experiments were also quantified at 5, 10 and 15 days using the same ELISA kit.

6.3.5 **Biological activity of VEGF from loaded systems**

The bioactivity of the loaded protein was tested by evaluating its effect on the proliferation of human umbilical vein endothelial cells (HUVEC). Cells were cultured with Endothelial Growth Medium (EGM) (Lonza, Switzerland) supplemented with SingleQuants (Lonza, Switzerland). Loaded and unloaded samples were placed on 96-well plate with a cell density of 4,000 cells per well. Cell proliferation after 3 and 7 days of culture was studied using a MTT assay (Roche). VEGF supplemented cell culture medium and cells only were used as positive control and negative control, respectively. Cell proliferation enhancement was obtained correcting cell proliferation of VEGF loaded bioSiC by cell proliferation with unloaded bioSiC for each sample.

Cell morphology was analysed using confocal microscopy (LEICA TCS-SP2, Germany). Cells were fixed with 4% of paraformaldehyde, permeabilized with Triton X-100 and dyed using Alexa Fluor 488 faloidin and propidium iodide.

6.3.6 *In vivo* evaluation of the angiogenic activity of VEGF loaded bioSiCs

For this purpose, the chick embryo chorioallantoic membrane (CAM) assay was selected. The studies were carried out using the procedure developed by Ribatti and coworkers to test the angiogenic or anti-angiogenic effect of therapeutic molecules with light modifications (35, 36). Fertilized hen eggs were incubated for 8 days. After removing a small portion of the shell, VEGF loaded and unloaded bioSiCs were directly placed on the membrane and incubated until day 12 to study new vessel formation (37). Membranes were fixed with 10% formalin and the vessel formation was observed using an optical lense (Olympus, Japan).

Using the same procedure, the bioactivity of VEGF released at day 5 from the bioSiCs during the *in vitro* experiments was tested. An aliquot of the release medium (20 µL) was properly diluted with a commercial extracellular polymeric matrix (Matrigel® (BD Biosciences, USA)) commonly used on CAM assays (36) and placed on the membrane. Matrigel® diluted with PBS was used as negative control.

6.3.7 Evaluation of hMSCs differentiation to osteoblast by real-time polymerase chain reaction (qPCR)

VEGF loaded and unloaded biomorphic silicon carbide samples were cultured on 24-well plates with hMSCs at a cell density of 100,000 cells per well in order to achieve a high density culture. Cell culture medium was replaced for fresh medium every three days. At 5, 10 and 15 days, samples were removed, placed in a new cell culture plate and washed with PBS. Trypsin diluted with PBS (1 mL) was added in order to remove the cells. Then, cells were centrifuged at 250 g for 5 min and resuspended in lysis solution supplemented with 2 M dithiothreitol (DTT) (Sigma-Aldrich, USA). Cells cultured with differentiation medium were used as the positive control. Cells cultured without samples or additives were used as the negative control.

The RNA extraction from the cell lysates was carried out according to GeneJET RNA Purification commercial kit protocol. Extracted RNA concentration was quantified using a Fluorometer (Qubit 2.0) with a Qubit Assay kit for RNA. The concentration of the RNA was adjusted to 10 mg/mL for the amplification with RevertAid H Minus First Strand cDNA synthesis kit (Fermentas) in a thermo cycler (Thermo Scientific Piko Thermal Cycler, Fisher). Thirty five cycles of the following stages were performed: 42 °C for 5 seconds, 50 °C for 50 seconds and 70 °C for 15 seconds.

The expression of IL-6 (5´-3´ GATGGCTGAAAAAGATGGATG; 5´-3´ GCTTGTTCCTCACTACTCTC), Tumor necrosis factor alpha (TNF-α) (5´-3´ GTGGCAGTCTCAAACTGA; 5´-3´ TATGGAAAGGGGCACTGA), protein wnt3a (5´-3´ ATAGCCTGCATCCGCTCTGA; 5´-3´ TGGTGACCATTGCCTCAACA) and β-catenin (5´-3´ CGAAGGGGGTAGGGCTGCCA; 5´-3´ GGCGGTCGACTCCACCTCAA) were quantified using glyceraldehyde-3-phosphate dehydrogenase (GAPDH) (5´-3´ ACCACAGTCCATGCCATCAC; 5´-3´ TCCACCACCCTGTTGCTGTA) as control gen.

The quantification carried out in the "Unidade de Biología Molecular" of University of A Coruña using SYBR Green as intercalating dye. Results were normalized according to the $2^{-\Delta\Delta CT}$ method (38).

6.3.8 **Statistical analysis**

Experimental results were expressed as means and standard deviations. The statistical significant differences between treatments were established by the analysis of variance (ANOVA). When the F-ratio suggests significant differences between groups, the least significant difference (LSD) test was used to compare them by pairs. ANOVA and LSD were performed by Statgraphics Centurion®X64 software (USA).

6.4 Results

6.4.1 **Biomorphic silicon carbide characterization**

Using the mercury porosimetry results, PoreXpert® software allows the simulation of the void structures of the different bioSiC samples which are represented as series of interconnected unit cells. Each unit cell comprises 1,000 nodes equally spaced and packed in a cubic-close-array. Cubic pores are centered at each node, and connected by cylindrical throats in each Cartesian direction.

This kind of simulation allows the prediction of some interesting parameters that can affect the ceramic biological behavior as thermal conductivity, permeability, tortuosity and fluid uptake, etc. Figure 6.1 shows fluid uptake simulation of the three materials. Blue cubes correspond to pores filled by water molecules after 100 ms at 0 MPa whereas orange cubes are unfilled pores. The highest number of water filled pores was observed for oak bioSiC with values of 68.59% of fluid uptake followed by sapelli bioSiC with 49.98% and pine bioSiC with 31.01%. According to the model simulation sapelli bioSiC shows the highest values of pore interconnectivity, crucial for cell and tissue ingrowth (39), followed by oak and pine.

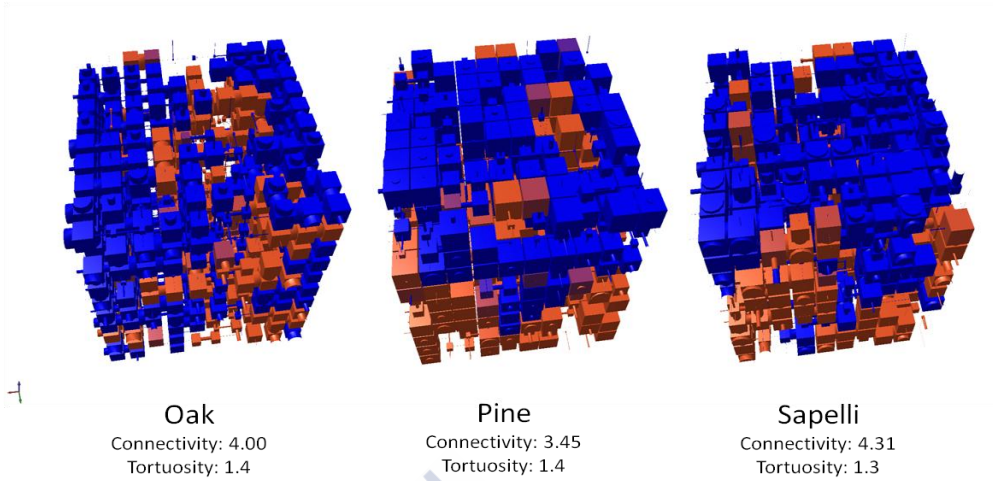

Figure 6.1 Characterization of biomorphic silicon carbide samples void porosity models of oak, pine and sapelli bioSiC samples from PoreXpert® simulation, Blue cubes correspond to pores filled by water molecules after 100 ms at 0 MPa whereas orange cubes are unfilled pores.

The image software analySIS® allows the macropores size of silicon carbide samples to be estimated, being oak bioSiCs 250 ± 20 µm, sapelli bioSiCs 140 ± 30 µm and pine silicon carbide samples 50 ± 20 µm.

Sample	Energy	Dispersive	Polar	Acid	Base
Oak bioSiC	-102.021	47.246	-149.267	36.431	152.892
Pine bioSiC	17.255	40.767	-23.512	2.209	62.570
Sapelli bioSiC	-9.765	44.351	-54.116	8.856	82.672

Table 6.1 Values of surface energy using Lewis acid/base with geometry combining rule software for oak, pine and sapelli samples.

Surface energy was evaluated by means of contact angle measurements using polar and apolar solvents. All samples are characterized by a basic non polar behavior, the higher energy values being obtained by pine biomorphic silicon carbide samples (Table 6.1).

Moreover, the FT-IR spectrum of these materials (Figure 6.2) shows together with the typical absorption bands of silicon carbide at 782 cm^{-1} and 798 cm^{-1} associated to Si-C stretching vibration mode, carbonate (C-O) groups identified by two absorption bands 877 cm^{-1} and 750 cm^{-1}, Si-O groups with bands at 1,100 cm^{-1} and 800 cm^{-1}, carboxyl groups (C=O) with a peak at 1,568 cm^{-1} and hydroxyl functional groups (-OH) at around 3,571 cm^{-1} with a shoulder at 3,550 cm^{-1} (40).

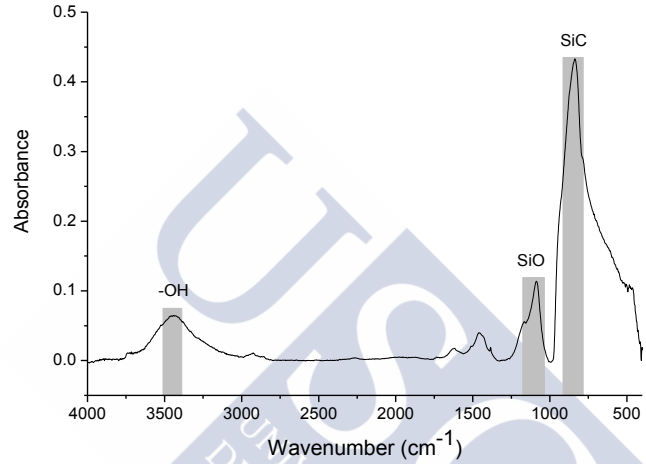

Figure 6.2 Example of FT-IR profile using the KBr technique of pine biomorphic silicon carbide.

6.4.2 **Evaluation of silicon carbide biocompatibility with hMSCs**

The cell response to the three different biomorphic silicon samples as a function of biomaterial microstructure was evaluated. Figure 6.3 shows the confocal micrographs of hMSCs cultured for 15 days on the surface of the bioSiC samples. As it can be seen, all the samples show low cell mortality (red cells) together with high number of alive attached cells, particularly for oak bioSiC samples. Cells not only were able to grow on the external surface but also covering the internal structure as it is shown in Figure 6.3D and/or connecting the two sides of the pore channels.

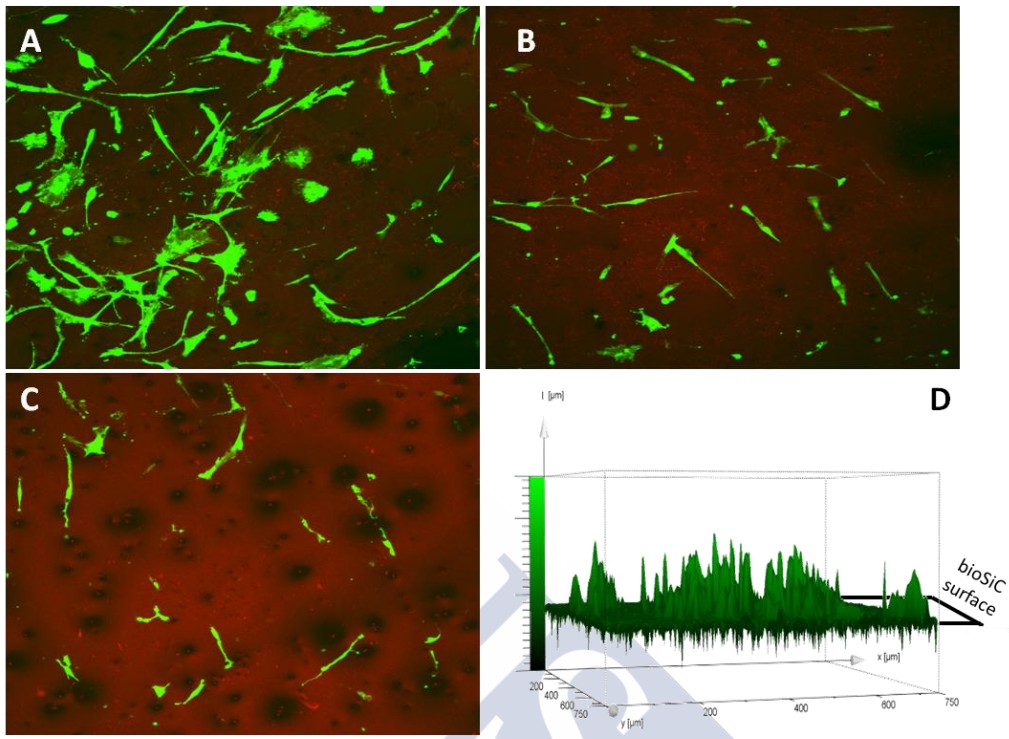

Figure 6.3 Alive cells (in green) and dead cells (in red) after culturing hMSC for 15 days on oak bioSiC (A), sapelli bioSiC (B) and pine bioSiC (C). Example of the growth of cells inside the pores of the samples obtained by the confocal images software analysis (D).

Quantitative cell viability results (Figure 6.4A) are in agreement with the confocal images. All the samples show cell viability percentages around 100% at the different culture times studied. As it can be observed cell proliferation percentage decreases with time for oak and sapelli samples whereas it increases for pine bioSiC samples reaching the maximum value after 15 days of assay.

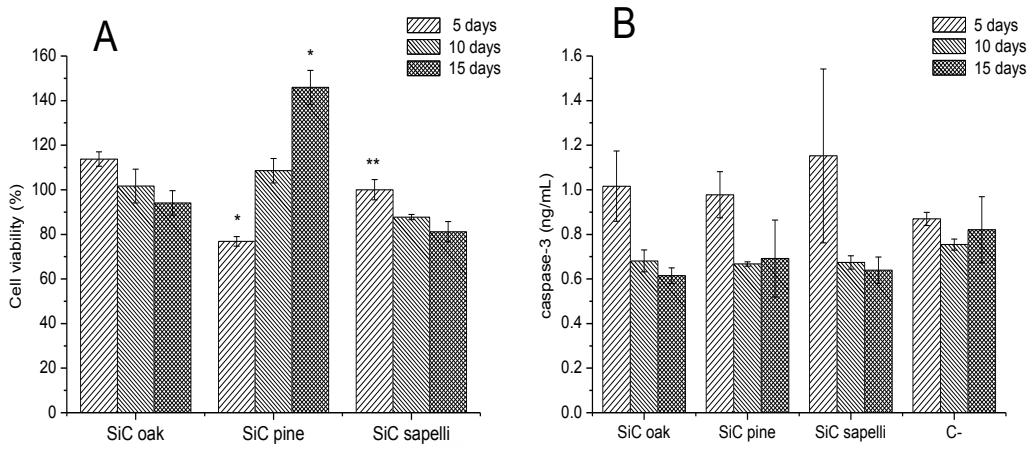

Figure 6.4 (A) Cell viability percentage and levels of caspase-3 (B) secreted by hMSC cultured on oak, pine and sapelli bioSiC. The homogeneous groups are indicated by an equal number of asterisks (*) above the columns ($\alpha < 0.05$).

Cell apoptosis was evaluated by the quantification of the caspase-3 levels after 5, 10 and 15 days of cell culture (Figure 6.4B). After a quantity higher than the negative control caspase-3 level at the first time (5 days) cells were able to attach and proliferate on the bioSiC samples without toxic effects and with no statistical significant differences between them. Moreover, the acute cytotoxicity, quantified by the proinflammatory cytokine (IL-1β), did not show detectable levels for any bioSiC sample after 24 hours of cell culture, which means that these materials do not cause an inflammatory response.

6.4.3 **Evaluation of hMSCs differentiation on bioSiC samples**

Bone marrow derived mesenchymal stem cells (hMSCs) have the ability of differentiating into cells of connective tissue lineages, including bone, cartilage, fat and muscle, thus having high potential for regenerative medicine and tissue engineering applications (4). Figure 6.5 shows the common indicators used for quantifying

osteoblastic differentiation; ALP, osteopontin and osteocalcin. ALP is a widely used marker of matrix mineralization for early osteogenesis, while osteocalcin and osteopontin are indicators for later osteogenic activity evaluation (12).

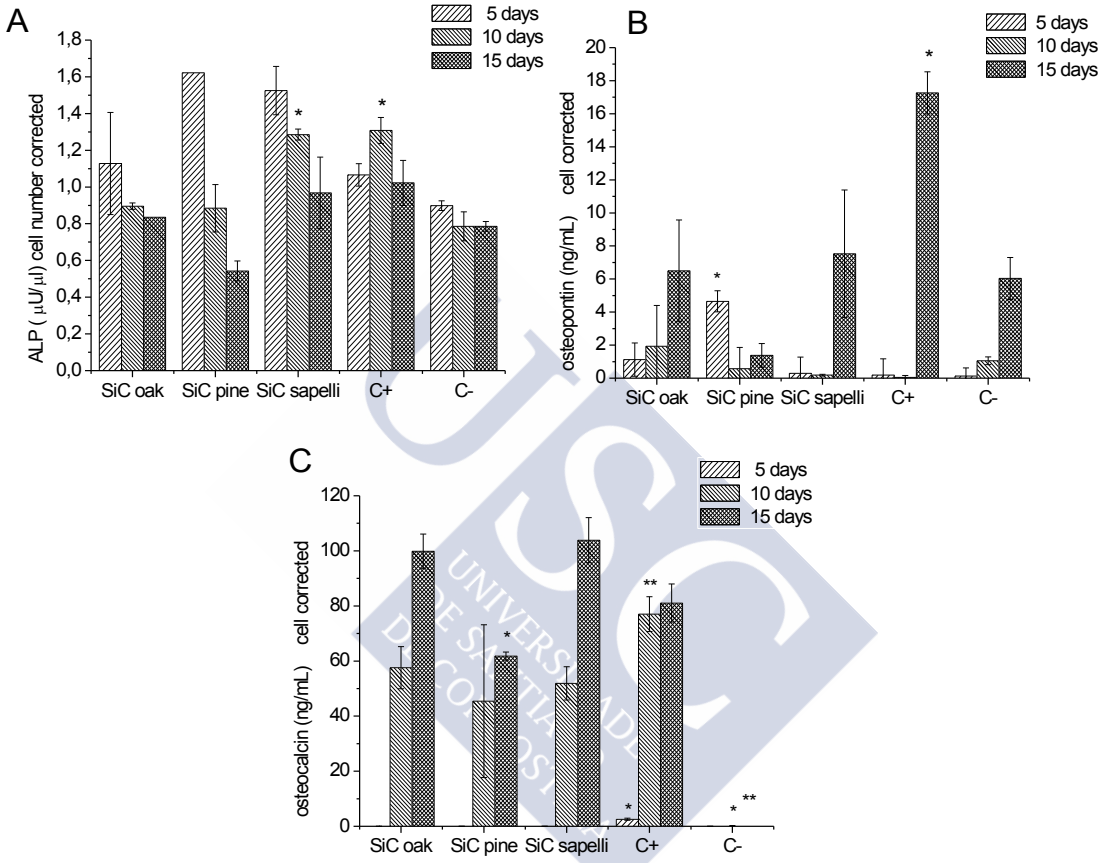

Figure 6.5 Concentration of osteoblastic markers secreted by hBMSCs corrected by cell number, of cells cultured on oak, pine and sapelli bioSiC of (A) alkaline phosphatase; (B) osteopontin and (C) osteocalcin. The homogeneous groups are indicated by an equal number of asterisks (*) above the columns ($\alpha < 0.05$).

Cells cultured on biomorphic silicon carbide were able to secrete a similar amount of ALP (Figure 6.5A) than the positive control, a specific osteogenic differentiation medium, thus indicating their osteoblastic differentiation. The level of ALP at the first

stage (5 days) decreases with time when the mineralization starts to take place (18). These results agree with the idea derived from Figure 6.4A; after the first week of culture the decrease in cell growth rate on oak and sapelli silicon carbide samples could be attributed to a period of late osteoblastic differentiation, matrix maturation and mineralization which may be correlated with the higher levels of osteopontin and osteocalcin observed on these samples especially after fifteen days of cell culture (Figure 6.5B-C).

6.4.4 **Silicon carbide VEGF loading and *in vitro* release**

The quantification of unloaded protein showed lower levels than 0.5% for all bioSiCs, meaning that they were able to retain most of VEGF on their surface and therefore, having a suitable loading ability.

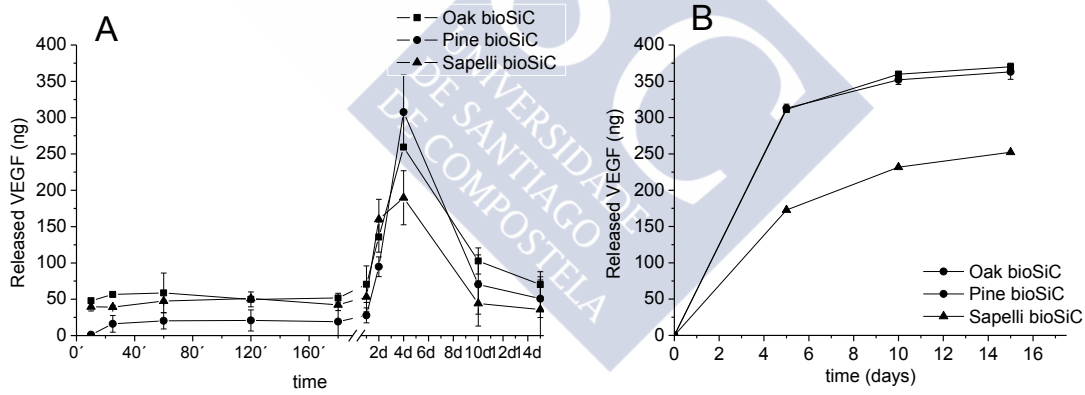

Figure 6.6 Release profiles for the three of VEGF loaded systems in (A) PBS supplemented with 0.1% of BSA and (B) DMEM cell culture medium supplemented with FBS and antibiotics.

Protein release profiles in PBS and in DMEM are shown in figure 6.6A and 6.6B respectively. The profiles using DMEM were obtained in order to simulate the release in cell culture conditions. Loaded systems were able to achieve a controlled release for

up to five days. After this time point the protein released in PBS is degraded which explain the decrease in the percentage of VEGF released. Despite it being described that salts and proteins such as BSA can be used to stabilize VEGF (23), the addition of 0.1% of BSA was unable to inhibit the protein degradation after 5 days of assay in PBS. However, when using DMEM, the percentage of VEGF achieved 100% after fifteen days of assay. The increase in salt concentration improves the stability of VEGF as suggested by other authors (20).

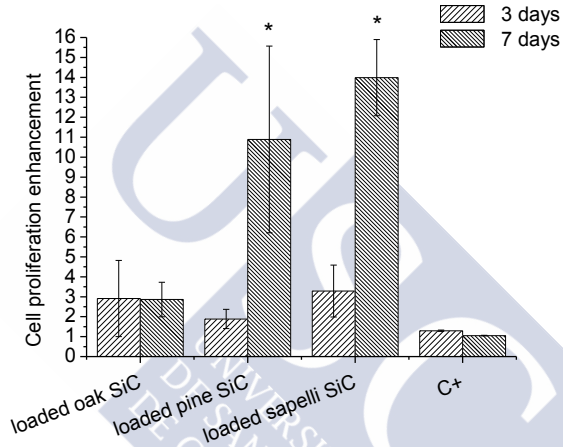

Figure 6.7 Cell proliferation enhancement of HUVEC cells of VEGF loaded silicon carbide samples compared to unloaded systems. The homogeneous groups are indicated by an equal number of asterisks (*) above the columns ($\alpha < 0.05$).

As VEGF is an endothelial cell specific mitogen (22), the bioactivity of loaded systems can be evaluated by its proliferation effect on the human umbilical vein endothelial cells (HUVEC). Figure 6.7 shows HUVEC proliferation both after 72 hours and 7 days of their culture with VEGF loaded samples. As it can be seen the VEGF release from loaded systems enhance HUVEC proliferation compared to the positive control specially after seven days of cell culture on the surface of loaded bioSiC. Moreover, confocal images show that HUVEC grow (Figure 6.8) around the macropores or even connecting both sides of porous structures.

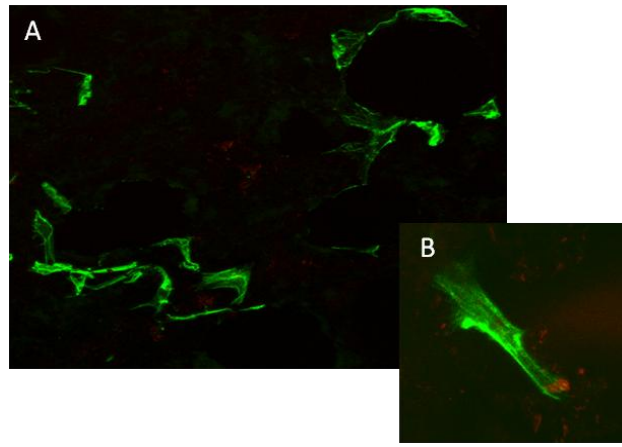

Figure 6.8 Confocal micrographs of HUVEC cells cultured on the surface of VEGF loaded bioSiC samples. Alive cells in green and dead cells in red. Cells growing around the pores of sapelli silicon carbide (A) and cells growing in the porous structure of oak silicon carbide (B).

6.4.5 **Evaluation of *in vivo* angiogenesis of VEGF loaded bioSiC**

Angiogenesis process is necessary to ensure cell viability and enhances bone integration of the implanted materials (41). CAM experiment was used to test angiogenesis *in vivo*. After the incubation of VEGF loaded silicon carbide samples and equivalent amounts of VEGF as previously described, all the chicks died.

Nevertheless when the dose of VEGF is low, as it is in the bioSiC release medium diluted with Matrigel® the angiogenic effect can be observed (Figure 6.9A-D). A similar number of new blood vessels with a large amount of branches are generated for the samples derived from the three bioSiCs tested. No new vessel formation can be seen either in negative control or in Matrigel® alone. Interestingly, unloaded oak and sapelli biomorphic silicon carbide used as negative controls were invaginated by the membrane (Figure 6.9A and 6.9C), whereas pine bioSiC samples remain in the membrane surface (Figure 6.9B).

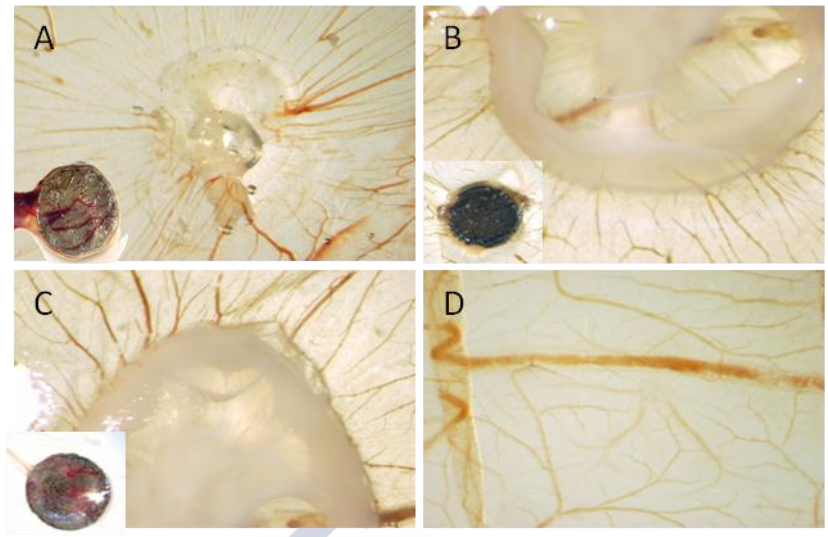

Figure 6.9 New vessels on chick embryo chorioallantoic membrane after 8 days of incubation with released medium of VEGF loaded systems diluted with Matrigel® for (A) oak biomorphic silicon carbide (B) pine biomorphic silicon carbide (C) sapelli biomorphic silicon carbide and (D) negative control. Small images in the lower left correspond to the unloaded ceramics that were invaginated by (A and C) or remained on (B) the chorionic membrane.

6.4.6 **Evaluation of hMSCs differentiation to osteoblast by real-time polymerase chain reaction (qPCR)**

In order to evaluate the synergistic effect of loaded VEGF and material surface properties on cell attachment and differentiation of hMSCs, qPCR was carried out for the genes encoding, interleukin 6 (IL-6), tumor necrosis factor alpha (TNF-α), beta-catenin (β-catenin) and protein wnt-3a.

As it can be concluded from the experimental data the expression of inflammatory cytokines (IL-6; TNF-α) for all, loaded and unloaded systems, is similar to the negative control (Figure 6.10A-B) indicating the absence of a cellular toxic reaction.

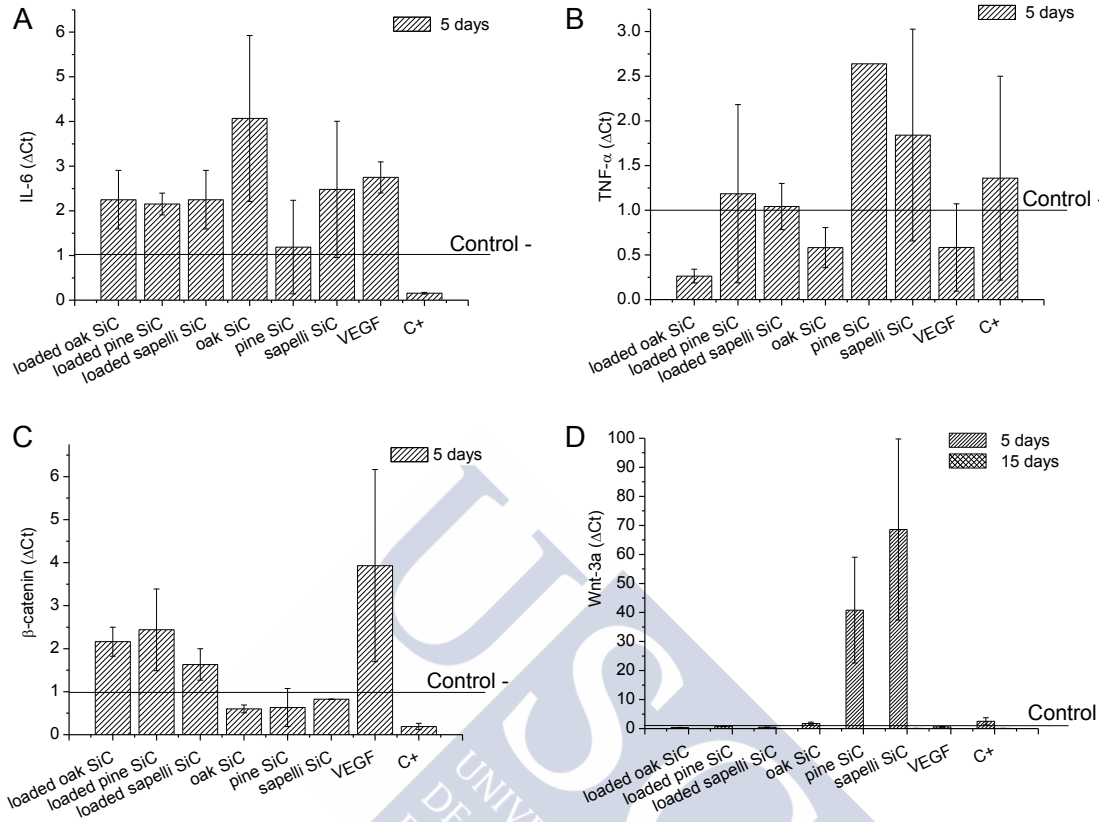

Figure 6.10 Quantification of RNAm expression of hBMSCs cultured with loaded and unloaded systems by qPCR according to the $2^{-\Delta\Delta_{CT}}$ method corrected by GAPDH expression for (A) IL-6 (B) TNF-α (C) β-catenin (D) Wnt-3a.

Figure 6.10C-D shows that after 5 days, the levels of beta-catenin expression and wnt-3a for VEGF loaded systems are higher and lower, respectively, than for the unloaded systems. VEGF loaded bioSiCs and the protein added to the cell culture were able to significantly increase the expression of β-catenin and decrease the expression of wnt-3a in comparison with the negative control after five days of cell culture. On the other hand unloaded bioSiCs and differentiation medium were found to decrease the expression of β-catenin and significantly increase the expression of wnt-3a when they are compared to negative control.

Statistical significant differences were found between unloaded bioSiCs with regard to the expression of wnt-3a which was lower for oak bioSiC one. After fifteen days of cell culture no levels of wnt-3a were detected neither for loaded nor for unloaded systems which indicates that the differentiation process was carried out for both systems.

6.5 Discussion

According to previously reported (16, 42) the use of different natural precursors for the bioSiC synthesis samples leads to the production of porous ceramics whose properties depend on the initial microstructure, pore size and porosity of the template materials. It has also been found that such properties are able to modulate their biological response and the drug release profile of a loaded antibiotic (16).

The use of PoreXpert® software has made possible the simulation of the pore structure of the three biomorphic silicon carbide samples used. The values of fluid uptake show strong differences between the behavior of the three structures. These variations in fluid uptake modify the accessibility of material surface to the cell suspensions and cell culture medium modulating cell viability and attachment.

Hard-connective tissues replacement should ensure the suitable mechanical properties/density/porosity relationship to guarantee enough resistance together with effective nutrient supply, gas diffusion and metabolic waste removal that allows cell ingrowth and osteointegration avoiding problems of stress shielding and implant failure (39, 43, 44). Based on microstructural results, oak and sapelli, with bigger pore size, interconnectivity and water uptake predicted parameters can be postulated as better candidates for allowing cell adhesion and tissue ingrowth.

Surface energy has been correlated with surface wettability and roughness (45) and modulates the interaction between cells and biomaterial surface. Despite the three

bioSiC being hydrophilic (Table 6.1), differences in pine bioSiC behavior, with high surface energy, can be related to its lower total porosity, pore size and water uptake.

The presence of functional groups on the ceramic surfaces, hydroxyl and SiO (Figure 6.2) detected by the FT-IR analysis, could be explained by the oxidation of the unreacted silicon atoms after the infiltration process of carbon performing with molten silicon (46). Hydroxyl groups can increase the bioSiC loading ability through the interaction with numerous therapeutic molecules.

Previous authors (33, 47, 48) have proposed some biomorphic silicon carbides as easy to obtain materials suitable for bone regeneration due to their high strength and toughness, their interconnected porosity and biocompatibility. However, as far as we know those studies have only been carried out using cell lines and the effect of material properties on cell behavior has not been established. In this study, the biocompatibility has been evaluated using human bone marrow derived mesenchymal stem cells (hMSCs). Confocal micrographs show cells growing on the surface of biomorphic silicon carbide (Figure 6.3) exhibiting a stellae shape with filopodia characteristic of rough surfaces with high size islands (49) obtained by the formation of silicon carbide crystals during the infiltration process in the ceramic synthesis (50).

The differences obtained in hMSCs biocompability (Figure 6.4A) for the three bioSiCs could be justified by a possible differentiation of hMSCs to osteoblasts in oak and sapelli bioSiC samples. Differentiation slows down cell proliferation as pointed out by other authors (51). However, no significant differences could be observed on cell toxicity (caspase-3, IL-1β) for all the bioSiCs with the negative control indicating the high potential of these systems as tissue engineering scaffolds.

As it was pointed out in the introduction, surface roughness plays an important role on cell attachment, proliferation and differentiation, controlling cell-material surface

interactions. The spontaneous chemical reaction taking place during biomorphic silicon carbide production leads to a material with a variable rough surface due to the silicon carbide crystallization process depending on the pore structure (52). It is well documented that rough surface increases cell differentiation when compared to flat surfaces and the presence of groves on the surface modulates cell contact guidance growth (53-56).

Silicon is a crucial element for the development of connective and skeletal tissues, playing a role in the mineralization front of growing bone. It was found that high dietary support of silicon is associated with a superior bone mineral density and also that the *in vitro* culture of osteoblasts with a component containing silicon increased extracellular matrix synthesis, proliferation, alkaline phosphatase activity and osteocalcin synthesis (57). We hypothesize that the presence of silicon in the porous scaffolds could also contribute to the enhancement of the osteoblastic differentiation and the mineralization of bone marrow derived mesenchymal stem cells. The presence of silicon atoms together with pore size, interconnectivity and surface nanotopography, energy and roughness of oak and sapelli bioceramics could justify the osteoblastic differentiation detected (Figure 6.5A-C). Those properties improve the osteogenic response of mesenchymal stem cells, the vessel formation and the bone tissue ingrowth, explaining the better results achieved with those samples (17, 44, 58, 59). Moreover, the lower surface energy of oak and sapelli silicon carbides could also contribute to the enhancement to osteoblastic cell differentiation as pointed out by other authors (13).

VEGF release profiles (Figure 6.6A-B) show differences between the three release profiles. The higher porosity of oak silicon carbide could explain the fast VEGF release because of the presence of higher amount of liquid inside the pores that elute the growth factor. The higher surface area of sapelli biomorphic silicon carbide led to

higher surface interactions between the protein and the ceramic and therefore decreases the release rate of VEGF. The release profiles of VEGF (Figure 6.6A) for all the bioSiCs showed an increase in protein release after five days of study. These release profiles should be adequate for tissue engineering applications as it is known that in the normal bone healing process the concentration of VEGF increases at day five and decreases at day ten (27, 60).

The extended release profiles in DMEM for a period of 15 days can be justified by the interaction between VEGF and the hydroxyl groups (Figure 6.2). Vascular endothelial growth factor has its isoelectric point at pH 8.5 (61). At the pH of the study 7.4 the protein is positively charged and could interact with the negatively charged –OH and SiO groups by hydrogen bonding and electrostactic interactions (62). This mechanism should control the release of the protein.

VEGF is a labile protein with a short half-life, which stability and effectiveness can be improved by its inclusion into polymeric particles or by its immobilization on metallic surfaces (63, 64). According to the effect of loaded bioSiC samples on HUVEC proliferation (Figure 6.7), the inclusion of VEGF into the ceramics not only does not affect the activity of the protein but also promotes cell proliferation to a greater extent than the cell culture medium supplemented with VEGF (Control +). The significant differences between the positive control and the loaded systems can be justified by the higher efficacy of the protein when administered through a controlled release mechanism versus a higher single dose, as described by other authors (63). The faster release profiles obtained from oak biomorphic silicon carbide could explain the lower HUVEC cell proliferation enhancement observed for this material as the faster the growth factor is released the faster it is degraded.

The effect of VEGF loaded systems on *in vivo* angiogenesis was studied using the CAM assay. Despite of human VEGF is commonly used for this assay (62, 65, 66) it seems

that high doses of protein may trigger an immunological response which ultimately leads to the animal death observed in the VEGF loaded bioSiCs and equivalent amounts of protein. However, the use of unloaded systems has led to the invagination of the ceramics by the membrane for oak and sapelli bioSiCs that should be correlated with the excellent biocompatibility of the systems. Pine bioSiC was not included in the membrane that must be related to their lower porosity and higher surface energy.

The low expression of TNF-α and IL-6 for all the loaded and unloaded samples quantified by qPCR indicates the low toxicity of these biomaterials.

VEGF has been found to be crucial for endochondral ossification by coupling cartilage resorption with bone formation, extracellular matrix mineralization and endothelial cell recruitment (67, 68). Furthermore this factor is able to stimulate osteoblasts proliferation and differentiation increasing new bone maturation by stimulating endothelial cells to produce osteoanabolic growth factors.

Beta-catenin signalling pathway plays an important role in osteoblast differentiation, maturation and bone formation. It has been found that beta-catenin is the central gene to increase osteoblast differentiation and proliferation while wnt/beta-catenin ratio is involved in the effect of implant topography on osteoblastic differentiation. It was reported that an increase in beta-catenin mRNA expression is associated to osteoblastic differentiation (51, 69).

The higher expression of beta-catenin and lower expression of wnt-3a observed after five days of cell culture for VEGF loaded systems could be justified by a synergistic effect of the surface roughness and VEGF on cell attachment and differentiation of hMSCs cultured with loaded bioceramics that promotes a faster osteoblastic differentiation of hMSCs. The higher expression of wnt-3a for the unloaded systems should cause an increase in cell proliferation to achieve a high enough number of cells

able to undergo osteoblastic differentiation observed at long periods (51). After 15 days, the decrease in the wnt-3a expression to undetectable levels observed for unloaded bioSiCs corroborates with these findings in agreement with the osteoblastic differentiation results from ELISA quantification of ALP, osteocalcin and osteopontin (Figure 6.5A-C). The addition of VEGF to biomorphic silicon carbide samples is able to achieve a faster differentiation of hMSCs than the materials themselves.

6.6 Conclusions

We propose a new non degradable system, biomorphic silicon carbide with excellent biocompatibility, high stability and good mechanical properties, able to load and release the bioactive vascular endothelial growth factor at a rate modulated by its porous structure. The particular morphology and surface properties of bioSiC from oak and sapelli is able to stimulate the differentiation of mesenchymal stem cells to osteoblasts after 15 days of cell culture. The microstructure of sapelli bioSiC achieves a more controlled release of VEGF, stimulating the most the proliferation of HUVEC. The addition of VEGF to bioSiC samples increases the expression of β-catenin at day five of study which could indicate a faster osteoblastic differentiation than that observed on bioSiC alone showing a synergistic effect of materials properties and VEGF loading. Based on these results sapelli bioSiC is the most promising material to be used for tissue engineering applications.

6.7 References

1. Biggs MJP, Richards RG, Gadegaard N, Wilkinson CDW, Dalby MJ. The effects of nanoscale pits on primary human osteoblast adhesion formation and cellular spreading. J Mater Sci: Mater Med. 2007;18(2):399-404.

2. Adachi T, Osako Y, Tanaka M, Hojo M, Hollister SJ. Framework for optimal design of porous scaffold microstructure by computational simulation of bone regeneration. Biomaterials. 2006;27(21):3964-72.

3. Ayala R, Zhang C, Yang D, Hwang Y, Aung A, Shroff SS, et al. Engineering the cell-material interface for controlling stem cell adhesion, migration, and differentiation. Biomaterials. 2011;32(15):3700-11.

4. Barrias CC, Ribeiro CC, Lamghari M, Miranda CS, Barbosa MA. Proliferation, activity, and osteogenic differentiation of bone marrow stromal cells cultured on calcium titanium phosphate microspheres. J Biomed Mater Res, Part A. 2005;72A(1):57-66.

5. Intranuovo F, Favia P, Sardella E, Ingrosso C, Nardulli M, d'Agostino R, et al. Osteoblast-like cell behavior on plasma deposited Micro/Nanopatterned coatings. Biomacromolecules. 2011;12(2):380-7.

6. Collie AMB, Bota PCS, Johns RE, Maier RV, Stayton PS. Differential monocyte/macrophage interleukin-1β production due to biomaterial topography requires the β2 integrin signaling pathway. J Biomed Mater Res, Part A. 2011;96A(1):162-9.

7. Kammerer PW, Gabriel M, Al-Nawas B, Scholz T, Kirchmaier CM, Klein MO. Early implant healing: Promotion of platelet activation and cytokine release by topographical, chemical and biomimetical titanium surface modifications *in vitro*. Clin Oral Implants Res. 2012;23(4):504-10.

8. Ravichandran R, Liao S, Ng CC, Chan CK, Raghunath M, Ramakrishna S. Effects of nanotopography on stem cell phenotypes. World J Stem Cells. 2009;1(1):55-66.

9. Badami AS, Kreke MR, Thompson MS, Riffle JS, Goldstein AS. Effect of fiber diameter on spreading, proliferation, and differentiation of osteoblastic cells on electrospun poly(lactic acid) substrates. Biomaterials. 2005;27(4):596-606.

10. Bakeine GJ, Ban J, Grenci G, Pozzato A, Dal Zilio S, Prasciolu M, et al. Design, fabrication and evaluation of nanoscale surface topography as a tool in directing differentiation and organisation of embryonic stem-cell-derived neural precursors. Microelectron Eng. 2009;86(4-6):1435-8.

11. Dulgar-Tulloch AJ, Bizios R, Siegel RW. Differentiation of human mesenchymal stem cells on nano- and micro-grain size titania. Mater Sci Eng, C. 2011;31(2):357-62.

12. Chen X, Cai K, Lai M, Zhao L, Tang L. Mesenchymal stem cells differentiation on hierarchically Micro/Nano-structured titanium substrates. Adv Biomater (Weinheim, Ger). 2012(3):B216-23.

13. Le Guehennec L, Lopez-Heredia M, Enkel B, Weiss P, Amouriq Y, Layrolle P. Osteoblastic cell behaviour on different titanium implant surfaces. Acta Biomater. 2008;4(3):535-43.

14. Lienemann PS, Lutolf MP, Ehrbar M. Biomimetic hydrogels for controlled biomolecule delivery to augment bone regeneration. Adv Drug Delivery Rev. 2012;64(12):1078-89.

15. Filardo G, Kon E, Tampieri A, Cabezas-Rodriguez R, Di Martino A, Fini M, et al. New bio-ceramization processes applied to vegetable hierarchical structures for bone regeneration: An experimental model in sheep. Tissue Eng, Part A. 2014;20(3-4):763-73.

16. Diaz-Rodriguez P, Perez-Estevez A, Seoane R, Gonzalez P, Serra J, Landin M. Suitability of biomorphic silicon carbide ceramics as drug delivery systems against bacterial biofilms. ISRN Pharm. 2013:104529, 9.

17. Klenke FM, Liu Y, Yuan H, Hunziker EB, Siebenrock KA, Hofstetter W. Impact of pore size on the vascularization and osseointegration of ceramic bone substitutes *in vivo*. J Biomed Mater Res, Part A. 2008;85A(3):777-86.

18. Gomes ME, Sikavitsas VI, Behravesh E, Reis RL, Mikos AG. Effect of flow perfusion on the osteogenic differentiation of bone marrow stromal cells cultured on starch-based three-dimensional scaffolds. J Biomed Mater Res, Part A. 2003;67A(1):87-95.

19. Sun X, Kang Y, Bao J, Zhang Y, Yang Y, Zhou X. Modeling vascularized bone regeneration within a porous biodegradable CaP scaffold loaded with growth factors. Biomaterials. 2013;34(21):4971-81.

20. De la Riva B, Nowak C, Sanchez E, Hernandez A, Schulz-Siegmund M, Pec MK, et al. VEGF-controlled release within a bone defect from alginate/chitosan/PLA-H scaffolds. Eur J Pharm Biopharm. 2009;73(1):50-8.

21. Clevert D, Bahramsoltani M, De Spiegelaere W, Janczyk P, Hiebl B, Cornillie P, et al. Quantitation of angiogenesis *in vitro* induced by VEGF-A and FGF-2 in two different human endothelial cultures - an all-in-one assay. Clin Hemorheol Microcirc. 2010;46(2-3):189-202.

22. Tille J, Pepper MS. Mesenchymal cells potentiate vascular endothelial growth factor-induced angiogenesis *in vitro*. Exp Cell Res. 2002;280(2):179-91.

23. Kim J, Kim T, Jin G, Park J, Yun Y, Jang J, et al. Mineralized poly(lactic acid) scaffolds loading vascular endothelial growth factor and the *in vivo* performance in rat subcutaneous model. J Biomed Mater Res, Part A. 2013;101A(5):1447-55.

24. Zhang W, Wang X, Wang S, Zhao J, Xu L, Zhu C, et al. The use of injectable sonication-induced silk hydrogel for VEGF165 and BMP-2 delivery for elevation of the maxillary sinus floor. Biomaterials. 2011;32(35):9415-24.

25. Kempen DHR, Lu L, Heijink A, Hefferan TE, Creemers LB, Maran A, et al. Effect of local sequential VEGF and BMP-2 delivery on ectopic and orthotopic bone regeneration. Biomaterials. 2009;30(14):2816-25.

26. Chen F, Chen R, Wang X, Sun H, Wu Z. *In vitro* cellular responses to scaffolds containing 2 microencapsulated growth factors. Biomaterials. 2009;30(28):5215-24.

27. Shah NJ, MacDonald ML, Beben YM, Padera RF, Samuel RE, Hammond PT. Tunable dual growth factor delivery from polyelectrolyte multilayer films. Biomaterials. 2011;32(26):6183-93.

28. Huang Y, Kaigler D, Rice KG, Krebsbach PH, Mooney DJ. Combined angiogenic and osteogenic factor delivery enhances bone marrow stromal cell-driven bone regeneration. J Bone Miner Res. 2005;20(5):848-57.

29. Gonzalez P, Borrajo JP, Serra J, Chiussi S, Leon B, Martinez-Fernandez J, et al. A new generation of bio-derived ceramic materials for medical applications. J Biomed Mater Res, Part A. 2009;88A(3):807-13.

30. Johnson, A., Roy, I.M., Matthews, G.P., Patel, D. An improved simulation of void structure, water retention and hydraulic conductivity in soil with the pore-cor three-dimensional network. Eur J Soil Sci. 2003;54:477-89.

31. Schoelkopf J, Ridgway CJ, Gane PAC, Matthews GP, Spielmann DC. Measurement and network modeling of liquid permeation into compacted mineral blocks. J Colloid Interface Sci. 2000;227(1):119-31.

32. Laudone GM, Matthews GP, Gane PAC. Modelling the shrinkage in pigmented coatings during drying: A stick-slip mechanism. J Colloid Interface Sci. 2006;304(1):180-90.

33. Diaz-Rodriguez P, Landin M, Rey-Rico A, Couceiro J, Coenye T, Gonzalez P, et al. Bio-inspired porous SiC ceramics loaded with vancomycin for preventing MRSA infections. J Mater Sci: Mater Med. 2011;22(2):339-47.

34. Rey-Rico A, Silva M, Couceiro J, Concheiro A, Alvarez-Lorenzo C. Osteogenic efficiency of in situ gelling poloxamine systems with and without bone morphogenetic protein-2. Eur Cells Mater. 2011;21:317-40.

35. Ribatti D, Nico B, Vacca A, Presta M. The gelatin sponge-chorioallantoic membrane assay. Nat Protoc. 2006;1(1):85-91.

36. Lokman NA, Elder ASF, Ricciardelli C, Oehler MK. Chick chorioallantoic membrane (CAM) assay as an *in vivo* model to study the effect of newly identified molecules on ovarian cancer invasion and metastasis. Int J Mol Sci. 2012;13:9959-70.

37. Morioka H, Morii T, Vogel T, Hornicek FJ, Weissbach L. Interaction of plasminogen-related protein B with endothelial and smooth muscle cells *in vitro*. Exp Cell Res. 2003;287(1):166-77.

38. VanGuilder HD, Vrana KE, Freeman WM. Twenty-five years of quantitative PCR for gene expression analysis. BioTechniques. 2008;44(5):619-26.

39. Miao X, Sun D. Graded/gradient porous biomaterials. Materials. 2010;3:26-47.

40. Lopez-Alvarez M, Gonzalez P, Serra J, de Carlos A, Chiussi S, Leon B. Innovative bioinspired SiC ceramics from vegetable resources. Section title: Pharmaceuticals; 2012.

41. Wernike E, Hofstetter W, Liu Y, Wu G, Sebald H, Wismeijer D, et al. Long-term cell-mediated protein release from calcium phosphate ceramics. J Biomed Mater Res, Part A. 2010;92A(2):463-74.

42. Lopez-Alvarez M, de Carlos A, Gonzalez P, Serra J, Leon B. Cytocompatibility of bio-inspired silicon carbide ceramics. J Biomed Mater Res, Part B. 2010;95B(1):177-83.

43. Mour M, Das D, Winkler T, Hoenig E, Mielke G, Morlock MM, et al. Advances in porous biomaterials for dental and orthopaedic applications. Materials. 2010;3:2947-74.

44. Oh SH, Park IK, Kim JM, Lee JH. *In vitro* and *in vivo* characteristics of PCL scaffolds with pore size gradient fabricated by a centrifugation method. Biomaterials. 2007;28(9):1664-71.

45. Guelcher SA, Hollinger JO. An introduction to biomaterials. Guelcher SA and Hollinger JO, editors. Florida: CRC-Taylor & Francis; 2006.

46. Robledo MJL, Ferrer RES, Leon AB, Fernandez JM, De Arellano Lopez AR. Mechanical properties of porous biomorphic SiC. Bol Soc Esp Ceram Vidrio. 2005;44(5):318-23.

47. de CA, Borrajo JP, Serra J, Gonzalez P, Leon B. Behaviour of MG-63 osteoblast-like cells on wood-based biomorphic SiC ceramics coated with bioactive glass. J Mater Sci Mater Med. 2006;17(6):523-9.

48. de Carlos A, Borrajo JP, Serra J, Gonzalez P, Liste S, Leon B. *In vitro* cytotoxicity testing of wood-based biomorphic SiC ceramics. Key Eng Mater. 2005;284-286:581-4.

49. Lim JY, Hansen JC, Siedlecki CA, Runt J, Donahue HJ. Human foetal osteoblastic cell response to polymer-demixed nanotopographic interfaces. J R Soc Interface. 2005;2(2):97-108.

50. Pappacena KE, Johnson MT, Xie S, Faber KT. Processing of wood-derived copper-silicon carbide composites via electrodeposition. Compos Sci Technol. 2010;70(3):485-91.

51. Boland GM, Perkins G, Hall DJ, Tuan RS. Wnt 3a promotes proliferation and suppresses osteogenic differentiation of adult human mesenchymal stem cells. J Cell Biochem. 2004;93(6):1210-30.

52. Díaz-Rodríguez P, González P, Serra J, Landin M. Key parameters in blood-surface interactions of 3D bioinspired ceramic materials. Materials Science and Engineering: C. 2014 8/1;41(0):232-9.

53. Wang P, Li W, Yu J, Tsai W. Modulation of osteogenic, adipogenic and myogenic differentiation of mesenchymal stem cells by submicron grooved topography. J Mater Sci : Mater Med. 2012;23(12):3015-28.

54. Nikkhah M, Edalat F, Manoucheri S, Khademhosseini A. Engineering microscale topographies to control the cell-substrate interface. Biomaterials. 2012;33(21):5230-46.

55. McNamara LE, Sjoestroem T, Burgess KEV, Kim JJW, Liu E, Gordonov S, et al. Skeletal stem cell physiology on functionally distinct titania nanotopographies. Biomaterials. 2011;32(30):7403-10.

56. Ravichandran R, Liao S, Ng CC, Chan CK, Raghunath M, Ramakrishna S. Effects of nanotopography on stem cell phenotypes. World J Stem Cells. 2009;1(1):55-66.

57. Jugdaohsingh R. Silicon and bone health. J Nutr, Health Aging. 2007;11(2):99-110.

58. Wang P, Clements LR, Thissen H, Jane A, Tsai W, Voelcker NH. Screening mesenchymal stem cell attachment and differentiation on porous silicon gradients. Adv Funct Mater. 2012;22(16):3414,3423, S3414/1-S3414/6.

59. Kuboki Y, Takita H, Kobayashi D, Tsuruga E, Inoue M, Murata M, et al. BMP-induced osteogenesis on the surface of hydroxyapatite with geometrically feasible and nonfeasible structures: Topology of osteogenesis. J Biomed Mater Res. 1998;39(2):190-9.

60. De la Riva B, Sanchez E, Hernandez A, Reyes R, Tamimi F, Lopez-Cabarcos E, et al. Local controlled release of VEGF and PDGF from a combined brushite-chitosan system enhances bone regeneration. J Controlled Release. 2010;143(1):45-52.

61. Ferrara N, Houck K, Jakeman L, Leung DW. Molecular and biological properties of the vascular endothelial growth factor family of proteins. Endocr Rev. 1992;13(1):18-32.

62. Singh S, Wu BM, Dunn JCY. Delivery of VEGF using collagen-coated polycaprolactone scaffolds stimulates angiogenesis. J Biomed Mater Res, Part A. 2012;100A(3):720-7.

63. Golub JS, Kim Y, Duvall CL, Bellamkonda RV, Gupta D, Lin AS, et al. Sustained VEGF delivery via PLGA nanoparticles promotes vascular growth. Am J Physiol. 2010;298(6, Pt. 2):H1959-65.

64. Hu X, Neoh K, Shi Z, Kang E, Poh C, Wang W. An *in vitro* assessment of titanium functionalized with polysaccharides conjugated with vascular endothelial growth factor

for enhanced osseointegration and inhibition of bacterial adhesion. Biomaterials. 2010;31(34):8854-63.

65. Anderson SM, Siegman SN, Segura T. The effect of vascular endothelial growth factor (VEGF) presentation within fibrin matrices on endothelial cell branching. Biomaterials. 2011;32(30):7432-43.

66. Silva-Correia J, Miranda-Goncalves V, Salgado AJ, Sousa N, Oliveira JM, Reis RM, et al. Angiogenic potential of gellan-gum-based hydrogels for application in nucleus pulposus regeneration: *In vivo* study. Tissue Eng, Part A. 2012;18(11 and 12):1203-12.

67. Tengood JE, Kovach KM, Vescovi PE, Russell AJ, Little SR. Sequential delivery of vascular endothelial growth factor and sphingosine 1-phosphate for angiogenesis. Biomaterials. 2010;31(30):7805-12.

68. Mayr-Wohlfart U, Waltenberger J, Hausser H, Kessler S, Gunther K-, Dehio C, et al. Vascular endothelial growth factor stimulates chemotactic migration of primary human osteoblasts. Bone (NY, U S). 2002;30(3):472-7.

69. Wang W, Zhao L, Ma Q, Wang Q, Chu PK, Zhang Y. The role of the wnt/β-catenin pathway in the effect of implant topography on MG63 differentiation. Biomaterials. 2012;33(32):7993-8002.

Capítulo 7

Alginate-poloxamer-silicon carbide composites for the controlled release of indomethacin decrease *in vitro* inflammation

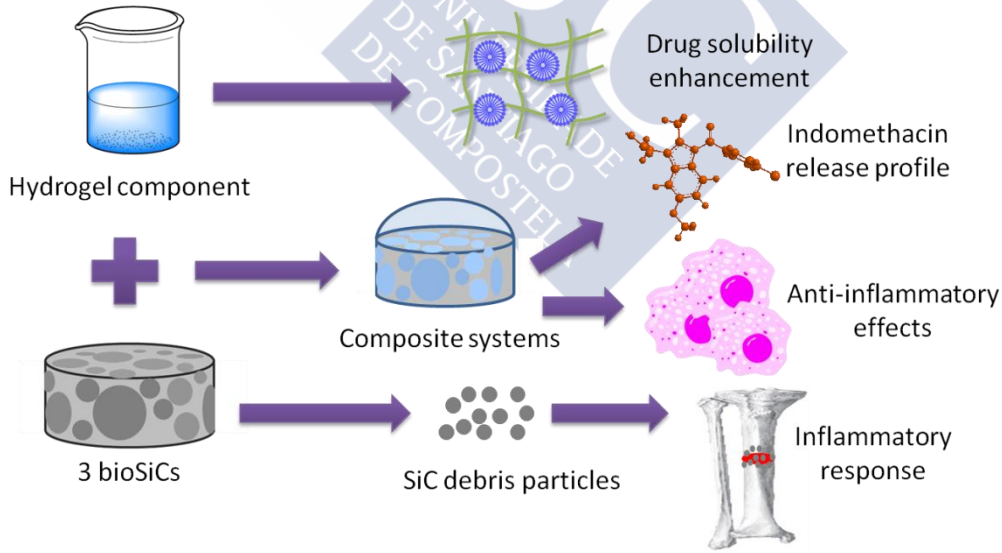

USC
UNIVERSIDADE
DE SANTIAGO
DE COMPOSTELA

7.1 Abstract

Composites of biomorphic silicon carbides (bioSiCs) and hydrogels are proposed in order to obtain materials able to load and release poor soluble drugs with application in bone pathologies therapy. Hydrogels composed by alginate and poloxamer were loaded with indomethacin, incorporated into the ceramics and crosslinked. The indomethacin release profile is dependent on the microstructure of the bioSiC selected. The loaded oak and sapelli bioSiCs composites have adequate release profiles to promote the decreasing of the secretion of pro-inflammatory cytokines in LPS stimulated macrophages, showing stronger anti-inflammatory effects than pine bioSiC composites. The released indomethacin is able to modulate the degradation of chondrocytes extracellular matrix and promote the formation of new collagen.

Particles derived from mechanical wear of biomorphic silicon carbides do not show high toxicity, being similar to the zirconia particles.

7.2 Introduction

Bone is a complex hierarchically organized tissue formed by an organic matrix, mainly collagen which is sequential mineralized with an inorganic component, hydroxyapatite (HAp), by the action of specific cells (1, 2). Due to this complex structure the development of new bone biomimetic materials has led to the production of new porous 3D composite systems formed by the combination of one or more than one organic component (natural or synthetic polymers) with an inorganic component. Composite systems should be able to meet all the physical and biological requirements for bone regeneration, combining the advantages of all components (3).

These composite systems have been found to be adequate also for the release of growth factors as BMP-2 (4-6), VEGF (7), platelet derived growth factors (8, 9) or drugs such as dexamethasone (10, 11), vancomycin (12, 13) and gentamicin (14). In the last few years, they have been also proposed for releasing a combination of therapeutic molecules such as BMP-2 and vancomycin (15), amikacin and gentamicin (16) or BMP-2 and VEGF (17). This new approach makes them an attractive alternative for the treatment of several bone pathologies.

Biomorphic silicon carbide ceramics (bioSiCs) obtained from natural resources (18) have been shown to maintain the original structure of their precursors being highly porous and biocompatible materials (19) suitable for the regeneration and revascularization of tissues. The incorporation of a polymer component into their structure must increase their therapeutic value. The use of ionic crosslinking polymers, such as alginate makes it possible to easily obtain a three dimensional network polymer through the addition of divalent ions (20). Alginate hydrogels can exert the function of an organic matrix suitable for cellular growth and encapsulation within the ceramic system and also facilitate the incorporation of drugs and growth factors into its three dimensional structure while modulating their release. Therefore, the combination of

alginate hydrogels and bioSiCs can be presented as a promising strategy in the development of complex systems for tissue regeneration and controlled drug release.

The addition of synthetic block copolymers such as poloxamers or poloxamines to the hydrogel component should be able to increase the solubility of low aqueous solubility drugs. The ability of these polymers to form micelles in an aqueous solution, where hydrophobic drugs can be incorporated, leads to an increase on their solubility and therefore makes their administration possible (21, 22). Furthermore, it was observed than poloxamines were able to stimulate the osteoblastic differentiation of adipose derived mesenchymal stem cells by themselves (23). The use of poloxamers has also been found to inhibit P-glycoprotein function decreasing the resistance of multidrug resistant (MDR) cell lines (24, 25).

Currently, the long-term stability of the prosthesis continues to be a challenge in the development of bone substitutes. Material wear debris is one of the main drawbacks associated to the use of artificial materials as implantable systems. The production of material particles may cause aseptic loosening and the activation of the surrounding macrophages leading to bone destruction and periprosthetic osteolysis (26-28). Several parameters modulate the inflammatory reaction caused by material particles such as their size (29) or their chemical composition (30, 31). Despite the fact that biomorphic silicon carbide has been previously described as a highly biocompatible material the inflammatory reactions caused by its potential debris have not been documented.

The aim of the present work is to develop composites able to load by entrapment and release an anti-inflammatory drug, indomethacin. The development of composite systems formed by a natural (alginate) and a synthetic polymer (poloxamer) together with the biomorphic ceramic (silicon carbide) should allow us to obtain an implant material suitable to load and release, in a controlled way, the indomethacin with an

amount enough to show an adequate anti-inflammatory effect on osteoarthritic chondrocytes.

Additionally, the potential toxic effects of particles obtained by mechanical wear of biomorphic silicon carbides are evaluated.

7.3 Materials and methods

7.3.1 **Preparation of composite systems**

Three different types of biomorphic silicon carbide (bioSiC) samples were obtained as described elsewhere from oak (*Quercus robur*), pine (*Pinus pinnaster*) and sapelli (*Enthandrophragma cylindricum*). Disks of 6 mm in diameter were sterilized by autoclaving at 121 °C for 20 min (32).

Two polymeric components were used; Poloxamer 407 (Pluronic F127® (PF127)) that was kindly donated from BASF (Ludwigshafen, Germany) and sodium alginate (GRINDSTED® Alginate PH 155) was purchased from Danisco (Copenhagen, Denmark).

Pluronic was dissolved in phosphate buffer (PBS) to achieve a final concentration of 2.5%. After its complete dissolution, indomethacin (2.38 mg/mL) and alginate (2%) were sequentially added. The final solution was autoclaved at 121 °C for 20 min.

30 µL of the polymeric solution was added on the bioSiC samples and crosslinked by the immersion of the loaded sample into a sterile solution of calcium chloride (Panreac; Barcelona, Spain) at a concentration of 20% for 10 seconds. After the crosslinking, systems were washed twice with 2 mL of PBS for ten seconds.

Crosslinked alginate-poloxamer beads prepared by dropping the polymeric solution into the calcium chloride solution were used as control.

7.3.2 **Characterization of the polymeric component**

The mechanical stability of the crosslinked and uncrosslinked polymeric systems was analyzed before and after the autoclaving process using a controlled stress rheometer (Rheolyst AR-1000N TA instruments, Surrey, UK). Ramps of temperature from 15 °C to 60 °C at 2 °C/min with an oscillatory stress of 0.1 Pa at 5 rad/s were carried out for all the samples.

The differential scanning calorimetric (DSC Q200, TA instruments, Surrey, UK) was used to evaluate the potential degradation of the polymeric chains during the autoclaving procedure. Ramps of temperature were carried out first from room temperature to -30 °C at 10 °C/min and then from this temperature to 50 °C at 10 °C/min.

7.3.3 **Isolation of human osteoarthritic chondrocytes**

Human osteoarthritic cartilages were provided by the Instituto de Ortopedia y Banco de Tejidos Musculoesqueléticos of the University of Santiago de Compostela. Pieces of the tissue were cut and placed into sterile tubes with trypsin and cell culture medium. The tissue was maintained in the solution at 37 °C for 30 min in order to kill the fibroblasts present in the extracts. Then, tissue samples were immersed in collagenase 1.5% in culture medium and kept overnight at 37 °C under mechanical stirring.

The solutions were centrifuged at 1,056 g for 4 min. Cells were resuspended in DMEM supplemented with 10% of fetal bovine serum and 1% penicillin/streptomycin and cultured at 37 °C with 5% of CO_2 and 90% of relative humidity.

7.3.4 ***In vitro* release of indomethacin**

Loaded composite systems were immersed in 3 mL of phosphate buffer at 37 °C. At preset times the concentration of indomethacin was quantified by UV-visible spectrophotometry at 320 nm. All the experiments were carried out in triplicate.

7.3.5 **Anti-inflammatory effect of indomethacin loaded composites**

The anti-inflammatory effects of loaded indomethacin composites were evaluated in two cell types, extracted human osteoarthritic chondrocytes and a murine macrophage cell line (Raw 264.7).

The macrophage cell line was cultured in DMEM-F12 HAM supplemented with 10% FBS and 1% penicillin/streptomycin and maintained at 37 °C with 5% of CO_2 and 90% relative humidity. Loaded composite systems were placed in 24-well plates, cultured with 100,000 cells per well and stimulated with lipopolysaccharide (LPS) at a concentration of 100 ng/mL.

The composites anti-inflammatory effect was evaluated after 24 and 72 hours of culture by the quantification of prostaglandin E_2 (PGE_2) (Arbor), TNF-α (eBioScience), nitric oxide (Cayman) and IL-1α (eBioScience).

The composites cytotoxicity was analyzed by the quantification of lactate dehydrogenase (LDH) (Roche). Indomethacin at 100 μM, unloaded silicon carbide samples, and the polymeric solution were used as controls.

Composites were also cultured with osteoarthritic chondrocytes in 24-well plates at a density of 60,000 cells per well with 2 mL of supplemented DMEM. The effect on extracellular matrix synthesis of osteoarthritic chondrocytes was evaluated by the quantification of glycosaminoglycans (GAGs) and collagen (I-V) production after 15 days of culture.

Cell culture supernatants were centrifuged at 10,000 g for 10 min. Two colorimetric assays were used, Blyscan (Biocolor) for GAGs and Sircol Collagen Assay kit (Biocolor) for collagen. Single cell culture medium was used as negative control and cells treated with indomethacin at a concentration of 100 μM equivalent to 100% of drug release were used as a positive control. Unloaded bioSiCs and crosslinked loaded and unloaded polymeric components were also used as controls.

Additionally, the concentration of inflammatory cytokine (IL-1β) and the secreted PGE_2 were measured at 1, 2, 5 and 15 days through an ELISA assay (BenderMedSystem) and a commercial colorimetric assay (Arbor) respectively.

7.3.6 **Evaluation of inflammation caused by silicon carbide released particles**

Particles were obtained by direct mechanical friction of two oak silicon carbide samples. One of the samples was immobilized on the surface of a sterile plastic container whereas the other was fixed on an impeller attached to a rotor (Ika RW20DZM) rotating at 150 rpm for one week. Ultrapure water (milliQ) was added to the container in order to facilitate the recovery of the particles. Particle size was analyzed by Scanning Electron Microscopy (ZEISS EVO LS 15, Germany) and their composition by EDX using the same equipment. Particles size distribution was analyzed using a zetasizer (Zetasizer Nano ZSP, Malvern, United Kingdom).

The inflammation caused by the particles was evaluated using a macrophage cell line (Raw 264.7) and cultured as previously described. Cells were seeded in 24-well plates with 1 mL of cell culture medium and particles were 10-fold diluted and added to the wells. Cells stimulated with 1 μg/mL of LPS were used as a positive control of inflammation and commercial Zirconium (IV) oxide particles as reference material (Sigma, USA).

Inflammatory cytokines were quantified after 24 hours of culture, IL-1α and TNF-α (Bender MedSystems).

7.3.7 **Statistical Analysis**

Experimental results were expressed as means and standard deviations. The statistical significant differences between treatments were established by the analysis of variance (ANOVA). When the F-ratio suggests significant differences between groups, the least significant difference (LSD) test was used to compare them in pairs. ANOVA and LSD were performed by Statgraphics Centurion®X64 software (USA).

7.4 Results and discussion

7.4.1 **Characterization of the polymeric component**

A strong interaction could be observed between alginate and poloxamer, this interaction is modified by the autoclaving process. Figure 7.1 shows the dynamic and elastic moduli of both, Alg and Alg-PF127 formulations before (Figure 7.1A) and after (Figure 7.1B) the autoclaving process. The addition of poloxamer to alginate solution caused an increase in both moduli and consequently in the complex viscosity at 37 °C (from 1.94 to 3.12 Pa.s) (Figure 7.1A). The sterilization process led to a markedly decrease in the complex viscosity values at 37 °C, being 0.06 Pa.s and 0.04 Pa.s for the Alg and Alg-PF127 formulations respectively. After this process the elastic modulus could not be detected. Interestingly, whereas in unsterilized systems the incorporation of poloxamer increased the complex viscosity, after autoclaving these seem to have the opposite effect. Complex interactions were established between alginate chains and poloxamer micelles in the unsterilized systems. Polysaccharide chains could be placed around the micelles hampering the interaction between poloxamer and water and increasing micelle-micelle interactions and therefore, the viscosity of the system (33). In the same way, Lin and coworkers found that the addition of alginate to poloxamer

solutions increased the gel strength of the systems. This fact could be attributed to the formation of hydrogen bonds between the two polymers where the water molecules act as crosslinking agent (34).

The autoclaving process could lead to the hydrolysis of the alginate chains (35). The decrease in the Alg molecular weight strongly affects the viscosity of the dispersions and additionally, in binary systems also reduces the Alg capability of hampering the interaction between poloxamer and water.

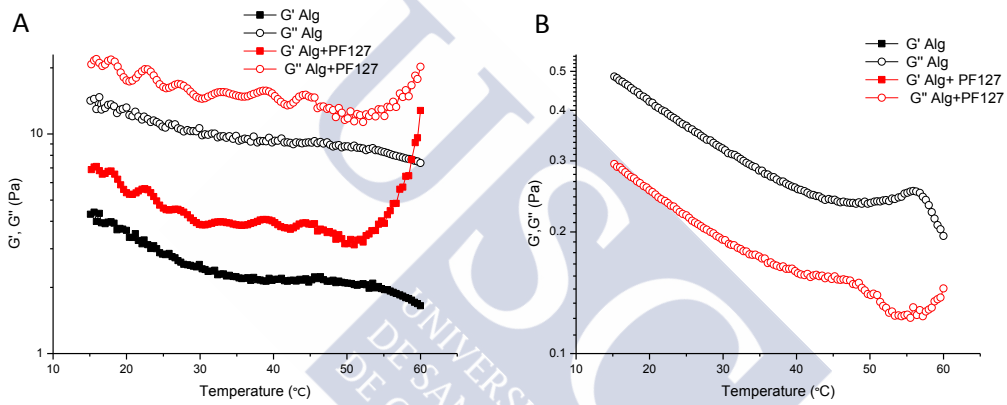

Figure 7.1 Values of storage moduli (G') and loss moduli (G´´) of the systems; (A) before, (B) after the autoclaving process from 15 °C to 60 °C at 2 °C/min with an oscillatory stress of 0.1 Pa at 5 rad/s.

This hypothesis was confirmed by the DSC results. Samples were sequentially frozen and heated in order to obtain the water melting temperature of both systems. Water melting temperature was higher for the autoclaved formulations (3.09 °C) than for non-autoclaved formulation (2.45 °C). The increase in the melting point is related to the molar concentration of the polysaccharide and therefore, suggests an increase in the number of chains by the hydrolysis promoted during the autoclaving process.

The capability of solubilization of indomethacin by the poloxamer-alginate formulation was compared to its solubility in water and in an aqueous solution of poloxamer alone at an equivalent concentration (2.5%). Poloxamer solution was able increased the solubility of indomethacin 18.44 ± 3.09 fold. The incorporation of alginate (2%) to the poloxamer solution decreased the solubility of the indomethacin. Due to the pH dependence solubility of indomethacin, this reduction in the solubility could be attributed to a change in the pH promoted by alginate chains. Despite this, biphasic systems were able to increase the hydrosolubility of indomethacin 7.31 ± 1.7 fold.

Rheological results of the studies carried out on the crosslinked Alg-PF127 formulations showed that the binary systems, formed by the polymeric mixtures both before and after the autoclaving process, exhibits high complex viscosity values at 37 °C. The hydrogel maintains its structure in the range of temperatures analyzed. The addition of the autoclaving step in the crosslinked hydrogel synthesis increased the complex viscosity of the hydrogel because of the presence of higher number of alginate chains that could interact with the calcium ions.

7.4.2 *In vitro* release of indomethacin

Porous biomorphic silicon carbide ceramics obtained from oak, pine or sapelli woods have been previously characterized with regard to their microstructure and surface properties (19, 32, 36). They show different capabilities of loading and releasing antibiotics and growth factors and also of interacting with cells. On this basis, it is presumed that the incorporation of a hydrogel into the pores, produces composite systems with different release behaviors when they are loaded with insoluble drugs.

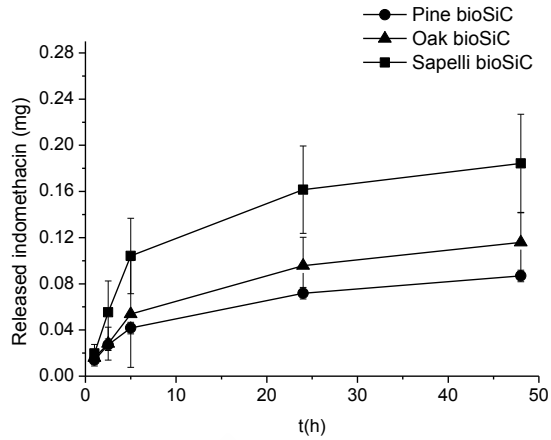

Figure 7.2 Release profiles of indomethacin at 37 °C in PBS from pine, oak and sapelli bioSiC composites.

Indomethacin release profiles from the different composite systems are shown in Figure 7.2. The release rate would be firstly controlled by the water uptake of the material, the hydration of the hydrogel and the diffusion of drug molecules. All the profiles fit the Higuchi model characteristic of a release process controlled by diffusion. The selection of low porosity ceramics (pine bioSiC) causes a more prolonged release of the anti-inflammatory drug. Once the hydrogel is incorporated into the ceramic matrix their low porosity hinders the interaction of the release medium with the hydrogel and therefore decreases the release rate of the drug. The use of ceramics with a higher porosity and pore size (sapelli and oak bioSiC) increases the release rate. Sapelli bioSiC has been found to be able to achieve the higher amount of drug released after two days reaching a 100% drug loading. The high interconnectivity of sapelli bioSiC may facilitate the release medium uptake and this could explain its faster drug release.

7.4.3 **Study of indomethacin anti-inflammatory effects**

Despite all the components being highly biocompatible, the cytotoxicity of the composites was studied by the quantification of lactate dehydrogenase (LDH). Figure 7.3 shows the percentage of cytotoxicity for each composite together with the corresponding values for single polymeric ingredients and the bioSiCs used. None of the samples cause values higher than 20% of cytotoxicity after three days of cell culture, therefore showing an excellent cytocompatibility.

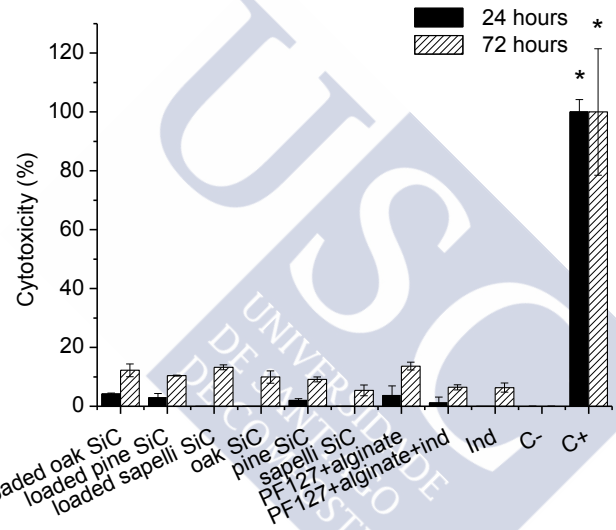

Figure 7.3 Cytotoxicity values obtained by the quantification of lactate dehydrogenase (LDH) levels after 24 and 72 hours of cell culture corrected by the positive control (lysis buffer). The homogeneous groups are indicated by an equal number of asterisks (*) above the columns ($\alpha < 0.05$).

Indomethacin is a non-steroidal anti-inflammatory drug (NSAID) widely used in the treatment of osteoarthritis (OA) to reduce pain. It is a non-selective inhibitor of the enzyme cyclooxygenase (COX), which catalyzes the formation of prostaglandins and thromboxane from arachidonic acid (37, 38).

One of the most common ways of evaluating the anti-inflammatory effect of a therapeutic molecule is to analyze the decreasing in cytokines secretion of macrophages, stimulated by LPS, when the molecule is added to the cell culture medium. In this regard, several molecules can be analyzed; nitric oxide (NO), tumour necrosis factor alpha (TNF-α) and prostaglandin (PGE_2) (39).

Murine macrophages stimulated with LPS were treated with drug loaded composites. The concentrations of TNF-α and IL-1β after 24 and 72 hours of cell culture were determined. As it is shown in Figure 7.4A, all loaded composites were able to promote a statistically significant reduction of the production of TNF-α after 72 hours of cell culture in comparison to unloaded bioSiCs. Composites including sapelli and oak bioSiC were able to promote a significant decrease in the production of TNF-α, even higher than the addition of an equivalent concentration of indomethacin (Ind) in the culture medium. Those results can be justified by the controlled release of the drug from these types of system that seems to improve its therapeutic activity. Conversely, the excessive slowing down in the release rate of indomethacin from composites including pine bioSiC does not favor the appearance of the beneficial anti-inflammatory effects.

The levels of IL-1β were undetectable or low in the most of the analyzed samples (Figure 7.4B), which is positive considering that IL-1β levels are directly correlated to the osteoclast activation and bone resorption (27). Only loaded and unloaded pine bioSiC composites promoted a statistically significantly higher secretion of IL-1β levels after 72 h of cell culture than the negative control (C-). These results may be justified by the production of higher concentration of silicon carbide particles during the cell culture process of pine silicon carbide samples which also affects the secretion of TNF-α when using pine bioSiC.

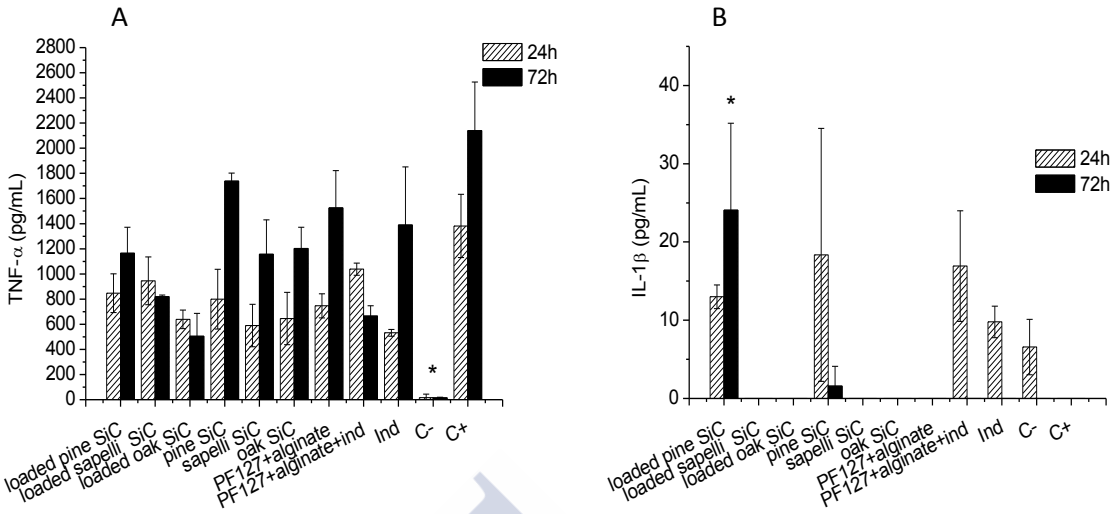

Figure 7.4 Levels of TNF-α and IL-1β secreted by LPS stimulated macrophages after 24 and 72 h of cell culture. The positive control (C+) and the negative control (C-) are macrophages stimulated or not stimulated with LPS respectively. The homogeneous groups are indicated by an equal number of asterisks (*) above the columns ($\alpha < 0.05$).

The production of nitric oxide (Figure 7.5A) was similar for the loaded and unloaded systems, the non-stimulated macrophages (C-) and the stimulated macrophages (C+) after 24 hours of cell culture. However, after 72 hours of cell culture stimulated macrophages were able to significantly increase the production of NO when they are compared to negative control and the composite systems. Furthermore, at this time indomethacin loaded composite systems were able to significantly decrease the amount of NO secreted in comparison with the negative control.

All the formulations, including indomethacin were able to significantly inhibit the synthesis of prostaglandin E_2 (Figure 7.5B) at 24 and 72 hours of cell culture reaching similar levels to non-stimulated macrophages (C-).

The controlled release of indomethacin by the composite systems, particularly those produced using oak and sapelli bioSiC, promote the highest anti-inflammatory effect according to all the analyzed cytokines.

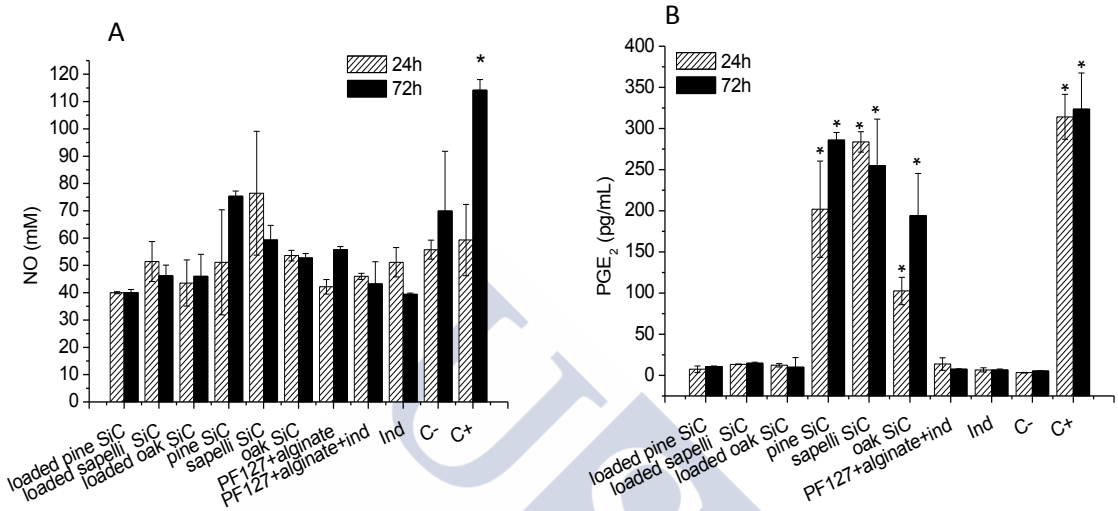

Figure 7.5 Levels of NO and PGE_2 secreted by LPS stimulated macrophages after 24 and 72 of cell culture. (C-) is macrophages not stimulated and (C+) is macrophages stimulated with LPS without any treatment. The homogeneous groups are indicated by an equal number of asterisks (*) above the columns ($\alpha < 0.05$).

Osteoarthritis (OA) is a non-inflammatory joint disease and the most common form of arthritis. It is characterized by the loss of cartilage from the articulating surfaces, ostophyte formation, changes in the synovial membrane, subchondral bone sclerosis and an increased volume of synovial fluid with less viscosity and poor lubrication properties (40, 41). Its current treatment is symptomatic, including intra-articular injections of glucocorticoids and hyaluronic acid formulations or the administration of non-steroidal anti-inflammatory drugs (NSAIDs) (40, 42). It is also well known that an imbalance between its metabolism and degradative signals is present in osteoarthritic cartilage. Osteoarthritic chondrocytes increase the secretion of inflammatory cytokines

and decrease the collagen synthesis (43). It has been reported that the secretion of prostaglandin E_2 is enhanced in osteoarthritic cartilage, synovium and synovial fluid (38).

Cell viability and the secretion of proinflammatory cytokines after 15 days of cell culture have been analyzed for osteoarthritic chondrocytes treated with the different formulations.

Cell viability results, all higher than 60%, (Figure 7.6), show no statistically significant differences between indomethacin alone and drug loaded systems. The addition of the drug to the cell culture medium, shows a slight toxicity and promotes a decrease in cell viability.

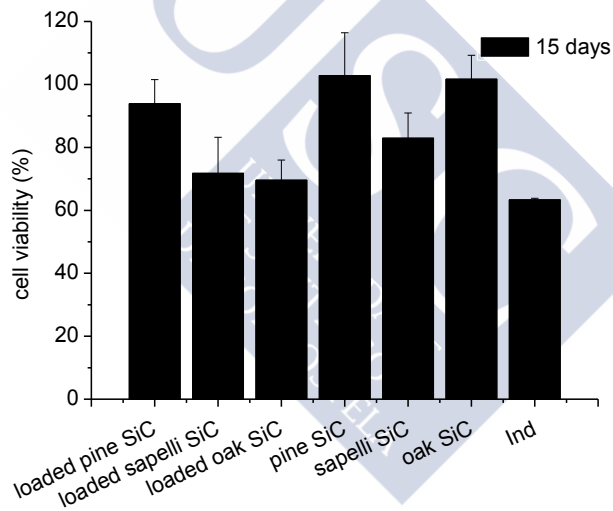

Figure 7.6 Cell viability values obtained by MTT assay after 15 days of cell culture corrected by the negative control (culture plates). No statistical significant differences were observed ($\alpha < 0.05$).

The levels of NO and PGE_2 secreted by osteoarthritic chondrocytes after 48 hour of treatment with the different formulations (Figure 7.7) point out that loaded composites promote a significant decrease in cytokines production in comparison to untreated chondrocytes (C-).

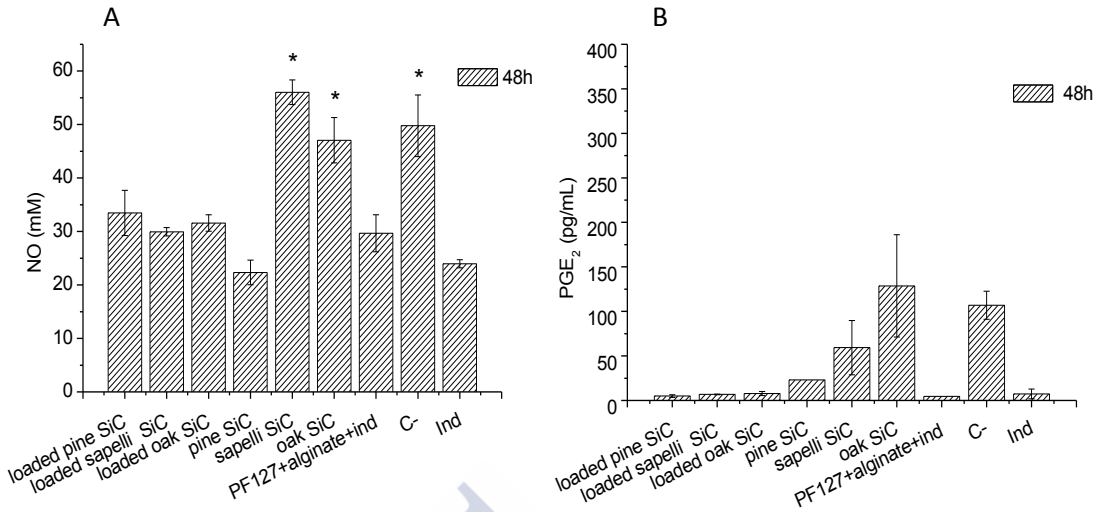

Figure 7.7 Levels of NO and PGE_2 secreted by osteoarthritic chondrocytes after 48 hours of cell culture. The negative control (C-) is osteoarthritic chondrocytes without treatment. The homogeneous groups are indicated by an equal number of asterisks (*) above the columns ($\alpha < 0.05$).

The secretion of IL-1β induces the catabolic cascade of osteoarthritic chondrocytes including the activity of cyclooxygenase enzymes and, therefore, the production of PGE_2, the main pro-inflammatory factor (38). The Levels of IL-1β were undetectable for all the treatments studied.

In order to evaluate the extracellular matrix catabolism and metabolism, the concentration of the main structural macromolecules, glycosaminoglycans (GAGs) and collagen I-V, in the cell culture medium after fifteen days of assay have been quantified. Figure 7.8 shows the not statistically significant differences between materials with regard to the amount of released GAGs and synthetized collagen for both loaded and unloaded composites. The release of indomethacin from loaded composites promotes a significant decrease in GAGs together with a significant increase in collagen production from the osteoarthritic chondrocytes which can be explained by the

decreasing of their anabolic activity, leading to the synthesis of new collagen molecules and to the reduction of the digestion of the extracellular matrix.

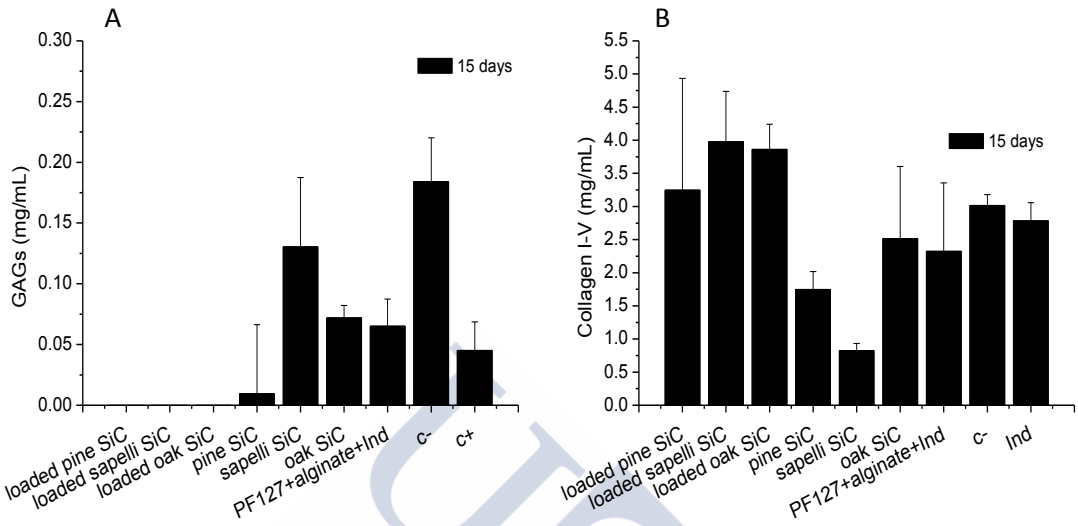

Figure 7.8 Levels of GAGs (A) and collagen I-V (B) secreted by osteoarthritic chondrocytes after 15 days of cell culture. The negative control (C-) is osteoarthritic chondrocytes without any treatment.

7.4.4 **Evaluation of inflammation caused by silicon carbide released particles**

Despite the excellent tribological properties of silicon carbides and their high corrosion resistance under normal biological conditions (26), it is relevant to evaluate the inflammation and macrophage activation caused by their mechanical wear debris after their hypothetical *in vivo* implantation. The simulation of mechanical wear between two silicon carbide samples allowed the obtaining of small particles characterized by a mean diameter of 481.33 nm to (Figure 7.9). The analysis of particle composition show that they were mainly composed by silicon and carbon atoms according to EDX measurements.

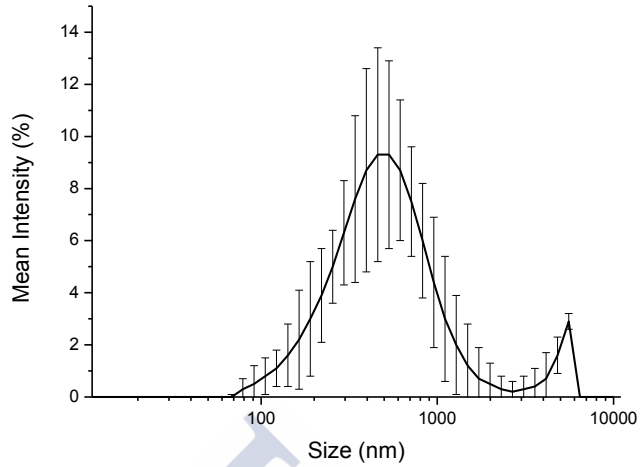

Figure 7.9 Particle size distribution obtained using a particle size analyzer at room temperature.

Macrophages were able to uptake wear debris from the medium as can be seen in Figure 7.10 where the particles are present inside the cytoplasm of the cells (black points) while the nuclei remain transparent.

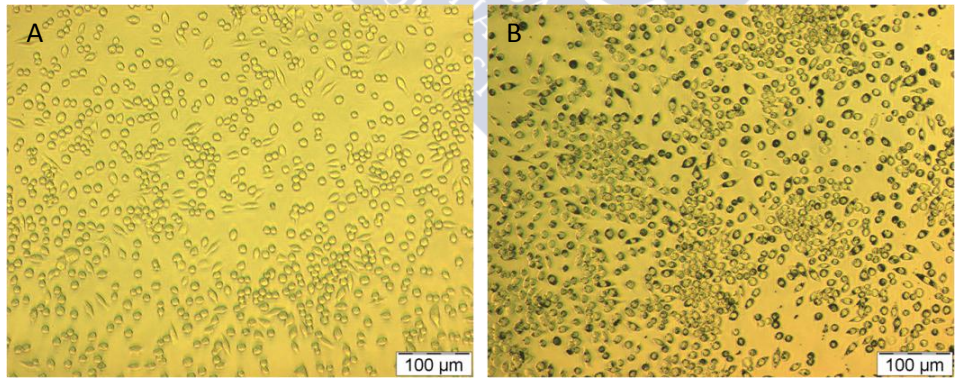

Figure 7.10 Macrophage cellular uptake of biomorphic silicon carbide particles after 24 hours of cell culture (B) compared to negative control (A) at 20X.

The activation of macrophages causes the secretion of numerous pro-inflammatory cytokines that cause the inflammatory cell recruitment as IL-1β, TNF-α, IL-6, and IL-8

(44). Two cytokines were selected to evaluate the activation of macrophages; tumor necrosis factor alpha (TNF-α) that had been found to be crucial mediating inflammatory cell recruitment derived from particulate systems, (45) and interleukin-1 (IL-1) that stimulates bone resorption and the consequent periprosthetic osteolysis (30). The levels of TNF-α and IL-1 were compared with the cytokines secreted after a similar treatment with zirconia particles.

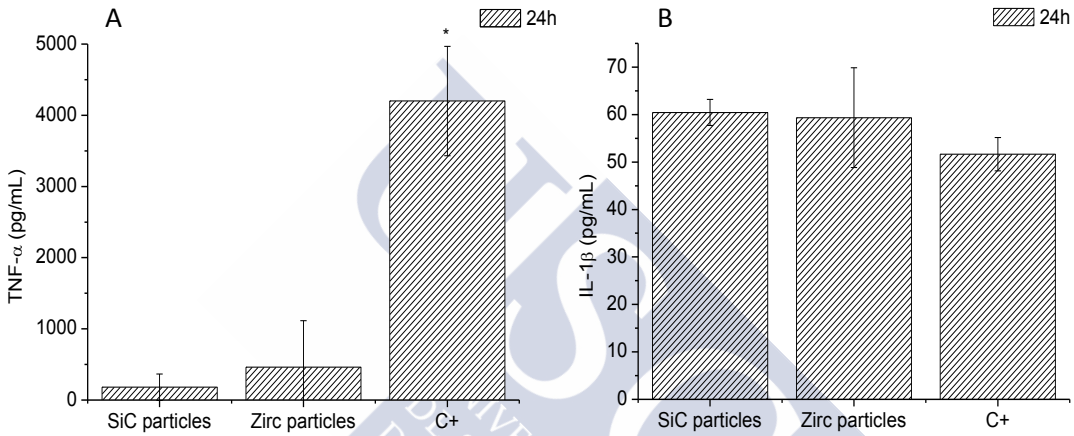

Figure 7.11 Levels of tumor necrosis alpha (TNF-α) and interleukin 1 beta (IL-1β) secreted by the murine macrophage cell line compared to positive control (cells stimulated with lipopolisaccharide). The homogeneous groups are indicated by an equal number of asterisks (*) above the columns ($\alpha < 0.05$).

After the addition of particles obtained by mechanical wear similar levels of TNF-α secretion than for zirconia particles (46) were found. Both levels were significantly lower than those promoted by the positive control (Figure 7.11). On the other hand the secretion of IL-1β was quantitatively similar to the one promoted by the positive control and the zirconia particles. It was found that the addition of lipopolisaccharide (control+) was not able to stimulate the production of IL-1β. It has been shown that zirconia particles show similar levels of inflammation to alumina with better results

than polymers like high-density polyethylene (46). Although the presence of zirconia particles may produce some adverse reactions, they are less intense than those promoted by titanium particles, therefore zirconia is considered the most suitable biomaterial in terms of inflammation promoted by material debris (47). Similar results were obtained for silicon carbide and zirconia particles showing the acceptable biocompatibility of our biomorphic silicon carbide particles.

7.5 Conclusions

New composite systems including biphasic alginate-poloxamer hydrogels and bioSiCs from different precursors have been developed and analyzed with regard to their capability of loading and control indomethacin release. All the ceramic-hydrogel composites have shown high biocompatibility. The loaded oak and sapelli bioSiCs composites had adequate release profiles able to promote the decreasing of the pro-inflammatory cytokines secretion in LPS stimulated macrophages, showing stronger anti-inflammatory effects than pine bioSiC composites. Those differences could not be observed when treating osteoarthritic chondrocytes. In those cases the indomethacin released from the composites was also able to modulate the degradation of chondrocyte extracellular matrix and promote the formation of new collagen.

Particles derived from wear debris of biomorphic silicon carbide did not show high toxicity, being similar to the zirconia particles.

These developed composites present great potential for the local treatment of bone pathologies.

7.6 References

1. Raghavan RN, Muthukumar T, Somanathan N, Sastry TP. Biomimetic mineralization of novel silane crosslinked collagen. Mater Sci Eng, C. 2013;33(4):1983-8.

2. Silverman LD, Lukashova L, Herman OT, Lane JM, Boskey AL. Release of gentamicin from a tricalcium phosphate bone implant. J Orthop Res. 2007;25(1):23-9.

3. Dessi M, Borzacchiello A, Mohamed THA, Abdel-Fattah WI, Ambrosio L. Novel biomimetic thermosensitive β-tricalcium phosphate/chitosan-based hydrogels for bone tissue engineering. J Biomed Mater Res, Part A. 2013;101A(10):2984-93.

4. Hernandez A, Sanchez E, Soriano I, Reyes R, Delgado A, Evora C. Material-related effects of BMP-2 delivery systems on bone regeneration. Acta Biomater. 2012;8(2):781-91.

5. Kim J, Jeong I, Lee K, Jung U, Kim C, Choi S, et al. Volumetric bone regenerative efficacy of biphasic calcium phosphate-collagen composite block loaded with rhBMP-2 in vertical bone augmentation model of a rabbit calvarium. J Biomed Mater Res, Part A. 2012;100A(12):3304-13.

6. MacDonald ML, Samuel RE, Shah NJ, Padera RF, Beben YM, Hammond PT. Tissue integration of growth factor-eluting layer-by-layer polyelectrolyte multilayer coated implants. Biomaterials. 2011;32(5):1446-53.

7. Suarez-Gonzalez D, Barnhart K, Migneco F, Flanagan C, Hollister SJ, Murphy WL. Controllable mineral coatings on PCL scaffolds as carriers for growth factor release. Biomaterials. 2012;33(2):713-21.

8. McCanless JD, Jennings LK, Cole JA, Bumgardner JD, Haggard WO. Induction of the early inflammatory-mediated cellular responses of fracture healing *in vitro* using platelet releasate-containing alginate/$CaPO_4$ biomaterials for early osteoarthritis prevention. J Biomed Mater Res, Part A. 2012;100A(5):1107-14.

9. Phipps MC, Xu Y, Bellis SL. Delivery of platelet-derived growth factor as a chemotactic factor for mesenchymal stem cells by bone-mimetic electrospun scaffolds. PLoS One. 2012;7(7):e40831.

10. Son JS, Choi Y, Park E, Kwon T, Kim K, Lee K. Drug delivery from hydroxyapatite-coated titanium surfaces using biodegradable particle carriers. J Biomed Mater Res, Part B. 2013;101B(2):247-57.

11. Son JS, Appleford M, Ong JL, Wenke JC, Kim JM, Choi SH, et al. Porous hydroxyapatite scaffold with three-dimensional localized drug delivery system using biodegradable microspheres. J Controlled Release. 2011;153(2):133-40.

12. Thanyaphoo S, Kaewsrichan J. Synthesis and evaluation of novel glass ceramics as drug delivery systems in osteomyelitis. J Pharm Sci. 2012;101(8):2870-82.

13. Ma T, Shang B, Tang H, Zhou T, Xu G, Li H, et al. Nano-hydroxyapatite/chitosan/konjac glucomannan scaffolds loaded with cationic liposomal vancomycin: Preparation, *in vitro* release and activity against staphylococcus aureus biofilms. J Biomater Sci, Polym Ed. 2011;22(12):1669-81.

14. Cai S, Zhai Y, Xu G, Lu S, Zhou W, Ye X. Preparation and properties of calcium phosphate cements incorporated gelatin microspheres and calcium sulfate dihydrate as controlled local drug delivery system. J Mater Sci: Mater Med. 2011;22(11):2487-96.

15. Doty HA, Leedy MR, Courtney HS, Haggard WO, Bumgardner JD. Composite chitosan and calcium sulfate scaffold for dual delivery of vancomycin and recombinant human bone morphogenetic protein-2. J Mater Sci: Mater Med. 2014:Ahead of Print.

16. Belcarz A, Zima A, Ginalska G. Biphasic mode of antibacterial action of aminoglycoside antibiotics-loaded elastic hydroxyapatite-glucan composite. Int J Pharm (Amsterdam, Neth). 2013;454(1):285-95.

17. Shah NJ, MacDonald ML, Beben YM, Padera RF, Samuel RE, Hammond PT. Tunable dual growth factor delivery from polyelectrolyte multilayer films. Biomaterials. 2011;32(26):6183-93.

18. Gonzalez P, Borrajo JP, Serra J, Chiussi S, Leon B, Martinez-Fernandez J, et al. A new generation of bio-derived ceramic materials for medical applications. J Biomed Mater Res, Part A. 2009;88A(3):807-13.

19. Diaz-Rodriguez P, Landin M, Rey-Rico A, Couceiro J, Coenye T, Gonzalez P, et al. Bio-inspired porous SiC ceramics loaded with vancomycin for preventing MRSA infections. J Mater Sci: Mater Med. 2011;22(2):339-47.

20. Drury JL, Mooney DJ. Hydrogels for tissue engineering: Scaffold design variables and applications. Biomaterials. 2003;24(24):4337-51.

21. Simoes SMN, Veiga F, Torres-Labandeira JJ, Ribeiro ACF, Sandez-Macho MI, Concheiro A, et al. Syringeable pluronic-α-cyclodextrin supramolecular gels for sustained delivery of vancomycin. Eur J Pharm Biopharm. 2012;80(1):103-12.

22. Diaz-Rodriguez P, Landin M. Smart design of intratumoral thermosensitive β-lapachone hydrogels by artificial neural networks. Int J Pharm (Amsterdam, Neth). 2012;433(1-2):112-8.

23. Rey-Rico A, Silva M, Couceiro J, Concheiro A, Alvarez-Lorenzo C. Osteogenic efficiency of in situ gelling poloxamine systems with and without bone morphogenetic protein-2. Eur Cells Mater. 2011;21:317-40.

24. Kabanov AV, Batrakova EV, Alakhov VY. An essential relationship between ATP depletion and chemosensitizing activity of pluronic block copolymers. J Controlled Release. 2003;91(1-2):75-83.

25. Kabanov AV, Batrakova EV, Alakhov VY. Pluronic block copolymers for overcoming drug resistance in cancer. Adv Drug Delivery Rev. 2002;54(5):759-79.

26. Mahmoodi M, Ghazanfari L. Fundamentals of biomedical applications of biomorphic SiC. Prop Appl Silicon Carbide. 2011:297-343.

27. St. Pierre CA, Chan M, Iwakura Y, Ayers DC, Kurt-Jones EA, Finberg RW. Periprosthetic osteolysis: Characterizing the innate immune response to titanium wear-particles. J Orthop Res. 2010;28(11):1418-24.

28. Gallo J, Raska M, Mrazek F, Petrek M. Bone remodeling, particle disease and individual susceptibility to periprosthetic osteolysis. Physiol Res (Prague, Czech Repub). 2008;57(3):339-49.

29. Kranz I, Gonzalez JB, Doerfel I, Gemeinert M, Griepentrog M, Klaffke D, et al. Biological response to micron- and nanometer-sized particles known as potential wear products from artificial hip joints: Part II: Reaction of murine macrophages to corundum particles of different size distributions. J Biomed Mater Res, Part A. 2009;89A(2):390-401.

30. Nordsletten L, Hogasen AKM, Konttinen YT, Santavirta S, Aspenberg P, Aasen AO. Human monocytes stimulation by particles of hydroxyapatite, silicon carbide and diamond: *In vitro* studies of new prosthesis coatings. Biomaterials. 1996;17(15):1521-7.

31. Granchi D, Amato I, Battistelli L, Ciapetti G, Pagani S, Avnet S, et al. Molecular basis of osteoclastogenesis induced by osteoblasts exposed to wear particles. Biomaterials. 2005;26(15):2371-9.

32. Díaz-Rodríguez P, González P, Serra J, Landin M. Key parameters in blood-surface interactions of 3D bioinspired ceramic materials. Materials Science and Engineering: C. 2014 8/1;41(0):232-9.

33. Mayol L, Biondi M, Quaglia F, Fusco S, Borzacchiello A, Ambrosio L, et al. Injectable thermally responsive mucoadhesive gel for sustained protein delivery. Biomacromolecules. 2011;12(1):28-33.

34. Lin H, Sung KC, Vong W. In situ gelling of Alginate/Pluronic solutions for ophthalmic delivery of pilocarpine. Biomacromolecules. 2004;5(6):2358-65.

35. Oliveira SM, Almeida IF, Costa PC, Barrias CC, Ferreira MRP, Bahia MF, et al. Characterization of polymeric solutions as injectable vehicles for hydroxyapatite microspheres. AAPS PharmSciTech. 2010;11(2):852-8.

36. Diaz-Rodriguez P, Perez-Estevez A, Seoane R, Gonzalez P, Serra J, Landin M. Suitability of biomorphic silicon carbide ceramics as drug delivery systems against bacterial biofilms. ISRN Pharm. 2013:104529, 9.

37. Omatsu T, Naito Y, Handa O, Hayashi N, Mizushima K, Qin Y, et al. Involvement of reactive oxygen species in indomethacin-induced apoptosis of small intestinal epithelial cells. J Gastroenterol. 2009;44(Suppl. 19):30-4.

38. Jeffrey JE, Aspden RM. Cyclooxygenase inhibition lowers prostaglandin E_2 release from articular cartilage and reduces apoptosis but not proteoglycan degradation following an impact load *in vitro*. Arthritis Res Ther. 2007;9(6):No pp. given.

39. Yang Y, Yu T, Jang H, Byeon SE, Song S, Lee B, et al. *In vitro* and *in vivo* anti-inflammatory activities of polygonum hydropiper methanol extract. J Ethnopharmacol. 2012;139(2):616-25.

40. Gerwin N, Hops C, Lucke A. Intraarticular drug delivery in osteoarthritis. Adv Drug Delivery Rev. 2006;58(2):226-42.

41. Ou Y, Tan C, An H, Jiang D, Quan Z, Tang K, et al. The effects of NSAIDs on types I, II, and III collagen metabolism in a rat osteoarthritis model. Rheumatol Int. 2012;32(8):2401-5.

42. Fioravanti A, Tinti L, Pascarelli NA, Di Capua A, Lamboglia A, Cappelli A, et al. *In vitro* effects of VA441, a new selective cyclooxygenase-2 inhibitor, on human osteoarthritic chondrocytes exposed to IL-1Î². J Pharmacol Sci (Tokyo, Jpn). 2012;120(1):6-14.

43. Meini S, Cucchi P, Catalani C, Bellucci F, Giuliani S, Maggi CA. Bradykinin and B2 receptor antagonism in rat and human articular chondrocytes. Br J Pharmacol. 2011;162(3):611-22.

44. Hallab NJ, Jacobs JJ. Biologic effects of implant debris. Bull NYU Hosp Jt Dis. 2009;67(2):182-8.

45. Driscoll KE, Carter JM, Hassenbein DG, Howard B. Cytokines and particle-induced inflammatory cell recruitment. Environ Health Perspect Suppl. 1997;105(5):1159-64.

46. Ingham E, Fisher J. Biological reactions to wear debris in total joint replacement. Proc Inst Mech Eng H. 2000;214(1):21-37.

47. Obando-Pereda GA, Fischer L, Stach-Machado DR. Titanium and zirconia particle-induced pro-inflammatory gene expression in cultured macrophages and osteolysis, inflammatory hyperalgesia and edema *in vivo*. Life Sci. 2014;97(2):96-106.

USC
UNIVERSIDADE
DE SANTIAGO
DE COMPOSTELA

Capítulo 8

Controlled release of rAAV vectors from alginate-poloxamer-silicon carbide composite systems

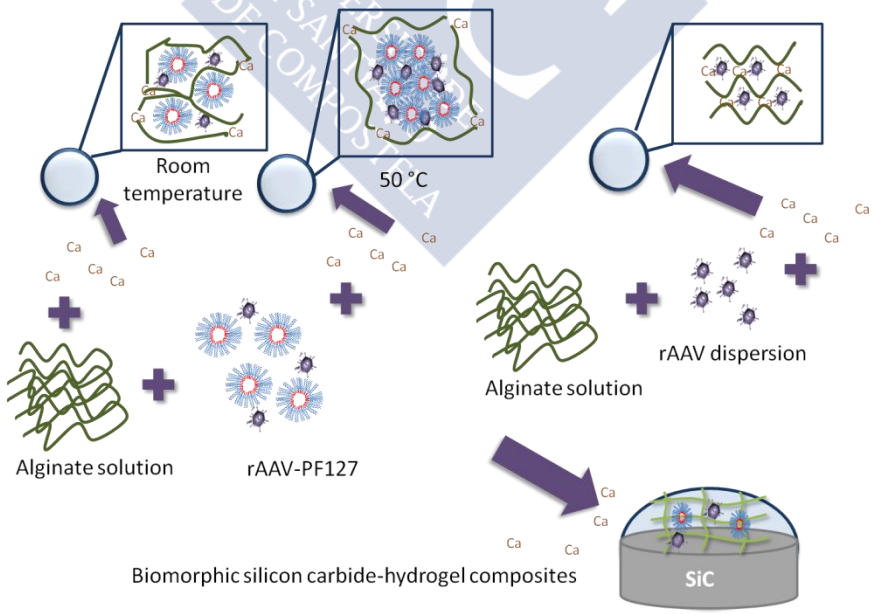

USC
UNIVERSIDADE
DE SANTIAGO
DE COMPOSTELA

8.1 Abstract

Viral vectors are commonly used to deliver a gene into a specific cell type in order to restore its normal protein expression. The inclusion of viral vectors into implantable systems is a promising alternative to the conventional therapy. However, little is known about the requirements of release systems to successfully include viral vectors and achieve a suitable transgenic expression. This work is focused on the development of different hydrogel structures, able to include recombinant adeno-associated viral vectors (rAAV) and promote their controlled release in order to elucidate the best conditions to achieve the highest transduction efficiency. The inclusion of rAAV loaded hydrogels into silicon carbide ceramics allow the obtaining of implantable systems for the release of viral vectors for local administration. The transduction efficiencies of the loaded hydrogels systems were in agreement with their *in vitro* release profiles. The addition of poloxamer to the systems was able to enhance viral vectors transduction efficiencies after one day of study. The incorporation of loaded hydrogels into bioSiCs has not been able to obtain adequate transduction efficiencies, being required additional studies.

8.2 Introduction

Gene therapy is an attractive approach for the treatment of numerous diseases due to its ability to stably introduce a functional gene into a target cell, allowing for the sustained production of a therapeutic candidate molecule. This can be performed either via direct injection of DNA, by encapsulation of DNA in cationic lipids or polymers, or through viral gene delivery systems (1, 2). Several non-integrating and integrating viral vectors are available to achieve this goal. Non-integrating vectors such as those derived from adenoviruses or the herpes simplex virus (1, 3) are of relatively limited clinical interest due to the initiation of deleterious, virus-specific immune and/or toxic reactions by the host. The development of adequate delivery systems is thus necessary in order to ensure that safe gene expression may occur at appropriate levels over extended periods of time using such vectors (3, 4).

The most commonly used viral vectors are based on retroviral and recombinant adeno-associated viral (rAAV) vectors (1). Administration of rAAV vectors that derive from the human nonpathogenic AAV virus is the goal of human gene therapy. They have been found to be most adequate as they can transduce both dividing and non-dividing cells in marked contrast with the retroviral vectors that can only modify dividing cells, carrying the additional risk of insertional mutagenesis. Furthermore, rAAV allow for the direct, effective transduction in animal models with low immunogenicity, being suitable for the treatment of human pathologies, especially those that affect the articular cartilage (traumatic defects, osteoarthritis) (5, 6). Transduction efficiencies up to 80% have been reported in articular chondrocytes *in vitro*, *in situ*, and *in vivo* using reporter but also therapeutic candidate genes including the insulin-like growth factor I (IGF-I), transforming growth factor beta (TGF-β), and fibroblast growth factor 2 (FGF-2), restoring a close to normal metabolic balance in osteoarthritic cartilage (7, 8). rAAV have been also successful to activate the processes of

chondrogenic differentiation in human bone marrow derived mesenchymal stem cells (hMSCs) *in vitro* upon gene transfer of the cartilage-specific transcription factor SOX9 (9) and to enhance the healing of osteochondral defects following direct administration of the same vector construct (10). Overall, these findings suggest that this vector type might be the most adapted gene vehicle to elaborate future, effective treatments against cartilage injuries in patients. While systemic injection of rAAV vectors can be performed in human subjects, the high amounts of vectors generally needed to achieve a therapeutic effect (~ 5×10^{13} vg/kg) severely restrict their use in the clinics via this route of administration (11). Several approaches have been explored to improve the delivery of such vectors by including them into polymeric systems through different technological approaches as a means to increase their stability while decreasing potential immune responses that may be raised against the viral capsids (3, 12, 13). The ideal system would increase the levels and duration of transgene expression and improve the safety of the gene transfer system through controlled release of the vectors, ensuring longer residence time by reduction of the viral clearance (3, 14). To achieve this goal, several natural and synthetic polymeric systems like fibrin, gelatin, collagen, poly(ethylene glycol) (PEG), and agarose have been tested (15, 16). Parenteral administration or co-administration of cationic polymers such as poly-L-lysine or poly-arginine have been also described, allowing to enhance the efficacy of rAAV gene delivery. Such polymers may affect the permissivity of the targets to the vector particle either by modifying the charge of the capsid or by increasing the interactions between the viral particle and its cell membrane receptor, a heparan sulfate proteoglycan (11).

Despite recent advances, the development of controlled viral vector release systems remains challenging. The high size of viral particles generally impairs their release from the most conventional pharmaceutical technology approaches. Some studies showed the ability of poloxamers like Pluronic F68® to increase rAAV-mediated transgene

expression in different tissues like adipose tissue (17). Biomorphic silicon carbide (bioSiC) ceramics have been reported for their excellent mechanical properties, with an adequate porosity and pore interconnectivity to promote bone regeneration and a good biocompatibility to induce the osteoblastic differentiation of hMSCs (18). To our best knowledge, such compounds have never been examined for their ability to release rAAV vectors as a means to improve the vector delivery process for cartilage repair. The goal of the present work was therefore to produce porous alginate-poloxamer systems in a suitable network structure that is capable of releasing such promising, clinically relevant gene delivery vectors for optimal transduction efficacy of reporter genes in hMSCs. The inclusion of the optimized hydrogel into a porous bioSiC ceramic may provide adequate biphasic systems for future applications to treat articular cartilage defects in patients.

8.3 Materials and methods

8.3.1 **Reagents**

Sodium alginate (GRINDSTED® AlgPH155) was purchased at Danisco (Copenhagen, Denmark). Poloxamer 407 (Pluronic F127® (PF127)) was kindly provided by BASF (Ludwigshafen, Germany). Biomorphic silicon carbide (bioSiC) samples were obtained from sapelli wood (*Enthandrophragma cylindricum*) as previously reported (19). The Cell Proliferation Reagent WST-1 and β-gal Staining Set were from Roche Applied Science (Mannheim, Germany). The Beta-Glo® Assay System was from Promega (Mannheim, Germany).

8.3.2 **Cells**

Human bone marrow derived mesenchymal stem cells (hMSCs) were prepared from bone marrow aspirates obtained from the distal femurs of patients undergoing total knee arthroplasty (n = 5). The study was approved by the Ethics Committee of the

Saarland Physicians Council. All patients provided informed consent before inclusion in the study. All procedures were performed in accordance with the Helsinky Declaration. Cells were isolated, expanded in DMEM, 100 U/mL penicillin and 100 µL/mL streptomycin, 10% FBS (growth medium), and characterized for cell surface markers and multilineage potential as previously described (9, 20). Culture medium was replaced every 2-3 days. Cells at passage 1-2 were used for the experiments.

8.3.3 **rAAV plasmids and vectors**

The constructs were derived from pSSV9, an AAV-2 genomic clone (21, 22). rAAV-*lacZ* carries the *lacZ* gene for E. coli β-galactosidase and rAAV-RFP a *Discosoma* sp. red fluorescent protein (RFP) cDNA fragment, both under the control of the cytomegalovirus immediate-early (CMV-IE) promoter (5, 8-10, 23). The vectors were packaged as conventional (not self-complementary) vectors using a helper-free, two-plasmid transfection system in the 293 cell line (an adenovirus-transformed human embryonic kidney cell line) with the packaging plasmid pXX2 and the Adenovirus helper plasmid pXX6 as previously described (8). The vector preparations were purified by dialysis and titered by real-time PCR (5, 8-10, 23), avering 10^{10} transgene copies/mL.

8.3.4 **Capsule preparation and characterization**

In order to achieve adequate vector stability and release profiles, three different conditions were selected from the initial conditions studied. Capsules were prepared with 0.3% alginate (AlgPH155) or with alginate containing 9% PF127 (AlgPH155 + PF127) in a solution of 10% sucrose. In the latter case, the effects of temperature upon viscosity and final structure of the combination containing a thermosensitive polymer were examined by crosslinking the systems at room temperature (AlgPH155 + PF127 [C]) or at 50 °C (AlgPH155 + PF127 [H]). Unloaded and rAAV vector-loaded capsules

were prepared by dropping the dispersion of polymers alone or containing rAAV to a calcium chloride solution (102 mM) in a 2 mL tube using a syringe with a needle of 18 ½ G. The crosslinking procedure was performed at room temperature or at 50 °C for a brief period of time (30 sec) to avoid irreversible crosslinking of all the polymeric bead. Capsules were then kept in culture in 96-well plates. Polymeric dispersions of AlgPH155 and AlgPH155 + PF127 in sucrose 10% were prepared by direct dissolution and used as controls.

The rheological properties of the polymeric dispersions were evaluated using a rheometer (Rheolyst AR-1000N TA instruments, UK) equipped with a Peltier plate for temperature control and a cone-plate geometry (60-mm diameter with an angle of 1.58°, gap 59 µm). Ramps of temperature from 15 °C to 60 °C at 2 °C/min with an oscillatory stress of 0.1 Pa at 5 rad/sec were carried out. Gel temperature (Tgel) was estimated from the cross point between the storage moduli (G´) and loss moduli (G´´).

8.3.5 **rAAV vector encapsulation efficiency**

The ability of the capsules to entrap rAAV during crosslinking was evaluated by measuring the number of viral particles in each bead. The capsules were placed in 50 µL of bead dissolution medium (55 mM sodium citrate, 0.15 M sodium chloride, 30 mM EDTA) (24), vortexed for 2 min followed by the addition of 50 µL viral dilution buffer (10% SDS, 1 M Tris pH 7.5, 0.5 M EDTA) and incubated for 10 min at 56 °C. After a quick spin, the vector concentrations were measured spectrophotometrically at 260 nm ($VP_{capsule}$). The initial amount of viral particles in the loading solution was also evaluated ($VP_{loading}$) and used as 100% of rAAV vector encapsulation efficiency (EE) calculated as:

$$EE\ (\%) = [VP_{capsule}/VP_{loading}] \times 100$$

8.3.6 **Capsule stability and degradation**

The stability of the vector-loaded and unloaded capsules was evaluated by testing their weight and size upon immersion in cell culture medium in the presence or absence of hMSCs. Each type of bead was placed in a well of 96-well plates containing 150 µL of growth medium. At preset times (0, 1, 3, 5, 10 and 21 days), each capsule was weighted and the mean diameters and total areas were measured under light microscopy (Olympus BX45, Hamburg, Germany) using the analySIS® program (Olympus). Similarly, stability against dilution was analyzed by modifying the medium volume where the capsules were immersed. The results were expressed as the percentage of area loss or weight loss of the initial area and weight, respectively.

8.3.7 **rAAV vector release from the capsules**

The vector release profiles were obtained by placing the capsules in 96-well plates containing 150 µL of growth medium. At preset times (1, 3, 5, 10 and 21 days), the release medium was removed and replaced by fresh medium. The number of viral particles in the removed medium at the selected time points was estimated by spectrophotometry as described above. Unloaded capsules were used as negative controls and loading solutions as positive controls. After 21 days, the capsules were placed in 50 µL of bead dissolution medium and the number of remaining viral particles was estimated in a similar way.

8.3.8 **Cell viability**

hMSC viability was estimated by placing rAAV-*lacZ*-loaded or unloaded capsules in contact with cells in monolayer culture (3,500 cells/well in 96-well plates) for 1, 3, 5, 10 or 21 days using the Cell Proliferation Reagent WST-1, with OD proportional to the cell numbers as previously described (9). Equivalent vector solutions with or without alginate and poloxamer were used as controls.

8.3.9 **Transduction efficiencies from released rAAV vectors**

In order to analyze the potential effects of alginate and poloxamer on the rAAV transduction efficiencies, hMSCs in monolayer culture (7,500 cells/well in 96-well plates) were treated with rAAV-*lacZ* solutions with and without equivalent concentrations of polymers used to prepare the beads. After 24 h, the efficiencies were measured from the luminescence produced after 30 min of incubation with the Beta-Glo® assay according to the manufacturer's recommendations. The values obtained were expressed as Relative Luminescence Units (RLUs) normalized to the cell numbers as determined by using the Cell Proliferation Reagent WST-1 (9).

The transduction efficiencies of released vectors were quantitatively and qualitatively using hMSCs in monolayer culture (109,400 cells/cm^2). For the first approach based on rAAV-*lacZ* gene transfer, X-Gal staining was performed following fixation of the cells and further processing according to the manufacturer's recommendations to examine positive staining under light microscopy (Olympus BX45). Quantitative estimation of the transduction efficiencies of rAAV-lacZ-loaded and unloaded capsules was carried out measuring the luminescence produced after 30 min of incubation with the Beta-Glo® assay as described above with RLUs normalized to the cell number. The transduction efficiencies were qualitatively estimated by detection of live fluorescence in transduced cells as with polymers alone after 1, 3, 5 and 10 days of contact with polymeric rAAV-RFP-loaded capsules under a fluorescent microscope with a 568 nm filter (Olympus CKX41).

8.3.10 **Hydrogel-ceramic composites**

In order to evaluate the possibility to include the hydrogel systems in a ceramic matrix, known amounts of each optimized polymeric solution were added to bioSiC samples. The composite systems obtained were then crosslinked with calcium chloride by

immersion in calcium solution (102 mM) for 30 sec. The transduction efficiencies of the composite systems using rAAV-*lacZ* were evaluated by X-Gal staining after 1, 5 and 10 days of monolayer culture with hMSCs (12,500 cells/well in 24-well plates). The effects of the presence of bioSiC on the transduction efficiencies were evaluated similarly.

8.3.11 **Statistical analysis**

All experiments were performed in quintuplicate for each condition and time point. Results are expressed as mean ± standard deviation. Statistical significant differences between treatments were evaluated by analysis of variance (ANOVA) using the Statgraphics Centurion® X64 software (Statpoint Technologies, USA). P values of less than 0.05 were considered statistically significant.

8.4 Results

8.4.1 **Hydrogel and bead characterization**

The potential interactions between AlgPH155 and PF127 were studied by analyzing the rheological properties of the polymeric dispersions. The dispersion of AlgPH155 in water produced a viscous solution characterized by a complex viscosity that decreases as the temperature increases with no gelation phenomena. The low concentration of AlgPH155 selected produced solutions with negative values of elastic modulus at all the temperatures studied (data not shown). PF127 dispersion showed a gelation temperature of 55.50 °C (Figure 8.1A). The combination AlgPH155 + PF127 promoted a reduction in the gel temperature to a lower value (44.55 °C) (Figure 8.1B), probably due to enhanced interactions of poloxamer chains via AlgPH155 (Figure 8.1C).

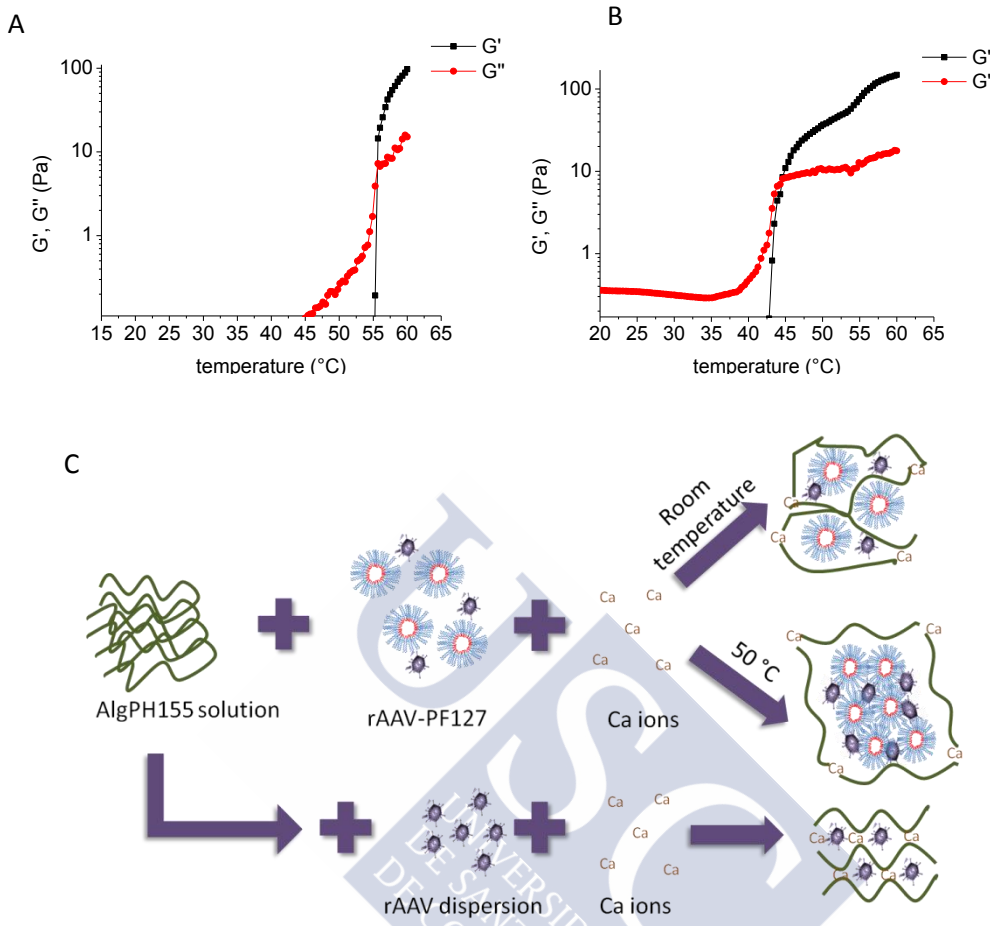

Figure 8.1 Hydrogel and bead characterization. The rheological properties of the polymeric dispersions were analyzed by using ramps of temperature from 15 °C to 60 °C at 2 °C/min with an oscillatory stress of 0.1 Pa at 5 rad/sec. Values of storage moduli (G´) and loss moduli (G´´) are shown for PF127 (A) and AlgPH155 + PF127 (B). The gel temperatures were obtained by the cross point between both moduli. A schematic distribution of polymeric chains after crosslinking with calcium ions is depicted in (C).

The stability parameters as evaluated by measuring the loss of capsule area and weight are presented in Figure 8.2. The differences in porous structures resulted in variations

in capsule area loss (Figure 8.2A). Lower compact external hydrogels AlgPH155 + PF127 [H] lost 58.7 ± 1.8% of total area after 21 days while medium compact external hydrogels AlgPH155 + PF127 [C] lost 49.4 ± 7.4% (1.18-fold difference, P = 0.3329). AlgPH155 capsules with the closest structure and denser hydrogel network provided more stable systems, with only 27.8 ± 1.6% of total lost area at a similar time point (2.1- and 1.8-fold difference versus AlgPH155 + PF127 [H] and AlgPH155 + PF127 [C], respectively, P = 0.1489 and P = 0.0368). Overall, a plateau was rapidly reached in all the capsules on day 10. The differences in capsule weight loss were more marked, with a regular increase over time (Figure 8.2B). Inclusion of PF127 at either crosslinking temperature led to the formation of capsules with high solubility that lost 86.9 ± 7.1% of weight after 21 days, while those made of AlgPH155 alone lost only 55.1 ± 10.26% (P = 0.0033), and although the area loss in such capsules was lower. This is probably due to their porous structure that might allow the diffusion of fluids inside the capsule in a porosity-dependent manner, leading to a shrinkage external hydrogel layer.

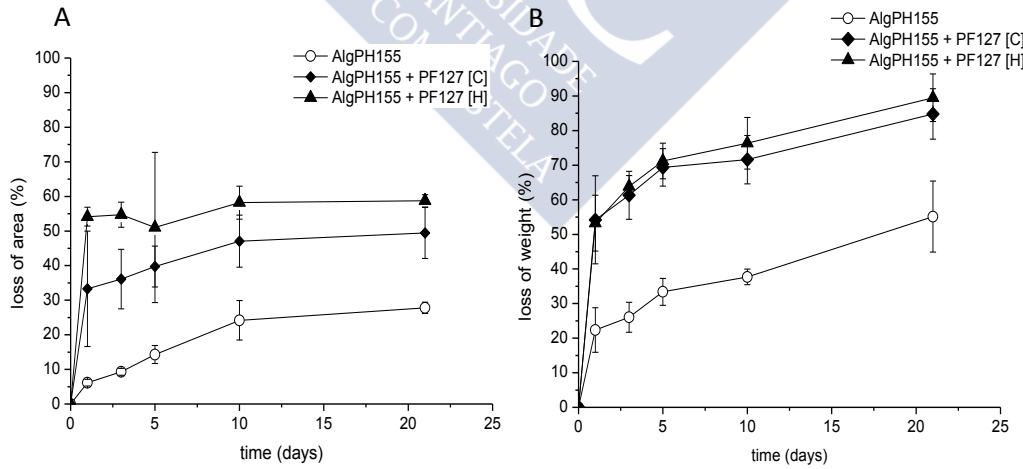

Figure 8.2 Hydrogel and bead stability. The loss of capsule area (A) and of capsule weight (B) in static conditions was measured by image analysis and analytical balance, respectively, as described in the Materials and Methods.

8.4.2 **Evaluation of entrapment and release of rAAV vectors from the capsules**

The ability of the different hydrogels to entrap the rAAV preparations was analyzed upon addition of either rAAV-*lacZ* or rAAV-RFP to the polymeric solutions prior to crosslinking by measuring the efficacies of encapsulation. All the hydrogels permitted high entrapment efficiencies with values of 92.1 ± 5.4%, 98.4 ± 2.9%, and 90.0 ± 3.1% for AlgPH155, AlgPH155 + PF127 [C], and AlgPH155 + PF127 [H], respectively, without statistical significance between capsule types (P = 0.6985; P = 0.2453). The higher viscosity of the combined polymers versus that of each independent polymer, leading to a decrease in the gel temperature of the block polymer, probably increased the entrapment ability of the systems in those systems with low pore size (AlgPH155 +PF127 [C]). The vector-loaded capsules had a higher stability than the unloaded ones for all the conditions studied, with a dissolution of the beads achieved at a dilution of 1:50 versus 1:33, respectively (P = 0.0808). There was no statistically significant difference (P = 0.1939) in the area loss between inert experiments (with cell culture medium without cells) and studies carried out in the presence of hMSCs for either vector-loaded and unloaded capsules. The loss of area for rAAV-*lacZ*-loaded capsules after 21 days was of 21.15 ± 0.09% and 15.16 ± 6.57% for AlgPH155 (P = 0.6985), of 59.95 ± 2.22% and 44.36 ± 12.18% for AlgPH155 + PF127 [C] (P = 0.2453), and 46.23 ± 14.18% and 47.92 ± 12.57% for AlgPH155 + PF127 [H] in the presence and in the absence of cells, respectively (P = 0.6985).

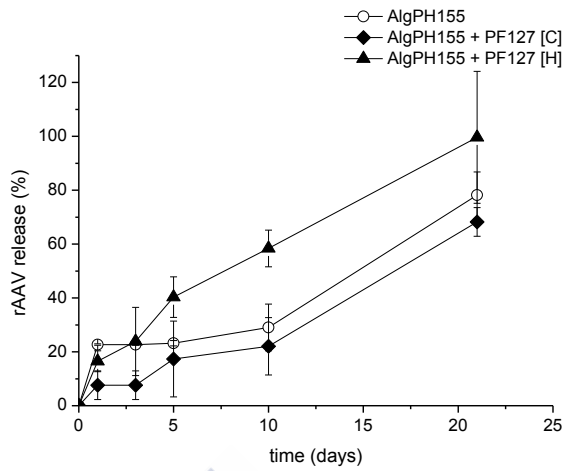

Figure 8.3 rAAV release study from capsules in static conditions. The vector tested was rAAV-*lacZ* as described in the Materials and Methods.

The differences between the systems in their network structure and stability may lead changes in the release profile of the selected hydrogels. All the systems show an initial burst of rAAV-*lacZ* followed by its controlled release for 21 days of assay (Figure 8.3). The initial burst (up to a 20% for the alginate capsules) may be explained the release of the viral particles placed on the external surface of the capsules. After this stage, the rAAV vector release is controlled by diffusion mechanism through the external cover of crosslinked polymer (25). The rAAV vector, because of its large size have steric hindrance for their difusion through the polymer, which slows down their release, for this fact we have selected capsules as rAAV vector release systems. The release profiles from the binary systems significantly fit zero order kinetics rAAV (%) = Kt + m, where K is the release constant from the system and m the y-intercept. The equations obtained were:

rAAVreleased (%) = 4 x 10^{11} t (days) + 1 x 10^{12} for AlgPH155 + PF127 [H] with R^2 = 0.989 and

rAAVreleased (%)= 2 x 10^{11} t (days) + 3 x 10^{11} for AlgPH155 + PF127 [C] with R^2 = 0.973.

The release profile of capsules formed by single alginate does not fit zero kinetics. After burst release a lag period of 10 days when the capsules loss stability (Figure 8.3) was observed. During those 10 days the small size of pores of the structure does not allow the release of the vectors.

After 21 days, the capsules were solubilized and the amounts of viral particles remaining in the samples were quantitatively estimated. The alginate capsules still contained 12.28 ± 0.02% of their loaded viral particles, whereas the amounts for room temperature crosslinked alginate-poloxamer were 3.52 ± 0.01% and of 20.16 ± 3.80% for hot-crosslinked formulation.

8.4.3 **Cell viability and transduction efficiency of polymers**

The hMSC viability and the transduction efficiency of rAAV in contact with the polymers were evaluated. Incorporation of rAAV vectors into alginate dispersion does not decrease cell viability (Figure 8.4A) but promotes a significant reduction in the rAAV-*lacZ* transduction efficiency (Figure 8.4B).

On the contrary, as it can be seen, addition of PF127 at the studied concentration (0.9%) to the medium produces a decrease in cell survival (Figure 8.4A) that can be justified by the surfactant properties of PF127 which may modify cell membrane permeability. However, the addition of PF127 (Figure 8.4B) is able of significantly increasing the transduction efficiency of rAAV in comparison with the vector itself and the vector within alginate.

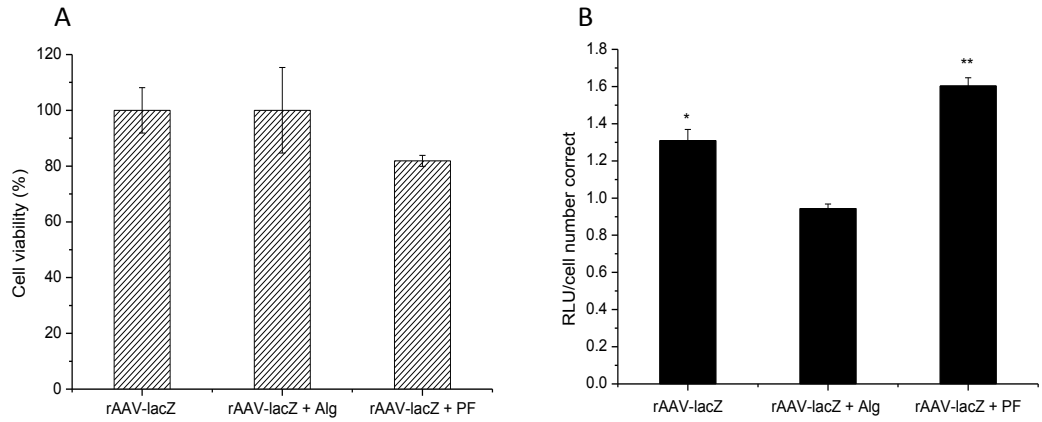

Figure 8.4 Effect of alginate and PF127 on the viability (A) and transduction efficiency (B) of rAAV-*lacZ* in hMSCs after 24 h of treatment. The homogeneous groups are indicated by an equal number of asterisks (*) above the columns ($P < 0.05$).

8.4.4 **Cell viability**

The studied capsules were characterized by high cell viability values at the different times evaluated. Neither the presence of the viral particles nor the addition of polymeric capsules to the cell culture increased significantly cell death. The PF127 toxicity pointed out before cannot be observed when the cells are treated with the capsules where the polymer is included into the network (Figure 8.5). The interaction between the poloxamer and the alginate should decrease the amount of PF127 chains as unimers reducing their surfactant capacity.

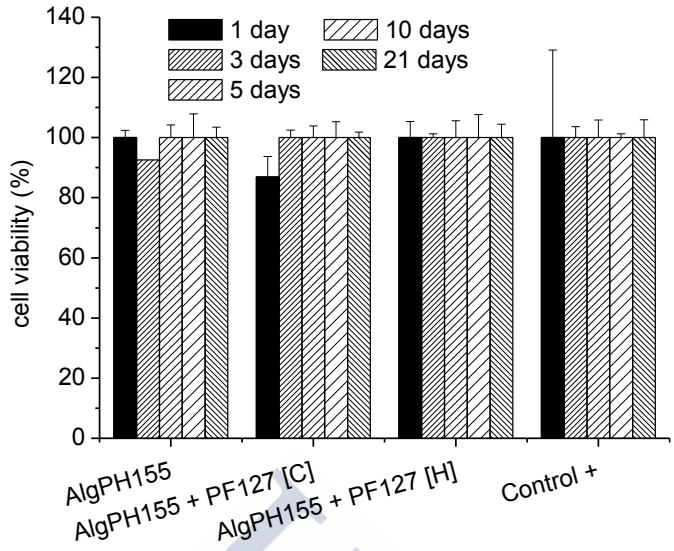

Figure 8.5 Cell viability of hMSCs in monolayer culture treated with rAAV-*lacZ*-loaded capsules. No statistically significant differences could be observed ($P < 0.05$).

8.4.5 **Transduction efficiency of released rAAV from loaded systems**

Transduction efficiencies based on released rAAV were qualitatively assessed by live fluorescence emission in monolayer cultures of hMSCs treated with alginate or alginate plus PF127 unloaded or rAAV-RFP-loaded capsules.

None of the unloaded capsules showed fluorescence emission at any time. The fluorescence emission of transduced cells in the presence of loaded capsules showed similar values to the positive control which corresponds to equal amounts of rAAV-RFP added in solution (Figure 8.6). Furthermore, at the latest evaluated times, 5 and 10 days, after the treatment with AlgPH155 and AlgPH155 + PF127 [H] capsules, the fluorescence emission was even higher than for the positive control. This may justified by the controlled release of the vector achieved by the capsules which enhances RFP expression, leading to higher transduction efficiency for the latest times.

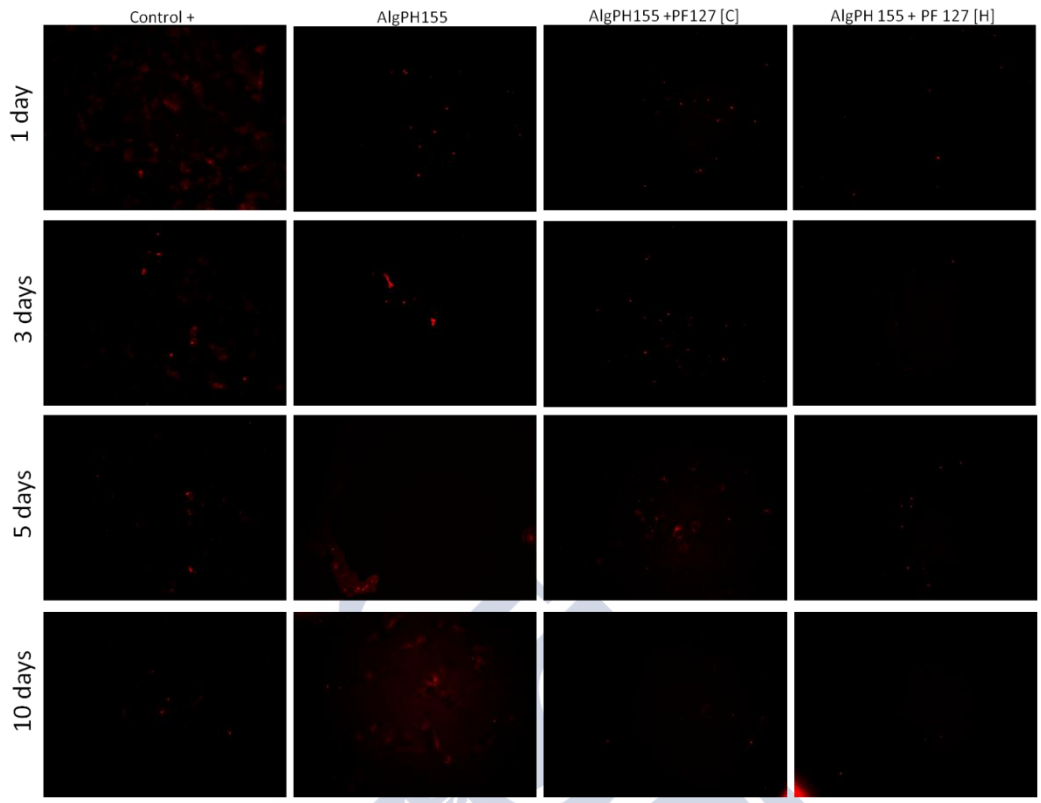

Figure 8.6 Live fluorescence emission of transduced hMSCs in monolayer cultures after 1, 3, 5 and 10 days of treatment with rAAV-RFP-loaded capsules.

Qualitative analysis was also carried out by X-Gal staining of hMSCs treated with unloaded and rAAV-*lacZ*-loaded capsules. Figure 8.7 shows *lacZ* expression after 1, 3, 5 and 10 days. Capsules containing alginate and poloxamer crosslinked at room temperature and at 50 °C showed higher staining after one day of treatment than capsules formed by alginate alone. On the other hand, capsules containing single AlgPH155 or AlgPH155 + PF127 [H] showed higher transduction efficiencies after one day of assay. Different cell morphology was observed in these two types of capsules, cells treated with alginate capsules show fibrous shape whereas cells treated with AlgPH155 + PF127 capsules show round shape. It was clearly observed that while positive control suffered a decrease in *lacZ* expression after 3 days of culture,

AlgPH155 and AlgPH155 + PF127 [H] maintained staining intensity over the time. Controlled release of rAAV was able to promote a suitable transduction efficiency over time in such systems.

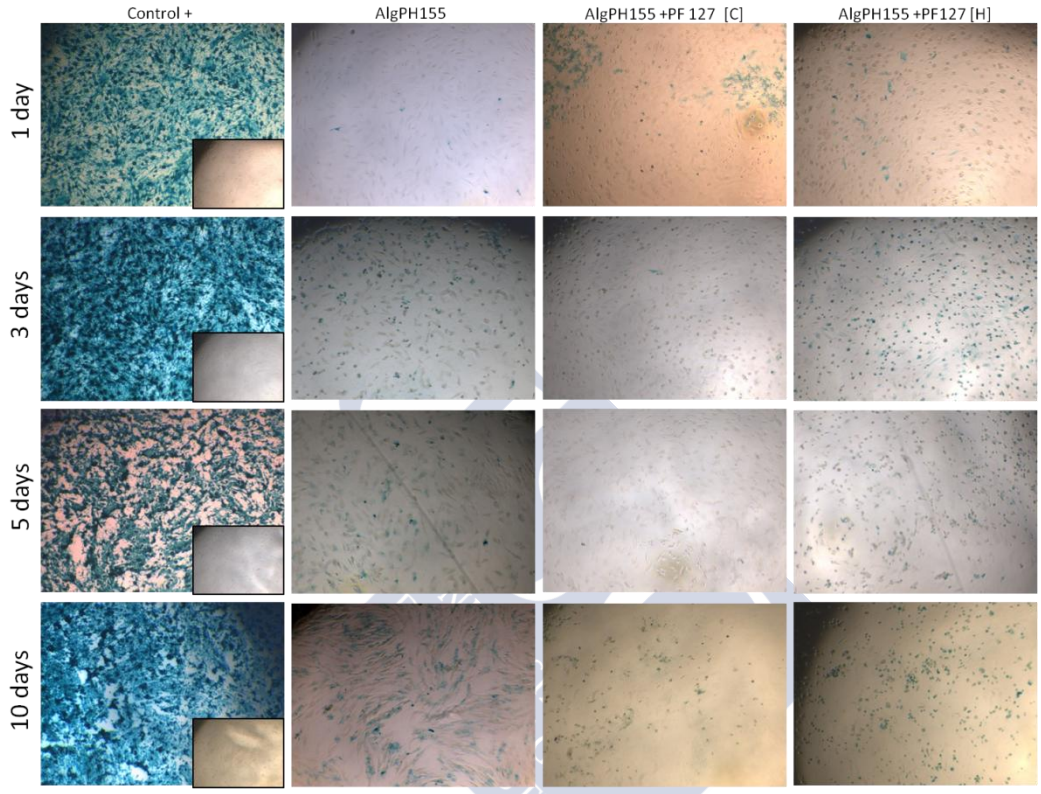

Figure 8.7 X-Gal staining of hMSCs in monolayer culture after 1, 3, 5 and 10 days of treatment with capsules including rAAV-*lacZ*.

Estimation of the transduction efficiencies was carried out using rAAV-*lacZ*-loaded and unloaded capsules as controls. Figure 8.8 shows RLUs/cell number for each one of the studied conditions at different times. According to the experimental results, all systems were able to achieve significant higher values of transgene expression than negative control (Control -). Capsules including PF127 were found to be able of increasing cell transduction in comparison with both, the positive control and single alginate capsules formed after 24 h of study. This effect may be attributed to the initial burst release

and/or the polymer itself in agreement with our previous results (Figures 8.3 and 8.4B). The addition of poloxamer is able to increase the transduction efficiencies of the vectors.

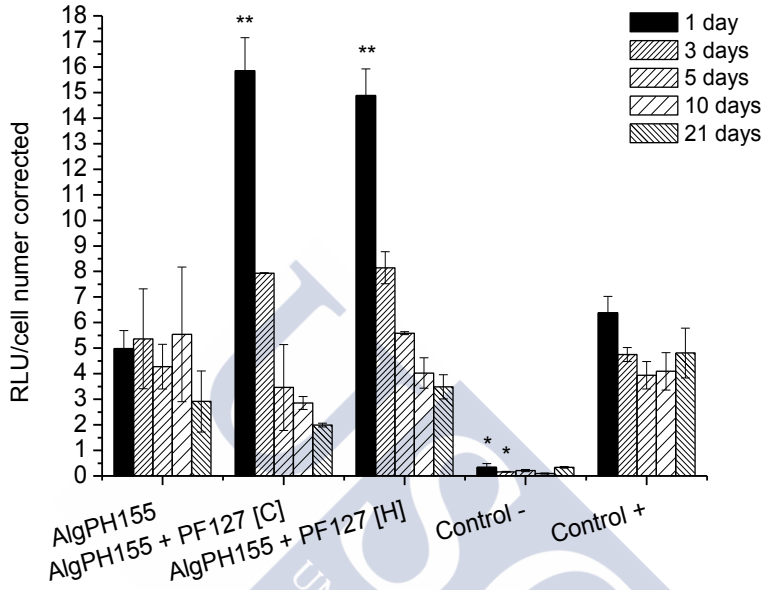

Figure 8.8 Transduction efficiencies of released rAAV-*lacZ* from capsules containing AlgPH155 with or without PF127. The homogeneous groups are indicated by an equal number of asterisks (*) above the columns ($P < 0.05$).

After the first time point of cell culture, poloxamer-alginate capsules shown similar levels of gene transduction efficiencies than alginate capsules but significantly higher than negative and positive controls. Furthermore, single alginate capsules formed by AlgPH155 were able to achieve stable cell transduction with similar RLU values at all time points evaluated whereas for the other capsules, the transduction efficiencies decreased with time. In spite of the effect of alginate decreasing transduction efficiency found for this polymer alone (Figure 8.4B), the controlled release achieved in these samples was able to promote an adequate *in vitro* transduction efficiency with statistically significant higher levels to negative control and AlgPH155 + PF127 [C] even

after 21 days of cell culture. Interestingly, capsules formed by the two polymers crosslinked at room temperature were not able to achieve higher levels of transduction efficiencies than negative control after 10 and 21 days of cell culture. According to the experimental data capsules formed by alginate alone have been shown the best release profiles and a more prolonged increase in trangene expression. Poloxamer-alginate capsules crosslinked at 50 °C have also shown good experimental results. These two hydrogel structures were selected for their incorporation into bioSiC ceramics.

8.5.6 **Hydrogel-ceramic composites**

Selected hydrogels including rAAV vector were used to be loaded into ceramic matrices in order to obtain a composite system able of promoting a local controlled release of rAAV useful for bone repair implants. Two compositions were selected for this purpose in light of their better *in vitro* results: AlgPH155 and AlgPH155 + PF127 [H]. As controls, equivalent concentrations of rAAV were directly loaded in the bioSiC samples, vectors added to cell culture medium were used as positive control and cells cultured without any treatment as negative controls. Figure 8.9 shows the results of X-Gal staining for the studied conditions. Both positive control and silicon carbide containing rAAV-lacZ showed similar staining intensity at different times studied. The presence of this ceramic thus did not affect the transduction efficiency. On the other hand, low staining was observed on both composite systems. Aginate-bioSiC showed few transduced cells while no stained cells were observed using AlgPH155 + PF127-bioSiC. This may be due to the lower hydrogel-cell culture interfacial surface that decreases the release rate of the vectors, thus decreasing transduction. Optimization of the composite process need to be next performed to obtain the desirable therapeutic effect for these composite systems.

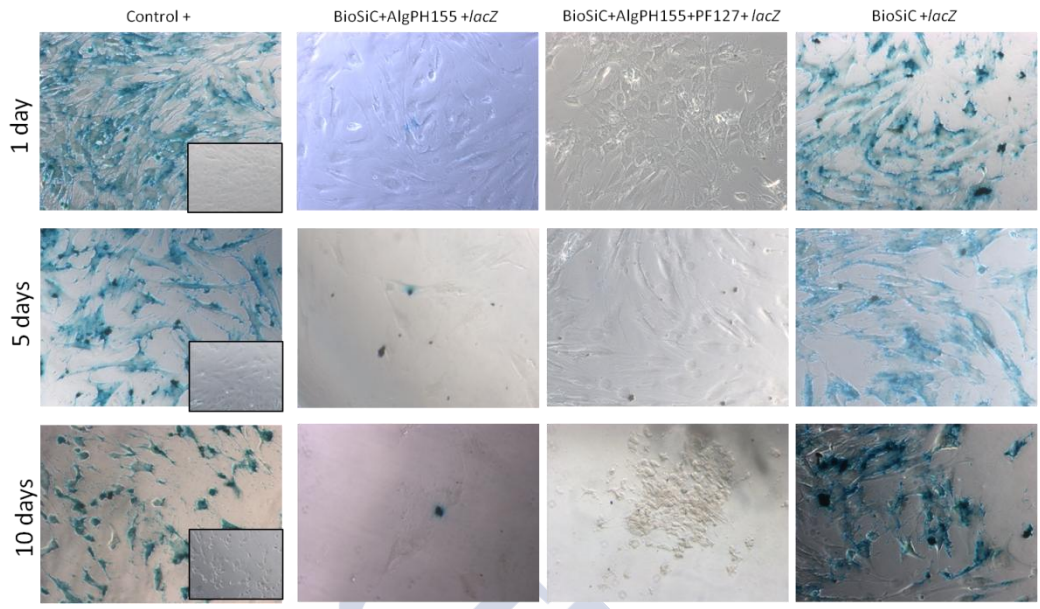

Figure 8.9 X-Gal staining of hMSCs in monolayer cultures after 1, 3, 5 and 10 days of treatment with the hydrogel-bioSiC composites including rAAV-*lacZ*.

8.5 Discussion

The combination of two polymers allowed to generate polymeric systems capable of combining the advantages of each polymer. Alginate is a safe natural polymer extracted from brown algae commonly used as tablet binding agent and as a diffusion barrier in controlled release formulations, decreasing drug molecules migration (25). The selection of alginate as part of the polymeric composition allows obtaining crosslinked hydrogels by simple addition of divalent ions (26). Synthetic block polymers such as poloxamers are capable of forming micelles in aqueous solutions with a hydrophilic shell and a hydrophobic core adequate for hydrophobic drug inclusion, increasing their solubility. Moreover, poloxamers can undergo a sol-to-gel transition at a temperature higher than the gel temperature (27).

The addition of alginate to poloxamer dispersions was able to decrease the gel temperature of the systems. This effect could be caused by complex interactions between the chains of both polymers where water could act as crosslinking agent forming hydrogen bonds between the polymers (28).

The ionotropic crosslinking of the polymeric dispersions with calcium chloride at two different temperatures was carried out being the obtained capsules of different characteristics. The selection of a crosslinking temperature higher than the gel temperature of the mixture alginate-poloxamer should make possible to obtain hydrogel systems with different porous structures. The aggregation of micelles after the gel temperature (50 °C) could be used as templates in order to obtain systems with higher porous size. The complex interactions between the two polymers where alginate chains should be placed around the polymeric micelles could increase the hydrophobicity of micelles and enhance micelle-micelle interactions and the consequent gelation as is shown in Figure 8.1B.

The significant differences in capsule stability parameters suggest that the presence of block polymeric micelles in alginate medium modifies the interaction between alginate chains and calcium ions during the crosslinking process. Micelles could impair these interactions giving final highly porous hydrogels therefore with lower stability. When the crosslinking procedure was carried out at 50 °C, a temperature over the sol-gel transition (Tgel 44.50 °C), the pluronic micelles can undergo aggregation. The increase in viscosity which strongly may hinder the ionic interactions between alginate and calcium together with presence of micelle aggregates, which act as porogen agents, may cause the synthesis of an even more porous hydrogel with larger pore size (Figure 8.2).

Good encapsulation efficiencies were obtained for all the systems studied. However, despite the higher viscosity of the polymeric composition, the lowest encapsulation efficiency was obtained for high temperature crosslinked systems. This might be result

of the higher porous structure on their external hydrogel surface layer, leading to a loss of rAAV from the particles when is compared to systems crosslinked at room temperature.

The controlled rAAV release was governed by a diffusion mechanism through the hydrogel matrix. The three porous structure obtained were able to achieve different release profiles as a function of the variations in hydrogel structure that are in agreement with the stability results.

The evaluation of the effect of the polymer presence on transduction efficiencies has pointed out an increase of trangene expression for PF127 according to a similar phenomenon that has been previously described for a similar block copolymer, PF68 (29). On the contrary the addition of alginate decreases the transduction efficiency. It has been reported that this polymer could decrease the rate of virus transport, thus decreasing the *in vivo* transfection of cancer cells, but not affecting the bioactivity of the vectors (30).

Qualitative evaluation of trangene expression of capsule released vectors through live fluorescence emission and X-Gal staining showed an enhancement on the transduction efficiency for the controlled release vectors when they are compared to positive control at long periods of time. It was previously reported that an adequate rAAV release profile is able to increase transgene expression of cells and reduce macrophage activation, increasing the therapeutic utility of the systems (13).

According to the quantitative analysis of transduction efficiencies data it is an evidence that the presence of pluronic in the capsule composition enhance the transduction efficiency of the release vectors after one day of study. This fact could be attributed to a change in the cellular membrane permeability (27) and was previously reported for lentiviral and adenoviral vectors (31).

Biomorphic silicon carbide ceramics have been shown to have highly porous structures in which the optimized hydrogels could be included. The addition of viral vectors to the ceramic structures did not affect the activity of the vectors.

8.6 Conclusions

In the present study, we were able to develop three hydrogel networks due to the thermosensitive properties of PF127 and their complex interactions with alginate chains during calcium crosslinking. These systems were stable against dilution and were able to produce three different release profiles of rAAV. The presence of PF127 was able to increase the transduction efficiency of rAAV. Crosslinked capsules showed excellent biocompatibility results and their transduction efficiency evaluation had lead to better results for systems containing alginate alone because of the long time controlled release observed for such systems. Despite the effect of PF127 on the transduction efficiency the faster release on these systems was not able to achieve higher long-term transduction efficiencies than negative control after five days of assay for room temperature crosslinked systems. The inclusion of the hydrogels in a porous ceramic was not able to achieve an adequate transduction efficiency due to the lower hydrogel surface and the consequent lower vector release. Further studies should be done in order to achieve adequate ceramic-hydrogel combinations for the treatment of osteochondral defects.

8.7 References

1. Kootstra NA, Verma IM. Gene therapy with viral vectors. Annu Rev Pharmacol Toxicol. 2003;43:413-39.

2. Ibraheem D, Elaissari A, Fessi H. Gene therapy and DNA delivery systems. Int J Pharm. 2014;459(1-2):70-83.

3. Wang C, Pham P. Polymers for viral gene delivery. Expert Opin Drug Deliv. 2008;5(4):385-401.

4. Xu X, Yang J, Cheng Y. Pharmacokinetic study of viral vectors for gene therapy: Progress and challenges. Viral Gene Ther. 2011:435-50.

5. Weimer A, Madry H, Venkatesan JK, Schmitt G, Frisch J, Wezel A, et al. Benefits of recombinant adeno-associated virus (rAAV)-mediated insulin-like growth factor I (IGF-I) overexpression for the long-term reconstruction of human osteoarthritic cartilage by modulation of the IGF-I axis. Mol Med. 2012;18(3):346-58.

6. Huang S, Kamihira M. Development of hybrid viral vectors for gene therapy. Biotechnol Adv. 2013;31(2):208-23.

7. Cucchiarini M, Thurn T, Weimer A, Kohn D, Terwilliger EF, Madry H. Restoration of the extracellular matrix in human osteoarthritic articular cartilage by overexpression of the transcription factor SOX9. Arthritis Rheum. 2007;56(1):158-67.

8. Venkatesan JK, Rey-Rico A, Schmitt G, Wezel A, Madry H, Cucchiarini M. rAAV-mediated overexpression of TGF-beta stably restructures human osteoarthritic articular cartilage *in situ*. J Transl Med. 2013;11:211-24.

9. Venkatesan JK, Ekici M, Madry H, Schmitt G, Kohn D, Cucchiarini M. SOX9 gene transfer via safe, stable, replication-defective recombinant adeno-associated virus vectors as a novel, powerful tool to enhance the chondrogenic potential of human mesenchymal stem cells. Stem Cell Res Ther. 2012;3(3):22-36.

10. Cucchiarini M, Orth P, Madry H. Direct rAAV SOX9 administration for durable articular cartilage repair with delayed terminal differentiation and hypertrophy *in vivo*. J Mol Med. 2013;91(5):625-36.

11. Moulay G, Boutin S, Masurier C, Scherman D, Kichler A. Polymers for improving the *in vivo* transduction efficiency of AAV2 vectors. PLoS One. 2010;5(12): e15576-83.

12. Zeng Y, Tseng S-, Kempson IM, Peng S, Wu W, Liu J. Controlled delivery of recombinant adeno-associated virus serotype 2 using pH-sensitive poly(ethylene glycol)-poly-l-histidine hydrogels. Biomaterials. 2012 12;33(36):9239-45.

13. Lee S, Kim J, Chu HS, Kim G, Won J, Jang J. Electrospun nanofibrous scaffolds for controlled release of adeno-associated viral vectors. Acta Biomaterialia. 2011 11;7(11):3868-76.

14. Kilpatrick LA, Li Q, Yang J, Goddard JC, Fekete DM, Lang H. Adeno-associated virus-mediated gene delivery into the scala media of the normal and deafened adult mouse ear. Gene Ther. 2011;18(6):569-78.

15. Kidd ME, Shin S, Shea LD. Fibrin hydrogels for lentiviral gene delivery *in vitro* and *in vivo*. J Control Release. 2012;157(1):80-5.

16. Tseng S-, Kempson IM, Peng S, Ke B, Chen H, Chen P, et al. Environment acidity triggers release of recombinant adeno-associated virus serotype 2 from a tunable matrix. J Control Release. 2013;170(2):252-8.

17. Zhang F-, Jia S-, Zheng S-, Ding W. Celastrol enhances AAV1-mediated gene expression in mice adipose tissues. Gene Ther. 2011;18(2):128-34.

18. Díaz-Rodríguez P, Pérez-Estévez A, Seoane R, González P, Serra J, Landin M. Suitability of biomorphic silicon carbide ceramics as drug delivery systems against bacterial biofilms. ISRN Pharm. 2013:104529-36.

19. Díaz-Rodríguez P, Landin M, Rey-Rico A, Couceiro J, Coenye T, González P, et al. Bio-inspired porous SiC ceramics loaded with vancomycin for preventing MRSA infections. J Mater Sci Mater Med. 2011;22(2):339-47.

20. Elsler S, Schetting S, Schmitt G, Kohn D, Madry H, Cucchiarini M. Effective, safe nonviral gene transfer to preserve the chondrogenic differentiation potential of human mesenchymal stem cells. J Gene Med. 2012;14(7):501-11.

21. Samulski RJ, Chang LS, Shenk T. Helper-free stocks of recombinant adeno-associated viruses: Normal integration does not require viral gene expression. J Virol. 1989;63(9):3822-8.

22. Samulski RJ, Chang LS, Shenk T. A recombinant plasmid from which an infectious adeno-associated virus genome can be excised *in vitro* and its use to study viral replication. J Virol. 1987;61(10):3096-101.

23. Madry H, Cucchiarini M, Terwilliger EF, Trippel SB. Recombinant adeno-associated virus vectors efficiently and persistently transduce chondrocytes in normal and osteoarthritic human articular cartilage. Hum Gene Ther. 2003;14(4):393-402.

24. Park H, Kim P, Hwang T, Kwon O, Park T, Choi S, et al. Fabrication of cross-linked alginate beads using electrospraying for adenovirus delivery. Int J Pharm. 2012;427(2):417-25

25. Tonnesen HH, Karlsen J. Alginate in drug delivery systems. Drug Dev Ind Pharm. 2002;28(6):621-30.

26. Drury JL, Mooney DJ. Hydrogels for tissue engineering: Scaffold design variables and applications. Biomaterials. 2003;24(24):4337-51.

27. Kabanov AV, Batrakova EV, Alakhov VY. Pluronic block copolymers as novel polymer therapeutics for drug and gene delivery. J Control Release. 2002;82(2-3):189-212.

28. Lin H, Sung KC, Vong W. *In situ* gelling of alginate/pluronic solutions for ophthalmic delivery of pilocarpine. Biomacromolecules. 2004;5(6):2358-65.

29. Zhang X, Godbey WT. Viral vectors for gene delivery in tissue engineering. Adv Drug Deliv Rev. 2006;58(4):515-34.

30. Wang Y, Hu JK, Krol A, Li Y, Li C, Yuan F. Systemic dissemination of viral vectors during intratumoral injection. Mol Cancer Ther. 2003;2(11):1233-42.

31. Strappe PM, Hampton DW, Cachon-Gonzalez B, Fawcett JW, Lever A. Delivery of a lentiviral vector in a pluronic F127 gel to cells of the central nervous system. Eur J Pharm Biopharm. 2005 10;61(3):126-33.

Capítulo 9

Discusión general

USC
UNIVERSIDADE
DE SANTIAGO
DE COMPOSTELA

9. Discusión general

De acuerdo con los objetivos descritos en el capítulo dos de la presente memoria, el trabajo se ha centrado en el desarrollo de sistemas biofuncionales de carburo de silicio biomórfico con potencial aplicación en el tratamiento y la prevención de patologías óseas. La introducción en el estudio de carburos de silicio procedentes de diversas fuentes vegetales (madera de roble, sapelli y pino), con diferentes microestructuras debe permitir analizar el efecto de diversos parámetros como la porosidad o las características superficiales sobre el comportamiento y la funcionalidad de estas cerámicas y, en último término, seleccionar la/s más adecuadas para este fin.

9.1 Caracterización de las cerámicas de carburo de silicio

La necesidad de desarrollar sistemas implantables capaces de mantener la funcionalidad del tejido reemplazado, integrarse adecuadamente y no provocar efectos tóxicos ha llevado, en los últimos años, a la síntesis de numerosos materiales porosos complejos. Entre ellos pueden señalarse las cerámicas de carburo de silicio, obtenidas a partir de precursores vegetales, cuyas microestructuras mimetizan la estructura porosa y la interconectividad del tejido óseo que se pretende reemplazar. La utilización de la

propia naturaleza como modelo resulta una muy prometedora aproximación para la síntesis de materiales con aplicación en regeneración ósea (1, 2) (Capítulo 1.2).

La amplia variedad de materiales naturales que pueden ser usados como molde para la síntesis de las cerámicas biomórficas, permite la obtención de sistemas biomiméticos con potencialidad diversa. En este trabajo se han empleado carburos de silicio biomórfico (bioSiCs) elaborados mediante un procedimiento de bioceramización en dos etapas; pirolización de la madera e infiltración con silicio líquido. La caracterización tanto de las estructuras porosas como de las propiedades superficiales resulta clave para comprender las respuestas celulares, así como la capacidad de los bioSiCs para cargar y ceder diferentes moléculas terapéuticas.

Las preformas de carbón obtenidas de las tres maderas tras el proceso de pirolización, de naturaleza hidrofóbica, presentan una reducida densidad, con microestructuras caracterizadas por un elevada porosidad total, poros de diámetro similar a las tráqueas y traqueidas propias de su especie y una gran rugosidad superficial, especialmente para la madera de sapelli (Capítulo 5).

La infiltración posterior produce una reacción espontánea entre el carbono y el silicio que da lugar a la formación de cristales de carburo de silicio que tapizan el interior de los poros, obturando los de menor tamaño o reduciendo el diámetro de los más grandes, como puede deducirse de la Figura 9.1.

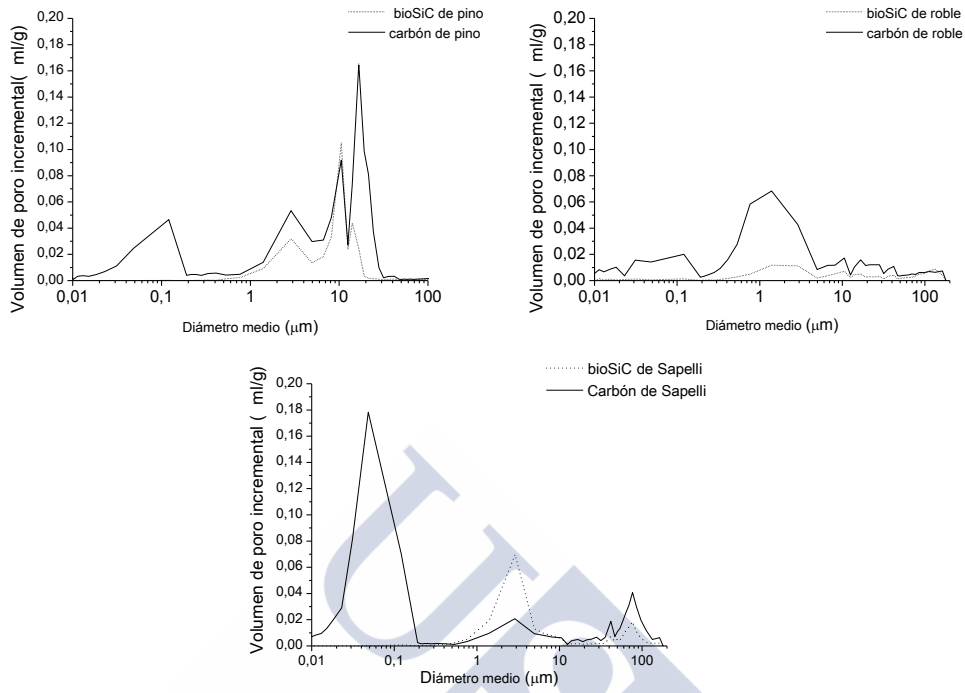

Figura 9.1 Relación entre la porosidad de los bioSiCs y sus preformas de carbón obtenida mediante porosimetría de intrusión de mercurio.

La figura 9.2 representa gráficamente algunos de los parámetros característicos de las cerámicas biomórficas producidas y sus precursores de carbón. Mientras que el pino genera la cerámica de mayor porosidad total (46.97%) y menor superficie específica, con macroporos de pequeño tamaño (50 ± 20 μm), el roble da lugar al bioSiC con menor porosidad total (27.85%) pero con la mayor superficie porosa, una densidad intermedia y macroporos de mayor tamaño 250 ± 20 μm (Capítulo 6).

Los bioSiCs obtenidos de la madera de sapelli se caracterizan por presentar: una distribución de tamaños de poro bimodal, una porosidad total similar a la del pino (40.72%), una superficie específica intermedia y la mayor densidad de los tres sistemas estudiados, con macroporos de un tamaño medio de 140 ± 30 μm.

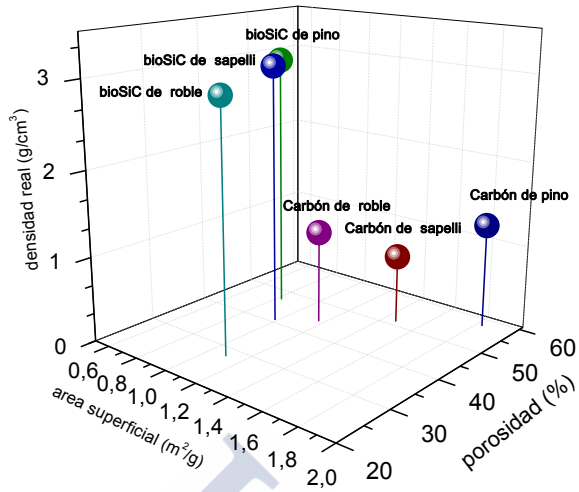

Figura 9.2 Relación entre porosidad, área superficial (obtenida por adsorción de nitrógeno) y densidad real (obtenida mediante picnometría de helio) de los tres sistemas cerámicos bioSiCs.

Los tres bioSiCs, a diferencia de sus correspondientes preformas de carbón, se caracterizan por ser materiales hidrofílicos, con un ángulo de contacto medio de 38 ± 7° (Capítulo 5) sin diferencias significativas entre ellos. Sin embargo, el empleo de fluidos de diferente naturaleza permite la estimación de valores de energía superficial variables. Así, los bioSiCs de pino presentaron una energía superficial positiva, mientras que los de roble y sapelli presentaron valores negativos (Capítulo 6).

La rugosidad superficial, evaluada mediante perfilometría interferométrica (Capítulo 5), también pone de manifiesto variaciones importantes. El bioSiC de sapelli presenta mayor rugosidad superficial con un Rq de 11.05 µm, muy superior al del pino y el roble, con valores de 6.91 µm y 5.91 µm respectivamente. El análisis de la superficie de los bioSiCs mediante FT-IR mostró en todas ellas, la presencia de grupos funcionales OH y SiO (Capítulo 6).

La modelización de la estructura porosa de los sistemas cerámicos a partir de las curvas de porosimetría de intrusión de mercurio mediante un software especializado (PoreXpert®) permite valorar la interconectividad de sus poros, su tortuosidad y también realizar predicciones sobre el potencial proceso de penetración de un fluido en la estructura porosa cuando la cerámica entre en contacto con un medio líquido (Capítulo 6). La Figura 9.3 presenta la cinética de captación de agua a 0 MPa simulada para los diferentes sistemas. Como puede observarse, es la microestructura del bioSiC de sapelli la que presumiblemente es capaz de captar más agua y más rápidamente. Este sistema presenta la mayor conectividad y la menor tortuosidad de los tres estudiados. A pesar de que la capacidad de captación de agua es similar en los bioSiCs de pino y de roble a 110 ms, la modelización pone de manifiesto que la conectividad del bioSiC de roble es superior a la del pino.

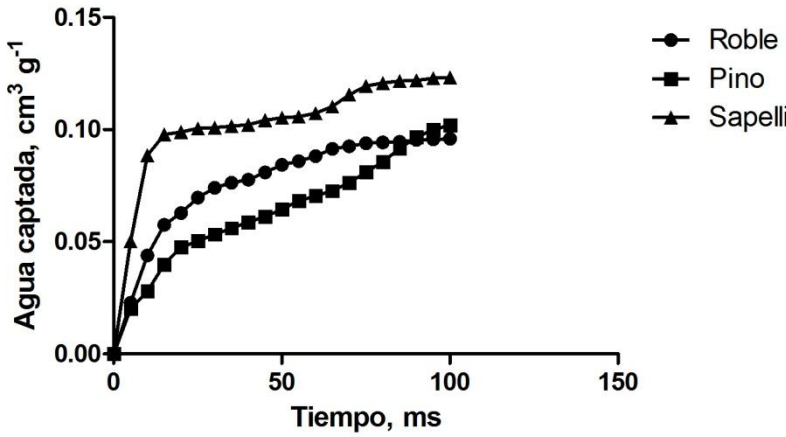

Figura 9.3 Simulación de la captación de agua por parte de los tres sistemas porosos bioSiCs obtenida tras la modelización de la estructura porosa con el software especializado PoreXpert®.

9.2 Evaluación de la respuesta celular e inmunológica a los bioSiCs

La captación de fluidos por parte de las estructuras porosa modifica no sólo la potencial capacidad de carga de fármacos, sino también la adhesión celular y la respuesta inflamatoria. Por ello, las diferentes estructuras de carburo de silicio deberían dar lugar a un comportamiento celular diferente y perfiles de carga y cesión variables. De esta manera la evaluación de la respuesta celular y tisular a los sistemas bioSiCs resulta crucial para analizar su potencial aplicación en regeneración ósea.

9.2.1 **Evaluación de la biocompatibilidad de los bioSiCs**

La introducción de nuevos materiales como sustitutos óseos ha de estar presidida por la capacidad del biomaterial para ejercer su función sin producir efectos adversos. El biomaterial ideal útil en regeneración ósea debe ser económico, fiable y seguro, a la vez que biocompatible, osteoinductivo, osteoconductivo y preferentemente biodegradable (3, 4). Si el defecto óseo es grande y el implante ha de fabricarse con material no biodegradable, es necesario que éste sea capaz de estimular la formación de tejido óseo y/o promover su osteointegración. En estos casos las características microestructurales y superficiales del material son críticas. Diversos autores han puesto de manifiesto que el tamaño de los poros del material condiciona la formación de nuevos vasos en el implante y, por tanto, el crecimiento del tejido óseo (5-8).

El estudio preliminar de la biocompatibilidad de los bioSiCs fue realizado con una línea celular de fibroblastos (BALB/3T3) usando como material cerámico el bioSiC de sapelli (Capítulo 3). Los resultados experimentales demostraron la excelente biocompatibilidad de los sistemas observándose la formación de una monocapa de células tras 15 días de estudio (Figura 9.4).

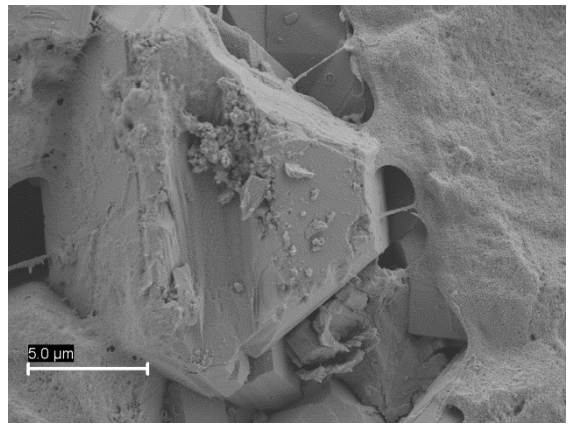

Figura 9.4 Fotografía de microscopía electrónica de barrido (SEM) de sapelli tras 15 días de cultivo con la línea celular fibroblástica BALB/3T3.

La biocompatibilidad de los tres sistemas bioSiCs (pino, roble y sapelli) fue posteriormente evaluada usando células madre mesenquimales obtenidas de médula ósea humana (Capítulo 6). Los resultados de viabilidad celular así como las imágenes de microscopía confocal, la cuantificación de citoquinas proinflamatorias (IL-1β) y de marcadores de apoptosis (caspasa-3), muestran que todos los sistemas son altamente biocompatibles con niveles no detectables de IL-1β y concentraciones de caspasa-3 equivalentes al control negativo a todos los tiempos estudiados. De esta manera, todos los carburos de silicio cumplen el requisito de biocompatibilidad.

9.2.2 **Efecto de las estructuras porosas de los bioSiCs sobre la interacción con los componentes sanguíneos**

Las características superficies de los materiales también determinan su interacción con los componentes sanguíneos en el momento de su implantación. La formación de coágulo, la activación de plaquetas y la inflamación condicionan el proceso normal de regeneración ósea y modulan el crecimiento óseo alrededor del implante y la osteoconducción (3, 9-12). También ha sido descrito que la energía superficial, el

ángulo de contacto, la liberación de iones, la resistividad y la rugosidad superficial modifican estas interacciones, y por tanto, la regeneración ósea (13-16).

La interacción de las superficies de los carburos de silicio y los componentes sanguíneos fue evaluada en lo que respecta a la hemólisis producida, la adsorción de proteínas, la coagulación, la adhesión de plaquetas y la activación del sistema de complemento con el fin de obtener los parámetros microestructurales clave que condicionan dichas interacciones (Capítulo 5). Así, se ha observado que el tamaño de poro es fundamental a la hora de predecir la hemólisis generada. La utilización de sistemas con menor tamaño de macroporo (pino y sapelli) da lugar a valores de hemolisis más reducidos.

La relación entre la adsorción de proteínas hidrofílicas (seroalbúmina bovina) y proteínas hidrofóbicas (fibrinógeno) condicionan la adhesión celular y como consecuencia la posterior osteointegración. Todos los bioSiCs estudiados se caracterizan por poseer una mayor adsorción de albúmina que de fibrinógeno lo que debe facilitar el reconocimiento celular de las superficies. Ello además, se correlaciona con una baja formación de trombo y con una mayor superficie específica de los materiales. De la misma manera, se observó que la activación del sistema de complemento, directamente relacionada con la respuesta inmune, está condicionada por la adsorción de proteínas. La adhesión de plaquetas por parte de los sistemas cerámicos mostró que éstas mantienen una morfología redondeada, lo que indica una adecuada adhesión celular, sin causar su activación.

La evaluación de formación de coágulo para los tres sistemas ensayados mostró mayores valores para el bioSiC de sapelli lo que está directamente correlacionado con la mayor rugosidad superficial. Se ha observado que la formación de coágulo es dependiente de la superficie externa mientras que la adsorción de proteínas se ve modulada tanto por la superficie externa como por la interna. Los resultados

experimentales obtenidos permiten concluir que las cerámicas de carburo de silicio biomórfico presentan una hemocompatibilidad adecuada para su aplicación como sistemas implantables.

Además, la formación de coágulo observada debería dar lugar a una adecuada integración de los implantes. La reducida respuesta inflamatoria podría indicar la ausencia de formación de tejido fibroso alrededor del implante favoreciendo su integración (17). De acuerdo con los resultados experimentales de rugosidad superficial y la formación de coágulo observada los carburos de silicio de sapelli se presentan como los más prometedores para una posible aplicación clínica.

9.2.3 **Efecto de la topografía de los bioSiCs sobre la diferenciación celular**

La rugosidad superficial, el ángulo de contacto, la cristalinidad y la composición química modulan la adhesión, la morfología, la funcionalidad y la migración celular en el interior del material lo que condiciona la fijación del implante y su integración (5, 18-27).

El efecto de las características topográficas de los carburos de silicio biomórficos así como de su estructura porosa sobre la diferenciación osteoblástica de células madre mesenquimales, se evaluó en función de la secreción de indicadores de diferenciación (osteocalcina, osteopontina y fosfatasa alcalina) (Capítulo 6). De acuerdo con datos bibliográficos previos, se ha observado que las propiedades de los bioSiCs modifican el comportamiento celular. Así, los carburos de silicio que presentan mayor tamaño de poro (roble y sapelli) son capaces de estimular la diferenciación osteoblástica de las células madre mesenquimales tras quince días de cultivo obteniéndose valores de osteocalcina y osteopontina similares a los de las células cultivadas en presencia de medio de diferenciación osteoblástica. Es posible que la diferenciación observada no sólo esté condicionada por la morfología de los sistemas, sino también por la presencia de silicio, ya que se ha descrito que este compuesto es capaz de promover la

diferenciación osteoblástica, e incrementar la proliferación de los osteoblastos y su producción de osteocalcina (28). Los resultados experimentales obtenidos permiten concluir que seleccionando un precursor con una estructura porosa adecuada se podrían obtener cerámicas de carburo de silicio biomórfico con capacidad osteoinductora.

9.2.4 **Actividad inflamatoria de las partículas de bioSiC obtenidas por desgaste mecánico**

Otro aspecto importante de los biomateriales es su potencial para generar productos de degradación tóxicos tras su implante. Por ejemplo, el uso de polímeros derivados del ácido láctico promueve la producción de sustancias de carácter ácido como producto de degradación que generan inflamación en los tejidos adyacentes (29).

El desgaste mecánico de los materiales implantados puede dar lugar a la formación de partículas, que causen la activación de los macrófagos circundantes, el desencadenamiento de una respuesta inflamatoria aguda y la consiguiente destrucción de tejido óseo y fallo del implante (30-32).

Los carburos de silicio biomórficos son materiales sólidos, poco friables, cuya velocidad de degradación es extremadamente lenta, menor de 30 nm por año en condiciones fisiológicas normales (30). Se estudió la capacidad de las partículas de carburo de silicio biomórfico para estimular macrófagos y provocar una respuesta inflamatoria con vistas a predecir su potencial toxicidad a largo plazo tras su implantación (Capítulo 7). Las partículas de carburo de silicio nanométricas obtenidas por desgaste mecánico a partir de dos piezas de carburo de silicio sometidas a rozamiento fueron internalizadas por los macrófagos, como se muestra en la Figura 9.5. A pesar de ello, la secreción de citoquinas proinflamatorias por los macrófagos (TNF-α e IL-1β) mostró valores similares a los obtenidos con las partículas de zirconio usadas como referencia. De

acuerdo con los resultados experimentales se puede afirmar que el carburo de silicio causa unos niveles aceptables de inflamación, similares a un material, el zirconio, que está reconocido como el más adecuado desde el punto de vista inflamación de partículas (33).

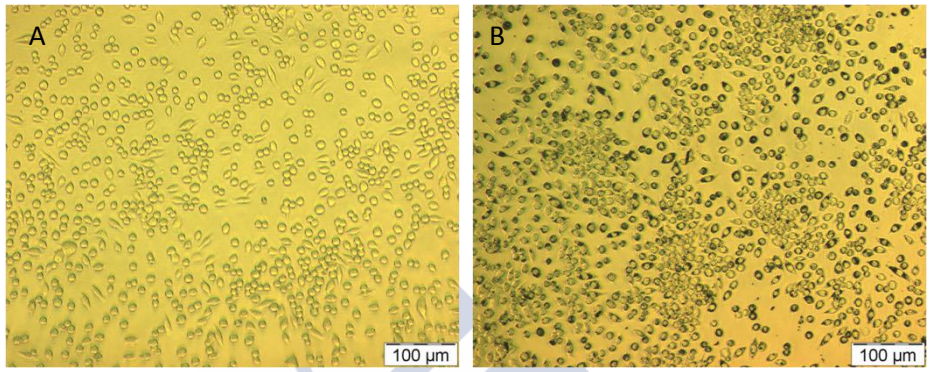

Figura 9.5 Captación de las partículas de carburo de silicio por parte de los macrófagos en comparación con el control negativo (A).

9.3 Desarrollo de sistemas biofuncionales de carburo de silicio

La incorporación de moléculas terapéuticas en sistemas implantables permite dotar de valor añadido a los materiales. De acuerdo con lo descrito en el Capítulo 1.1 existen diferentes mecanismos de carga que pueden ser empleados para la obtención de materiales biofuncionales y que condicionan los perfiles de liberación de fármaco obtenidos. En este trabajo se han utilizado tres mecanismos diferentes para la incorporación de moléculas terapéuticas: la adsorción inespecífica, las interacciones iónicas y la inclusión en una matriz.

9.3.1 **Adsorción inespecífica de antibióticos**

A pesar de los tratamientos preventivos con antibióticos a nivel sistémico, la osteomielitis postquirúrgica continúa siendo una seria complicación en la cirugía

ortopédica y dental (34). Los materiales implantados en el organismo son a menudo objeto de colonización microbiana, lo que evita la adhesión celular y da lugar al fallo de la prótesis (35). Cuando la contaminación es severa, la osteomielitis se cronifica y la administración sistémica de antibióticos no es capaz de erradicarla debido a las bajas concentraciones locales de fármaco que se alcanzan. El protocolo para el tratamiento de esta problemática supone la retirada de la prótesis y la implantación provisional de sistemas poliméricos de polimetil-metacrilato (PMMA) cargados con antibióticos capaces de alcanzar un adecuado perfil de liberación. El carácter no biodegradable del PMMA hace necesaria su retirada mediante una nueva cirugía (36, 37).

La posibilidad de desarrollar sistemas para la regeneración ósea, cargados con antibióticos que prevengan o traten la osteomielitis representa una prometedora alternativa en regeneración ósea.

En este estudio se han desarrollados sistemas de carburo de silicio biomórfico cargados con vancomicina mediante un mecanismo de adsorción inespecífica. La necesidad de alcanzar concentraciones elevadas de fármaco a tiempos cortos que funcionen como dosis de ataque a los microorganismos presentes en el medio y eviten la colonización del implante por parte de las bacterias hacen de este mecanismo el más adecuado *a priori* para el desarrollo de sistemas bioSiC cargados con vancomicina.

Como evaluación preliminar de la capacidad de carga y cesión de los bioSiCs se seleccionó el carburo de silicio obtenido a partir de madera de sapelli (Capítulo 3). La isoterma de adsorción del fármaco muestra la formación inicial de una monocapa de moléculas de vancomicina para luego dar lugar a consecutivas capas de fármaco a medida que la concentración de carga se ve incrementada de acuerdo con un perfil característico de adsorción inespecífica.

La potencial variabilidad en la carga y cesión de la vancomicina en función de la microestructura se evaluó incorporando al estudio muestras de bioSiC de roble y pino mediante el mismo procedimiento de adsorción inespecífica. Los perfiles de liberación de fármaco a partir de los sistemas cerámicos (Capítulos 3 y 4) mostraron una liberación en dos fases, propia del método de carga seleccionado. Así, se observó una importante cesión de fármaco a tiempos cortos, debida a la elevada solubilidad de la vancomicina, seguida de una liberación más lenta condicionada por la difusión de las moléculas de fármaco en el medio introducido en los poros de la matriz cerámica. Las diferentes estructuras porosas condicionan el perfil de liberación obteniéndose constantes de cesión más elevadas para los sistemas de sapelli y pino que son los que presentan mayor porosidad e interconexión respectivamente.

En el caso del bioSiC de sapelli, los sistemas cargados fueron capaces de inhibir la formación del biofilm bacteriano de *S. aureus* meticilin resistentes tras 72 horas de cultivo.

La erradicación del biofilm bacteriano es más compleja debido a que los polisacáridos que lo componen, reducen la penetración de los fármacos e incrementan la resistencia de las bacterias a los tratamientos (38, 39).

Los sistemas cargados con vancomicina son capaces de prevenir la formación de biofilm y/o tratar el biofilm de *S. aureus* ya formado. Los sistemas biofuncionales desarrollados han sido capaces de disminuir significativamente el número de bacterias presentes en el biofilm tras 48 horas de ensayo obteniéndose valores superiores a la adición de antibiótico en el biofilm (Figura 9.6). Además, se ha observado un efecto sinérgico entre la propia actividad del fármaco y las estructuras porosas ya que se alcanza una mayor erradicación del biofilm con los sistemas cargados que con la adición simple de fármaco.

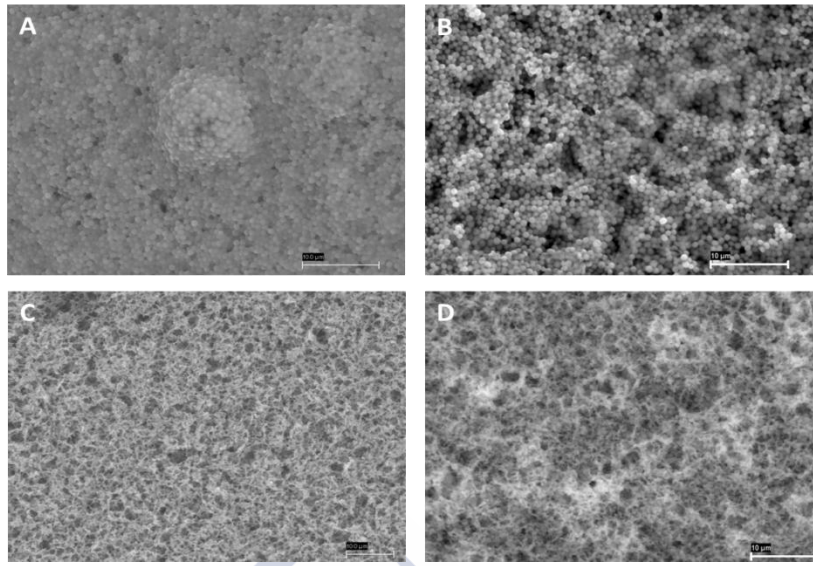

Figura 9.6 Fotografías de microscopía electrónica de barrido correspondientes a: (A) biofilm bacteriano; (B) biofilm bacteriano tratado con bioSiC de roble sin vancomicina a las 48 horas; (C) control negativo (soporte para el crecimiento del biofilm); (D) biofilm tratado con bioSiC cargado con vancomicina a las 48 horas.

9.3.2 **Interacciones iónicas con proteínas**

La incorporación de factores de crecimiento, tanto en la superficie externa como en el seno de los biomateriales, es una técnica ampliamente empleada en ingeniería de tejidos que mejora las propiedades de los materiales dotándolos de capacidad osteoinductiva (40, 41). Además, favorece la estabilidad de las proteínas y dilata su tiempo de permanencia en el lugar de acción, incrementando el éxito terapéutico del implante (42, 43). Los factores de crecimiento más empleados para la regeneración del tejido óseo son las proteínas morfogénicas óseas (BMPs) ya que modulan el proceso de regeneración ósea (44). Sin embargo, se ha observado que la utilización de otros factores como el factor de crecimiento del endotelio vascular (VEGF) además de incrementar la formación de vasos sanguíneos favoreciendo la osteointegración del

implante (45) puede promover la proliferación de los osteoblastos y la diferenciación celular (46, 47).

El proceso de angiogénesis o formación de nuevos vasos es crucial para asegurar la viabilidad celular ya que permite el flujo de nutrientes y la eliminación de productos de deshecho en el seno de los implantes (5, 6, 48). Por ello, y con el fin de obtener sistemas con elevado potencial en regeneración ósea y dilucidar el posible efecto sinérgico entre la superficie de los implantes y la incorporación de factores de crecimiento se han desarrollado sistemas biofuncionales bioSiC cargados con VEGF.

El empleo de factores de crecimiento a elevadas concentraciones o con perfiles de liberación no adecuados que no mimeticen la cascada normal de señalización celular, puede dar lugar a numerosos efectos adversos indeseados que deben evitarse (48). Por ello, el VEGF se ha cargado en los bioSiCs mediante un mecanismo de interacción iónico, por la interacción de la proteína con los grupos funcionales presentes en la superficie de los bioSiCs (-OH, SiO). Ello debe favorecer su cesión de forma controlada (Capítulo 6). Los bioSiCs obtenidos a partir de madera de sapelli se caracterizaron por poseer una liberación más lenta lo que se justifica por mayores interacciones proteína-bioSiC, debidas a su mayor superficie específica, la conectividad de sus poros y una menor tortuosidad. El máximo de concentración de proteína liberada que se obtiene tras 5 días de ensayo, permite simular las condiciones fisiológicas (49, 50).

La potencial modificación de la estabilidad de la proteína en los sistemas cargados se evaluó mediante su efectividad sobre la proliferación de células endoteliales (HUVEC). El proceso de carga y liberación de la proteína no modifica su actividad. Además, la cesión controlada de VEGF permite modular la respuesta celular obteniéndose una mayor proliferación celular en los sistemas capaces de producir una cesión más sostenida (sapelli). Se observó un efecto sinérgico entre el VEGF y los bioSiCs

obteniéndose mejores resultados en con los sistemas biofuncionales que los descritos tras la adición de VEGF al medio (51).

La capacidad de la proteína liberada para generar angiogénesis *in vivo* fue evaluada mediante un modelo animal (membrana corioalantóidea). La proteína liberada a partir de los sistemas bioSiCs diluida en una matriz polimérica ha sido capaz de estimular la formación de nuevos vasos (Figura 9.7). Es destacable además que los bioSiCs no cargados, de mayor porosidad, sapelli y roble fueron invaginados por la propia membrana lo que es indicativo de una excelente biocompatibilidad, mientras que los de pino se mantienen en la superficie de la membrana (Figura 9.7).

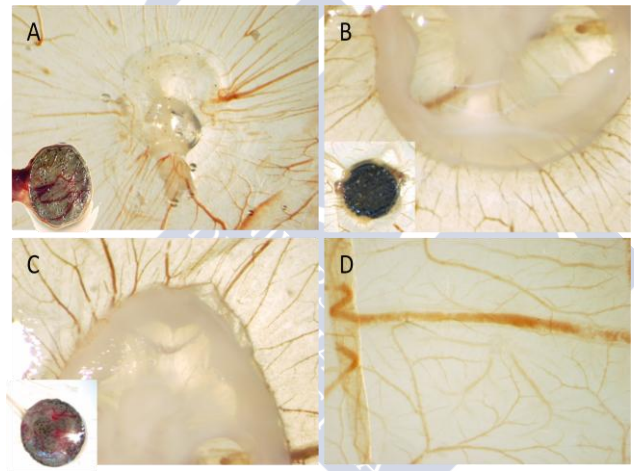

Figura 9.7 Formación de nuevos vasos de la proteína liberada de (A) bioSiC de roble; (B) bioSiC de pino; (C) bioSiC de sapelli y (D) control negativo. Las imágenes de tamaño reducido se corresponden con los bioSiCs colocados sobre la membrana e invaginados (roble y sapelli, A y C) o no invaginado (pino, B).

La evaluación del efecto sinérgico del VEGF y la morfología de los bioSiCs en cuanto a la diferenciación osteoblástica evaluada mediante PCR en tiempo real muestra que la adición de VEGF a los sistemas es capaz de promover una diferenciación más rápida,

mientras que los sistemas no cargados inducen inicialmente una elevada proliferación celular seguida de la diferenciación a tiempos más prolongados.

9.3.3 **Inclusión en una matriz de hidrogel**

Es frecuente el empleo de materiales compuestos, cerámicas de fosfato cálcico o vidrios bioactivos en matrices poliméricas, para simular la elevada complejidad del tejido óseo constituido por un componente orgánico, mayoritariamente colágeno, y un componente inorgánico, la hidroxiapatita (52, 53). Ello permite incrementar el valor terapéutico de cada uno de los materiales por separado (54, 55) o incluso establecer nuevas terápicas mediante el empleo de diversas moléculas activas con perfiles de liberación diferentes (49, 56, 57).

La adición de un sistema polimérico a las cerámicas porosas de carburo de silicio biomórfico debería permitir la obtención de sistemas compuestos hidrogel-cerámica con elevado potencial en regeneración ósea y en el tratamiento de defectos osteocondrales. Además, la incorporación de moléculas terapéuticas en la fase polimérica ha de dar lugar a perfiles de cesión controlada.

9.3.3.1 *Inclusión de antiinflamatorios en sistemas compuestos de bioSiCs*

Se desarrollaron sistemas compuestos hidrogel-bioSiC empleando como parte polimérica, reticulada con iones calcio, una combinación de un polímero natural, alginato, y un polímero bloque sintético, poloxamer 147 (Pluronic® F127) (Capítulo 7).

Se seleccionó el antiinflamatorio indometacina como fármaco modelo para su inclusión en la fase de hidrogel. Los perfiles de cesión de fármaco obtenidos son característicos de un proceso de liberación controlado por difusión. El medio de disolución penetra a través de los poros del material e interacciona con el alginato-poloxamer, dando lugar a un gel que controla la liberación. Los sistemas mostraron una clara dependencia de la

estructura porosa de la matriz cerámica, produciéndose una cesión más rápida en los sistemas obtenidos con bioSiC de sapelli. Ello puede justificarse, al igual que para la cesión de los factores de crecimiento, a su elevada porosidad e interconectividad que, como se señaló anteriormente, permite predecir una captación de agua más rápida y en mayor cantidad que para los otros dos materiales.

El efecto terapéutico de la indometacina liberada por los sistemas cargados se evaluó mediante su capacidad para reducir la inflamación de macrófagos estimulados con lipopolisacárido. Los sistemas cargados generaron reducciones significativas de la secreción de citoquinas proinflamatorias por los macrófagos (NO, PGE_2 y TNF-α) tras 24 y 72 horas, lo que indica un adecuado efecto antiinflamatorio.

Además, los sistemas compuestos cultivados con condrocitos osteoartríticos fueron capaces de modular la destrucción de la matriz extracelular. La indometacina liberada disminuye la secreción de citoquinas proinflamatorias (PGE_2, NO) por parte de los condrocitos incrementa la síntesis de colágeno y reduce la actividad catabólica de las células.

9.3.3.2 *Inclusión de vectores virales en sistemas compuestos*

El empleo de la terapia génica se presenta como una atractiva alternativa a la terapia convencional para el tratamiento de numerosas patologías. Su principal ventaja es su capacidad para inducir la expresión de un gen en un tipo celular concreto restableciendo el nivel normal de expresión proteica durante un período de tiempo prolongado (58, 59). Para la inducción del gen de interés en este tipo de terapia se emplean diversas técnicas como la inyección directa de ADN, la encapsulación de ADN en sistemas poliméricos o el empleo de vectores virales (58, 59).

Los vectores virales presentan una capacidad de transducción superior a la de las otras alternativas (Capítulo 8). Particularmente, los virus recombinantes adeno-asociados

(rAAV) han mostrado utilidad para la transducción de condrocitos (60, 61). Sin embargo, el elevado tamaño y la reducida estabilidad de estos virus dificulta su aplicación mediante sistemas de liberación convencionales, lo que abre interesantes perspectivas para el desarrollo de nuevas alternativas para su administración.

Como fase final de este trabajo hemos desarrollado combinaciones de estructuras porosas de carburo de silicio biomórfico con polímeros, alginato y poloxamer, con el objetivo de cargar y liberar de forma controlada estos vectores virales para su potencial aplicación en la regeneración de defectos osteocondrales.

La presencia de alginato y poloxamer modifica la eficacia de transducción de los vectores virales, de forma similar a lo observado por otros autores (62-64). Así, el poloxamer incrementa la eficacia de transducción, posiblemente debido a la modificación de la permeabilidad de la membrana (65), mientras que la adición de alginato al medio de cultivo reduce la eficacia de transducción de los vectores en solución.

La incorporación de los vectores virales en los sistemas binarios alginato-poloxamer reticulados con calcio da lugar a cápsulas con perfiles de liberación condicionados por su composición y condiciones de procesado. De esta manera, las cápsulas formadas por alginato solo poseen una estructura más compacta en su parte externa. Los sistemas formados por alginato y poloxamer reticulados a temperatura ambiente y a 50 °C poseen una estructura menos compacta. En estos últimos, el realizar la reticulación a una temperatura superior a la de gelificación (44.55 °C) permitiría que los agregados micelares de poloxamer actuaran como moldes para obtener sistemas de mayor tamaño de poro.

Los perfiles de liberación obtenidos de los tres hidrogeles con estructura variable se correlacionan con la eficacia de transducción observada. El perfil de liberación más

controlado, obtenido por los sistemas que contienen solo alginato, fue el que logró una eficacia de transducción más prolongada. Los sistemas que contienen poloxamer mostraron un incremento de la capacidad de transducción de los vectores virales tras el primer día de cultivo. Sin embargo, este efecto no se observó a tiempos más prolongados.

La incorporación de los dos sistemas con mejor liberación en el seno de matrices poliméricas de bioSiC no logró un perfil de liberación adecuado capaz de alcanzar unos niveles deseados de transducción (Figura 9.8). La adición de los vectores virales en las cerámicas de carburo de silicio biomórfico no modificó la eficacia de transducción de los vectores. Las condiciones de síntesis de los sistemas complejos deberían de ser modificadas con el fin de alcanzar el nivel óptimo de transducción.

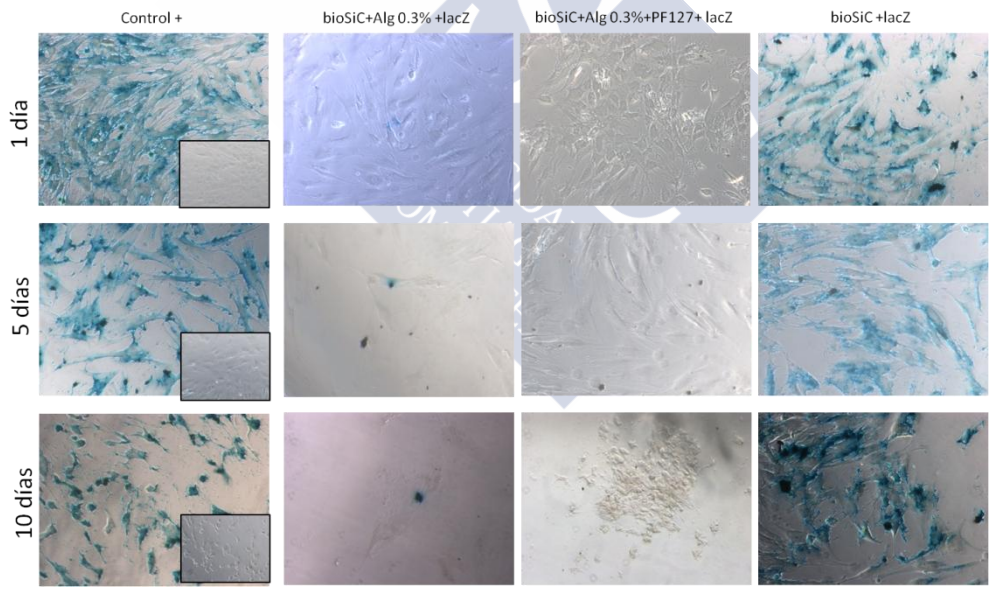

Figura 9.8 Tinción X-Gal correspondientes a células madre mesenquimales cultivadas en monocapa tras 1, 5 y 10 días de tratamiento con los sistemas compuestos hidrogel-bioSiC conteniendo el vector viral rAAV-*lacZ*.

9.4 Referencias

1. Filardo G, Kon E, Tampieri A, Cabezas-Rodriguez R, Di Martino A, Fini M, et al. New bio-ceramization processes applied to vegetable hierarchical structures for bone regeneration: An experimental model in sheep. Tissue Eng, Part A. 2014;20(3-4):763-73.

2. Chen X, Cai K, Lai M, Zhao L, Tang L. Mesenchymal stem cells differentiation on hierarchically Micro/Nano-structured titanium substrates. Adv Biomater (Weinheim, Ger). 2012(3):B216-23.

3. Park J, Lakes RS. Biomaterials an introduction. 3ª ed. Park J and Lakes RS, editores. New York: Springer; 2007.

4. Blitterswijk C, Thomsen P, Lindahl A, Hubbell JA, Williams D, Cancedda R, et al. Tissue engineering. 1ª ed. Blitterswijk C, editores. London: Academic Press: Elsevier; 2008.

5. Adachi T, Osako Y, Tanaka M, Hojo M, Hollister SJ. Framework for optimal design of porous scaffold microstructure by computational simulation of bone regeneration. Biomaterials. 2006;27(21):3964-72.

6. Klenke FM, Liu Y, Yuan H, Hunziker EB, Siebenrock KA, Hofstetter W. Impact of pore size on the vascularization and osseointegration of ceramic bone substitutes *in vivo*. J Biomed Mater Res, Part A. 2008;85A(3):777-86.

7. Gomes ME, Sikavitsas VI, Behravesh E, Reis RL, Mikos AG. Effect of flow perfusion on the osteogenic differentiation of bone marrow stromal cells cultured on starch-based three-dimensional scaffolds. J Biomed Mater Res, Part A. 2003;67A(1):87-95.

8. Sun X, Kang Y, Bao J, Zhang Y, Yang Y, Zhou X. Modeling vascularized bone regeneration within a porous biodegradable CaP scaffold loaded with growth factors. Biomaterials. 2013;34(21):4971-81.

9. Davies JE. Understanding peri-implant endosseous healing. J Dent Educ. 2003;67(8):932-49.

10. Lienemann PS, Lutolf MP, Ehrbar M. Biomimetic hydrogels for controlled biomolecule delivery to augment bone regeneration. Adv Drug Delivery Rev. 2012;64(12):1078-89.

11. Sinno H, Prakash S. Complements and the wound healing cascade: An updated review. Plast Surg Int. 2013;2013:146764.

12. Park JY, Davies JE. Red blood cell and platelet interactions with titanium implant surfaces. Clin Oral Implants Res. 2000;11(6):530-9.

13. Yang Y, Lai Y, Zhang Q, Wu K, Zhang L, Lin C, et al. A novel electrochemical strategy for improving blood compatibility of titanium-based biomaterials. Colloids Surf, B. 2010;79(1):309-13.

14. Zheng CL, Cui FZ, Meng B, Ge J, Liu DP, Lee I-. Hemocompatibility of C-N films fabricated by ion beam assisted deposition. Surf Coat Technol. 2005;193(1-3):361-5.

15. Okpalugo TIT, Ogwu AA, Maguire PD, McLaughlin JAD, Hirst DG. In-vitro blood compatibility of a-C:H:Si and a-C:H thin films. Diamond Relat Mater. 2004;13(4-8):1088-92.

16. Park JE, Barbul A. Understanding the role of immune regulation in wound healing. Am J Surg. 2004;187(5A):11S-6S.

17. Cazander G, Jukema GN, Nibbering PH. Complement activation and inhibition in wound healing. Clin Dev Immunol. 2012:534291, 14.

18. Biggs MJP, Richards RG, Gadegaard N, Wilkinson CDW, Dalby MJ. The effects of nanoscale pits on primary human osteoblast adhesion formation and cellular spreading. J Mater Sci: Mater Med. 2007;18(2):399-404.

19. Ayala R, Zhang C, Yang D, Hwang Y, Aung A, Shroff SS, et al. Engineering the cell-material interface for controlling stem cell adhesion, migration, and differentiation. Biomaterials. 2011;32(15):3700-11.

20. Barrias CC, Ribeiro CC, Lamghari M, Miranda CS, Barbosa MA. Proliferation, activity, and osteogenic differentiation of bone marrow stromal cells cultured on calcium titanium phosphate microspheres. J Biomed Mater Res, Part A. 2005;72A(1):57-66.

21. Intranuovo F, Favia P, Sardella E, Ingrosso C, Nardulli M, d'Agostino R, et al. Osteoblast-like cell behavior on plasma deposited Micro/Nanopatterned coatings. Biomacromolecules. 2011;12(2):380-7.

22. Collie AMB, Bota PCS, Johns RE, Maier RV, Stayton PS. Differential monocyte/macrophage interleukin-1β production due to biomaterial topography requires the β2 integrin signaling pathway. J Biomed Mater Res, Part A. 2011;96A(1):162-9.

23. Kammerer PW, Gabriel M, Al-Nawas B, Scholz T, Kirchmaier CM, Klein MO. Early implant healing: Promotion of platelet activation and cytokine release by topographical, chemical and biomimetical titanium surface modifications *in vitro*. Clin Oral Implants Res. 2012;23(4):504-10.

24. Ravichandran R, Liao S, Ng CC, Chan CK, Raghunath M, Ramakrishna S. Effects of nanotopography on stem cell phenotypes. World J Stem Cells. 2009;1(1):55-66.

25. Badami AS, Kreke MR, Thompson MS, Riffle JS, Goldstein AS. Effect of fiber diameter on spreading, proliferation, and differentiation of osteoblastic cells on electrospun poly(lactic acid) substrates. Biomaterials. 2005;27(4):596-606.

26. Bakeine GJ, Ban J, Grenci G, Pozzato A, Dal Zilio S, Prasciolu M, et al. Design, fabrication and evaluation of nanoscale surface topography as a tool in directing

differentiation and organisation of embryonic stem-cell-derived neural precursors. Microelectron Eng. 2009;86(4-6):1435-8.

27. Dulgar-Tulloch AJ, Bizios R, Siegel RW. Differentiation of human mesenchymal stem cells on nano- and micro-grain size titania. Mater Sci Eng, C. 2011;31(2):357-62.

28. Jugdaohsingh R. Silicon and bone health. J Nutr, Health Aging. 2007;11(2):99-110.

29. Prabaharan M, Rodriguez-Perez MA, de Saja JA, Mano JF. Preparation and characterization of poly(L-lactic acid)-chitosan hybrid scaffolds with drug release capability. J Biomed Mater Res, Part B. 2007;81B(2):427-34.

30. Mahmoodi M, Ghazanfari L. Fundamentals of biomedical applications of biomorphic SiC. Prop Appl Silicon Carbide. 2011:297-343.

31. St. Pierre CA, Chan M, Iwakura Y, Ayers DC, Kurt-Jones EA, Finberg RW. Periprosthetic osteolysis: Characterizing the innate immune response to titanium wear-particles. J Orthop Res. 2010;28(11):1418-24.

32. Gallo J, Raska M, Mrazek F, Petrek M. Bone remodeling, particle disease and individual susceptibility to periprosthetic osteolysis. Physiol Res (Prague, Czech Repub). 2008;57(3):339-49.

33. Ingham E, Fisher J. Biological reactions to wear debris in total joint replacement. Proc Inst Mech Eng H. 2000;214(1):21-37.

34. Hetrick EM, Schoenfisch MH. Reducing implant-related infections: Active release strategies. Chem Soc Rev. 2006;35(9):780-9.

35. Mourino V, Boccaccini AR. Bone tissue engineering therapeutics: Controlled drug delivery in three-dimensional scaffolds. J R Soc Interface. 2010;7(43):209-27.

36. Gonzalez Corchon MA, Salvado M, de la Torre BJ, Collia F, de Pedro JA, Vazquez B, et al. Injectable and self-curing composites of acrylic/bioactive glass and drug systems. A histomorphometric analysis of the behavior in rabbits. Biomaterials. 2006;27(9):1778-87.

37. Kanellakopoulou K, Tsaganos T, Athanassiou K, Koutoukas P, Raftogiannis M, Skiadas I, et al. Comparative elution of moxifloxacin from norian skeletal repair system and acrylic bone cement: An *in vitro* study. Int J Antimicrob Agents. 2006;28(3):217-20.

38. Steward PS. Theoretical aspects of antibiotic diffusion into microbial biofilms. Antimicrob Agents Chemother. 1996;40(11):2517-22.

39. Stewart PS, William Costerton J. Antibiotic resistance of bacteria in biofilms. Lancet. 2001;358(9276):135-8.

40. Cushnie EK, Khan YM, Laurencin CT. Tissue-engineered matrices as functional delivery systems: Adsorption and release of bioactive proteins from degradable composite scaffolds. J Biomed Mater Res, Part A. 2010;94A(2):568-75.

41. Schnettler R, Pfefferle H, Kilian O, Heiss C, Kreuter J, Lommel D, et al. Glycerol-L-lactide coating polymer leads to delay in bone ingrowth in hydroxyapatite implants. J Controlled Release. 2005;106(1-2):154-61.

42. Hu Y, Cai K, Luo Z, Jandt KD. Layer-by-layer assembly of β-estradiol loaded mesoporous silica nanoparticles on titanium substrates and its implication for bone homeostasis. Adv Mater (Weinheim, Ger). 2010;22(37):4146-50.

43. Kelpke SS, Zinn KR, Rue LW, Thompson JA. Site-specific delivery of acidic fibroblast growth factor stimulates angiogenic and osteogenic responses *in vivo*. J Biomed Mater Res, Part A. 2004;71A(2):316-25.

44. Sun X, Su J, Bao J, Peng T, Zhang L, Zhang Y, et al. Cytokine combination therapy prediction for bone remodeling in tissue engineering based on the intracellular signaling pathway. Biomaterials. 2012;33(33):8265-76.

45. Kim J, Kim T, Jin G, Park J, Yun Y, Jang J, et al. Mineralized poly(lactic acid) scaffolds loading vascular endothelial growth factor and the *in vivo* performance in rat subcutaneous model. J Biomed Mater Res, Part A. 2013;101A(5):1447-55.

46. Tengood JE, Kovach KM, Vescovi PE, Russell AJ, Little SR. Sequential delivery of vascular endothelial growth factor and sphingosine 1-phosphate for angiogenesis. Biomaterials. 2010;31(30):7805-12.

47. Mayr-Wohlfart U, Waltenberger J, Hausser H, Kessler S, Gunther K-, Dehio C, et al. Vascular endothelial growth factor stimulates chemotactic migration of primary human osteoblasts. Bone (NY, U S). 2002;30(3):472-7.

48. De la Riva B, Nowak C, Sanchez E, Hernandez A, Schulz-Siegmund M, Pec MK, et al. VEGF-controlled release within a bone defect from alginate/chitosan/PLA-H scaffolds. Eur J Pharm Biopharm. 2009;73(1):50-8.

49. Shah NJ, MacDonald ML, Beben YM, Padera RF, Samuel RE, Hammond PT. Tunable dual growth factor delivery from polyelectrolyte multilayer films. Biomaterials. 2011;32(26):6183-93.

50. De la Riva B, Sanchez E, Hernandez A, Reyes R, Tamimi F, Lopez-Cabarcos E, et al. Local controlled release of VEGF and PDGF from a combined brushite-chitosan system enhances bone regeneration. J Controlled Release. 2010;143(1):45-52.

51. Golub JS, Kim Y, Duvall CL, Bellamkonda RV, Gupta D, Lin AS, et al. Sustained VEGF delivery via PLGA nanoparticles promotes vascular growth. Am J Physiol. 2010;298(6, Pt. 2):H1959-65.

52. Bose S, Tarafder S. Calcium phosphate ceramic systems in growth factor and drug delivery for bone tissue engineering: A review. Acta Biomater. 2012;8(4):1401-21.

53. Habraken WJEM, Wolke JGC, Jansen JA. Ceramic composites as matrices and scaffolds for drug delivery in tissue engineering. Adv Drug Delivery Rev. 2007;59(4-5):234-48.

54. Raghavan RN, Muthukumar T, Somanathan N, Sastry TP. Biomimetic mineralization of novel silane crosslinked collagen. Mater Sci Eng, C. 2013;33(4):1983-8.

55. Silverman LD, Lukashova L, Herman OT, Lane JM, Boskey AL. Release of gentamicin from a tricalcium phosphate bone implant. J Orthop Res. 2007;25(1):23-9.

56. Doty HA, Leedy MR, Courtney HS, Haggard WO, Bumgardner JD. Composite chitosan and calcium sulfate scaffold for dual delivery of vancomycin and recombinant human bone morphogenetic protein-2. J Mater Sci: Mater Med. 2014:Ahead of Print.

57. Belcarz A, Zima A, Ginalska G. Biphasic mode of antibacterial action of aminoglycoside antibiotics-loaded elastic hydroxyapatite-glucan composite. Int J Pharm (Amsterdam, Neth). 2013;454(1):285-95.

58. Kootstra NA, Verma IM. Gene therapy with viral vectors. Annu Rev Pharmacol Toxicol. 2003;43:413-39.

59. Ibraheem D, Elaissari A, Fessi H. Gene therapy and DNA delivery systems. Int J Pharm (Amsterdam, Neth). 2014;459(1-2):70-83.

60. Cucchiarini M, Thurn T, Weimer A, Kohn D, Terwilliger EF, Madry H. Restoration of the extracellular matrix in human osteoarthritic articular cartilage by overexpression of the transcription factor SOX9. Arthritis Rheum. 2007;56(1):158-67.

61. Venkatesan JK, Rey-Rico A, Schmitt G, Wezel A, Madry H, Cucchiarini M. rAAV-mediated overexpression of TGF-β stably restructures human osteoarthritic articular cartilage *in situ*. J Transl Med. 2013;11:211/1,211/14, 14.

62. Kidd ME, Shin S, Shea LD. Fibrin hydrogels for lentiviral gene delivery *in vitro* and *in vivo*. J Controlled Release. 2012;157(1):80-5.

63. Tseng S, Kempson IM, Peng S, Ke B, Chen H, Chen P, et al. Environment acidity triggers release of recombinant adeno-associated virus serotype 2 from a tunable matrix. J Controlled Release. 2013;170(2):252-8.

64. Moulay G, Boutin S, Masurier C, Scherman D, Kichler A. Polymers for improving the *in vivo* transduction efficiency of AAV2 vectors. PLoS One. 2010;5(12):No pp. given.

65. Kabanov AV, Batrakova EV, Alakhov VY. Pluronic block copolymers as novel polymer therapeutics for drug and gene delivery. J Controlled Release. 2002;82(2-3):189-212.

Capítulo 10

Conclusiones/Conclusions

USC
UNIVERSIDADE
DE SANTIAGO
DE COMPOSTELA

10. Conclusiones

El trabajo presentado y discutido en esta memoria permite establecer las siguientes conclusiones:

1. El procedimiento empleado para la síntesis de los bioSiCs mediante la pirolización e infiltración con silicio líquido de precursores naturales (maderas de pino, sapelli y roble) permite la obtención de tres sistemas cerámicos con propiedades variadas en cuanto a porosidad, distribución de tamaños de poro, características superficiales y densidad, que condicionan su utilidad como sustitutos óseos capaces de cargar y ceder moléculas terapéuticas.

2. Todos los materiales mostraron excelentes valores de biocompatibilidad cuando se ensayaron en una línea celular de fibroblastos (BALB/3T3) y células madre mesenquimales obtenidas de médula ósea humana. Además, la microestructura de los materiales promueve la diferenciación osteoblástica, particularmente para aquellos carburos de silicio con mayor tamaño de poro (roble y sapelli), para los que se obtuvieron, tras quince días de cultivo, valores de osteocalcina y osteopontina similares a los de las células cultivadas en presencia de medio de diferenciación osteoblástica.

Las partículas de carburo de silicio generadas por degaste mecánico no mostraron efectos tóxicos y si una respuesta celular aceptable.

En contacto con los componentes sanguíneos se observaron diferencias importantes en las interacciones de los bioSiCs y de sus respectivos precursores carbonáceos en función de sus características microestructurales y superficiales. Así, la respuesta hemolítica está determinada fundamentalmente por el tamaño de poro, mientras que la formación de coágulo depende de la rugosidad superficial y la adsorción de proteínas y la activación del complemento de la superficie específica.

3. La carga de los sistemas con antibiótico mediante interacciones inespecíficas genera capas sucesivas de moléculas de fármaco sobre la superficie del material que dan lugar a un proceso de cesión en dos fases, una más rápida inicial seguida de otra más lenta, dependiendo de la microestructura del material empleado. La menor porosidad del bioSiC de roble da lugar a los perfiles de cesión más sostenidos. Los sistemas cargados son capaces de inhibir la formación del biofilm bacteriano e incluso de tratar el previamente formado.

4. La incorporación de VEGF mediante interacciones iónicas da lugar a sistemas biofuncionales que mantienen la bioactividad de la proteína, incrementando la formación de vasos sanguíneos en un modelo animal *in vivo*. La adición del factor de crecimiento consigue estimular la diferenciación inicial de células madre mesenquimales, observándose un efecto sinérgico entre la proteína y la topografía de los materiales.

5. La combinación de bioSiCs con dos polímeros, alginato y poloxamer, permite incorporar fármacos de baja hidrosolubilidad, por su inclusión en las micelas generadas por el polímero sintético, y su cesión controlada, por su difusión en

el medio gelificado. Además, la microestructura del bioSiC condiciona el acceso del medio y la liberación del fármaco, por lo que se observaron diferencias significativas en el efecto antiinflamatorio promovido por los bioSiCs cargados con indometacina.

6. La combinación de estos polímeros, alginato y poloxamer ha permitido también la inclusión y liberación de vectores virales manteniendo su capacidad de transducción tras 21 días de ensayo, especialmente por aquellos sistemas que presentan un menor tamaño de poro. La incorporación de los hidrogeles en la matriz cerámica no ha permitido lograr sistemas que consigan alcanzar una adecuada transducción, lo que hace necesario trabajo de optimización adicional.

En su conjunto, los resultados de este trabajo confirman el elevado potencial de las cerámicas de carburo de silicio como sistemas biofuncionales con aplicación en implantes para el tratamiento de diversas patologías óseas. El gran número de precursores naturales y las diferentes técnicas de carga de moléculas activas disponibles debe permitir el desarrollo del sistema más adecuado en cada caso en función de la necesidad requerida.

USC
UNIVERSIDADE
DE SANTIAGO
DE COMPOSTELA

10. Conclusions

The work presented and discussed herein led to the following conclusions:

1. The bioceramization process employed for the synthesis of bioSiCs in two steps, pyrolyzation and infiltration with liquid silicon of natural precursors (pine, oak and sapelli wood) allows three ceramic systems with different properties of porosity, pore size distribution, surface properties and density to be obtained, which determine its usefulness as bone substitutes able to load and release therapeutic molecules.

2. All materials showed excellent biocompatibility values when tested on an fibroblast cell line (BALB/3T3) and mesenchymal stem cells derived from human bone marrow. Furthermore, the microstructure of materials promotes the osteoblastic differentiation, particularly those silicon carbides with larger pore size (oak and sapelli) in which, after fifteen days of cell culture, osteocalcin and osteopontin levels were similar to those of cells cultured in the presence of the osteoblastic differentiation medium.

   Silicon carbide particles produced by mechanical wear showed no toxic effect and an acceptable cellular response.

Significant differences in the interactions of bioSiCs and their respective carbon precursors in contact with blood components were observed according to their microstructure and surface properties. Thus, the hemolytic response is primarily determined by the pore size, while clot formation depends on the surface roughness and the protein adsorption and complement activation on the specific surface.

3. The antibiotic loading of the systems through unspecific interactions lead to multi layers of drug molecules on the surface of the material. These distribution results in a two phase release profile with an initial burst followed by a slower release, dependent on the microstructure of the material selected. The lower porosity of oak bioSiC leads to more sustained release profiles. Loaded systems are able to inhibit bacterial biofilm formation and even to treat an already formed biofilm.

4. The inclusion of VEGF into the ceramics by ionic interactions leads to biofunctional systems which maintain the bioactivity of the protein, increasing the vessel formation in an *in vivo* animal model. The addition of the growth factor achieves an initial stimulation of the differentiation of mesenchymal stem cells, showing a synergistic effect between the protein and the material topography.

5. The combination of bioSiCs with two polymers, alginate and poloxamer, allows low aqueous solubility drugs to be loaded by the drug inclusion into the synthetic polymer micelles and the hydrogel diffusion controlled release. Furthermore, the bioSiC microstructure determines the medium access and drug release, so that significant differences in the anti-inflammatory effect of indomethacin loaded bioSiCs composites were observed.

6. The mixture of these polymers, alginate and poloxamer, has also allowed the loading and release of viral vectors maintaining their transduction efficiency after 21 days of assay, especially for those systems with closer structures. The incorporation of these hydrogels into the ceramic matrix has not produced systems that achieve adequate gene transduction, thus requires further optimization work.

Taken all together, the results of this study confirm the high potential of silicon carbide ceramics as biofunctional systems, with an application as implants for the treatment of various bone pathologies. The large number of natural precursors and different loading techniques available, should allow the selection of the right fit in each case according to the required needs.

USC
UNIVERSIDADE
DE SANTIAGO
DE COMPOSTELA

La obtención de cerámicas de carburo de silicio biomórfico (bioSiC) a partir de recursos naturales ha permitido obtener sistemas que mimetizan la compleja estructura del material original. Estos sistemas han mostrado una excelente respuesta celular y tisular, lo que indica su elevado potencial como sistemas implantables para la regeneración del tejido óseo. La incorporación de moléculas terapéuticas en el seno de las matrices cerámicas permite obtener sistemas biofuncionales con elevada actividad terapéutica para el tratamiento o la profilaxis de patologías óseas. Se observó un efecto sinérgico entre las cerámicas y los fármacos incorporados.

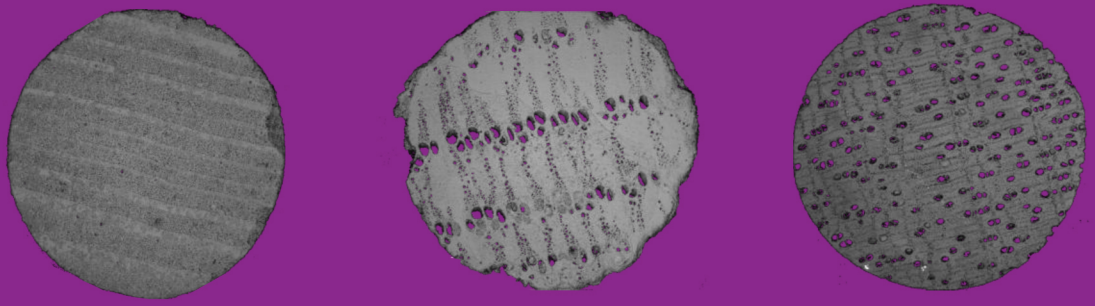

USC
UNIVERSIDADE DE SANTIAGO DE COMPOSTELA

UNIVERSIDAD DE SANTIAGO DE COMPOSTELA

Facultad de Farmacia

Departamento de Farmacia y Tecnología Farmacéutica